جامعة سيدي محمد بن عبد الله بفاس
UNIVERSITÉ SIDI MOHAMED BEN ABDELLAH DE FES

كلية العلوم والتقنيات فاس
FACULTÉ DES SCIENCES ET TECHNIQUES DE FÈS

N° d'ordre : 70/2023

Centre des Etudes Doctorales : Sciences et Techniques et Sciences Médicales
Formation Doctorale : SISPMI (Sciences de l'Ingénieur, Sciences Physiques, Mathématiques et Informatique)
Discipline : Génie Mécanique
Spécialité* : Génie Mécanique
Laboratoire : Génie Mécanique

** voir la liste des spécialités qui correspond à la formation doctorale sur le lien : https://fst-usmba.ac.ma/formations-doctorales/*

Thèse pour l'obtention de DOCTORAT

Modelling and analysing progressive damage in composite laminates: new perspectives for design and engineering applications

Préparée par : Mr. EL IDRISSI Hamza

Soutenue le 06 /10/2023 devant le jury :

Nom et Prénom	Etablissement	Grade	Qualité
Pr. HARRAS Bilal	FST, Fès	PES	Président
Pr. EL KHALFI Ahmed	FST, Fès	PES	Rapporteur
Pr. SAKA Abdelmjid	ENSA, Fès	PES	Rapporteur
Pr. CHAABA Moulay Ali	ENSAM, Meknès	PES	Rapporteur
Pr. ABOUTAJEDDINE Ahmed	FST, Fès	PES	Examinateur
Pr. RZINE Bouchra	FST, Fès	PH	Examinateur
Pr. EL HAINI Jamila	ENSA, Fès	PH	Examinateur
Pr. SEDDOUKI Abbass	FST, Fès	PES	Directeur de thèse
Pr. GARZIAD Mouad	FST, Fès	Invité	

بسم الله الرحمن الرحيم

عَنْ أَبِي الدَّرْدَاءِ، قَالَ: سَمِعْتُ رَسُولَ اللَّهِ ﷺ، يَقُولُ: مَنْ سَلَكَ طَرِيقًا يَبْتَغِي فِيهِ عِلْمًا سَهَّلَ اللَّهُ لَهُ طَرِيقًا إِلَى الْجَنَّةِ، وَإِنَّ الْمَلَائِكَةَ لَتَضَعُ أَجْنِحَتَهَا لِطَالِبِ الْعِلْمِ رِضًا بِمَا يَصْنَعُ، وَإِنَّ الْعَالِمَ لَيَسْتَغْفِرُ لَهُ مَنْ فِي السَّمَوَاتِ وَمَنْ فِي الْأَرْضِ حَتَّى الْحِيتَانُ فِي الْمَاءِ، وَفَضْلُ الْعَالِمِ عَلَى الْعَابِدِ كَفَضْلِ الْقَمَرِ عَلَى سَائِرِ الْكَوَاكِبِ، وَإِنَّ الْعُلَمَاءَ وَرَثَةُ الْأَنْبِيَاءِ وَإِنَّ الْأَنْبِيَاءَ لَمْ يُوَرِّثُوا دِينَارًا وَلَا دِرْهَمًا وَإِنَّمَا وَرَّثُوا الْعِلْمَ، فَمَنْ أَخَذَهُ أَخَذَ بِحَظٍّ وَافِرٍ. رواهُ أَبُو داود والترمذيُّ.

ACKNOWLEDGEMENTS

First and foremost, I am immensely grateful to my supervisor Mr. SEDDOUKI Abbass for his unwavering support, guidance, and expertise have been invaluable throughout this journey. The fact that he believed in my abilities and devoted himself to my academic development played a decisive role in the outcome of this thesis. I am truly fortunate to have been privileged to work under his mentorship.

I would like to extend my sincere thanks to the members of the jury for their time, insight, and valuable feedback. I would like to thank Professor Mr. HARRAS Bilal for the honour of presiding over the jury for my thesis. I would like to express my deep gratitude to Mr. EL KHALFI Ahmed, Mr. SAKA Abdelmjid and Mr. CHAABA Moulay Ali for agreeing to be the rapporteur of this thesis and for the interest they have shown in the content of this manuscript. Their perceptive comments and constructive criticism have contributed immensely to the refinement of this work. I am very grateful to Mr. ABOUTAJEDDINE Ahmed, Mrs. RZINE Bouchra and Mrs. EL HAINI Jamila for giving me the honour of examining my work and for agreeing to take part in this jury. I am glad for their thoughtful evaluation and for the opportunity to learn from their expertise. I extend my sincere appreciation to Mr. GARZIAD Mouad for his presence and support during this important moment in my academic journey. Thank you for being a part of my thesis defense and for your valuable perceptions and encouragement.

I would also like to acknowledge the Department of Mechanical Engineering at the Faculty of Sciences and Techniques. The faculty members and staff have created an enriching academic environment that has fostered my intellectual growth. Their commitment to excellence and their passion for knowledge have inspired me throughout my studies.

To my dear parents and family, words cannot express the depth of my gratitude. Your unwavering love, encouragement, and support have been the foundation of my academic pursuits. You have believed in me, even when I doubted myself, and your constant presence has given me the strength to overcome challenges. I am forever indebted to you for your sacrifices, understanding, and boundless belief in my potential. This achievement is as much yours as it is mine, and I am profoundly grateful for your unwavering love and support.

To my dear friends, thank you for standing by my side throughout this journey. Your friendship, laughter, and unwavering support have provided solace during moments of stress and have made this experience all the more meaningful. Your encouragement, late-night study sessions, and shared moments of celebration have brought joy to my academic pursuits. I am grateful for your presence in my life and for the memories we have created together.

Last but not least, I would like to express my deepest gratitude and appreciation to all those who have supported and contributed to the completion of this thesis.

ABSTRACT

Composite structures are becoming increasingly prominent within the contemporary aircraft industry, assuming a significant role. The utilization of composite materials has transcended the boundaries of aircraft design, extending its presence to diverse sectors such as automotive, athletics, and recreational equipment, among others. The exceptional attributes of composite materials, namely their lightweight nature and remarkable specific strength, contribute to the development of vehicles that exhibit enhanced fuel efficiency and longevity. To gain a comprehensive understanding of the impact of design parameters concerning the application of composite materials in these domains, a thorough examination of laminated composite structures necessitates a comprehensive investigation into failure analysis encompassing both damage initiation and propagation.

Composite laminates are widely used in engineering applications due to their excellent mechanical properties and lightweight nature. However, accurately predicting their behaviour and damage evolution remains challenging. Accordingly, this thesis proposes an in-depth assessment into the modelling and assessment of progressive damage in different composite laminates.

The thesis focuses on three key aspects. Firstly, it addresses the tensile loading behaviour of notched laminates and proposes various evaluation methods based on Puck’s failure criteria and damage mechanics. A new computational analysis was developed using the UMAT subroutine integrated into the Abaqus finite element analysis package, the study successfully predicts failure loads, failure modes, and load-displacement curves, demonstrating the potential of the proposed models for designing laminates involving holes and notches.

Secondly, the flexural behaviour of composite structure was studied using experimental tests and numerical modelling. We have employed Puck's failure criteria in conjunction with the Element Weakening Method, allowing for precise simulation of composite laminates behaviour. Furthermore, the study explored the influence of geometrical parameters on the bending behaviour of the composite laminate within the context of the 2D element model. Specifically, the ratio between the span and height (l/h) of the specimens, along with the width of the specimens, were found to significantly impact the successive failure and overall resistance of the composite laminate. The implemented model has effectively captured the complex behaviour and failure modes observed under bending load.

Lastly, the thesis proposes a novel 3D progressive damage model to predict the flexural behaviour and damage evolution of composite laminates under three-point bending. The model incorporates a progressive failure algorithm and gradual stiffness degradation rules, considering both inter and intralaminar failure modes. The study validates the model using different composite laminates and successfully predicts load vs. deflection, ultimate load and stiffness. Additionally, the thesis explores the interaction between matrix cracking and delamination, highlighting the significance of interface strength and addressing the mesh dependency for accurate simulations.

Overall, this thesis contributes to the advancement of progressive damage modelling in composite laminates. The findings enhance the understanding of progressive failure mechanisms and provide valuable insights for the design and engineering of composite laminates in various applications.

TABLE OF CONTENTS

ACKNOWLEDGEMENTS ..... **i**
ABSTRACT ..... **ii**
LIST OF FIGURES ..... **vi**
LIST OF TABLES ..... **ix**
ABBREVIATION ..... **x**
Chapter 1: Introduction **1**
1.1. Overview of failure in composite 2
1.2. Motivation from the WWFE 3
1.3. Summary of the objectives of this work 4
1.4. Organization of chapters 4
Chapter 2: Development of theories and the state of art **5**
2.1. Introduction 6
2.2. Background on composite materials 6
2.2.1. Definition of a composite material 6
2.2.2. Areas of use for composite materials 7
2.2.3. Classification of composite materials 7
2.2.4. Composites: Tools for Innovation and competitiveness 9
2.2.5. Interest of fiber orientation on deformation 10
2.2.6. Reinforcements 11
2.2.7. Laminates Based on Unidirectional Threads or Fabrics 15
2.2.8. Design rules for parts based on laminates 16
2.3. Failure analysis of laminated composite structures 16
2.3.1. Scales and coordinate systems of the material 16
2.3.2. Failure mechanism 18
2.4. Modelling of intralaminar behaviour initiation 21
2.4.1. Global theories 23
2.4.2. Failure criterion related to the specific failure mode 26
2.5. Progressive failure of intralaminar behaviour 40
2.5.1. Discount method 41
2.5.2. Continuum damage mechanics (CDM) 45
2.6. Modelling of interlaminar behaviour 50
2.6.1. Initiation failure criteria 50
2.6.2. Linear elastic fracture mechanics 51
2.6.3. Cohesive zone elements 54

2.7. Numerical modelling technique ... 57
2.7.1. Element type ... 58
2.7.2. Numerical solution ... 61
2.8. Numerical implementation ... 63
2.8.1. Umat subroutine ... 63
2.8.2. implementation via Umat in Abaqus ... 63
2.9. Conclusion ... 64
Chapter 3: Progressive failure analysis of composite laminates under tensile loading ... 63
3.1. Introduction ... 64
3.2. Computational analyse procedure ... 65
3.3. Results and discussion ... 67
3.3.1. T300/1034C Carbon/Epoxy composite laminates ... 67
3.3.1.1. Composite laminates with an open-hole ... 67
3.3.1.2. Validation for failure load and the load-displacement curves ... 69
3.3.1.3. Analysis results and discussions for progressive failure and load-displacement curves ... 72
3.3.1.4. Mesh dependency study using T300/1034C ... 81
3.3.2. AS4/PEEK composite laminates ... 84
3.3.2.1. Analysis Results and discussions for failure load and progressive damage ... 86
3.3.2.2. Mesh dependency study using AS4/PEEK ... 90
3.4. Conclusion ... 92
Chapter 4: Flexural behaviour modelling of carbon/epoxy laminates using the Puck-EWM approach ... 97
4.1. Introduction ... 98
4.2. Intralaminar damage initiation and evolution ... 98
4.3. Experimental setup ... 99
4.3.1. Materials ... 99
4.3.2. Preparation of the samples ... 100
4.4. Numerical simulation ... 101
4.4.1. Finite element model ... 101
4.4.2. Properties for model input ... 103
4.4.3. Model implementation ... 103
4.5. Result and discussion ... 106
4.5.1. Analysis results and discussions for failure load ... 106
4.5.2. Discussion and analysis results for progressive damage and load-deflection curves ... 109
4.5.3. Mesh dependency ... 117
4.6. Conclusion ... 119

Chapter 5: Intra/interlaminar damage modelling of composite laminates using a 3D progressive failure model 121

5.1. Introduction 122

5.2. Failure theory 126

5.2.1. Intralaminar damage initiation 126

5.2.2. Intralaminar damage evolution 126

5.2.3. Interlaminar damage initiation and evolution 127

5.3. Modelling 127

5.3.1. Initial/progressive failure analysis procedure using Abaqus Umat subroutine 127

5.3.2. Materials for computational analysis 129

5.3.3. Samples of composite laminates 129

5.3.4. Finite element model 132

5.4. Results and discussion 134

5.4.1. IMS194/CYCOM977-2 134

5.4.2. AS4/PEEK 144

5.5. Conclusion 151

Chapter 6: Conclusions and recommendations for future research studies 153

6.1. Introduction 154

6.2. Conclusions 154

6.3. Recommendation for future research works 157

REFERENCES 158

LIST OF FIGURES

Figure 1.1: The application of composite materials in the Airbus A380 [1]. 2
Figure 2.1: Composite material. 7
Figure 2.2: Composite materials classification. 8
Figure 2.3: Composite materials in aerospace (Boeing 787). 9
*Figure 2.4: a) The carbon fiber demand expansion in thousand tones over the years 2008–2022 (*estimate). b) The carbon Fiber demand in thousand tones per field of application (2013) [11]* 10
Figure 2.5: Influence of fiber orientation (Tensile test). 11
Figure 2.6: Classification of reinforcement. 11
Figure 2.7: Carbon fiber consisting of several hundred filaments [15]. 12
Figure 2.8: Unidirectional web. 13
Figure 2.9: Canvas fabric. 14
Figure 2.10: Serge fabric. 14
Figure 2.11: Satin fabric [12]. 14
Figure 2.12: Constitution of a laminate. 15
Figure 2.13: Example of a laminate designation. 15
Figure 2.14: Scales of a Unidirectional FRP: (a) The micro-mechanical level, (b) the lamina level, and (c) the laminate level. 17
Figure 2.15: Different forms of microdefects in the lamina: (a) hackles caused by shear stress $\tau_{\perp\parallel}$, (b) local matrix cracks and fiber-matrix debonding caused by fiber perpendicular stress $\sigma_{\perp}$, and (c local matrix failure caused by fiber parallel stress $\sigma_{\parallel}$ 19
Figure 2.16: (a to c) In-Situ Laser Scanning Microscope [25] captures the progression of micro-damage to inter-fiber fracture under tensile $\sigma_{\perp}$ [25], (d) (close- ups: (i) Scanning Electron Microscope micrograph showing the area in front of the crack tip, (ii) Onset of micro-delamination. 20
Figure 2.17: (a) Fracture modes according to conventional fracture mechanics, (b) In a $\pm 45^{0}$ laminate, delamination jumps between two interfaces due to inter-fiber fracture. 20
Figure 2.18: Biaxial first-ply failure (FPF) stress envelope for AS4/3501 laminates under biaxial loading [17, 18]. 22
Figure 2.19: Biaxial last-ply failure (LPF) stress envelope for AS4/3501 laminates under biaxial loading [17, 18]. 23
Figure 2.20: Tsai-Hill criterion failure envelopes for various σ_{12} [34]. 24
Figure 2.21: The Tsai-WU criterion failure envelopes for various σ_{12} [34] 25
Figure 2.22: (a) Stresses acting on the failure plane, (b) resultant shear stress on the failure plane. .. 27
Figure 2.23: Projection of the failure initiation surface on the (a) $\sigma_{n1}-\sigma_{nt}$ plane, $\sigma_{nn}= 0$, and (b) $\sigma_{nn}-\sigma_{n\psi}$ plane for $\sigma_{nn}\geq 0$. 33
Figure 2.24: Projection of the failure initiation surface on the $\sigma_{nn}-\sigma_{n1}$ stress plane; $\sigma_{nt}= 0$. 33
Figure 2.25: The matrix failure modes in Puck and Schürmann's failure criteria. 38
Figure 2.26: The wedge effect showing the fractured pieces gliding one against another in Mode C of matrix failure. 39
Figure 2.27: Representative Volume Element with damage. 46
Figure 2.28: Equivalent stress versus equivalent displacement. 48
Figure 2.29: Principle of the VCCT method [86]. 52
Figure 2.30: Presentation of different propagation criteria for G_{IC} = 350 J/m² and G_{IIC} = 1500 J/m² [78]. 54
Figure 2.31: Principle of a cohesive zone model. 55
Figure 2.32: Description of the different parts, with several possible shapes, of a cohesive zone model. 55
Figure 2.33: Upper row: 2D elements, lower row: 3D elements. Quadratic elements feature an extra node along each edge of the element. 58

Figure 2.34: Continuum shell elements SC8R. *61*
Figure 2.35: Flow chart for AbaqusTM and Umat integration. *64*
Figure 3.1: The computational algorithm used. *66*
Figure 3.2: Geometrical of T300/1034C test specimen. *67*
Figure 3.3: Loading and boundary conditions for T300/1034C composite laminates. *68*
Figure 3.4: One-quarter of the finite element model of open-hole laminate. *68*
Figure 3.5: Plies stacking sequence with different cases and with identical thickness for T300/1034C composite laminate. *69*
Figure 3.6: Predicted load vs. displacement curves of T300/1034C $[0/(\pm 45)_3/(90)_3]_s$ *composite laminates.* *72*
Figure 3.7: Predicted load vs. displacement curves of T300/1034C $[0/(\pm 45)_2/(90)_5]_s$ *composite laminates.* *73*
Figure 3.8: Predicted load vs. displacement curves of T300/1034C $[0/(\pm 45)/(90)_7]_s$ *composite laminates.* *73*
Figure 3.9: Load vs. displacement curves for the different methods used in this work. *77*
Figure 3.10a: The progress of failure for PUCK+CSE. *78*
Figure 3.10b: The progress of failure for PUCK+EWM. *79*
Figure 3.10c: The progress of failure for Built-in model. *80*
Figure 3.10: The progress of failure for different progressive damage models. *80*
Figure 3.11: Different mesh numbers near the open-hole to verify the mesh dependency of PFA. *81*
Figure 3.12: Load vs. displacement curves for different mesh cases using the Built-in model. *82*
Figure 3.13: Load vs. displacement curves for different mesh cases using the PUCK+EWM model. *82*
Figure 3.14: Load vs. displacement curves for different mesh cases using the PUCK+CSE model. *83*
Figure 3.15: Failure load values according to the number of elements near the open-hole. *84*
Figure 3.16: Load vs. displacement curve for the Present model. *89*
Figure 3.17: Load vs. displacement curve for the built-in model. *89*
Figure 3.18: Relationships between failure load and different diameters. *90*
Figure 3.19: Various mesh densities around the hole. *91*
Figure 3.20: Load-displacement curves for different mesh cases with a diameter of $D = 2$. *92*
Figure 3.21: Failure load value according to the number of elements near the open-hole. *92*
Figure 4.1: Three-point bending test. *99*
Figure 4.2: The geometry of the composite specimens for three-point bend experiments. *100*
Figure 4.3: The CNC milling machine: (a) Cutting the specimens by CNC milling machine; (b) The specimens obtained by cutting *101*
Figure 4.4: The FE models. *102*
Figure 4.5: The computational algorithm. *104*
Figure 4.6: Experimental macroscopic curves with damage progressive of specimen K. *106*
Figure 4.7: Load-deflection curves of specimen K. *110*
Figure 4.8: Load-deflection curves of specimen A. *110*
Figure 4.9: Load-deflection curves of specimen B. *111*
Figure 4.10: Load-deflection curves of specimen C. *111*
Figure 4.11: Load-deflection curves of specimen D. *112*
Figure 4.12: Progressive failure contours using the applied method for specimen K, A and D. *113*
Figure 4.13: Failure patterns of Prepreg T700: (a) Fiber damage progressive in the 0° ply; (b) Matrix damage progressive in the 90° ply *115*
Figure 4.14: Contours of stress's Mises (MPa) in the 90° ply: (a) stress contour of specimen k at first ply failure; (b) stress contour of specimen A at first ply failure; (c) stress contour of specimen D at first ply failure. *116*
Figure 4.15: Load vs. deflection curves for the different mesh sizes. *118*
Figure 4.16: Different mesh numbers to verify the mesh dependency of the applied model. *119*
Figure 4.17: Failure load values according to the number of elements. *119*

Figure 5.1: The illustrative synopsis. *125*
Figure 5.2: The computational algorithm of the progressive damage simulation using UMAT subroutine. *128*
Figure 5.3: Plies stacking sequence with cohesive plies for IMS194/CYCOM977-2 composite laminates. *131*
Figure 5.4: Plies stacking sequence with cohesive plies for AS4/PEEK composite laminate. *131*
Figure 5.5: Computer-Aided Design (CAD) model using Abaqus software. *133*
Figure 5.6: 3-Dimensional FEM for bending loading of the specimens. *133*
Figure 5.7: Predicted load vs. deflection curves of IMS194/CYCOM977-2 composite laminates. *135*
Figure 5.8: Damage contour of fiber tension/compression of IMS194/CYCOM977-2 composite laminates. *136*
Figure 5.9: Delamination initiation at Failure load. *137*
Figure 5.10: Damage contour of Matrix tension/compression of IMS194/CYCOM977-2 composite laminates. *138*
Figure 5.11: Intra/interlaminar damage contour at second/third fracture of IMS194/CYCOM977-2 composite laminates *140*
Figure 5.12: Distributions of σ_{13} along path A-B of IMS194/CYCOM977-2 composite laminates. *140*
Figure 5.13: Status of all damage modes of IMS194/CYCOM977-2 composite laminates. *141*
Figure 5.14 : Compression matrix damage contour. (a) model without CZE, (b) model with CZE. *142*
Figure 5.15: The comparison of load vs deflections of two model. *142*
Figure 5.16: load-deflection curves for different sizes. *143*
Figure 5.17: Different mesh numbers to verify the mesh dependency of the applied model. *144*
Figure 5.18: Failure load values according to the number of elements. *144*
Figure 5.19: Predicted load vs. deflection curves of AS4/PEEK composite laminates *145*
Figure 5.20: Matrix damage obtained from the experiments [153] and the damage contour from the simulation at failure load. *147*
Figure 5.21: Intra/interlaminar damage contour at second fracture of AS4/PEEK composite laminates. *148*
Figure 22. Damage contour of fiber tension/compression of AS4/PEEK composite laminates. *149*
Figure 5.23: Delamination obtained from post-tested with delamination damage contour obtained from simulation at failure load. *150*
Figure 5.24: Status of all damage modes. *150*

LIST OF TABLES

Table 2.1. Area of use for composite materials. 7
Table 2.2. Advantages and disadvantages of carbon fiber. 12
Table 2.3. Main characteristics of the reinforcements. 13
Table 2.4. The suggested values for Puck's inclination parameters. 38
Table 2.5. EWM and CSE conditions for each failure mode. 45
Table 3.1. Marking. 66
Table 3.2. Dimensions of the specimen used in this study. 68
Table 3.4. Comparison of the failure stresses of T300/1034C carbon/epoxy laminates (Label D). 70
Table 3.5. Dimensions of the specimen used in this study. 85
Table 3.6. Material properties of AS4/PEEK test specimen [64]. 85
Table 3.7. The failure loads (KN) of AS4/PEEK carbon/epoxy laminates. 86
Table 4.1. Dimensions of the specimens used in this study in (mm). 100
Table 4.2. Material properties of the specimens used. 103
Table 4.3. Marking. 105
Table 4.4. Comparison of the failure load and the displacement at failure load with the test results. 107
Table 4.5. Results obtained by finite element method for test specimen A, D and K. 114
Table 5.1. Labelling. 128
Table 5.2. The mechanical properties of the materials used in this study. 130
Table 5.3. The materials properties of the cohesive plies. 130
Table 5.4. The parameters of three-point bending experiments. 130
Table 5.5. Comparison of the failure load and the deflection at failure load with the test results. 145

ABBREVIATION

ASTM : *American Society for Testing and Materials*

AMR : *Adaptive Mesh Refinement*

Al : *Alumina*

C : *Carbon*

CDM : *Continuum Damage Mechanics*

CAE : *Computer-Aided Engineering*

CLT : *Classical Laminate Theory*

CSE : *Constant Stress Exposure*

CFRP : *Carbon Fiber Reinforced Polymer*

CZE : *Cohesive Zone Element*

CS : *Continuum Shell*

CNC : *Computer Numerical Control*

CAD : *Computer-Assisted Design*

DOF : *Degree of Freedom*

EWM : *Element Weakening Method*

FRC : *Fiber Reinforced Composite*

FF : *Fiber Failure*

FPF : *First Ply Failure*

f_S : *Stretch Factor*

f_E : *Stress exertion*

FI_M : *Failure Index for Matrix*

FI_F : *Failure Index for a Fiber*

FEA : *Finite Element Analysis*

FSDT : *First Shear Deformation Theory*

HR : *High Resistance*

HM : *High Module*

IFF : *Inter-Fiber Fracture*

GFRP : *Glass Fiber Reinforced Polymer*

LPF : *Last Ply Failure*

MVCCT : *Modified Virtual Crack Closure Technique*

MMC : *Metal Matrices Composite*

MS : *Margin of Safety*

OHT : *Open-hole Tension*

OMC : *Organic Matrix Composite*

PFA : *Progressive Failure Analysis*

PAN : *Polyacrylonitrile*

PVD : *Principle of Virtual Displacement*

PDM : *Progressive Damage Model*

PEEK : *Polyether Ether Ketone*

RVE : *Representative Volume Element*

RP : *Reference Point*

SiC : *Silicon Carbide*

STATEV : *State Variables*

SDEG : *Scalar Stiffness Degradation*

TSL : *Traction-Separation Law*

UK : *United Kingdom*

UD : *Unidirectional*

Umat : *User Material*

VCCT : *Virtual Crack Closure Technique*

VCE : *Virtual Crack Extension*

WWFE : *World-Wide Failure Exercise*

Chapter 1: Introduction

Overview

- *Overview of failure in composite*
- *Motivation from the WWFE*
- *Summary of the objectives of this work*
- *Organization of chapters*

1.1. Overview of failure in composite

Composite materials have become increasingly popular in a wide range of applications, from aerospace and automotive engineering to sports equipment and biomedical devices. These materials, which consist of a combination of fibers and a matrix, offer unique advantages such as high strength-to-weight ratios, improved stiffness, and improved resistance to fatigue and impact damage and their ability to be tailored for various designs. This evolution is expected to continue well into the future. It will bring significant improvements in fuel economy and passenger comfort, among other benefits. Recently, composites have begun to make real inroads into replacing conventional materials in commercial structural assemblies. Civil aircraft are using more and more composites in primary structures. Indeed, a number of recent designs, such as the Airbus A380 and Boeing 787, even use composites for major structural elements such as wing spars and fuselage skins, resulting in lightweight structures without compromising the overall airworthiness of the aircraft (see Fig. 1.1) [1].

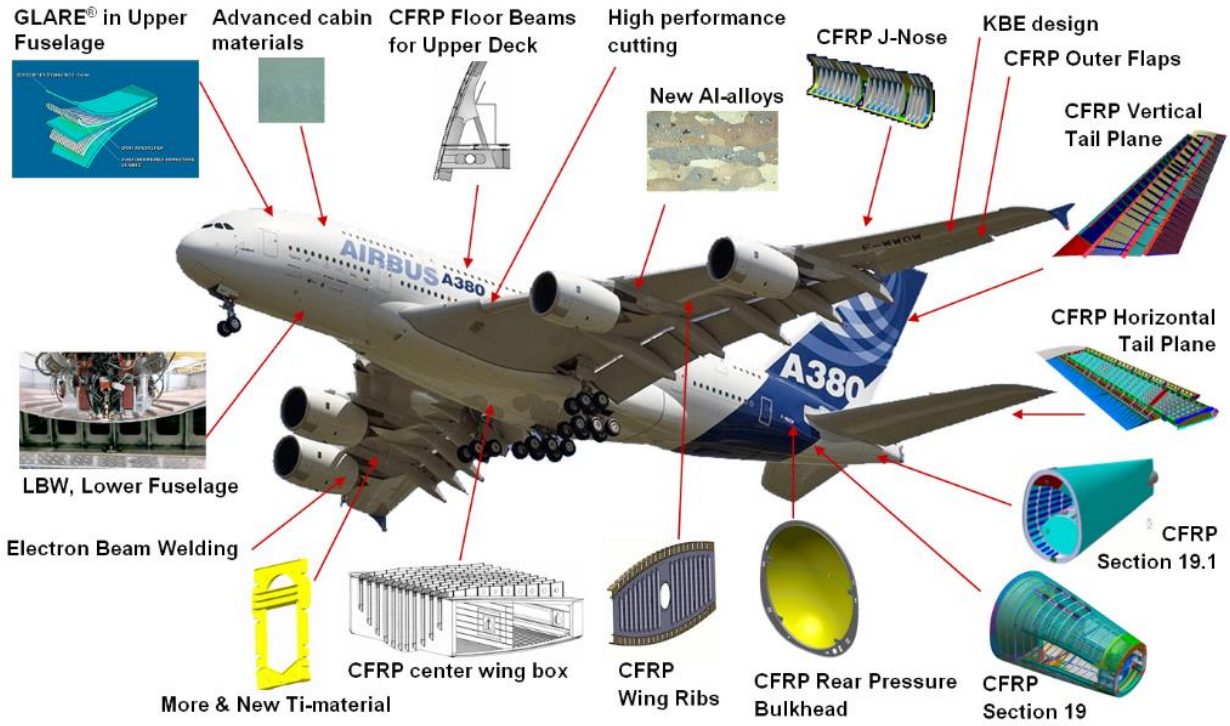


Figure 1.1: The application of composite materials in the Airbus A380 [1].

The performance requirements for composite structures are increasing. This means that the design boundaries for composite structures need to be carefully developed. In addition, the difficulty of predicting service life and the certification process still limit the use of composites in civil aircraft structures. The complexity of the failure mechanisms of laminated composites is related to many factors, such as interfacial fiber/matrix decohesion, matrix cracking, delamination between plies and fiber failure (buckling or kinking) in independent or mixed modes.

Due to the high anisotropy of these structures and the dependence on temperature, time, ambient light and humidity, many measurements are required to fully qualify a material. Also, the difficulty in predicting the structural failure modes requires better planned test program to reach the design requirements.

Therefore, more robust failure theories and damage propagation methods are needed to adequately forecast the complex failure mechanisms in composite materials. Driven by the observation that extensive testing of composite structures is extremely expensive, predictive tools are becoming increasingly important. Accurate numerical prediction, which is becoming increasingly important, would be very desirable to avoid expensive experiments. Moreover, on the basis of the increasing reliability of in-plane failure prediction [2], the application of FRC (Fiber Reinforced Composite) has been pushed to more complex geometries, which include primary load-bearing components, leading eventually to 3D loading of the material. Efficient and reliable failure prediction under common 3D loading conditions is required for safe design of such materials and structures. This is done by using computational models and methods and validating their predictions with experimental data.

Nevertheless, the intricate nature of composites, characterized by anisotropy, non-linear stress-strain characteristics, and intricate failure processes, present considerable challenges when attempting to model their structural behaviour, particularly regarding failure initiation and propagation. The complex interplay of various failure mechanisms further compounds the difficulty in accurately capturing structural failure phenomena, serving as a significant obstacle to the broader utilization of laminate composites. The prediction of composite behaviour is inherently demanding due to the involvement of diverse failure modes, including matrix cracking, delamination, and fiber-dominated failures, all of which contribute to structural shortcomings, with the matrix (resin) playing a dominant role in certain failure mechanisms.

1.2. Motivation from the WWFE

The World-Wide Failure Exercise (WWFE) took place in St Albans (UK) in 1991 with the aim of investigating the current state of the art in failure theory for polymer composites [2]. The WWFE was organised in three distinct phases. Firstly, participants were selected on the basis of rigorous criteria as outlined by Soden and Hinton [2] and were provided with test cases, material definitions, geometries and loads as pronounced [3] to establish a comprehensive framework. Subsequently, Part A of the WWFE involved the collection of technical papers from each participant presenting their respective failure theories and predictions for the specified test cases [4].

A significant outcome of the WWFE was the presentation by the organisers of a special issue of the journal Composites Science and Technology, which presented the results of a head-to-head comparison of the predictive capabilities of different failure theories. This comparative analysis was the first time that researchers in the field of composites compared failure predictions using different models and theories for the same set of geometry, loading conditions and material properties.

During the third phase of the exercise, Part B of the WWFE [5], all test cases were provided with experimental details, showing the test methods used. There was a collection of technical papers from all participants, and a comparison of the predictions of their theories with the experimental results was then made. Deficiencies in the different theories and experimental approaches were also identified. The WWFE has been expanded further in Part C, as referred to in [6]–[8], where the scale of the investigation has been enhanced. It incorporated five failure theories, including predictions based on modifications of the original theories, that had been found to be successful during the study.

A full discussion of their weaknesses and strengths was provided. Guidelines for designers of composite structures in the selection of appropriate failure theories were also given, together with

recommendations for the research community to advance the current state of the art in composite failure prediction. In particular, one of the five failure theories developed by Puck and Schürmann [9] was found to have the greatest number of consistent predictions based on the experimental data from the WWFE, and to capture more general features of the experimental data.

1.3. Summary of the objectives of this work

The objective of this thesis is to accurately predict the mechanical response and progressive damage of composite materials under various loading conditions. It aims to address the need for a suitable approach that can assess the growth of damage leading to final failure while reducing computational time and costs, and fully exploiting the advantages of composite structures.

To achieve this objective, a progressive failure model for composite laminated structures will be developed within the finite element framework, using the commercial software package Abaqus. This model will enable simple and accessible failure analysis by implementing a user-defined subroutine (Umat). The model will incorporate the Puck failure criteria coupled with damage mechanics models that are not part of the commercial package.

The progressive failure analysis (PFA) approach will be adopted, which focuses on the analysis of structures and materials with a particular emphasis on the degradation of material properties after failure initiation. The developed model will be applied to various example problems, considering different damage modes. The analysis will include the generation of damage contour plots, load-displacement curves as well as the mesh dependency analysis.

Two main example problems, namely the open hole tension (OHT) specimen and a composite plate under three-point bending, will be studied in detail. The numerical predictions obtained from the developed model will be thoroughly compared with existing experimental and numerical findings available in the literature.

By accomplishing these objectives, this thesis will contribute to advancing the understanding of progressive failure in composite materials and provide valuable insights for practical applications in composite structure design and analysis.

1.4. Organization of chapters

Chapter 1: Provides an introduction to the research background and problem, along with a clear statement of the aims and objectives.

Chapter 2: Reviews different approaches found in the literature, and presents a comprehensive overview of composite materials and their behaviour as well as the modelling guideline.

Chapter 3: Describes the modelling of progressive damage in an open-hole carbon/epoxy composite laminate subjected to tensile loading using different assessment methods coupled with finite element method.

Chapter 4: Presents an experimental study and numerical modelling using the Puck-Ewm approach of carbon/epoxy laminates subjected to bending loading.

Chapter 5: Propose an improved three-dimensional PFA that takes into account the interaction of intra/interlaminar failure modes, to accurately predict the flexural behaviour and damage evolution of thick laminates under three-point bending.

Chapter 6: Presents the main findings and conclusions together with recommendations for future work.

Chapter 2: Development of theories and the state of art

Overview

- *Introduction*
- *Background on composite materials*
- *Failure analysis of laminated composite structures*
- *Modelling of intralaminar behaviour initiation*
- *Progressive failure of intralaminar behaviour*
- *Modelling of interlaminar behaviour*
- *Numerical modelling technique*
- *Numerical implementation*

2.1. Introduction

Composite materials have emerged as a promising solution to meet the growing demand for high-performance materials in various industries. Composites are a type of engineered material with different properties. These materials are widely used in various industries such as aerospace, automotive, marine, and sporting goods due to their high strength-to-weight ratio, durability, and corrosion resistance.

In this chapter, we provide an in-depth overview of composite materials, covering various aspects such as their definition, areas of use, classification, and design rules for parts based on laminates. We also delve into the failure analysis of laminated composite structures, including the scales and coordinate systems of the material and failure mechanisms associated with it. Furthermore, we discuss the modelling of intralaminar behaviour initiation, including global theories and failure criteria associated with the failure mode, such as Hashin, Puck and Shurmann's failure criteria. The progressive failure of intralaminar behaviour is also examined using various methods such as the discount method and continuum damage mechanics (CDM). In addition, the modelling of interlaminar behaviour has likewise been studied in this chapter, including the initiation of failure criteria using linear elastic fracture mechanics and zone cohesive elements. We also discuss the numerical modelling techniques used to simulate and analyse the behaviour of composite materials, including the selection of the appropriate element type and numerical solution method for the analysis. Finally, we cover the numerical implementation of composite material models using the UMAT subroutine and Abaqus software, which are commonly used tools in the industry.

Overall, the insights provided in this chapter can aid in the design and development of composite materials for improved performance and reliability, which is crucial in various industries where high-performance materials are required. By gaining a comprehensive understanding of composite materials, their behaviour, and modelling techniques, researchers and engineers can make informed decisions in selecting the appropriate materials and design strategies to meet the needs of their specific applications.

2.2. Background on composite materials

2.2.1. Definition of a composite material

A composite material is a substantial manufactured by combining the physical or chemical properties of two or more constituent materials to create a material with improved and unique properties compared to its individual components. The individual components are usually referred to as the matrix and the reinforcement. The matrix is typically a polymer, metal, or ceramic material that serves as a binder for the reinforcement material and transfers stresses between them, which is typically composed of fibers, particles, or other materials that add strength, stiffness, or other desired properties to the composite (See Fig. 2.1). The resulting composite material can exhibit properties including a superior strength-to-weight ratio, excellent durability, corrosion resistance and thermal stability, making them useful in a wide range of applications in industries such as aerospace, automotive, construction, and equipment's sport.

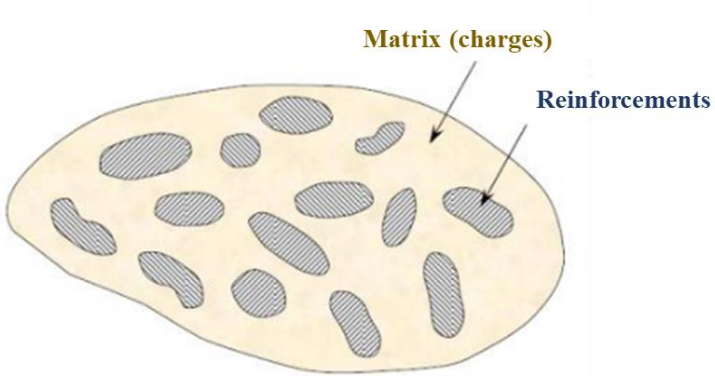


Figure 2.1: Composite material.

2.2.2. Areas of use for composite materials

Composite materials are nowadays taking a prominent place in various fields due to their simplicity of manufacture, their lightness and their mechanical properties. In contrast to conventional materials, which have intrinsic mechanical characteristics, composite materials can meet the requirements of different types of stresses, based on a judicious elaboration and choice of matrix and reinforcement, especially in different fields. Table 2.1 shows the different composite materials, their constituents and applications.

Table 2.1. Area of use for composite materials.

Type of composite	Constitutions	Fields of application
Organic matrix composites	Cellulose fibers, resin, wood chips, wood fibers, glass fibers, carbon fibers, etc.	Printing, packaging, carpentry Roofing, decking, sports, automotive.
Matrix composites Cement/Sand/aggregate Or ceramic matrix composites	Cement, sand, aggregates, carbon, Ceramic, etc.	Civil Engineering Aircraft
Metal matrix composites	Aluminium, boron fiber	Space
Sandwiches Metal, laminate, foam, honeycomb	Metals, laminate, honeycomb foam, balsa wood.	Multiple fields

2.2.3. Classification of composite materials

Composite materials are defined as an arrangement of reinforcements embedded in a matrix with different mechanical features. The matrix retains the geometric layout of the reinforcements and transfers loads between them. Furthermore, the arrangement of the fibers and their orientation, enable the enhancement of the mechanical properties of the structure.

Composite materials are categorized according to the composite matrix nature (See Fig. 2.2). In order to improve the rigidity of plastic materials, polymer and carbon matrices named organic matrix composite (OMC) are mostly used. In this case, the different constituents do not have any chemical affinity and do not react together. In contrast, metal matrices composite (MMC) typically used for high-temperature environments can often react chemically, but it must be ensured that the

high chemical reactivity of the metals does not lead to the formation of brittle compounds at the interface; which would lead to a degradation of the mechanical properties of the composite. The advantage of these compositions is that the intrinsic mechanical characteristics of metals are commonly prosperous. It is, therefore, possible to rely on the matrix behaviour and to reinforce only specific zones, or to use only unidirectional reinforcements; which is generally not possible with polymer matrices (because of their low strength) or ceramic (due to their fragility). Polymer and metal matrices are more ductile than fibers, but their resistance and rigidity are lower. Indeed, metal matrix composite (CMM) generally involves reinforcement of two types:

- Either particles or short ceramic fibers; the mechanical properties are then slightly greater than that of the metal matrix, and traditional manufacturing process of metals can generally be employed.
- Long ceramic or metallic fibers; the properties are much higher than the matrix characteristics, and the manufacturing processes are more expensive.

On the other hand, the ceramic matrix (CMC) which offers the excessively high-temperature resistance aims to improve the low tenacity of the matrix without increasing its rigidity inherently raised. For thermo-mechanical applications, the CMCs are among the most efficient materials. In this instance, the reinforcements and the matrix are often made of silicon carbide (Sic), carbon (C) or alumina (Al2O3). It is relatively common that the reinforcements and the matrix are made of the same material. The role of the composite structure, in this case, is beyond the combination of the properties of the different constituents. The composite provides new mechanical properties, namely toughness, and ductility. A particularity of CMCs is that often the fibers are less rigid than the matrix!

Architecturally, CMCs generally have continuous long fibers braided into wires which are then organized into 2D or 3D fabrics; as for CMOs, there are also short fiber reinforced CMCs, whose manufacturing processes are much closer to traditional ceramics.

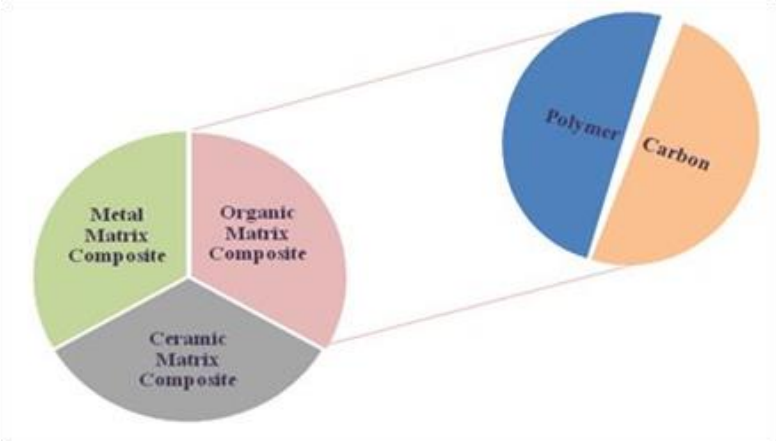


Figure 2.2: Composite materials classification.

Ultimately, there are 3 main categories of reinforcements: Organic (Glass Fibers, aramid ...), mineral (Carbon fiber, ceramics...) and Metallic (Boron fiber, alumina...). These reinforcements can be available under different structures:

- Particles
- Short or long fibers

- Multiaxial weaving
- Braiding
- Three-dimensional assembly ...

2.2.4. Composites: Tools for Innovation and competitiveness

Modern technology is driven by many competing criteria, such as materials with high mechanical properties and low densities. Therefore, materials with the highest property-to-density ratio, strength and stiffness are desirable.

Composite materials provide great potential for innovation because of their technical performance related to their mechanical properties, their conductivity and their resistance to corrosion. Indubitably, composites offer a wide possibility to be used within the different segments of the market and their applications are almost limitless.

Composite materials are widely used in the aircraft. In fact, 50 % of the structural parts of planes are made from composite materials [10] (See Fig. 2.3). In the aerospace, rockets can take heavier loads thanks to composite materials. Growing global demand for composites in these fields has contributed to the improvement of the technology.

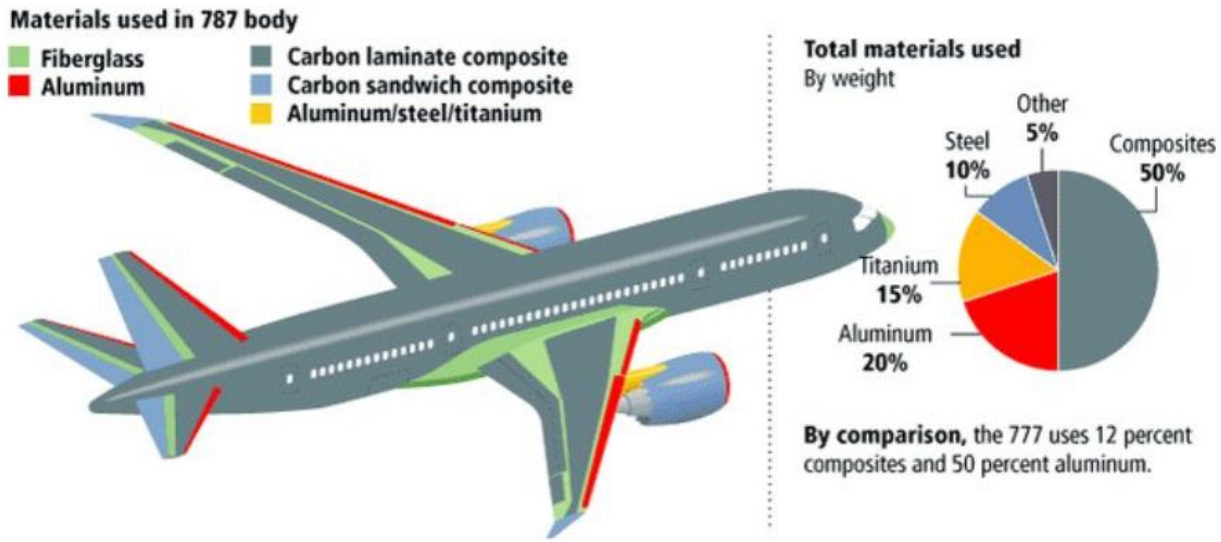


Figure 2.3: Composite materials in aerospace (Boeing 787).

Currently, the multifunctional potential of the composite is used for an increasing range of applications. Industrial and electronic equipment already account for 26 % of the market for organic matrix composites. Despite the strong biocompatibility constraints, composites play an increasing role in the dental sector (implants) and biomedical (prosthetic materials).

For the record, the production of musical instruments (pianos, harpsichords, violins, and even accordions) can offer opportunities for prestigious niches. Composite materials are also vital in the automotive area. In fact, the proportion of composite in the different sectors fluctuates according to the composite type. The Fig. 2.4 below illustrates the example of carbon composite:

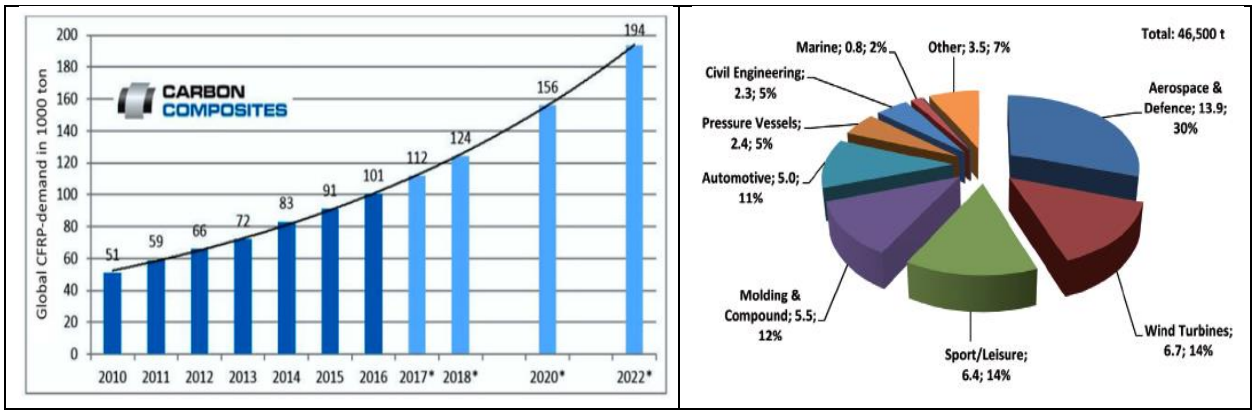


Figure 2.4: a) The carbon fiber demand expansion in thousand tones over the years 2008–2022 (*estimate). b) The carbon Fiber demand in thousand tones per field of application (2013) [11]

However, the use of composites is still confined to large-scale applications. Therefore, to spread them even more widely, manufacturers will have to overcome a number of obstacles:

- Technical challenge
- Increase in material cost
- Increase in quality control requirements
- Low automation
- Sensitivity to moisture, erosion, lightning damage
- The difficulty to detect damage
- Variability in material properties.
- The need to enhance competitiveness around the quadriptych performance-cycle-cost-sustainability of composite materials.
- Laminate architectures with weak interfaces.
- Fire resistance and temperature resistance (lower than metals).

2.2.5. Interest of fiber orientation on deformation

The orientation of the fiber is chosen to be adaptable to the load directions. The fibers are arranged in such a way that they resist tensile and compressive loads, Fig. 2.5. In order to resist the shear effect as well, two orthogonal fibers are used, so that one fiber withstands the compression or tension effect and the other the shear effect.

In addition, there is an influence of the reinforcement shape on the deformation. Indeed, the stiffness obtained with a woven reinforcement will be less than that observed by superimposing two directionals crossed at 90°. This is due to the curvature of the fibers as a result of the weaving operation, which makes the woven ply more deformable than crossed unidirectionals under the same load [12].

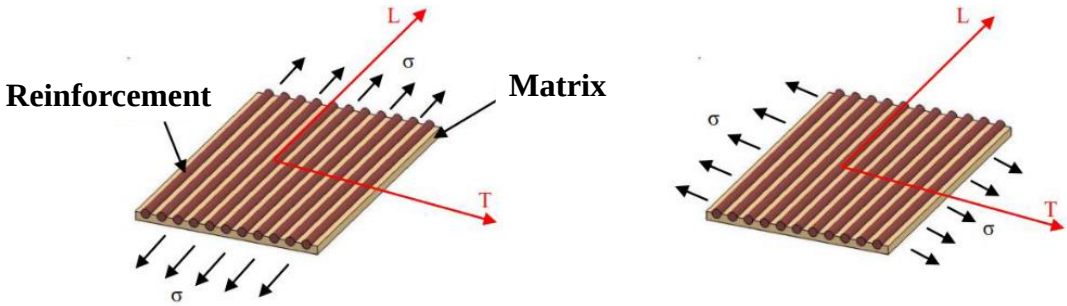


Figure 2.5: Influence of fiber orientation (Tensile test).

2.2.6. Reinforcements

The reinforcements ensure the mechanical properties of the composite material and a large number of fibers are available on the market, depending on the costs required for the structure. A large number of fibers are available on the market depending on the cost of the structure. Reinforcements consisting of fibers come in the following forms: linear (yarns, rovings), surface fabrics (fabrics, mats), multidirectional (braid, complex fabrics, tri-directional weaving or more) [13]. The classification of commonly encountered reinforcement types is shown in Fig. 2.6:

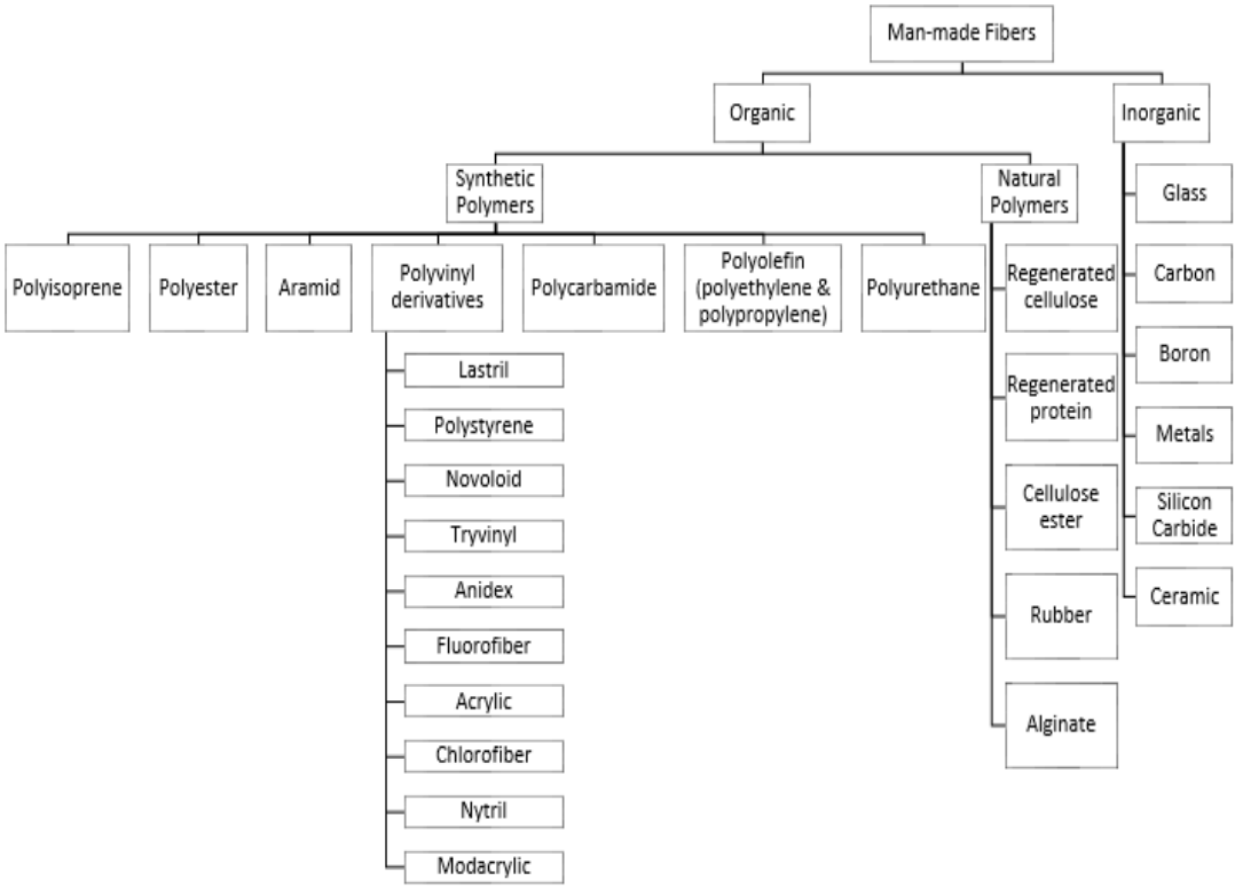


Figure 2.6: Classification of reinforcement.

2.2.6.1. Carbon fiber

It is the most widely used fiber in high performance applications. It is obtained by carbonisation of PAN (Polyacrylonitrile) fiber, (see Fig. 2.7). Its advantages and disadvantages are listed in Table

2.2. Depending on the combustion temperature, two types of carbon fibers can be distinguished [14].

- Fibers (HR): for a combustion of 1000 to 1500 °C.
- Fibers (HM): for a combustion temperature of 2500 to 3000 °C.

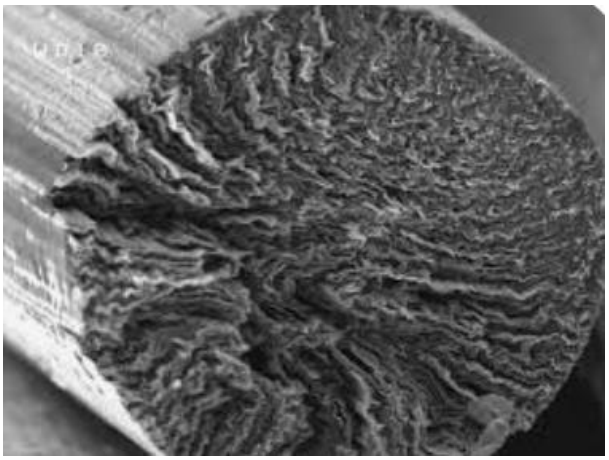


Figure 2.7: Carbon fiber consisting of several hundred filaments [15].

Table 2.2. Advantages and disadvantages of carbon fiber.

Advantages	Disadvantages
✓ High tensile strength and longitudinal rigidity. ✓ Very high temperature resistance without loss of properties (up to 1500°C in non-oxidising atmosphere). ✓ Corrosion and chemical resistance. ✓ Very low coefficient of longitudinal expansion.	✗ Fragility to impact ✗ Fragile when bent or folded ✗ High cost

2.2.6.2. Renforcement architecture

Composite structures are anisotropic. Most reinforcements work well in tension, but perform less well in compression and shear (see Table. 2.3). It is therefore imperative to play with the texture and geometry of the reinforcements to create a suitable architecture. There are different geometries and textures of reinforcements [12].

Unidirectional (UD):

In a unidirectional web, the yarns are aligned parallel to the warp direction, and they are joined by a thin yarn in the weft direction (See Fig. 2.8). Thus, the web is unidirectional with high performance in the warp direction [14].

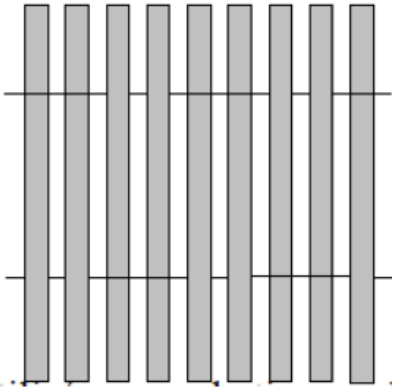


Figure 2.8: Unidirectional web.

Table 2.3. Main characteristics of the reinforcements.

Reinforcements Features	**Glass E**	**Glass R**	**Carbon HM**	**Carbon HR**	**Kevlar**	**Boron**	**Alumina silicate**
Filament diameter (µm)	3 to 30	3 to 30	6.5 to 8	7 to 8	12	100 to 200	8
Density	2.5 to 2.6	2.48 to 2.5	1.8	1.9 to 1.75	1.45	2.53 to 2.6	2.6
Longitudinal modulus of elasticity (GPa)	73 to 74	86	350 to 400	180 to 230	130	400	200
Shear modulus (GPa)	30	/	20	50	12	-	-
Poisson's ratio	0.25	0.2	0.35	0.3	0.4	-	-
Coefficient of thermal expansion (C^{-1}) *10^5	0.5	0.3	0.08	0.02	-0.2	0.4	-
Tensile strength (MPa)	2500 to 3400	3200 to 4400	2500 to 2500	3200 to 2800	2900 to 3100	3400 to 3500	3000
Elongation at rupture (%)	3.5 to 4.8	4 to 5.4	0.6	1.3	2.3	0.8	1.5

The fabrics:

Fabrics are made up of warp and weft threads running perpendicular to each other. They are characterised by the way they are interlaced or woven [16].

Canvas or taffeta: each warp thread passes over and then under each weft thread, and vice versa, (see Fig.2.9). The fabric has good flatness and relative stiffness, but is not very deformable for processing. The numerous successive interweaving generates a significant amount of caking and reduce the mechanical properties [17].

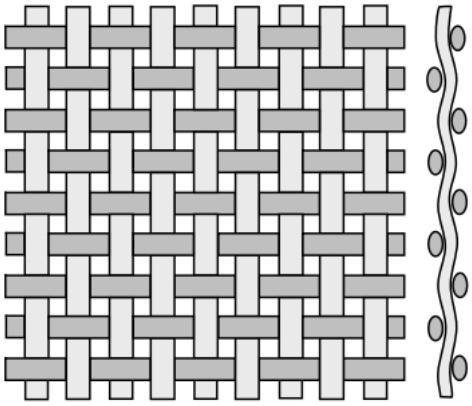


Figure 2.9: Canvas fabric.

Serge: each warp thread passes over several (n) weft threads and each weft thread floats over (m) warp threads, (See Fig. 2.10). This results in a weave that is more flexible than taffeta with a good thread density [16].

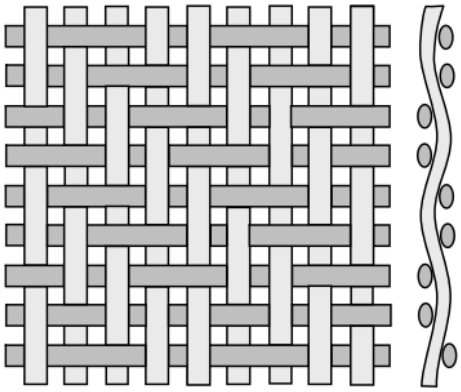


Figure 2.10: Serge fabric.

Satin: each warp thread passes over several (n-1) weft threads and vice versa, (See Fig. 2.11). These fabrics have different aspects on each side. These fabrics are quite flexible and suitable for shaping parts with complex surfaces. This type of fabric has a high specific gravity. As a fabric is difficult to deform on a left-hand surface, two- or three-dimensional weaves are also produced for specific uses [17].

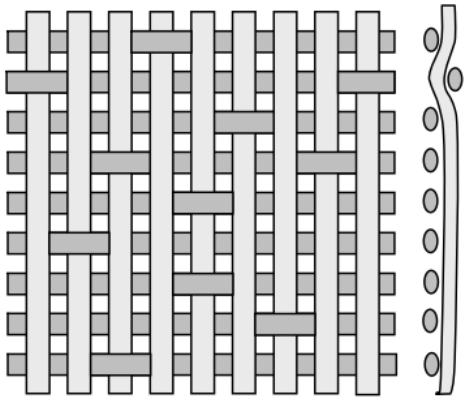


Figure 2.11: Satin fabric [12].

2.2.7. Laminates Based on Unidirectional Threads or Fabrics

Laminates based on unidirectional yarns or fabrics are a basic type of laminate to which any other type of laminate can theoretically be related. These laminates consist of layers of unidirectional yarns or fabrics, the direction of which is offset in each layer, (See Fig 2.12) [16].

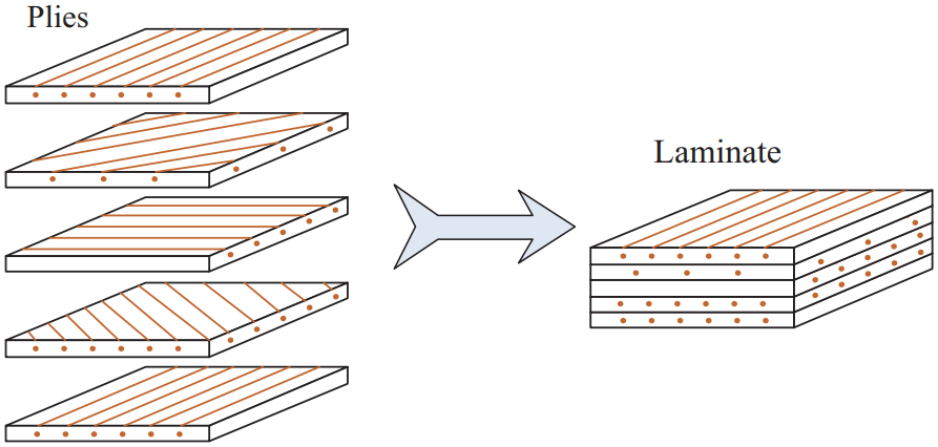


Figure 2.12: Constitution of a laminate.

The designation of these laminates is usually done according to the subsequent code:

- ✓ Each ply is identified by a numerical value representing the angle, in degrees, whereby the direction of the fibers is shifted from the reference x-axis (see Fig. (2.13)).
- ✓ If successive layers have different angles, they are separated by a slash (/).
- ✓ Consecutive plies having the same orientation are given a numerical code.
- ✓ Layers are named sequentially from one side towards the other.
- ✓ The start and end of the code are enclosed in square brackets (or parentheses).
- ✓ The name of the layers depends on the selected axis system.
- ✓ In cases where layers have equal angles in absolute values with opposite signs, either (+) or (-) should be used. The choice of positive or negative angles corresponds to the chosen axis system.

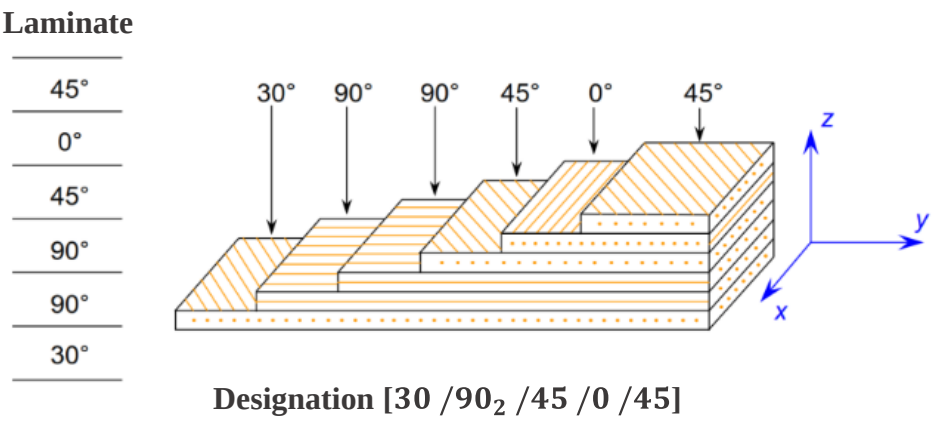


Figure 2.13: Example of a laminate designation.

The direction known as "at 0°" corresponds to the direction of application of the preponderant load, or to a privileged direction of the part considered, or to the axis of abscissas of the chosen reference frame.

2.2.8. Design rules for parts based on laminates

In general, a minimum proportion of layers (5% to 10%) in each of the 0°, +45°, -45° and 90° directions is expected. The minimum thickness of the laminate should be about 1 mm. The proportion and number of layers in each direction at 0°, +45°, -45° and 90° take into account the mechanical stresses on the laminate in the area under consideration. In addition, there are three criteria that concern the designer when deciding on the ply arrangement [13]:

- Supporting the load flows without deterioration.
- Limiting the deformation of the loaded part of which the laminate is a component.
- Minimise the mass of the materials involved.

Besides, when defining the laminate (orientations and number of layers), the following provisions should be observed as far as possible:

- 90° plies placed on the surface, then plies at +45 or -45, when the predominant load flow is in the 0° direction.
- No more than 4 consecutive folds in any one direction.

2.3. Failure analysis of laminated composite structures

Composite materials consist of several originally separate phases. This study focuses on laminates, which fall into the category of composites in two ways. Firstly, laminates consist of stacked layers, called laminae, which in turn consist of fibers embedded in a matrix material.

The primary failure modes observed in fiber reinforced polymer (FRP) composites include matrix compression, matrix tension, fiber compression, fiber tension and delamination between adjacent laminae. These failure modes are known as intra/interlaminar failure modes. Intralaminar failure can manifest as fracture in the fibers and/or matrix, as well as fiber kinking or buckling under compression. In this thesis, the intralaminar failure modes are described using phenomenological theories that consider stress levels as initiators of damage or fracture. These theories can be effectively studied using finite element analysis of structural problems.

Furthermore, in unidirectional laminates, predictions of intralaminar failure are based on the analysis of strains and stresses within each lamina, with failure criteria evaluated for each individual layer. It's important to note that failure initiated in one lamina does not necessarily mean ultimate failure of the entire laminate. Degradation models of the material must be used to accurately model damage propagation.

2.3.1. Scales and coordinate systems of the material

Continuous glass fibers typically have a diameter ranging from 3 to 20 μm, with the majority falling around 12 μm. On the other hand, carbon and graphite fibers have an approximate diameter of 8 μm. The thickness of a single ply in carbon fiber-reinforced polymer (FRP) composites, as well as glass FRP composites, is approximately 125 μm. These values hold true for carbon FRP composites with a typical fiber volume fraction of 0.7, and glass FRP composites with a typical fiber volume fraction of 0.45.

In the field of mechanics and materials engineering, the micro-level modelling focuses on a physical scale of 10 μm, while the meso-level modelling considers a larger physical scale of 1 mm. However, in the present study, our emphasis is on the mesoscale modelling at the lamina level. The objective is to understand and predict the response and failure of an individual lamina in order to anticipate the progressive failure of the laminate as a whole. For this purpose, the material properties at the meso-level are assumed to be predetermined. Based on the setup of unidirectional (UD) fiber-reinforced composites, there are four levels at which the composite can be analysed, each providing unique insights into its behaviour.

2.3.1.1. Micro-mechanical level

At the micro-mechanical level, the fibers and matrix are considered distinct materials exhibiting different constitutive behaviours, as depicted in Fig. 2.14a. Although explicit analysis of Puck's failure criteria is not conducted at the micro-mechanical level, key mechanisms are condensed and extrapolated to the lamina level.

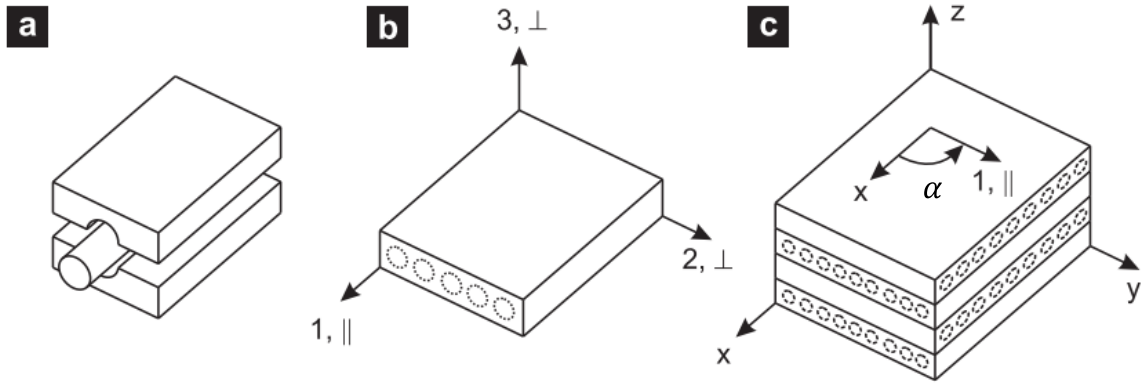


Figure 2.14: Scales of a Unidirectional FRP: (a) The micro-mechanical level, (b) the lamina level, and (c) the laminate level.

2.3.1.2. Lamina level

At the lamina level, the fiber-matrix composite is treated as a homogeneous continuum but anisotropic material, possessing effective material properties as illustrated in Figure 2.14b. In the case of a unidirectional (UD) lamina, it exhibits transverse isotropy due to the presence of two inherent directions: fiber-parallel (indexed as ∥) and fiber-perpendicular (indexed as ⊥). The transverse (index 2) and through-thickness (index 3) directions of the lamina behave identically, while the longitudinal direction (index 1) displays different characteristics. To capture this behaviour, common orthotropic material models are employed.

The constitutive behaviour and strength of the lamina can be determined through experimental coupon tests or derived from the individual behaviours of the fibers and matrix using mixture rules, analytical micro-mechanical models, or Representative Volume Element (RVE) approaches [18]. These methods aim to characterize the lamina by homogenized stiffnesses (E_{11}, E_{22}, E_{33}, G_{12}, G_{13}, G_{23}) and strengths [19], [20]. Most failure criteria, including Puck's Theory, rely on the stresses or strains calculated at the lamina level. As a result, these criteria serve as layer-wise indicators for intra-laminar failure.

2.3.1.3. Laminate level

At the laminate level, the scale expands to approximately 10^0 m and encompasses various structural elements such as beams, columns, and plates. The material is considered as a stacked composition comprising multiple laminae, including their interfaces, as depicted in Fig. 2.14c. The orientation of each lamina is determined by the angle α, which represents the deviation between a laminate-related x-axis and the fiber orientation (1-direction) within the respective lamina.

The primary objective of stress analysis at the laminate level is to determine the inter- and intralaminar stresses within individual laminae and at the interfaces, resulting from the applied loads on the entire laminate. Consequently, stress analysis at this level forms the foundation for intra-laminar failure analysis and the prediction of delamination.

In contrast to the behaviour at the lamina level, a unidirectional (UD) fiber-reinforced lamina may exhibit true orthotropic properties when it is confined within a laminate. This phenomenon, known as the in-situ effect, influences the lamina's strength characteristics.

2.3.1.4. Structural level

At the structural level, the focus shifts to considering complete components, which can possess intricate geometries and complex local stacking sequences. Stress analyses conducted at this level aim to determine the local stress distribution at any given position within the component, resulting from external loads applied to the component.

The ultimate objective of failure analysis in practical applications is to achieve a dependable prediction of failure within a structural level analysis. This entails accurately identifying the points where failure is likely to occur and understanding the factors that contribute to structural failure. By gaining insights through structural level analysis, one can effectively anticipate and mitigate potential failures in real-world components.

2.3.2. Failure mechanism

2.3.2.1. Micro-damage

The degradation process of any material initiates at the micro-mechanical level. In the case of a fiber-polymer lamina, even during the manufacturing process of the fiber-matrix composite, micro-damage is already introduced. This is attributed to the disparities in thermal expansion coefficients between the fiber and matrix, as well as the matrix shrinkage during polymerization. As a result, significant residual stresses are present in the matrix following the curing process [21].

These residual stresses can lead to flaws, such as local fiber-matrix debonding and microscopic matrix cracks, as depicted in Fig. 2.15b. When subjected to an increasing load, these initial micro-defects swiftly propagate in both size and number. Additionally, under shear loading, microscopic hackles form within the matrix, as shown in Fig. 2.15a. Furthermore, when subjected to a load parallel to the fibers, the early fracture of individual fibers induces the failure of the adjacent matrix due to the localized increase in load, as seen in Fig. 2.15c.

It is important to note that these micro-defects initiate and progress well before a macroscopic crack becomes visible. However, their presence can be detected through observations such as the material transitioning to an opaque appearance, a reduction in stiffness, or acoustic emission analysis. These indicators provide evidence of the existence and development of micro-defects within the material.

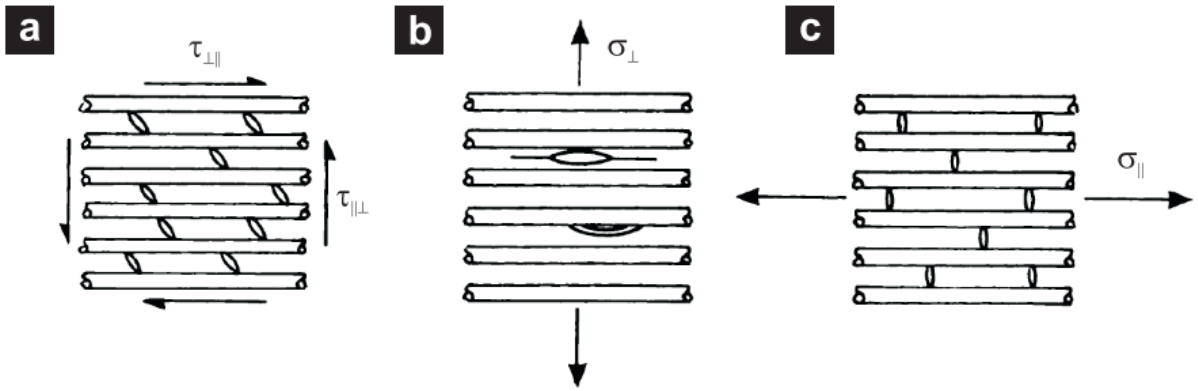


Figure 2.15: Different forms of microdefects in the lamina: (a) hackles caused by shear stress $\tau_{\perp\parallel}$, (b) local matrix cracks and fiber-matrix debonding caused by fiber perpendicular stress $\sigma_{\perp}$, and (c local matrix failure caused by fiber parallel stress $\sigma_{\parallel}$.

2.3.2.2. Fiber fracture

The failures observed in a fiber-matrix composite at the lamina level can be categorized into two macroscopic types: fiber fracture (FF) and inter-fiber fracture (IIF). Fiber fracture refers to the complete fracture of most or all fibers within a lamina, rather than the fracture of individual fibers, which typically begins at around 50% to 70% of the fiber fracture limit. A fiber fracture criterion defines the load condition at which the entire lamina experiences a sudden separation in the fiber-parallel direction. When considering the lamina as a homogeneous material, such criteria are determined based on the maximum load that can be sustained in the fiber-parallel, longitudinal direction.

The behaviour of a lamina in the fiber-parallel direction differs significantly under tension and compression. Under fiber-parallel tension, the material separates along a fracture plane perpendicular to the fibers. The load-bearing capacity in this direction is predominantly governed by the fibers, meaning that micro-damage in the matrix resulting from additional fiber-perpendicular or shear loads [22] does not significantly affect the load-bearing capacity in the fiber direction. However, the load-bearing capacity in the fiber direction is influenced by fiber-perpendicular loads due to the differential lateral contraction behaviour of the fibers and matrix. This effect is accounted for in Puck's extended fiber fracture criterion.

In the case of fiber-parallel compressive loading, the occurrence of fiber fracture (FF) heavily depends on the interaction between fibers and matrix, which varies among different material systems. In situations where fibers are perfectly supported and aligned, they may break due to shear within the fibers, resulting in an inclined fracture plane and mutual sliding of the newly exposed surfaces, if kinematically possible. However, this behaviour has rarely been observed and, if at all, it is exclusively observed in anisotropic carbon fibers [23]. The more common mechanism for relieving the load on the fibers is buckling. The activation of this mechanism, ranging from micro-buckling to macroscopic fiber kinking, where fibers in large continuous regions deflect in the same direction, depends on the material system and the fiber volume fraction. Unlike tension-induced fiber fractures, the supporting capacity of the matrix plays a role under compressive loading. Therefore, the presence of matrix defects resulting from fiber-perpendicular or shear loads influences the compressive load-bearing capacity of the lamina [24]. However, this effect has not yet been incorporated into Puck's Theory.

2.3.2.3. Inter-fiber fracture

When subjected to fiber-perpendicular tension, fiber-perpendicular compression, or shear loading, the lamina will ultimately experience failure through an inter-fiber fracture (IFF). This term refers to a macroscopic crack that extends through the matrix material or along the boundaries between fibers and the matrix, spanning the entire lamina (refer to Fig. 2.16). The outcome is a fracture plane that appears macroscopically planar. The significance of an IFF in terms of the load-bearing capacity of a laminate varies from being relatively benign to potentially catastrophic, depending on the orientation of the fracture plane and the magnitude of the transmitted load.

Puck's Theory is capable of distinguishing between fiber fractures and inter-fiber fractures, and it can predict both the orientation of the IFF plane and the stresses acting on that plane. By providing insights into the behaviour and characteristics of inter-fiber fractures, Puck's Theory enables a deeper understanding of the failure mechanisms within laminates, facilitating the analysis and prediction of laminate performance under various loading conditions.

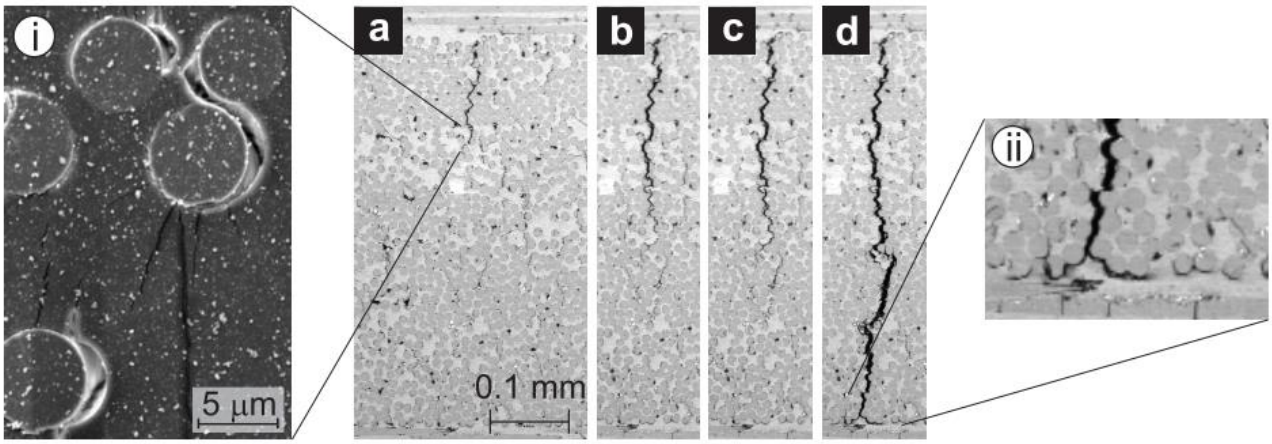


Figure 2.16: (a to c) In-Situ Laser Scanning Microscope [25] captures the progression of micro-damage to inter-fiber fracture under tensile $\sigma_{\perp}$ [25], (d) (close- ups: (i) Scanning Electron Microscope micrograph showing the area in front of the crack tip, (ii) Onset of micro-delamination.

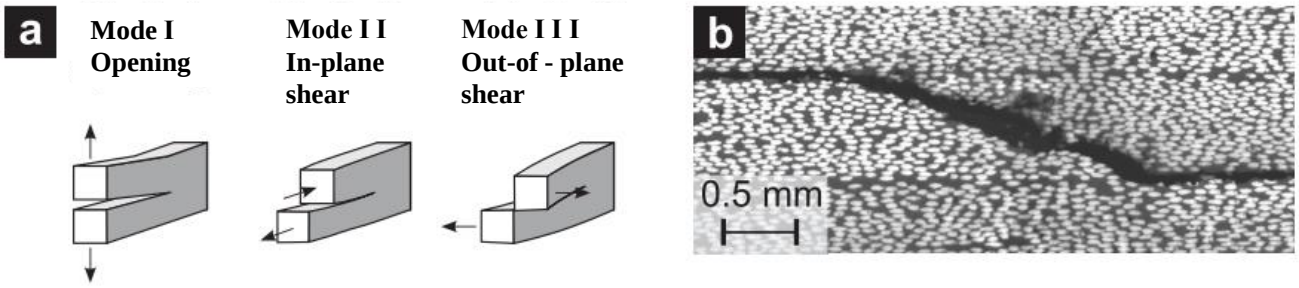


Figure 2.17: (a) Fracture modes according to conventional fracture mechanics, (b) In a ±45⁰ laminate, delamination jumps between two interfaces due to inter-fiber fracture.

2.3.2.4. Delamination

Delamination, the separation of layers within a laminate, can occur due to inter-laminar stresses such as through-thickness tension or through-thickness shear. Bending is a common deformation that induces significant inter-laminar shear, while in-plane loading can also lead to inter-laminar shear depending on the laminate's stacking sequence. Various analytical models, typically based

on traction-separation laws and energy terms, have been developed to study delamination onset and growth [26].

In this work, delamination is considered in the post-failure analysis, and its interaction with inter-fiber fractures (IFFs) has been studied (refer to Chapter 5). It has been observed that delamination often initiates at the point where a macroscopic inter-fiber crack intersects the interface between two laminae (see Fig. 2.16, ii). Furthermore, IFFs can propagate and facilitate delamination across different interfaces (see Fig. 2.17b). These effects are influenced by local stress concentrations at the crack tips. At the structural level, areas damaged by IFFs affect inter-laminar stresses through their reduced stiffness, leading to changes in the overall stress distribution within the laminate.

2.4. Modelling of intralaminar behaviour initiation

Ensuring the absence of irreversible damage in composite structures under operational loads is crucial for the design of load-carrying components. Understanding the initiation of damage is necessary, particularly for UD-laminas subjected to simple longitudinal loading, where comparing the applied load with the specimen's strength value can provide valuable information. The simple maximum stress criterion is generally sufficient for reliably determining failure in such cases. However, in practical scenarios, components experience more complex stress states, where normal and shear stress components interact, rendering the simple maximum stress criterion invalid.

In the case of metals, the von Mises yield criterion is utilized to transform the three-dimensional stress state into a single scalar value, allowing for comparison with the material's tensile strength. However, complications arise when assessing laminates due to their anisotropic material behavior, which cannot be characterized by a single equivalent value. To address this challenge, numerous failure criteria have been developed by researchers worldwide. By 1986, there were already 30 different failure criteria, but only a few of them had sufficient experimental data to support their validity.

Recognizing this limitation, an international effort was initiated in 1992, known as the World-Wide Failure Exercise (WWFE), organized by Hinton et al [2]–[8]. In the WWFE, the authors of commonly used failure criteria were tasked with analyzing their criteria for various laminate types and materials. A total of 14 test cases were conducted, with all participants using the same provided data. The results were compared and published in part A of the WWFE, revealing significant discrepancies among the individual criteria, with variations reaching as high as 570% in some cases. Part B of the exercise involved assessing the results against experimental data provided by the organizers, offering insights into the validity of the criteria. Part C provided an opportunity for participants to comment on their results and make corrections if necessary. Subsequent WWFE iterations were conducted to evaluate the validity of three-dimensional stress states.

Throughout the WWFE, many new criteria were developed based on the exercise's experimental data, contributing to the advancement of laminate analysis theories. It also highlighted the strengths and limitations of individual theories in accurately predicting failure. This underscored the need for further research to enhance the quality of laminate assessments. The results of the WWFE are utilized in this framework to determine the most suitable failure criteria for a given stress state and laminate type. Puck's failure criterion, as one of the winners of the WWFE, has been implemented in the FE program Abaqus. Polar plots have been established to aid in selecting the appropriate failure criterion for a specific stress state and particular laminate type. While not all laminate types and stacking sequences could be covered, the most commonly used sequences have been taken into account.

The chosen theories are described in detail below. Besides, several investigations have been carried out to evaluate the effectiveness of Puck failure criteria within simulating the first ply failure of composite laminates [3], [5], [27]–[31]. M. Appaso et al. [32] have investigated the failure stress envelopes under various settings using Puck's failure criterion, which they compared to Tsai–Wu and Tsai–Hill failure criteria as shown in Figs. (2.18, 2.19). Furthermore, they found that the FPF and LPF stress envelopes calculated using Puck's failure criterion accord well with analytical, computational and experimental data reported in the literature. However, as there is a significant difference between FPF and LPF stress envelopes under all situations, it is necessary to analyse the failure of composite laminated up to the last ply in order to fully use the laminate's strength. However, these failure criteria can be divided into two main categories:

- Global criteria
- Failure criteria related to the failure mode.

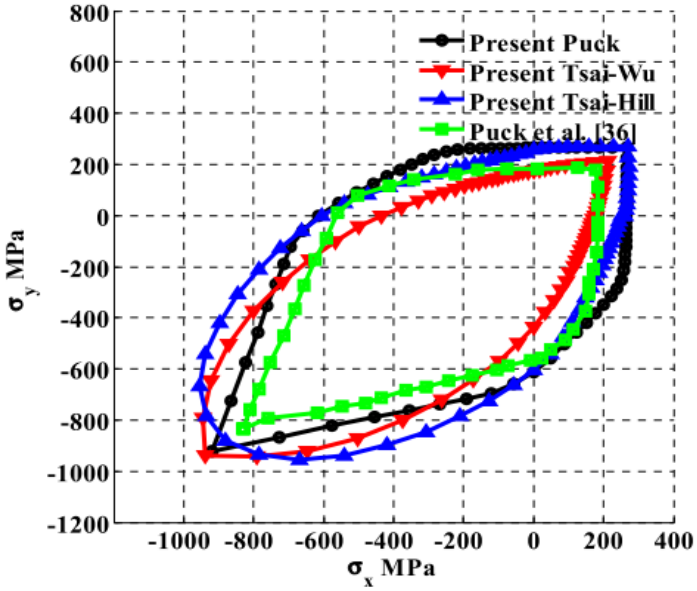


Figure 2.18: Biaxial first-ply failure (FPF) stress envelope for AS4/3501 laminates under biaxial loading [17, 18].

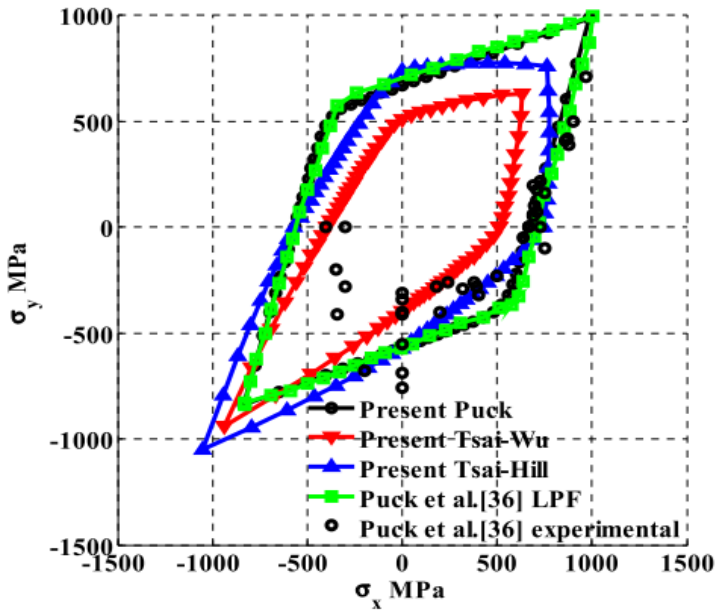


Figure 2.19: Biaxial last-ply failure (LPF) stress envelope for AS4/3501 laminates under biaxial loading [17, 18].

A failure criterion is a mathematical representation of a "failure surface" that defines the load-carrying capacity limit of a lamina. In simple terms, failure happens when a vector (stress exertion f_E) formed by the plane stress components σ_{11}, σ_{22} and σ_{12} intersects the failure surface. The margin of safety (MS) or safety margin is a crucial parameter in FRP analysis which is determined by the stretch factor (f_S) as shown in Eq. (2.1).

$$MS = f_S - 1 \tag{2.1}$$

The margin of safety in any application must always exceed zero to ensure a reliable design. The specific safety margin required depends on the level of risk associated with failure and its potential consequences. The stretch factor (f_S) is defined as the reciprocal value of the stress exertion f_E. It is important to note that this relationship holds true when residual stresses can be disregarded.

2.4.1. Global theories

Global criteria offer the advantage of simplicity in their application. Typically, these criteria are formulated as second-order elliptical equations, utilizing the strength properties of the lamina to establish the boundary conditions for the failure envelope. However, a major drawback of global criteria is the limited insight they provide into the specific failure mode of the lamina. A single scalar failure index fails to indicate the nature of the failure, whether it is the less severe inter-fiber fracture (IFF) or the more severe fiber failure. While this approach has faced criticism from researchers, the widespread adoption of global criteria persists due to their ease of use.

2.4.1.1. Azzi-Tsai-Hill Criterion

The Azzi-Tsai-Hill theory closely resembles the criterion put forth by Tsai and Hill [33]. The main distinction lies in the coupling term between σ_{11} and σ_{22}, where the absolute value is employed, as demonstrated in Eq. (2.3). Hill's theory, on the other hand, represents an orthotropic adaptation of the Von Mises yield criterion.

A failure is deemed to have transpired when the specified equation is fulfilled.

$$f(\sigma_{ij}) = F(\sigma_{22} - \sigma_{33})^2 + G(\sigma_{33} - \sigma_{11})^2 + H(\sigma_{11} - \sigma_{22})^2 + 2L\sigma_{23}^2 + 2M\sigma_{13}^2 + 2N\sigma_{12}^2 = 1 \tag{2.2}$$

The material strength parameters, denoted as F, G, H, L, M, and N, can be derived by conducting a series of controlled experiments. In these experiments, the material is subjected to individual stress directions while maintaining all other stresses at zero.

As an example, let's consider pure shear in the 1-2 plane, where only σ_{12} is non-zero while all other stresses are set to zero. In this case, the yield condition can be expressed as $2N = \frac{1}{S^2}$, where S represents the shear strength. By performing similar experiments for different stress components, we can determine the remaining strength parameters in a similar manner.

Once all the strength parameters have been determined, the failure criterion for a plane stress condition can be expressed as follows:

$$\left(\frac{\sigma_{11}}{R_{||}^{c,t}}\right)^2 - \frac{|\sigma_{11}\sigma_{22}|}{\left(R_{||}^{c,t}\right)^2} + \left(\frac{\sigma_{22}}{R_{\perp}^{c,t}}\right)^2 + \left(\frac{\sigma_{12}}{R_{||\perp}}\right)^2 \leq 1 \tag{2.3}$$

The strength of the material in the fiber direction and perpendicular to the fiber direction is denoted by $R_{||}$ and $R_{\perp}$ respectively. The superscripts c and t indicate compression and tension respectively. Geometrically, this criterion takes the form of an ellipsoid in the (σ_{11}, σ_{22}) plane, as illustrated in Fig. 2.20.

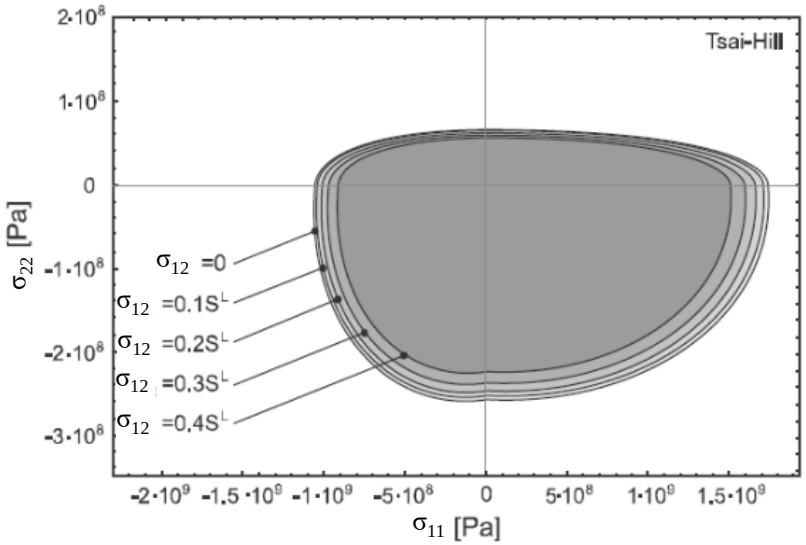


Figure 2.20: Tsai-Hill criterion failure envelopes for various σ_{12} [34].

2.4.1.2. Tsai-Wu Criterion

The Tsai-Wu criterion, based on the Hill theory for orthotropic materials, is widely used as a failure criterion for laminates [35]. It has shown good agreement with experimental data, leading to its implementation in various analysis programs.

However, quadratic failure criteria, like the Tsai-Wu criterion, have a limitation in that they do not account for the difference in tensile and compressive strength when determining the strength parameters. To address this drawback, the tensor polynomial criterion has been developed. This criterion involves a scalar polynomial of strength and stress tensors, making it invariant and allowing for the application of tensor transformation laws when there is a coordinate axis transformation [36].

The expression for the failure surface within the tensor polynomial criterion can be represented as follows:

$$f(\sigma_i) = F_i\sigma_i + F_{ij}\sigma_i\sigma_j = 1 \tag{2.4}$$

The failure surface within the tensor polynomial criterion is determined by the constants F_i and F_{ij}, which represent the components of two tensors of rank 2 and rank 4, respectively. The linear terms, F_i, account for potential variations in the material's behavior under tension and compression. On the other hand, the quadratic terms, F_{ij} define an ellipsoid in the stress space, capturing the interactions between the individual stress components, σ_i and σ_j.

The formulation developed by Tsai-Wu holds significant interest due to the following reasons:

- The invariance of the Eq. (2.4) in any change of basis
- The strength parameters are transformed in a change of axis in the same way as the elasticity constants.
- The relationships between the strength parameters depend on the symmetry of the material.

- The linear terms reflect the difference between tensile and compressive failure.

The theory assumes the presence of a closed failure surface, which simplifies to the following form in a two-dimensional stress state:

$$\left(\frac{1}{R_{||}^{t}}-\frac{1}{R_{||}^{c}}\right)\sigma_{11}+\left(\frac{1}{R_{\perp}^{t}}-\frac{1}{R_{\perp}^{c}}\right)\sigma_{22}+\left(\frac{1}{R_{||}^{t}R_{||}^{c}}\right)\sigma_{11}^{2}+\left(\frac{1}{R_{\perp}^{t}R_{\perp}^{c}}\right)\sigma_{22}^{2} - 2\sqrt{\frac{1}{R_{\perp}^{t}R_{\perp}^{c}R_{||}^{t}R_{||}^{c}}}\,\sigma_{22}\sigma_{11}+\frac{\sigma_{12}^{2}}{R_{||\perp}^{2}}\leq 1 \tag{2.5}$$

The expression $\sqrt{\frac{1}{R_{\perp}^{t}R_{\perp}^{c}R_{||}^{t}R_{||}^{c}}}$ is often given as F_{12} where is an interaction coefficient considered as an empirical coefficient, adjusted according to the experimental results. There are several forms of this criterion depending on the approximation used to evaluate the interaction factor. More than twenty-seven values have been used for this factor. The accuracy required for the measurement of this factor depends both on its value, the quadrant where the point $(\sigma_{11},\sigma_{22})$ is located and the stress ratio. Wu proposed an iterative method for calculating the optimal stress ratio and the required experimental conditions depending on the type of biaxial loading. The geometric representation of the fracture surface is an ellipse in the $(\sigma_{11},\sigma_{22})$ plane for σ_{12} fixed. The inclination of the ellipse as well as the length of its half axes depend on the interaction coefficient F_{12}. The best correlation with the experimental results case was obtained for $F_{12}=0$ (see Fig. 2.21).

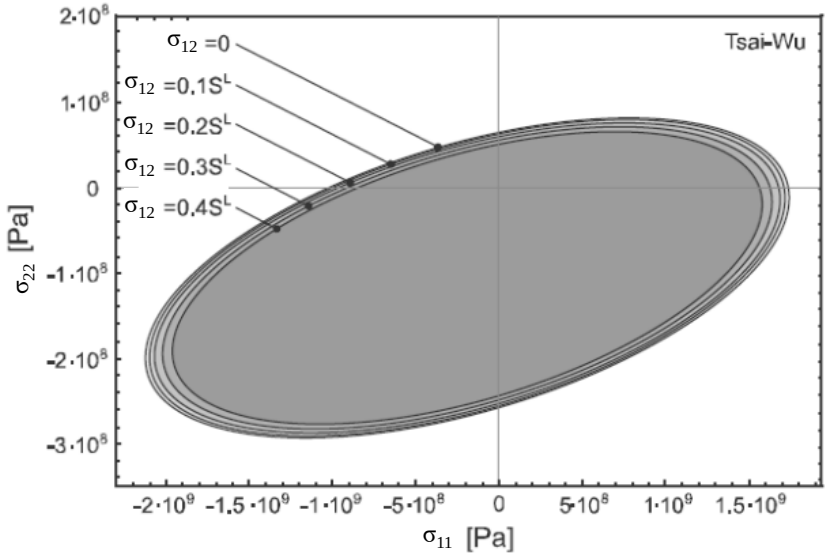


Figure 2.21: The Tsai-WU criterion failure envelopes for various σ_{12} [34] .

In this case, the failure envelope has a fixed centre and orientation. So far, the approximations used to calculate this factor are suitable for particular situations and no systematic method to formally evaluate it has been proposed. It can be determined, for example, either by[13]:

- A biaxial test, e.g. a biaxial tension ($\sigma_1=\sigma_2=\sigma$) and the other stresses are zero. The value of F_{12} will be calculated by measuring σ during the test.
- A 45° tension or compression test ($\sigma_1=\sigma_2=\sigma_6=\frac{1}{2}\sigma_{45}$) and the other stresses are zero. The value of F_{12} corresponds to the value of σ_{45} in a 45° failure test.

2.4.1.3. Comparison between the two criteria

The use of these criteria requires biaxial tests which are difficult to implement and their results vary depending on the type of specimen and the type of loading. The implementation of these criteria varies greatly from one author to another.

The polynomial criterion is derived from the Hill criterion which is specific to metallic materials. Metallic materials are homogeneous and isotropic, while the composite materials are considered anisotropic and heterogeneous and have different failure modes.

The above-mentioned failure criteria cannot adequately describe the complexity of failure behaviour of composite materials. However, they can be used in practice, when their accuracy is satisfactory and no other method is available.

Some criticisms have been made by Puck [37], Hashin [38] and recently by Hart Smith [23] addressing the problems cited in Echaabi et al [39] in particular:

- ➔ Uncertainty of the parameters required for a biaxial test;
- ➔ Fracture stresses that refer to different failure modes are used to obtain a regular set, but the failure criterion is physically unacceptable. This problem is particularly important in the unidirectional case and even less so in the (0/90) case.
- ➔ These methods are global (any loading in one region has no influence on the other regions. This phenomenon is physically unacceptable).
- ➔ Only one geometric form can be obtained for a single set of force parameters (there is not enough flexibility to describe the wide variety of fracture behaviour observed in composites).
- ➔ Only failure envelopes that are regular and continuous are possible, although experience has shown, in several cases, that the rupture envelope is presented by a set of lines;
- ➔ The mode of rupture is not predicted and its effect is not incorporated into the criterion equation.

2.4.2. Failure criterion related to the specific failure mode

Considering the non-homogeneous nature of materials, various failure modes can be observed in a lamina when subjected to loading. This category of failure criteria takes into account this unique phenomenon.

2.4.2.1. Hashin's failure criteria

Significant contributions to the development of intralaminar failure initiation criteria, utilizing the mechanics of materials approach, have been made by researchers such as Hashin [38], Hashin and Rotem [40], Dávila et al. [41], Puck and Schürmann [9], and Pinho et al. [42]. In this context, we will review the failure initiation criteria proposed by Hashin, Puck and Schürmann.

Each criterion is defined in terms of a dimensionless failure index, denoted as FI_M for the matrix and FI_F for the fiber. The failure indices range from 0 to 1, where values between 0 and 1 indicate no failure, and a value of 1 corresponds to failure initiation.

Hashin [38] assumed brittle matrix failure occurring in a plane parallel to the fibers due to the stress components acting on that plane. The fracture plane is represented by Cartesian coordinate directions (x_1, x_n, x_t), obtained through the following transformation:

$$\begin{pmatrix} x_1 \\ x_n \\ x_t \end{pmatrix} = \begin{pmatrix} 1 & 0 & 0 \\ 0 & cos\ \alpha & \sin\alpha \\ 0 & -\sin\alpha & \cos\alpha \end{pmatrix} \begin{pmatrix} x_1 \\ x_2 \\ x_3 \end{pmatrix} \tag{2.6}$$

The stresses in the (x_1, x_n, x_t) coordinate system are represented by σ_{11} , σ_{nn}, σ_{tt} , σ_{nt}, σ_{t1}, and σ_{1n}. These stresses are related to the stresses in the principal material directions σ_{ij} where *i* and *j* can take values of 1, 2, or 3, through the stress transformation equations:

$$\begin{pmatrix} \sigma_{11} \\ \sigma_{nn} \\ \sigma_{tt} \\ \sigma_{nt} \\ \sigma_{1t} \\ \sigma_{1n} \end{pmatrix} = \begin{pmatrix} 1 & 0 & 0 & 0 & 0 & 0 \\ 0 & cos^2\alpha & sin^2\alpha & 2\cos\alpha\sin\alpha & 0 & 0 \\ 0 & sin^2\alpha & cos^2\alpha & -\cos\alpha\sin\alpha & 0 & 0 \\ 0 & -\cos\alpha\sin\alpha & \cos\alpha\sin\alpha & cos^2\alpha - sin^2\alpha & 0 & 0 \\ 0 & 0 & 0 & 0 & \cos\alpha & -\sin\alpha \\ 0 & 0 & 0 & 0 & \sin\alpha & \cos\alpha \end{pmatrix} \begin{pmatrix} \sigma_{11} \\ \sigma_{22} \\ \sigma_{33} \\ \sigma_{23} \\ \sigma_{13} \\ \sigma_{12} \end{pmatrix} \tag{2.7}$$

The fracture plane is defined as the $x_1 - x_t$ plane, with the x_n direction perpendicular to the plane. The stress components acting on the fracture plane obtained from Eq. (2.7) can be expressed as follows:

$$\sigma_{1n} = \sigma_{12}\cos\alpha + \sigma_{13}\sin\alpha \tag{2.8a}$$

$$\sigma_{nn} = \frac{(\sigma_{22}+\sigma_{33})}{2} + \frac{(\sigma_{22}-\sigma_{33})}{2}\cos 2\alpha + \sigma_{23}\sin 2\alpha \tag{2.8b}$$

$$\sigma_{nt} = \frac{-(\sigma_{22}-\sigma_{33})}{2}\sin 2\alpha + \sigma_{23}\cos 2\alpha \tag{2.8c}$$

The stress components exerted on the fracture plane are displayed in the Fig. 2.22.

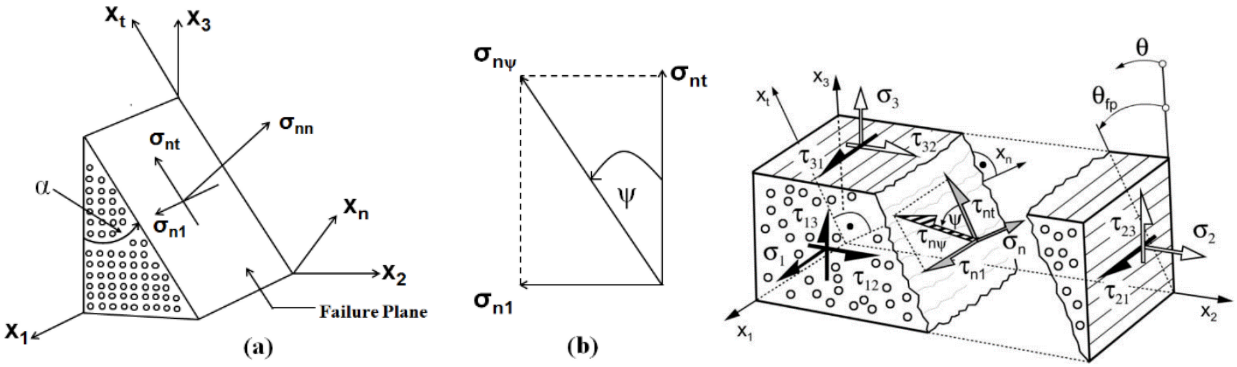


Figure 2.22: (a) Stresses acting on the failure plane, (b) resultant shear stress on the failure plane.

It should be noted that the stress component σ_{11} does not feature in the criterion derived from the stress components on the fracture plane as indicated in Eq. (2.8). Hashin introduced a quadratic formulation considering three of the five stress invariants associated with the rotation of the $x_2 - x_3$ plane around the x_1 axis. Terms involving the first stress invariant $I_1 = \sigma_{11}$ are excluded from the criterion, and the fifth invariant, being cubic in stresses, is not incorporated into the quadratic

criterion consisting of integer powers of the invariants. The failure criterion is expressed as follows:

$$A_2 I_2 + B_2^2 I_2 + A_3 I_3 + A_4 I_4 = 1 \tag{2.9}$$

where coefficients A_2, B_2, A_3, and A_4 in the equation need to be determined using experimental data, while the three stress invariants are given by:

$$I_2 = \sigma_{22} + \sigma_{33}; \qquad I_3 = \sigma_{23}^2 - \sigma_{22}\sigma_{33}; \qquad I_4 = \sigma_{12}^2 + \sigma_{13}^2 \tag{2.10}$$

By conducting a pure transverse shear test, where the failure occurs at $\sigma_{nt} = S_T$, and a pure axial shear test, where the failure occurs at $\sigma_{n1} = S_L$, we can determine the values of A_3 and A_4 in the quadratic form as $A_3 = \frac{1}{S_T{}^2}$ and $A_4 = \frac{1}{S_L{}^2}$, respectively. However, there are still two coefficients in the quadratic form that remain unknown. These coefficients vary depending on whether the matrix failure occurs in tension ($\sigma_{nn} \geq 0$) or compression ($\sigma_{nn} < 0$).

Hashin highlighted the challenge of experimentally measuring the shear strength S_T in the fracture plane parallel to the fibers, as there may not be a specific test available for this purpose. However, an alternative approach is to conduct an in-plane shear test, where all stresses in the (x_1, x_2, x_3) coordinate system except σ_{12} are set to zero. In this test, the maximum value of σ_{12} corresponds to the longitudinal shear strength S_L.

Matrix Compression Mode

In the transverse compression test, the stress component σ_{22} reaches a value of $-Y_C$ at failure, while all other stress components in the (x_1, x_2, x_3) system become negligible. To determine the two unknown coefficients in the quadratic criterion, additional information is needed. Hashin suggests that if the material fails under a transversely isotropic pressure, denoted as $\sigma_{22} = -\rho_h$, the hydrostatic pressure at failure (ρ_h) is significantly larger than the compressive strength in transverse compression (Y_C), i.e., $\rho_h \gg Y_C$. Based on this assumption, the quadratic criterion for matrix failure in compression can be formulated in terms of Y_C and the ratio Y_C/ρ_h. The quadratic criterion is then expanded in a series, with only the lowest-order terms retained. The resulting expression for the matrix failure in compression is:

$$\begin{aligned} FI_M = \frac{1}{Y_C}\left[\frac{Y_C}{2S_T} - 1\right](\sigma_{22} + \sigma_{33}) + \frac{1}{4S_T^2}(\sigma_{22} + \sigma_{33})^2 + \frac{1}{4S_T^2}(\sigma_{23}^2 - \sigma_{22}\sigma_{33}) \\ + \frac{1}{4S_T^2}(\sigma_{12}^2 + \sigma_{13}^2), \qquad \sigma_{nn} < 0 \end{aligned} \tag{2.11}$$

Hashin showed that $\sigma_{nn} < 0$ if the invariant $I_2 = \sigma_{22} + \sigma_{33} < 0$.

Matrix Failure in Tension

To obtain the two unknown coefficients in the quadratic form for matrix failure in tension, the results of two tests are necessary. The first test is the transverse tension test, where σ_{22} reaches the value of Y_T. In this test, it is assumed that the coefficient A_2, which is associated with the invariant I_2 in Eq. (2.9), is equal to zero. This assumption ensures a convex failure locus. As a result, Hashin's criterion for matrix failure in tension is expressed as follows

$$FI_M = \left(\frac{\sigma_{22}+\sigma_{33}}{Y_T}\right)^2 + \frac{\sigma_{23}^2-\sigma_{22}\sigma_{33}}{S_T^2} + \frac{\sigma_{12}^2+\sigma_{13}^2}{S_T^2} = 1, \ \ \sigma_{nn} \geq 0 \qquad (2.12)$$

Furthermore, it is important to note that $\sigma_{nn} \geq 0$ if the invariant $I_2 = \sigma_{22} + \sigma_{33} > 0$. It is worth mentioning that in the stress plane defined by σ_{22} and σ_{33}, for the failure locus $\llbracket FI_M = 1$ to have a convex shape resembling an ellipse, the condition $Y_T < 2S_T$ must be satisfied

Hashin's compression fiber failure mode

Considering that the understanding of the influence of shear on compressive fiber mode was limited at the time when the reference [38] was written, Hashin's criterion is formulated as a non-interacting maximum allowable compressive stress criterion. Consequently, the failure index can be expressed as follows:

$$FI_F = \frac{-\sigma_{11}}{X_C}, \qquad \sigma_{11} < 0 \qquad (2.13)$$

Hashin's tension fiber failure mode

In uniaxial tension tests, the plane of failure is defined as the $x_1 - x_3$ plane. Hashin proposed a quadratic stress criterion based on the stress invariants $I_1 = \sigma_{11}$ and I_4 as shown in Eq. (2.12). To ensure a convex failure locus in the stress space of σ_{11}, σ_{12} and σ_{13}, the linear term in the invariant I_1 is excluded from the failure criterion. The failure index for tensile fiber mode can be expressed as:

$$FI_F = \left(\frac{\sigma_{11}}{X_T}\right)^2 + \left(\frac{\sigma_{12}^2+\sigma_{13}^2}{S_L^2}\right), \qquad \sigma_{11} > 0 \qquad (2.14)$$

Hashin also gave the following approximation:

$$FI_F = \left(\frac{\sigma_{11}}{X_T}\right), \qquad \sigma_{11} > 0 \qquad (2.15)$$

In which the influence of longitudinal shear stresses σ_{12} and σ_{13} on fracture are neglected.

2.4.2.2. Discussion of hashin's criteria

Hashin introduced the concept of a fracture plane parallel to fibers to model matrix failure modes. However, due to the computational complexity involved in locating this plane in a three-dimensional stress state, it was abandoned. Instead, Hashin focused on developing fracture criteria based on a quadratic approximation of stress invariants. The intersection of the tensile and compression matrix failure modes occurs when the invariant I_2, which is the sum of the principal stresses $(\sigma_{22} + \sigma_{33})$, equals zero.

For $I_2 = 0$, the fracture plane is positioned at $\alpha = \mp 45°$, where the normal stress σ_{nn} is zero and the shear stress σ_{nt} is maximized and equal to $(\sigma_{22} - \sigma_{33})/2$. Hashin recognized that this observation, where fracture occurs on the plane with maximum transverse shear stress σ_{nt}, may not universally hold but is a consequence of the quadratic approximation.

The shear strength S_T, which is transverse to the fibers in the fracture plane and appears in the matrix mode criteria, cannot be directly obtained from standard tests. In the absence of a direct

measurement method for S_T, researchers using Hashin's criteria have either considered S_T equal to the longitudinal shear strength S_L or used the apparent interlaminar shear strength as an approximation. This approach is discussed in the review of composite failure criteria by Paris [43]. Additionally, Paris noted that for a plane stress state, the matrix compression criterion (Eq. 2.11) specifies the out-of-plane allowable strength S_T without considering the corresponding shear stress σ_{23}.

2.4.2.3. Puck and shurmann's failure criteria

Puck and Schürmann [9] introduced phenomenological models to analyse the failure behaviour of unidirectional FRP composites. Their failure criterion is dependent on the specific failure mode within a unidirectional ply and is expressed in terms of stresses on the principal planes of the material. Similar to Hashin's approach [38], they assume brittle matrix failure occurring on a plane parallel to the fibers. However, unlike Hashin's assumption of instantaneous matrix failure at a point, Puck and Schürmann distinguish between failure initiation and completion. They consider the degradation of matrix elastic moduli after failure initiation due to crack-induced weakening of the matrix.

To model this phenomenon, they employ the CDM (Continuum Damage Mechanics) approach, which spreads cracks over an infinitesimal volume with degraded material properties. Following Hashin's postulation of a brittle failure plane parallel to the x_1 −axis, Puck and Schürmann [9] develop an inter-fiber failure (IFF) criterion similar to the modified Coulomb-Mohr (C-M) criterion. In their criterion, the limiting shear stress on the failure plane increases with increasing magnitude of the normal compressive stress σ_{nn}.

Puck and Schürmann introduced criteria that consider different stress expressions for initiating failure under tensile and compressive normal stresses on the failure plane. Their criterion, known as the Inter-Fiber Failure (IFF) criterion, takes into account cracks that extend throughout the thickness of the unidirectional lamina. These cracks can originate from cohesive failure within the matrix or adhesive failure at the fiber-matrix interface. The normal to the matrix failure plane is assumed to be inclined at an angle α in a counter-clockwise direction with respect to the x_1 −axis, as illustrated in Fig. 2.22a. The stress components acting on the failure plane are determined using Equation (2.8). Puck and Schürmann propose that brittle failure on a plane parallel to the fibers is influenced by the presence of a tensile normal stress $\sigma_{nn} \geq 0$ and hindered by a compressive normal stress $\sigma_{nn} < 0$. As a result, they establish separate criteria for tension failure and compression failure to account for this behaviour.

Tensile Failure Criterion, $\sigma_{nn} \geq 0$

First, we will discuss the Puck and Schürmann criterion for matrix failure, specifically for $\sigma_{nn} \geq 0$, which is classified as Mode A failure. This criterion is applied in the uni-axial transverse tension test conducted along the $x_2 -$ direction, as well as in the in-plane $(x_1 - x_2)$ simple shear test. In both tests, the failure plane is oriented perpendicular to the $x_2 -$ direction, with α=0. From Eqs. (2.8) $\sigma_{n1} = \sigma_{12}$, $\sigma_{nn} = \sigma_{22}$, and $\sigma_{nt} = \sigma_{23}$.

During the uniaxial transverse tension test, the stress component σ_{22} equals the tensile strength Y_T at the point of failure initiation. At this stage, all other stresses in the x_1, x_2 and x_3 coordinate system are negligible. Similarly, in the $(x_1 - x_2)$ plane shear test, the stress component σ_{12} is equal to the longitudinal shear strength S_L at failure initiation, with all other stresses in the x_1, x_2 and x_3 system being negligible. The Puck and Schürmann criterion for failure initiation is

expressed as a quadratic function of the stress components acting on the failure plane and can be written as:

$$(1 - C_1)\left(\frac{\sigma_{nn}}{Y_T}\right)^2 + C_1\left(\frac{\sigma_{nn}}{Y_T}\right) + \left(\frac{\sigma_{nt}}{S_T}\right)^2 + \left(\frac{\sigma_{n1}}{S_L}\right)^2 = 1, \qquad \sigma_{nn} > 0 \tag{2.16}$$

The parameter S_T in Eq. (2.16) represents the shear strength transverse to the fibers in the failure plane $(x_1 - x_2)$. However, determining S_T is not straightforward as there is no direct test available for it. When the constant C_1 is less than 1, Eq. (2.16) defines an ellipsoidal surface in the stress space, with the axes representing σ_{nn}, σ_{nt} and σ_{n1}. The failure plane exhibits a resultant shear stress represented by $\sigma_{n\psi}$, where $\sigma_{n\psi} = \sqrt{{\sigma_{nt}}^2 + {\sigma_{n1}}^2}$. Additionally, the angle ψ, depicted in Fig. 2.22b, indicates the direction of $\sigma_{n\psi}$ on the failure plane. Substituting $\sigma_{nt} = \sigma_{n\psi}\cos\psi$ and $\sigma_{n1} = \sigma_{n\psi}\sin\psi$ in Eq. (2.16) yields:

$$(1 - C_1)\left(\frac{\sigma_{nn}}{Y_T}\right)^2 + C_1\left(\frac{\sigma_{nn}}{Y_T}\right) + \left(\frac{\sigma_{n\psi}}{S_\psi}\right)^2 = 1, \qquad \sigma_{nn} > 0 \tag{2.17}$$

where the shear strength S_ψ is defined by

$$\frac{1}{{S_\psi}^2} = \left(\frac{\cos^2\psi}{{S_T}^2} + \frac{\sin^2\psi}{{S_L}^2}\right) \tag{2.18}$$

The constant C_1 corresponds to the negative slope of $\sigma_{n\psi}$ with respect to σ_{nn} along the contour $\psi = constant$ on the ellipsoidal surface, specifically evaluated at $\sigma_{nn} = 0$. We represent the negative of this slope as $p_{n\psi}^{(+)}$.

$$p_{n\psi}^{(+)} = -\left.\frac{d\sigma_{n\psi}}{d\sigma_{nn}}\right|_{\sigma_{nn}=0} = 0; \qquad \psi = \text{Constant} \tag{2.19}$$

For a fixed value of ψ, differentiating Eq. (2.17) with respect to σ_{nn} followed by setting $\sigma_{nn} = 0$, and noting that at failure initiation, $\sigma_{n\psi} = S_\psi$, we get

$$C_1 = \frac{2Y_T}{S_\psi}p_{n\psi}^{(+)}, \qquad \psi = \text{Constant} \tag{2.20}$$

Substitute the value of C_1 from Eq. (2.20) into Eq. (2.17), we obtain

$$\left(1 - \frac{2Y_T}{S_\psi}p_{n\psi}^{(+)}\right)\left(\frac{\sigma_{nn}}{Y_T}\right)^2 + \frac{2Y_T}{S_\psi}p_{n\psi}^{(+)}\left(\frac{\sigma_{nn}}{Y_T}\right) + \left(\frac{\sigma_{n\psi}}{S_\psi}\right)^2 = 1, \qquad \sigma_{nn} > 0 \tag{2.21}$$

To get the final form of the tension failure criterion listed as Eq. (2.21) in Puck and Schürmann, we add the term $\left[p_{n\psi}^{(+)}\frac{Y_T}{S_\psi}\left(\frac{\sigma_{nn}}{Y_T}\right)\right]^2$ to both sides of Eq. (2.21), and rearrange the result to get

$$\left[1 - p_{n\psi}^{(+)}\frac{Y_T}{S_\psi}\right]^2\left(\frac{\sigma_{nn}}{Y_T}\right)^2 + \left(\frac{\sigma_{n\psi}}{S_\psi}\right)^2 = \left[1 - p_{n\psi}^{(+)}\frac{\sigma_{nn}}{S_\psi}\right]^2 \quad ; \quad \sigma_{nn} > 0 \tag{2.22}$$

Taking the positive square root of each side of Eq. (2.22), and using $\left(\frac{\sigma_{n\psi}}{S_\psi}\right)^2 = \left(\frac{\sigma_{nt}}{S_T}\right)^2 + \left(\frac{\sigma_{n1}}{S_L}\right)^2$ we define the index for the matrix failure initiation in tension as:

$$F\,I_M = \sqrt{\left[1 - \mathrm{p}_{n\psi}^{(+)}\frac{\mathrm{Y}_T}{\mathrm{S}_\psi}\right]^2\left(\frac{\sigma_{nn}}{\mathrm{Y}_T}\right)^2 + \left(\frac{\sigma_{nt}}{\mathrm{S}_T}\right)^2 + \left(\frac{\sigma_{n1}}{\mathrm{S}_L}\right)^2} + \mathrm{p}_{n\psi}^{(+)}\frac{\sigma_{nn}}{\mathrm{S}_\psi}, \qquad \sigma_{nn} > 0 \tag{2.23}$$

Projections of the failure initiation surface, $FI_M = 1$, on the $\sigma_{n1} - \sigma_{nt}$ plane ($\sigma_{nn} = 0$), and on the $\sigma_{n1} - \sigma_{n\psi}$ plane for $\sigma_{nn} > 0$ are shown in (Figs. (2.23a, 2.23b)), respectively.
For $\psi = 0$ and $\psi = \frac{\pi}{2}$ we write Eq. (2.19) as:

$$\mathrm{p}_{nt}^{(+)} = -\left.\frac{d\sigma_{nt}}{d\sigma_{nn}}\right|_{\sigma_{nn}=0}, \quad \psi = 0 \qquad ; \qquad \mathrm{p}_{n1}^{(+)} = -\left.\frac{d\sigma_{n1}}{d\sigma_{nn}}\right|_{\sigma_{nn}=0}, \quad \psi = \frac{\pi}{2} \tag{2.24}$$

The contour line of the failure initiation surface for $\psi = 0$ is defined by setting $\sigma_{n1} = 0$ in Eq. (2.16). For the $\psi = 0$ contour, we set $\sigma_{n1} = 0$ in Eq. (2.16), differentiate the resulting equation with respect to σ_{nn} and set $\sigma_{nn} = 0$ to get:

$$\frac{C_1}{\mathrm{Y}_T} = \frac{2}{\mathrm{S}_L}\mathrm{p}_{nt}^{(+)} \tag{2.25}$$

Following the same procedure for the $\psi = \frac{\pi}{2}$ contour for which $\sigma_{nt} = 0$, we get

$$\frac{C_1}{\mathrm{Y}_T} = \frac{2}{\mathrm{S}_L}\mathrm{p}_{n1}^{(+)} \tag{2.26}$$

After multiplying both sides of Eq. (2.25) by $\cos^2\psi$ and of Eq. (2.26) by $\sin^2\psi$, adding respective sides of the resulting equations, and substituting for C_1 from Eq. (2.20) we get:

$$\frac{\mathrm{p}_{n\psi}^{(+)}}{\mathrm{S}_\psi} = \frac{\mathrm{p}_{nt}^{(+)}}{\mathrm{S}_T}\cos^2\psi + \frac{\mathrm{p}_{n1}^{(+)}}{\mathrm{S}_L}\sin^2\psi \tag{2.27}$$

Equation (2.27) is listed as Eq. (18) in Puck and Schürmann [9]. It follows from Eqs. (2.25) and (2.21) that $\frac{\mathrm{p}_{n1}^{(+)}}{\mathrm{S}_L} = \frac{\mathrm{p}_{nt}^{(+)}}{\mathrm{S}_T}$

It should be noted that the value of FI_M is always limited to 1 or below. When $FI_M < 1$, failure does not initiate. In the case of $\sigma_{nt} = 0$, the failure surface in the $\sigma_{nn} - \sigma_{n1}$ plane is depicted in Fig. 2.24 for $\sigma_{nn} \geq 0$.

The tension failure index FI_M, as defined in Eq. (2.23), is influenced by the angle α of the failure plane. The optimum value of α that maximizes FI_M determines the orientation of the failure plane.

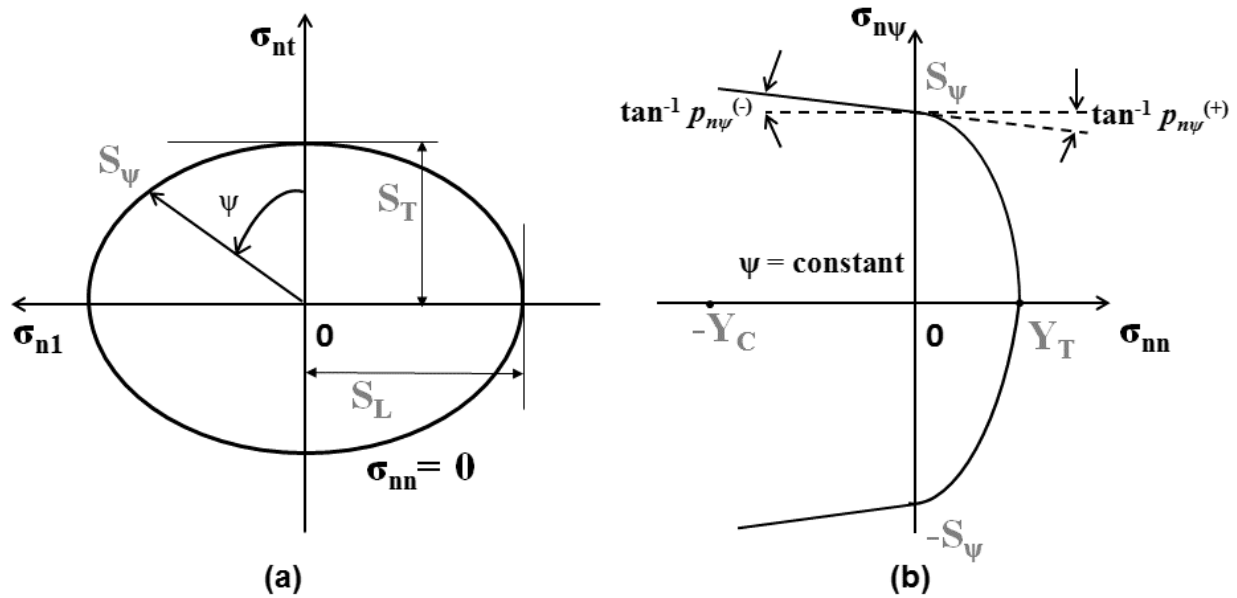


Figure 2.23: Projection of the failure initiation surface on the (a) $\sigma_{n1}-\sigma_{nt}$ plane, $\sigma_{nn}=$ 0, and (b) $\sigma_{nn}-\sigma_{n\psi}$ plane for $\sigma_{nn}\geq$ 0.

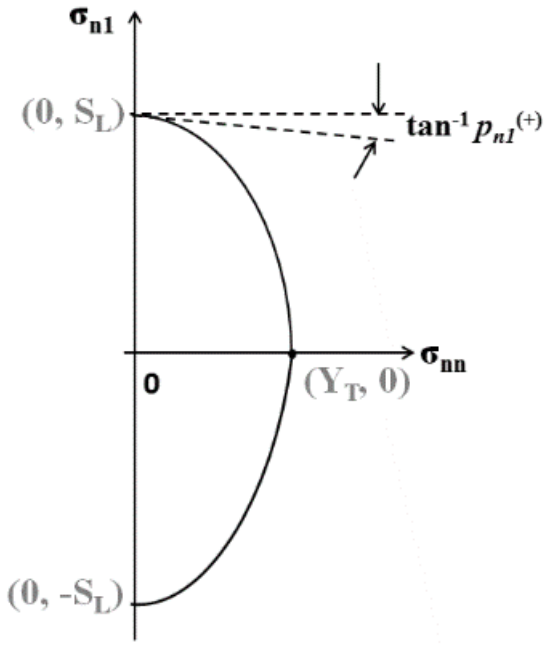


Figure 2.24: Projection of the failure initiation surface on the $\sigma_{nn}-\sigma_{n1}$ stress plane; $\sigma_{nt}=$ 0.

Compression Matrix Failure Initiation Criterion, $\sigma_{nn} < 0$.

Similar to the Coulomb-Mohr (C-M) criterion, the Puck and Schürmann criterion assumes that a compressive normal stress, $\sigma_{nn} < 0$, acts to resist failure caused by shear stresses σ_{nt} and σ_{n1}. In the $\sigma_{nn} - \sigma_{nt}$ and the $\sigma_{nn} - \sigma_{n1}$ planes, the C-M criterion can be expressed as $|\sigma_{nt}| - \mu|\sigma_{nn}| = S_T$ and $|\sigma_{n1}| - \mu|\sigma_{nn}| = S_L$, where μ represents the coefficient of friction. Building upon the C-M criterion, Puck and Schürmann [9] propose that there is no matrix failure under pure normal compressive stress on a plane. Instead, they introduce the following criterion for the initiation of matrix failure when $\sigma_{nn} < 0$, considering non-zero shear stresses:

$$\left(\frac{\sigma_{nt}}{S_T - p_{nt}^{(-)}\sigma_{nn}}\right)^2 + \left(\frac{\sigma_{n1}}{S_L - p_{n1}^{(-)}\sigma_{nn}}\right)^2 = 1, \qquad \sigma_{nn} < 0 \tag{2.28}$$

In the Eq. (2.28), the strengths in the denominators are augmented by the compressive normal stress, while ($p_{nt}^{(-)}$, $p_{n1}^{(-)}$) represent the inclination parameters in compression. When the stress state has $\sigma_{n1} = 0$, Eq. (2.28) simplifies to $\sigma_{nt} = S_T - p_{nt}^{(-)}\sigma_{nn}$. From this expression, the inclination parameter is interpreted as the negative slope of σ_{nt} with respect to σ_{nn}.

$$p_{nt}^{(-)} = -\left(\frac{d\sigma_{nt}}{d\sigma_{nn}}\right), \quad \sigma_{n1} = 0 \tag{2.29}$$

Likewise, in the stress state where $\sigma_{nt} = 0$, Eq. (2.28) can be simplified to $\sigma_{n1} = S_L - p_{n1}^{(-)}\sigma_{nn}$. From this expression, the inclination parameter $p_{n1}^{(-)}$ is interpreted as the negative slope of σ_{n1} with respect to σ_{nn}, where,

$$p_{n1}^{(-)} = -\left(\frac{d\sigma_{n1}}{d\sigma_{nn}}\right), \quad \sigma_{n1} = 0 \tag{2.30}$$

To achieve better agreement with experimental findings, Puck and Schürmann made adjustments to Eq. (2.28) by neglecting the quadratic terms involving σ_{nn}. The modified form is expressed as follows:

$$\frac{{\sigma_{nt}}^2}{{S_T}^2 - 2p_{nt}^{(-)}S_T\sigma_{nn}} + \frac{{\sigma_{n1}}^2}{{S_L}^2 - 2p_{n1}^{(-)}S_L\sigma_{nn}} = 1, \quad \sigma_{nn} < 0 \tag{2.31}$$

To simplify the mathematical formulation, Puck and Schürmann introduced an assumption that relates the inclination parameters as follows:

$$\frac{p_{nt}^{(-)}}{S_T} = \frac{p_{n1}^{(-)}}{S_L} = \frac{p}{R} \tag{2.32}$$

The variables p and R, as defined in Eq. (2.32), lead to a simplified form of Eq. (2.31), expressed as follows:

$$\left(\frac{\sigma_{nt}}{S_T}\right)^2 + \left(\frac{\sigma_{n1}}{S_L}\right)^2 + 2\left(\frac{p}{R}\right)\sigma_{nn} = 1\,, \qquad \sigma_{nn} < 0 \tag{2.33}$$

The failure initiation surface in the stress space (σ_{nn}, σ_{nt}, σ_{n1}), as described by Eq. (2.33), takes the form of an elliptic paraboloid. When this surface intersects with the plane $\sigma_{nn} = \text{Constant}$, it creates an ellipse with the shear stresses as the principal axes. It is important to note that the failure initiation surface does not intersect the negative σ_{nn} axis, as per the assumption that compressive normal stress hinders shear failure. By differentiating Eq. (2.33) with respect to σ_{nn} and utilizing Eq. (2.32), the inclination parameters can be related to the slopes of the failure initiation surface by:

$$\frac{1}{S_T}\frac{d\sigma_{nt}}{d\sigma_{nn}} = -\left(\frac{p_{nt}^{(-)}}{S_T}\right) = -\left(\frac{p}{R}\right) \quad \text{in the } (\sigma_{nt}, \sigma_{nn}) \quad \text{plane at} \quad (\sigma_{nt}, \sigma_{nn}) = (S_T, 0) \tag{2.34}$$

$$\frac{1}{S_L}\frac{d\sigma_{n1}}{d\sigma_{nn}} = -\left(\frac{p_{n1}^{(-)}}{S_L}\right) = -\left(\frac{p}{R}\right) \quad \text{in the } (\sigma_{n1}, \sigma_{nn}) \quad \text{plane at} \quad (\sigma_{n1}, \sigma_{nn}) = (S_T, 0) \tag{2.35}$$

For the elliptic failure envelope in the plane $\sigma_{nn} = \text{Constant}$ let $\sigma_{nt} = \overline{S_\psi}\cos\psi$ and $\sigma_{n1} = \overline{S_\psi}\sin\psi$ where $\overline{S_\psi} = \sqrt{{\sigma_{n1}}^2 + {\sigma_{nt}}^2}$ at failure (see Fig. 2.22b). Then the failure ellipse, from Eq. (2.33), reduces to

$$\overline{S_\psi}^2\left[\left(\frac{\cos\psi}{S_T}\right)^2 + \left(\frac{\sin\psi}{S_L}\right)^2\right] = 1 - 2\left(\frac{p}{R}\right)\sigma_{nn} \tag{2.36}$$

$$\text{where } \frac{1}{{S_\psi}^2} = \left(\frac{\cos\psi}{S_T}\right)^2 + \left(\frac{\sin\psi}{S_L}\right)^2 \tag{2.37}$$

Hence

$$\left(\frac{\overline{S_\psi}}{S_\psi}\right)^2 = 1 - 2\left(\frac{p}{R}\right)\sigma_{nn} \tag{2.38}$$

The derivative of $\overline{S_\psi}$ with respect to the normal stress σ_{nn} at $\sigma_{nn} = 0$ is given by

$$2\frac{\overline{S_\psi}}{{S_\psi}^2}\left(\frac{d\overline{S_\psi}}{d\sigma_{nn}}\right)\Bigg|_{\sigma_{nn}=0} = \frac{2}{S_\psi}\left(\frac{d\overline{S_\psi}}{d\sigma_{nn}}\right)\Bigg|_{\sigma_{nn}=0} = -2\left(\frac{p}{R}\right) \tag{2.39}$$

At the contour of the failure surface corresponding to a constant ψ, we define $p_{n\psi}^{(-)}$ as the negative slope of $\overline{S_\psi}$ with respect to σ_{nn} when σ_{nn} is equal to zero. Thus, Eq. (2.39) can be expressed as follows:

$$\frac{p_{n\psi}^{(-)}}{S_\psi} = \frac{p}{R} \qquad \text{where} \quad p_{n\psi}^{(-)} = -\frac{d\overline{S_\psi}}{d\sigma_{nn}} \tag{2.40}$$

Now multiply Eq. (2.34) by $\cos^2\psi$ and add it to Eq. (2.35) multiplied by $\sin^2\psi$to get

$$\frac{p_{nt}^{(-)}}{S_T}\cos^2\psi + \frac{p_{n1}^{(-)}}{S_L}\sin^2\psi = \frac{p}{R} \tag{2.41}$$

Substitute for $\frac{p}{R}$ from Eq. (2.33) in Eq. (2.34) to get

$$\frac{p_{n\psi}^{(-)}}{S_\psi} = \frac{p_{nt}^{(-)}}{S_T}\cos^2\psi + \frac{p_{n1}^{(-)}}{S_L}\sin^2\psi \tag{2.42}$$

Equation (2.42) is analogous to Eq. (2.27) for $\sigma_{nn} > 0$. Equation (2.33) is manipulated to a final form by the following algebraic steps: Substitute for $\frac{p}{R}$ from Eq. (2.40) in Eq. (2.33), add the term $\left(\frac{p_{n\psi}^{(-)}\sigma_{nn}}{S_\psi}\right)^2$ to each side of Eq. (2.33) and rearrange the terms to get

$$\left(\frac{\sigma_{nt}}{S_T}\right)^2 + \left(\frac{\sigma_{n1}}{S_L}\right)^2 + \left(\frac{p_{n\psi}^{(-)}\sigma_{nn}}{S_\psi}\right)^2 = \left[1 - \frac{p_{n\psi}^{(-)}\sigma_{nn}}{S_\psi}\right]^2 \tag{2.43}$$

Take the positive square root of both sides of Eq. (2.43) to get

$$FI_M = \sqrt{\left(\frac{\sigma_{nt}}{S_T}\right)^2 + \left(\frac{\sigma_{n1}}{S_L}\right)^2 + \left(\frac{p_{n\psi}^{(-)}\sigma_{nn}}{S_\psi}\right)^2} + p_{n\psi}^{(-)}\frac{\sigma_{nn}}{S_\psi}, \qquad \sigma_{nn} < 0 \tag{2.44}$$

The failure initiation surface is defined by $FI_M = 1$. Therefore, in order to determine if a matrix failure has initiated, it is necessary to identify the angle α that maximizes the failure index for a given stress state, and then verify if FI_M equals 1 at this particular value of α. The necessary condition for an extremum is $\frac{\partial FI_M}{\partial \alpha} = 0$, which can be solved numerically to obtain the angle α.

Failure Criteria for Plane State of Stress

In a plane stress state within the $(x_1 - x_2)$ plane, the failure plane is perpendicular to the x_2 −direction, with the angle α being 0. Referring to Eq. (2.8), we have, $\sigma_{n1} = \sigma_{21}$, $\sigma_{nn} = \sigma_{22}$, and $\sigma_{nt} = 0$. Consequently, the angle ψ depicted in (Fig. 2.22b) is equal to π/2. Utilizing Eq. (2.27), we obtain:

$$\frac{p_{n\psi}^{(+)}}{S_\psi} = \frac{p_{n1}^{(+)}}{S_L}$$

Hence, the failure index given by Eq. (2.23) reduces to

$$FI_M = \sqrt{\left[1 - p_{n1}^{(+)}\frac{Y_T}{S_L}\right]^2 \left(\frac{\sigma_{22}}{Y_T}\right)^2 + \left(\frac{\sigma_{21}}{S_L}\right)^2} + p_{n1}^{(+)}\frac{\sigma_{22}}{S_L}, \qquad \sigma_{22} \geq 0 \tag{2.45}$$

The determination of the longitudinal shear strength, S_L, in a unidirectional ply involves conducting in-plane shear tests that lead to failure through transverse matrix cracking parallel to the fibers, similar to the fracture observed in the transverse tension test. On the other hand, the shear strength, S_T, transverse to the fibers in the failure plane, referred to as the fracture resistance in the action plane by Puck and Schürmann, cannot be directly determined through simple tests. Instead, S_T, is derived from the uniaxial transverse compression test, where $\sigma_{22} = -Y_C$ at failure, and all other stresses in the xi-coordinate system are zero.

To establish the relationship between S_T and Y_C, we consider a plane stress state characterized by $\sigma_{n1} = \sigma_{21}\cos\alpha$, $\sigma_{nn} = \sigma_{22}\cos^2\alpha$, and $\sigma_{nt} = -\sigma_{22}\cos\alpha\, sin\alpha$. Substituting these stresses into the left-hand side of Eq. (2.33) and expressing the result as (when $FI_M(\alpha) = 1$) :

$$FI_M(\alpha) = \left(\frac{\sigma_{22}}{S_T}\right)^2 \sin^2\alpha\cos^2\alpha + \left(\frac{\sigma_{21}}{S_L}\right)^2 \cos^2\alpha + 2\frac{p}{R}\sigma_{22}\cos^2\alpha = 1, \qquad \sigma_{22} < 0 \tag{2.46}$$

The action plane orientated at the angle α_{fp} and parallel to σ_{11}, which is the angle where the highest risk of fracture occurs. This angle is determined by computing $FI_M(\alpha)$ for all planes with angles ranging from $\alpha = -90°$ to $\alpha = 90°$ with one step and the plane with the greatest stress exposure is the location where the fracture is to be expected. However, $[FI_M(\alpha)]_{MAX} = FI_M(\alpha_{fp})$ where α_{fp} represent the angle of the fracture plane.

On the other hands, using trigonometric identities, Eq. (2.46) is rewritten in terms of $\cos^2\alpha$, and then the necessary condition for a maximum can be written as:

$$\frac{dFI_M}{d\alpha} = \frac{dFI_M}{d\,(\cos^2\alpha)}(-\,2\cos\alpha\sin\alpha) = 0 \tag{2.47}$$

One solution of Eq. (2.47) is α = 0, which is the mode B (See Fig. 2.25) failure where the failure plane is normal to the x_2 −direction. The other solution of Eq. (2.47) gives:

$$\cos^2\alpha = \frac{1}{2}\left[1 + \left(\frac{S_T}{S_L}\right)^2\left(\frac{\sigma_{21}}{\sigma_{22}}\right)^2\right] + \frac{{S_T}^2}{\sigma_{22}}\frac{p}{R} \tag{2.48}$$

where the assumption in Eq. (2.32) has been used. Substitute Eq. (2.48) for $\cos\alpha^2$ in Eq. (2.46) to get

$$\begin{aligned} FI_M = \left(p_{nt}^{(-)}\right)^2 + \frac{1}{2}\left(\frac{\sigma_{21}}{S_L}\right)^2 + \frac{1}{4}\left(\frac{S_T}{\sigma_{22}}\right)^2\left(\frac{\sigma_{21}}{S_L}\right)^4 + p_{nt}^{(-)}\left(\frac{S_T}{\sigma_{22}}\right)\left(\frac{\sigma_{21}}{S_L}\right)^2 + p_{nt}^{(-)}\left(\frac{\sigma_{22}}{S_T}\right) \\ + \frac{1}{4}\left(\frac{\sigma_{22}}{S_T}\right)^2; \quad \sigma_{22} < 0 \qquad Mode\ C \end{aligned} \tag{2.49}$$

Equation (2.49) can be rewritten as

$$FI_M = \frac{1}{2(1 + p_{nt}^{(-)})}\left[\left(\frac{\sigma_{21}}{S_L}\right)^2 + \left(\frac{\sigma_{22}}{S_T}\right)^2\right]\left(-\frac{S_T}{\sigma_{22}}\right); \qquad \sigma_{22} < 0\,, \quad Mode\ C \tag{2.50}$$

The derived expression, given by Puck and Schürmann as their Eq. (26), takes the form of Eq. (2.50) when the degradation term associated with the longitudinal normal stress σ_{11} is disregarded.

By setting $FI_M = 1$, $\sigma_{21} = 0$, and $\sigma_{22} = -Y_C$ in Eq. (2.50), we can evaluate the transverse shear strength S_T, yielding the following result:

$$S_T = \frac{Y_C}{2(1 + p_{nt}^{(-)})} \tag{2.51}$$

Equation (2.51) is shown in Table 2.4 of Puck and Schürmann. If we set $FI_M = 1$ in Eq. (2.49) or Eq. (2.50), then Eq. (2.48) can be reduced to

$$\cos^2\alpha = -\frac{S_T}{\sigma_{22}} \tag{2.52}$$

Since $\cos^2\alpha \leq 1$, therefore for Mode C failure $\sigma_{22} \leq -S_T$. Equation (2.52) is Eq. (25) of Puck and Schürmann if we set their weakening factor $f_w = 1$.

For mode B failure in plane stress, set $\alpha = 0$ and $FI_M = 1$ in Eq. (2.46) to get

$$1 = \left(\frac{\sigma_{21}}{S_L}\right)^2 + 2p_{nt}^{(-)}\frac{\sigma_{22}}{S_T}, \qquad \sigma_{22} < 0 \qquad Mode\ B \tag{2.53}$$

The substitution of $\frac{P}{R}$ from Eq. (2.32) has been utilized to determine the transition values of stresses σ_{22} and σ_{21} between modes B and C. By solving Eq. (2.53) for σ_{21} and replacing this outcome in Eq. (2.49) with $FI_M = 1$, the following outcomes have been obtained:

$$\sigma_{22} = -S_T, \quad \sigma_{21} = S_L\sqrt{1 + 2p_{nt}^{(-)}} \tag{2.54}$$

Table 2.4. The suggested values for Puck's inclination parameters.

Parameter	Value	
	GFRP/epoxy	CFRP/epoxy
$P_{\perp\parallel}^{(+)}$	0.30	0.35
$P_{\perp\parallel}^{(-)}$	0.25	0.30
$P_{\perp\perp}^{(-)}$	0.20–0.25	0.25–0.30

In Fig. 2.25, a schematic of the three matrix failure modes, known as A, B and C, is shown.

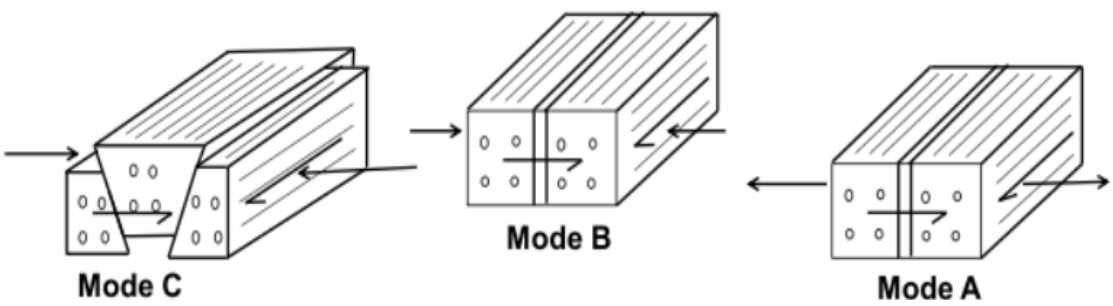


Figure 2.25: The matrix failure modes in Puck and Schürmann's failure criteria.

Summary of Matrix Failure Criteria

The failure indices for plane stress can be expressed as follows:

$$FI_M = \sqrt{\left[1 - \mathrm{p}_{n1}^{(+)} \frac{\mathrm{Y}_T}{\mathrm{S}_L}\right]^2 \left(\frac{\sigma_{22}}{\mathrm{Y}_T}\right)^2 + \left(\frac{\sigma_{21}}{\mathrm{S}_L}\right)^2} + \mathrm{p}_{n1}^{(+)} \frac{\sigma_{22}}{\mathrm{S}_L}, \qquad \sigma_{22} \geq 0\,, \qquad Mode\ A \tag{2.55}$$

$$FI_M = \left(\frac{\sigma_{21}}{\mathrm{S}_L}\right)^2 + 2\mathrm{p}_{nt}^{(-)} \frac{\sigma_{22}}{\mathrm{S}_L}, \qquad -\mathrm{S}_T \leq \sigma_{22} < 0\,,$$

$$\mathrm{S}_L < |\sigma_{21}| \leq \mathrm{S}_L \sqrt{1 + 2\mathrm{p}_{nt}^{(-)}}, \qquad Mode\ B \tag{2.56}$$

$$FI_M = \frac{1}{2(1 + \mathrm{p}_{nt}^{(-)})} \left[\left(\frac{\sigma_{21}}{\mathrm{S}_L}\right)^2 + \left(\frac{\sigma_{22}}{\mathrm{S}_T}\right)^2\right] \left(-\frac{\mathrm{S}_T}{\sigma_{22}}\right); \qquad -\mathrm{Y}_C < \sigma_{22} < -\mathrm{S}_T\,, \qquad Mode\ C \tag{2.57}$$

The shear strength value S_T is determined explicitly through the uniaxial transverse compression test, as given by Eq. (2.51). In their proposal, Puck and Knops [37] suggest setting $\mathrm{p}_{nt}^{(+)}$ equal to $\mathrm{p}_{nt}^{(-)}$, ensuring a continuous slope of the $(\sigma_{nt}, \sigma_{nn})$ failure curve (See Fig. 2.23) at the points where it intersects the σ_{nt} axis. By combining Eqs. (2.32) and Eq. (2.51), the following relationship between the inclination parameters $\mathrm{p}_{nt}^{(+)}$ and $\mathrm{p}_{n1}^{(-)}$ is derived:

$$\mathrm{p}_{nt}^{(+)} = \frac{1}{2}\left[\sqrt{1 + \frac{2\mathrm{Y}_C}{\mathrm{S}_L} \mathrm{p}_{n1}^{(-)}} - 1\right] \tag{2.58}$$

Table 2.4 provides the suggested ranges for inclination parameters.

In the case of WWFE [9], the inclination parameters $\mathrm{p}_{n1}^{(-)} = 0.25$ and $\mathrm{p}_{n1}^{(+)} = 0.30$, with $\mathrm{p}_{nt}^{(-)}$ calculated using Eq. (2.32), were employed. Puck, Kopp, and Knops [37] acknowledge the challenges associated with measuring the fracture angle from test coupons, emphasizing that the data exhibits significant scatter.

Wedge Effect in Mode C

The occurrence of matrix failure in Mode C can significantly impact laminate failure, particularly when the magnitude of σ_{22} is considerably larger than the shear stress σ_{21} ($|\sigma_{22}| >> \sigma_{21}$). This condition leads to the "wedge effect," where the continuous presence of high compressive σ_{22} values, along with the inclined fracture plane, plays a crucial role. As depicted in Fig. 2.26, when the normal stress overcomes the transverse compressive strength Y_C on the failure plane, one side of the fractured layer tends to slide over the other portion, causing an upward movement in the thickness direction. This phenomenon can result in local delamination and subsequent buckling of adjacent layers upon further loading. The behaviour of delamination is influenced by various factors, such as layer thickness, fiber orientation, the position of the affected layer within the laminate (inner or surface layer), and other local parameters.

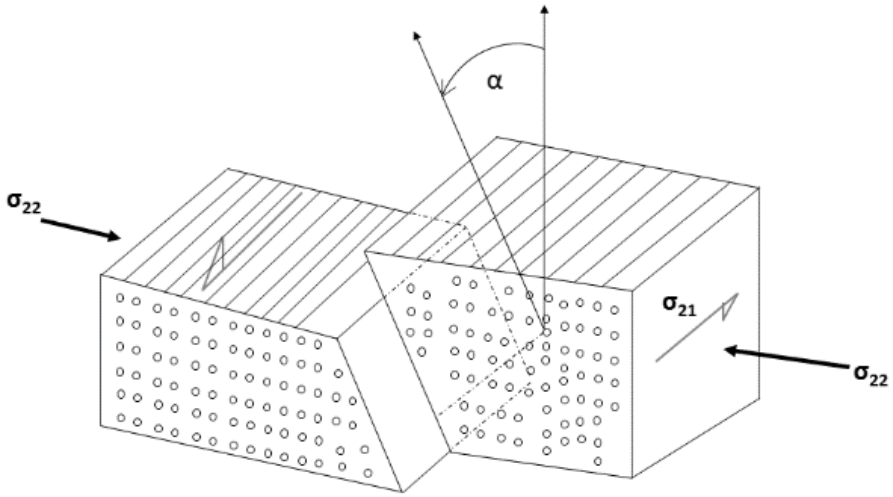


Figure 2.26: The wedge effect showing the fractured pieces gliding one against another in Mode C of matrix failure.

Fiber Failure Modes

Puck and Schürmann propose that fiber failure in tensile conditions takes place under a variety of stress states, where the axial stress in the fiber reaches its failure value as determined in a uniaxial tension test, denoted as X_T. Conversely, compressive failure of the fiber occurs when the negative axial stress matches the strength measured in a uniaxial compression test, represented as X_C. The failure indices for the fiber in tension and compression adhere to non-interactive maximum stress criteria, and they can be expressed as follows:

$$FF_T = \frac{\sigma_{11}}{X_T}, \quad \sigma_{11} > 0 \tag{2.59}$$

$$FF_C = -\frac{\sigma_{11}}{X_C}, \quad \sigma_{11} < 0 \tag{2.60}$$

In Eqs. ((2.59) − (2.60)), the indices FF_T and FF_C represent the failure modes of the fiber in tension and compression, respectively. Failure is observed when either FF_T or FF_C reaches a value of 1, indicating that the corresponding failure criterion has been satisfied.

For loading scenarios involving three-dimensional stress conditions, the fiber failure index in tension (with $\sigma_{11} > 0$) can be defined as follows:

$$\mathrm{FF}_T = \frac{1}{X_T}\left[\sigma_{11} - \left(\nu_{12} - \nu_{12f}\, m_{\sigma f}\frac{E_1}{E_{1f}}\right)(\sigma_{22} + \sigma_{33})\right] \tag{2.61}$$

and in compression ($\sigma_{11} < 0$) is given by

$$\mathrm{FF}_C = \frac{1}{|X_C|}\left[\sigma_{11} - \left(\nu_{12} - \nu_{12f}\, m_{\sigma f}\frac{E_1}{E_{1f}}\right)(\sigma_{22} + \sigma_{33})\right] \tag{2.62}$$

2.5. Progressive failure of intralaminar behaviour

From a phenomenological perspective, the initiation and propagation of defects in a material are closely linked to the degradation of its capacity, with the most apparent manifestation being the decline in the material's stiffness.

However, in standard engineering problems, the analysis of progressive failure typically follows the stress analysis. This approach holds true for composites as well, but only when linear analysis methods are employed. Once a nonlinear analysis is conducted, the stress analysis and fracture analysis become interdependent, necessitating an iterative process to determine the final load at which laminate failure occurs. The stress analysis of a component can be performed using analytical tools like the classical laminate theory (CLT) or through numerical approximations such as finite element analysis (FEA), as utilized in this study. Consequently, it becomes possible to represent the progressive failure of a composite laminate by numerically capturing the relationship between an increase in the material's internal damage and a corresponding decrease in its stiffness.

Several studies have been performed to assess the failure behaviour of composite materials using progressive failure analysis (PFA) which exploit the damage mechanics and material stiffness degradation methods [44]–[52]. F K Chang et al. [53] have evaluated the progressive failure behaviour of the notched T300/1034C graphite/epoxy composite laminate. They based on the classical lamination theory and a material degradation model included failure criterion that they proposed, to analyse the stress and calculate the damage progressive, respectively. Yoon et al. [54] using a PFA model by implementing the crack-band-model through FEM to predict the behaviour of a composite laminate containing an open-hole. The damage variable of Matzenmiller et al. [55] is currently used as a typical PFA tool.

Furthermore, there are a number of challenges in using progressive damage modelling. These include:

The complexity of the models: Progressive damage models can be very complex, as they need to account for the different damage mechanisms that can occur in a material, as well as the interaction between these mechanisms. This can make the models computationally expensive and difficult to calibrate.

The availability of data: In order to develop accurate progressive damage models, it is important to have a good understanding of the different damage mechanisms that can occur in a material. This data can be obtained from physical testing, but it can be time-consuming and expensive to collect.

The uncertainty in the models: Progressive damage models are inherently uncertain, as they are based on a number of assumptions about the material and the loading conditions. This uncertainty can make it difficult to make accurate predictions about the failure of a structure.

In recent decades, numerous researchers have dedicated their efforts to studying failure mechanisms and predicting damage initiation in composite laminates. Reddy and Pandey [56] introduced a finite element approach based on the first shear deformation theory (FSDT) to analyse the first ply failure of laminates. They employed various criteria including maximum stress, maximum strain, Tsai-Hill, Tsai-Wu, and Hoffman criteria for the failure analysis. Kam and Jan [57] proposed a finite element procedure utilizing the layer-wise linear displacement theory to investigate the first ply failure in laminated composites. They employed five failure theories, namely maximum stress (independent and polynomial), maximum strain, Hoffman, Tsai-Hill, and Tsai-Wu. Pal and Bhattacharya [58] conducted a progressive failure analysis of cross-ply laminated composite plates based on FSDT, utilizing maximum stress, maximum strain, Tsai-Wu, and Hoffman criteria. Prusty et al. [59] presented a first ply failure analysis of laminated panels using a computational procedure based on the finite element method. They employed Yeh-Stratton, maximum stress, maximum strain, Tsai-Hill, Tsai-Wu, and Hoffman failure criteria to predict the failure of the lamina.

On the contrary, first-ply failure (FPF) analysis tends to underestimate the complete load-carrying capabilities of the layers [36]. In the past, FPF analyses were prevalent due to the complexity involved in predicting failure evolution and the challenges in simulating it. However, with advancements over the years, engineers now seek to harness the full potential of these advanced materials. Considerable efforts have been made to achieve reliable predictions of final failure. Nonetheless, performing a full-layer progressive failure (LPF) analysis requires significant effort from the analysis engineer and is computationally demanding.

Currently, FPF and LPF analyses are employed in tandem. Typically, the FPF analysis is conducted to assess whether the component can withstand standard operational loads. In addition to FPF, the LPF analysis is utilized to simulate one-time events, such as component misuse or crashes. The fracture analysis for laminate composites is performed on a layer-by-layer basis. This means that for each lamina, the analysis engineer must apply an appropriate failure criterion to determine if the layer under investigation will fail or not. Another challenge arises from the fact that the plies do not fail simultaneously.

The discount analysis method used in this study accounts for successive fracture events, allowing for continuous stiffness reduction beyond FPF, resulting in a more realistic prediction of laminate failure. It also enables the engineer to observe if unacceptably large deformations occur. Additionally, the reduction of laminate stiffness affects the safety against instability, which can be monitored as well.

2.5.1. Discount method

As discussed in the preceding section, accurately predicting final failure is a complex task. One approach to monitor the degradation of stiffness during laminate failure is the ply-by-ply discount method. Knops[60] devised a procedure in which the stiffness parameters of each lamina are progressively reduced based on their stress levels. Meanwhile, Chang and Lessard [61], Goyal et al. [62], and Puck and Schürmann [9] have employed empirical methods to simulate material degradation.

Chang and Lessard [61] conducted a progressive failure analysis of a symmetrically laminated composite plate with a centrally located open hole under in-plane compression. Their analysis assumes plane stress, with no out-of-plane displacement of the plate's mid-plane, and considers

geometric linearity. However, their analysis incorporates the nonlinear shear stress/strain behaviour within the plane of a ply.

In a separate study, Goyal et al. [62] developed a progressive failure analysis for two scenarios: a flat composite panel subjected to quasi-static shear loading, and a curved composite panel subjected to quasi-static compression. Both panels feature a centrally located cut-out, and the lamina material properties correspond to AS4-3502 graphite-epoxy unidirectional tape. The analysis takes into account geometric nonlinearity and was performed using AbaqusTM software, utilizing the shear deformable shell element S4R and the user-defined field (USDFLD) option to degrade the intralaminar material properties. Moreover, Puck and Schürmann address material property degradation for IFF in Modes A, B, and C under plane stress deformations, specifically in the context of 2D problems. They incorporate a dimensionless degradation factor to account for this degradation.

One common approach for modelling the stiffness degradation of composite laminates is the use of damage evolution laws. These laws relate the extent of damage in each ply to the corresponding reduction in stiffness. Damage evolution laws can be derived from experimental data or theoretical models, and they typically take into account the type and severity of the damage, as well as the loading conditions. Another important aspect of the discount method is the use of finite element analysis (FEA) to predict the mechanical response of composite laminates under different loading conditions. FEA allows for the simulation of complex deformation and failure mechanisms in composite laminates, and it can be used to predict the stiffness degradation of composite laminates due to various types of damage.

Despite the well-established and widely accepted nature of these damage models, the numerical derivation and implementation procedure for finite elements can be significantly complex. This complexity arises due to two main reasons. Firstly, the majority of damage models have been developed for isotropic ductile materials, making it challenging to directly apply them to anisotropic brittle materials. Secondly, a substantial amount of effort is needed to accurately identify the material parameters of a damage model. This entails obtaining a large number of material test results in order to define the precise material parameters.

Otherwise, the element weakening method (EWM) and constant stress exposure (CSE), which enable us to track the stiffness degradation for both 2D and 3D problems and are part of discount methods , have been employed and presented in this work [9], [63]. Several advantages of these approaches including:

- The residual stiffness of a ply is taken into account.
- Accuracy: The discount method provides an accurate prediction of the onset and propagation of damage in composite laminates. By modelling the material behaviour as a continuum, the method can capture the behaviour of the material more accurately than other approaches.
- Simplicity: The method is relatively simple to implement and can be used with a range of commercial finite element software packages.
- Insight: The method provides insight into the failure mechanisms of composite laminates by identifying the locations and extent of damage in the structure.

2.5.1.1. Theoretical formulation

In quasi-static stress analysis, constituent models establish a relationship between the strain and stress states. This relationship assumes a linearly elastic material with transversely orthotropic behaviour. The constitutive relation can be expressed as follows:

$$\{\epsilon\} = [S]\{\sigma\} \text{ or } \{\sigma\} = [C]\{\epsilon\} \tag{2.63}$$

$$C_{11} = E_{11}(1 - \nu_{23}\nu_{32})\Delta \tag{2.64}$$

$$C_{22} = E_{22}(1 - \nu_{13}\nu_{31})\Delta \tag{2.65}$$

$$C_{33} = E_{33}(1 - \nu_{12}\nu_{21})\Delta \tag{2.66}$$

$$C_{12} = E_{11}(\nu_{21} - \nu_{31}\nu_{23})\Delta \tag{2.67}$$

$$C_{13} = E_{22}(\nu_{32} - \nu_{12}\nu_{31})\Delta \tag{2.68}$$

$$C_{23} = E_{33}(\nu_{31} - \nu_{21}\nu_{32})\Delta \tag{2.69}$$

$$\Delta = \frac{1}{1 - \nu_{12}\nu_{21} - \nu_{23}\nu_{32} - \nu_{31}\nu_{13} - 2\nu_{21}\nu_{32}\nu_{13}} \tag{2.70}$$

$$\begin{Bmatrix} \sigma_{11} \\ \sigma_{22} \\ \sigma_{33} \\ \sigma_{12} \\ \sigma_{13} \\ \sigma_{23} \end{Bmatrix} = \begin{bmatrix} C_{11} & C_{12} & C_{13} & 0 & 0 & 0 \\ C_{12} & C_{22} & C_{23} & 0 & 0 & 0 \\ C_{13} & C_{23} & C_{33} & 0 & 0 & 0 \\ 0 & 0 & 0 & 2G_{12} & 0 & 0 \\ 0 & 0 & 0 & 0 & 2G_{13} & 0 \\ 0 & 0 & 0 & 0 & 0 & 2G_{23} \end{bmatrix} \begin{Bmatrix} \epsilon_{11} \\ \epsilon_{22} \\ \epsilon_{33} \\ \epsilon_{12} \\ \epsilon_{13} \\ \epsilon_{23} \end{Bmatrix} \tag{2.71}$$

The equation represents the components of the material stiffness tensors, denoted as C_{ij}. The values of ν_{ij} represent the Poisson's ratios, E_{ij} represent the Young's moduli, and G_{ij} represent the shear moduli.

2.5.1.2. Element weakening method (EWM)

In this method, when the stress exposure reaches the value one, the elastic properties of selected elements are progressively reduced to zero, following the Eqs. ((2.72) − (2.82)). During inter-fiber failure, the modulus perpendicular to fibers and the in-plane shear modulus undergo degradation. However, in the case of fiber failure, all elastic properties are diminished. The specific degradation rules employed are listed in Table 2.5 below:

$$d_f = 1 - (1 - d_{ft})(1 - d_{fc}) \tag{2.72}$$

$$d_m = 1 - (1 - d_{mt})(1 - d_{mc}) \tag{2.73}$$

$$C_{11} = (1 - d_f)C_{11}^0 \tag{2.74}$$

$$C_{22} = (1 - d_f)(1 - d_m)C_{22}^0 \tag{2.75}$$

$$C_{33} = (1 - d_f)(1 - d_m)C_{33}^0 \tag{2.76}$$

$$C_{12} = (1 - d_f)(1 - d_m)C_{12}^0 \tag{2.77}$$

$$C_{13} = (1 - d_f)(1 - d_m)C_{13}^0 \tag{2.78}$$

$$C_{23} = (1 - d_f)(1 - d_m)C_{23}^0 \tag{2.79}$$

$$G_{12} = (1 - d_f)(1 - d_{mt}S_{mt})(1 - d_{mc}S_{mc})G_{12}^0 \quad (2.80)$$

$$G_{23} = (1 - d_f)(1 - d_{mt}S_{mt})(1 - d_{mc}S_{mc})G_{23}^0 \quad (2.81)$$

$$G_{31} = (1 - d_f)(1 - d_{mt}S_{mt})(1 - d_{mc}S_{mc})G_{31}^0 \quad (2.82)$$

The damage variables, d_f and d_m, represent the overall damage in the fiber and matrix materials, respectively. These variables capture the extent of damage under different stress states, including tensile and compressive conditions, as indicated by d_{ft}, d_{fc}, d_{mt} and d_{mc}. The loss control factors, S_{mt} and S_{mc}, govern the reduction in shear stiffness resulting from matrix tensile and compressive failures. In the context of the present study, it is noteworthy to mention that the chosen loss control factors are $S_{mt} = 0.9$ and $S_{mc} = 0.5$. These values imply that the shear stiffness reduction due to matrix tensile failure is limited to 90% of its original value, while for matrix compressive failure, the reduction is more substantial, reaching only 50% of the initial stiffness. Indeed, these factors values have been chosen by many authors such as [28].

2.5.1.3. Constant stress exposure method (CSE)

In this method, when fiber failure occurs, the entire stiffness of the lamina is degraded, similar to the EWM (Equivalent Weakening Material) approach. However, in the case of inter-fiber failure (IFF), only the stiffness related to IFF is gradually reduced. This degradation process is based on the concept of stress exposure (f_E) and maintains the significance of the fracture criterion, $FI_M = 1$. Therefore, when the stress exposure of a lamina reaches the value one, IFF is initiated, causing the lamina to redistribute some of its load. The degradation of the stiffness tensor, E_i and G_{ij}, is not uniform and follows a progressive damage rule. The specific details of the progressive damage rule for this method are outlined as follows [64]:

$$E_1 = (1 - d_{ft})(1 - d_{fc})E_1^0 \quad (2.83)$$

$$E_2 = (1 - d_{ft})(1 - d_{fc})(1 - d_{mt})(1 - d_{mc})E_2^0 \quad (2.84)$$

$$E_3 = E_2 \quad (2.85)$$

$$G_{12} = (1 - d_{ft})(1 - d_{fc})(1 - \mu d_{mt})(1 - \mu d_{mc})G_{12}^0 \quad (2.86)$$

$$G_{13} = G_{12} \quad (2.87)$$

$$G_{23} = (1 - d_{ft})(1 - d_{fc})(1 - \mu d_{mt})(1 - \mu d_{mc})G_{23}^0 \quad (2.88)$$

$$\nu_{21} = \frac{E_2}{E_1}\nu_{12} \quad (2.89)$$

$$\nu_{31} = \frac{E_3}{E_1}\nu_{13} \quad (2.90)$$

$$\nu_{32} = \frac{E_3}{E_2}\nu_{23} \quad (2.91)$$

However, the unequal stress distribution over the length of the layer after the cracks appear in the matrix is approximated by constant stress which has the magnitude of the mean value of the unequal stresses. Consequently, the effect of the cracks is spread over the fiber direction. In practical calculations, Puck et al. were able to use a reduction factor μ through a purely phenomenological approach to provide a linear fit to the nonlinear behaviour of the shear moduli.

The recommended values for μ are μ=77% for CFRP (Carbon Fiber Reinforced Polymer) and μ=41% for GFRP (Glass Fiber Reinforced Polymer), as proposed in the referenced study [9]. However, it is important to note that this approach does not consider the progression of damage over time and relies solely on load redistribution until the failure exposure reaches the value one.

Table 2.5. EWM and CSE conditions for each failure mode.

Failure mode	Condition for validity	Damage value
Tensile fiber mode	$\sigma_{11} > 0$	$d_{ft} = 1$
Compressive fiber mode	$\sigma_{11} < 0$	$d_{fc} = 1$
Tensile matrix mode	$\sigma_{n} > 0$	$d_{mt} = 1$
Compressive matrix mode	$\sigma_{n} < 0$	$d_{mc} = 1$

2.5.2. Continuum damage mechanics (CDM)

In this work, the second approach employed to predict the final failure is based on continuum damage mechanics (CDM). Despite their physical differences, engineering materials such as metals, polymers, ceramics, and composites exhibit similar qualitative mechanical behaviour. This suggests that common "mesoscopic" properties can be explained by energy mechanisms that apply to all these materials. These shared characteristics allow the application of CDM and thermodynamics theories to model their behaviour, regardless of the complexity and differences in their physical structures.

Constitutive damage models for intralaminar failure mechanisms have been developed using the thermodynamics of irreversible processes by researchers such as Ladevéze and Le Dantec [65], Maimí et al. [48], and Hassan and Batra [66]. The creation and growth of microvoids and microcracks are considered as damage processes [67]. The degradation of material properties under loading conditions can be simulated using internal variables to describe the progression of damage [68]. These approaches enable the simulation of the deterioration of material properties and the damage evolution during mechanical loading.

In a continuum medium, various forms of damage can manifest, including:

- Brittle damage: This occurs when cracks initiate at the mesoscale without significant plastic strains.
- Ductile damage: Nucleation and growth of microvoids and microcracks occur in the medium as a result of plastic strains [69].
- Creep damage: This type of damage occurs when a metallic structure is subjected to elevated temperatures, and plastic strains involve viscosity (Lemaitre, 1996).
- Low cycle fatigue damage: When a material is cyclically loaded at high stress or strain levels, damage can occur.
- High cycle fatigue damage: Under cyclic loads lower than a reference stress, the material undergoes deterioration.

These different forms of damage reflect the complex behaviour of materials under various loading conditions and provide insight into the mechanisms of damage initiation and propagation in continuum media. Moreover, in the classical formulation of Continuum Damage Mechanics (CDM), the presence of energy potentials is assumed, from which the state laws and constitutive equations are derived.

As discussed earlier, damage refers to the formation of micro-voids and microcracks, which are discontinuities on the surface. By considering the smallest volume in which measurements can be conducted, known as the Representative Volume Element (RVE), it becomes possible to formulate equations that describe the process of damage (see Fig. 2.27).

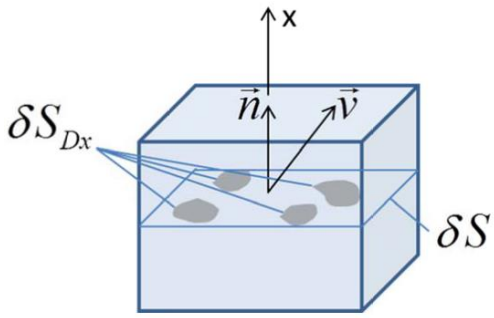


Figure 2.27: Representative Volume Element with damage.

The damage of this element can be defined as the ratio between the area of damage (δS_{D_x}) and the total area (δS).

$$D\ (\vec{n}, x)\ = \frac{\delta S_{D_x}}{\delta S} \tag{2.92}$$

When $D = 0$, the material is undamaged and when $D = 1$, it is fully damaged. Regarding a surface δS with normal $\vec{n}$ and a reference vector $\vec{v}$ (Fig. 2.27), a more general tensorial notation for damage is

$$\left(I_{ijkl} - D_{ijkl}\right)v_k n_l \delta S = v_i \hat{n}_j \delta \hat{S} \tag{2.93}$$

The effective normal vector, denoted by $\hat{n}$, is associate with the effective area ($\delta \hat{S}$). When considering anisotropic damage, accurately representing the underlying damage physics while ensuring compatibility with thermodynamics becomes more challenging. The effective stress can be expressed using the following equation:

$$v_i \hat{\sigma}_{ij} \hat{n}_j \delta \hat{S} = \ v_k \sigma_{kl} n_l \delta S \tag{2.94}$$

Using the Eq. (2.93), it is possible to write:

$$\hat{\sigma}_{ij}\left(I_{ijkl} - D_{ijkl}\right)v_k n_l \delta S = v_k \sigma_{kl} n_l \delta S \tag{2.95}$$

It is important to mention that the fourth order damage tensor D_{ijkl} has the following symmetries: ($D_{ijkl} = D_{ijlk} = D_{jikl} = D_{klij}$). Considering those symmetries, the effective stress tensor is

$$\hat{\sigma}_{ij} = \sigma_{kl}(I - D)^{-1}{}_{klij} \tag{2.96}$$

When considering the fourth-order damage tensor, certain constraints apply:

- The effective stress must exhibit symmetry.
- The effective stress should be independent of the strain behaviour and Poisson's coefficient.
- Compatibility with thermodynamics is necessary.
- The damage should have a distinct effect on the behaviour of hydrostatic stresses.

The resulting elasticity tensor, modified by the presence of damage, can be expressed as:

$$\left(I_{ijrs} - D_{ijrs}\right)E_{rskl} = \hat{E}_{ijkl} \tag{2.97}$$

In composite materials, the damage mechanism exhibits variations between tension and shear. As a result, two separate scalar variables are required to describe the impact on elastic shear and hydrostatic energy. These variables, denoted as D_s (for deviator stress components) and D_n (for hydrostatic stress), capture the influence of damage. Consequently, the anisotropic complementary energy density for damaged media can be expressed as:

$$w_e = \frac{1}{2} E_{ijkl}{}^{-1} \sigma_{ij}{}^{D} \sigma_{kl}{}^{D} + \frac{1}{2} E_{ijkl}{}^{-1} \sigma_H{}^{2} \delta_{ij} \delta_{kl} \tag{2.98}$$

In this equation, $\sigma_{ij}{}^{D}$ represents the deviator stress tensor, σ_H denotes the hydrostatic stress, and δ_{ij} corresponds to the Kronecker symbol.

$$Y_s = \frac{\delta w_e}{\delta D_s} \tag{2.99}$$

$$Y_n = \frac{\delta w_e}{\delta D_n} \tag{2.100}$$

These derivatives can be written, using engineering constants:

$$Y_s = \frac{\delta w_e}{\delta D_s} = \frac{\tau_{12}^2}{2G_{12}(1 - D_s)^2} \tag{2.101}$$

$$Y_n = \frac{\delta w_e}{\delta D_n} = \frac{\sigma_{22}^2}{2E_{22}(1 - D_n)^2} \tag{2.102}$$

When the principal directions of stress remain constant over time, the damage also aligns with these principal directions. As a result, the effective stresses corresponding to three-dimensional principal directions are given by:

$$\hat{\sigma} = \begin{bmatrix} \frac{\sigma_{11}}{(1 - D_1)} & 0 & 0 \\ 0 & \frac{\sigma_{22}}{(1 - D_2)} & 0 \\ 0 & 0 & \frac{\sigma_{33}}{(1 - D_3)} \end{bmatrix} \tag{2.103}$$

The damage variables in the principal directions for three-dimensional stress states are represented by D_1, D_2 and D_3.

However, CDM is a rather new but very promising method for commercial use which has been applied by several authors. For example, in previous studies, Donadon et al. [70] utilized a crack smeared formulation of Continuum Damage Mechanics (CDM) to model progressive failure mechanisms in composite structures. Pavan et al. [71] developed a material model incorporating viscoelastic effects within the CDM framework to study the failure process of composites. Flatscher et al. [72] conducted finite element analyses on open hole specimens under uniaxial tensile loads, combining CDM and Plasticity Theory. Zhou et al. [73] used continuum shell and cohesive zone elements for open-hole compression to model in-plane damage and delamination while taking into account the failure criteria of Tsai–Wu and Hoffman to simulate the onset of matrix damage.

However, different models have been employed including the built-in Abaqus model and Linde's model. Abaqus incorporates the Hashin criterion for predicting initial failure and utilizes Matzenmiller's approach [60] for modelling progressive damage. Linde has developed a three-dimensional damage evolution model based on strain failure criteria [74] and provided an Umat subroutine that can be executed within Abaqus. In the context of Continuum Damage Mechanics (CDM), damage variables (d) are introduced to capture the damage state within a ply, and the number of damage variables may vary depending on the specific CDM theory employed.

Furthermore, Abaqus has an integrated progressive damage model, for elastic brittle fiber reinforced materials with anisotropic behaviour, to allow the user to predict the initiation of damage and model the evolution progressive of damage using Eqs. ((2.12) − (2.15)) and Eqs. ((2.104) − (2.113)), respectively. Damage variables, which can have values ranging from 0 (undamaged state) to 1 (fully damage state for the mode corresponding to this damage variable), are used to track the reduction of material stiffness if a damage initiation criterion is met. The energy that is dissipated throughout the damage process is the basis of evolution's law, also known as fracture energy. The present law of evolution is a generalization of the approach suggested by [75]. Abaqus integrates a characteristic length into the formulation to reduce mesh dependency during material softening, resulting in the constitutive law being stated as a stress-displacement relationship. For each of the four failure modes, the damage variable will proceed in such a way that the stress-displacement behaves as depicted in (Fig. 2.28) below.

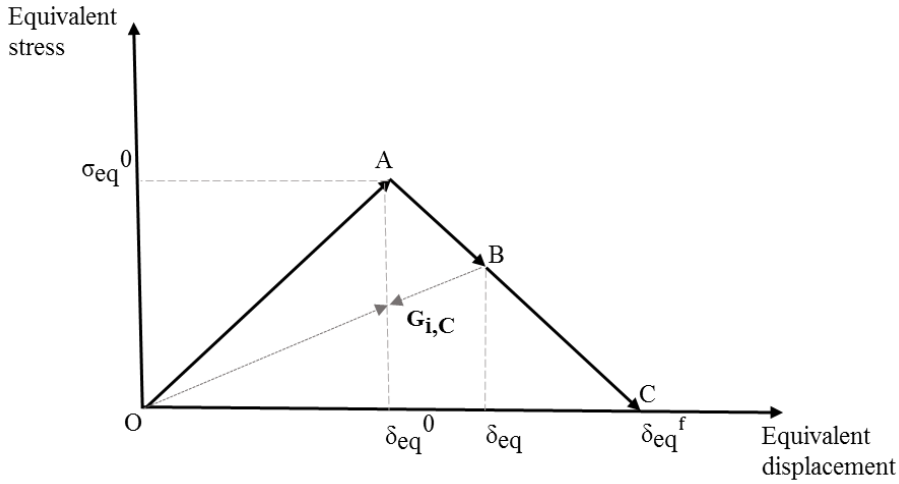


Figure 2.28: Equivalent stress versus equivalent displacement.

Before the onset of the damage, it is assumed a linear elastic behaviour of the material and when the damage has occurred, the negative slope is determined by the development of the appropriate damage variables using the equations shown below.

For each kind of damage, the equivalent displacements and stresses are stated as follows:
Fiber tension ($\sigma_{11} \geq 0$) :

$$\delta_{eq} = L_c\langle\varepsilon_{11}\rangle \tag{2.104}$$

$$\sigma_{eq} = \frac{L_c\langle\varepsilon_{11}\rangle\langle\sigma_{11}\rangle}{\delta_{eq}^{ft}} \tag{2.105}$$

Fiber compression ($\sigma_{11} < 0$) :

$$\delta_{eq} = L_c\langle -\varepsilon_{11}\rangle \tag{2.106}$$

$$\sigma_{eq} = \frac{L_c\langle -\varepsilon_{11}\rangle\langle -\sigma_{11}\rangle}{\delta_{eq}^{fc}} \tag{2.107}$$

Matrix tension ($\sigma_{22} \geq 0$) :

$$\delta_{eq} = L_c\sqrt{\langle\varepsilon_{22}\rangle^2 + \varepsilon_{12}^2} \tag{2.108}$$

$$\sigma_{eq} = \frac{L_c(\langle\varepsilon_{22}\rangle\langle\sigma_{22}\rangle + (\tau_{12}\varepsilon_{12}))}{\delta_{eq}^{mt}} \tag{2.109}$$

Matrix compression ($\sigma_{22} \leq 0$) :

$$\delta_{eq} = L_c\sqrt{\langle -\varepsilon_{22}\rangle^2 + \varepsilon_{12}^2} \tag{2.110}$$

$$\sigma_{eq} = \frac{L_c(\langle -\varepsilon_{22}\rangle\langle -\sigma_{22}\rangle + (\tau_{12}\varepsilon_{12}))}{\delta_{eq}^{mc}} \tag{2.111}$$

The symbol $< >$ denotes the Macaulay bracket operator in the equations above, which is defined for every $\alpha \in \mathcal{R}$ as $\langle\alpha\rangle = (\alpha + |\alpha|)/2$. Where L_c is the element's representative length, which is based on the element. geometry and formulation. For membranes and shells, it is a characteristic length determined as the square root of the area in the reference surface. Besides, a failure mode's equivalent displacement is written in terms of components, with the effective stress components used in the initiation criterion for that failure mode.

As the behaviour is shown in (Fig. 2.28) and after the initiation of damage (i.e., $\delta_{eq} \geq \delta_{eq}^0$), the damage variable for every failure mode i can be expressed as follow:

$$d_i = \frac{\delta_{i,eq}^f(\delta_{i,eq} - \delta_{i,eq}^0)}{\delta_{i,eq}(\delta_{i,eq}^f - \delta_{i,eq}^0)}; \quad i = \{ft, fc, mt, mc\} \tag{2.112}$$

Where $d_i \in [0,1]$

$\delta_{i,eq}^0$ is the initial equivalent displacement at which the initiation criterion is fulfilled and $\delta_{i,eq}^f$ is displays the equivalent displacement at which the material is completely damaged in this failure mode (i.e. $d_i = 1$). Moreover, for uniaxial deformations, the material softening is linear if the damage variable is computed by employing Eq. (2.112) in accordance with Eqs. ((2.104) − (2.111)). The $\delta_{i,eq}^f$ in Eq. (2.112) is unknown and can be divided from the following relation:

$$\delta_{i,eq}^f = \frac{2G_{i,C}}{\sigma_{i,eq}^0} \tag{2.113}$$

The values of $\delta_{i,eq}^0$ for different modes depend on the specific elastic stiffness and resistance parameters chosen to represent the respective damage initiation [76]. On the other hand, $G_{i,C}$ represents the critical energy release rate for each failure mode, and it is determined individually to correspond to the region within the triangle OAC as illustrated in Fig. 2.28. $\sigma_{i,eq}^0$ is the equivalent stress at which a mode's initiation is achieved.

One limitation of this damage progression model is its inability to accurately reproduce tensile fracture localization. However, this issue will be addressed by incorporating the crack band approach, which was originally proposed by Bažant and Oh [77]. The crack band model modifies

the post-peak behavior of the constitutive law (damage progression) to ensure that the energy dissipation matches the localized crack band observed in experimental studies.

Furthermore, finite element analysis (FEA) is a common approach to modelling the behaviour of composite laminates, and CDM can be applied within FEA to predict progressive failure. While this combination can be useful, there are some potential drawbacks to consider. Here are a few:

- Computational cost: FEA models can be computationally expensive, especially for large or complex geometries. When combined with CDM, the computational cost can increase further, as CDM requires additional calculations for damage evolution and failure prediction. This can limit the size and complexity of the models that can be analysed.
- Accuracy of input parameters: The accuracy of CDM predictions can depend heavily on the accuracy of the input parameters used in the model. These parameters may be challenging to obtain experimentally, especially for complex composite materials, which can lead to inaccurate predictions. Additionally, the CDM model may not account for all of the relevant failure modes, which can further limit its accuracy.
- Limited scope of damage: CDM typically focuses on one or two failure modes, such as fiber breakage or matrix cracking. However, composite laminates can fail due to a combination of several damage modes, such as delamination, transverse cracking, and fiber pull-out. CDM may not be able to accurately capture the interactions between different damage modes, leading to inaccurate predictions.

Overall, while CDM can be a useful approach for predicting progressive failure in composite laminates, it is essential to consider its limitations and potential drawbacks carefully.

2.6. Modelling of interlaminar behaviour

The prediction of the initiation and propagation of delamination is a major step forward in the description of structural strength. For this purpose, different approaches have been developed in recent years:

(i) Initiation criteria to predict crack onset

(ii) Linear elastic fracture mechanics to describe delamination propagation,

(iii) Bi-criteria, a combination of the first two approaches, for a better determination of initiation and the associated crack length (not included here see [78])

(iv) Cohesive zone models, based on damage mechanics, capable of describing initiation and delamination propagation

2.6.1. Initiation failure criteria

Over the past 30 years, numerous studies have focused on the initiation of delamination and have led to the prediction of this mechanism using stress or strain criteria. The principle of failure criteria is to determine the stress/strain field required to create a crack. This approach has the advantage of being fast, simple to implement and easy to use (usually as a post processing of a calculation). For this reason, this type of approach is used extensively by industry even if it is limited to delamination initiation. Among the most commonly used criteria [79] is the maximum stress, which consists of comparing the stress field with the maximum interlaminar stresses:

$$\sigma_{33} \geq Z_t, \ \tau_{13} \geq S_{13}, \qquad \tau_{23} \geq S_{23} \tag{2.114}$$

Where Z_t is the interlaminar resistance related to mode I, S_{13}, that related to mode II and S_{23} that associated with mode III. This criterion does not take into account the couplings between the different failure modes. This is why other criteria seem to be more suitable such as the quadratic criterion proposed by Hashin Eq. (2.115) or its extension proposed by Brewer Eq. (2.116) [80], which takes into account the possible difference between the out-of-plane stress in pure tension and in pure compression.

$$\left(\frac{\sigma_{33}}{Z_t}\right)^2 + \left(\frac{\tau_{13}}{S_{13}}\right)^2 + \left(\frac{\tau_{23}}{S_{23}}\right)^2 \geq 1 \tag{2.115}$$

$$\left(\frac{\langle\sigma_{33}\rangle_+}{Z_t}\right)^2 + \left(\frac{\langle\sigma_{33}\rangle_-}{Z_c}\right)^2 + \left(\frac{\tau_{13}}{S_{13}}\right)^2 + \left(\frac{\tau_{23}}{S_{23}}\right)^2 \geq 1 \tag{2.116}$$

Where Z_c is the interlaminar strength in compression. In reality, since initiation cannot occur in pure compression, this parameter corresponds to the failure of plies in a compression test on a thick plane plate.

In addition, in order to better predict the initiation of delamination, a reinforcement of the interface strength in compression/shear seems necessary, a criterion has been proposed by Charrier et al. [81]. The latter uses a parameter p (corresponding in practice to the inverse of the pure compressive strength Z_c) in order to obtain the shape that reflects the desired reinforcement:

$$\left(\frac{\langle\sigma_{33}\rangle_+}{Z_t}\right)^2 + \left(\frac{\langle\sigma_{33}\rangle_-}{Z_c}\right)^2 + \left(\frac{\tau_{13}}{S_{13}(1-p\sigma_{33})}\right)^2 + \left(\frac{\tau_{23}}{S_{23}(1-p\sigma_{33})}\right)^2 \geq 1 \tag{2.117}$$

Although this approach is efficient in describing the initiation of delamination, it does not describe the propagation of the crack after initiation. Furthermore, in order to use these criteria in the region of a point where the stress field is singular, it is necessary to calculate it by introducing an "internal length". Methods such as "Point stress" [82] for example, are used to define the initiation at the bottom of a notch by :

$$\sigma(0, d_c) > \sigma_c \tag{2.118}$$

With d_c the imposed internal length. This type of approach has been used to study delamination due to edge effects. The authors have shown that it is not possible to describe all the experimental cases (different thicknesses, different orientations between plies) with a single critical distance. Since our objective is to describe the initiation and propagation in general, we will not be interested in this type of approach in the following.

2.6.2. Linear elastic fracture mechanics

The description of crack propagation can be done using linear elastic fracture mechanics approaches. These allow the calculation of the energy restitution rate G at the crack tip. Propagation is then assured when this energy becomes greater than the critical energy restitution rate of the interface G_C [83].

The propagation condition can therefore be summarized as:

$$G \geq G_C \tag{2.119}$$

The crack propagation can be carried out in a stable or unstable way. The stability condition, with an imposed displacement, is expressed by the equation:

$$\frac{\partial G}{\partial a} < 0 \tag{2.120}$$

With (a) the length of the crack.

Thus, for a known interface toughness G_C, it is possible to describe the delamination propagation. From a practical point of view, it is therefore necessary to (i) calculate the energy restitution rate, (ii) calculate the mode mix and (iii) know the toughness as a function of the mode mix. To model crack propagation by finite elements, several tools have been developed, including the Virtual Crack Closure Technique (VCCT), by Rybicki and Kanninen [84], and the Virtual Crack Extension (VCE). The VCCT is the method that seems to be the most widely used in the literature. The work of Krueger [85] explains the principle of this method in detail.

The VCCT is based on Irwin's [86] assumption that the energy ΔE^e required to open a crack of length a to length $a + \Delta a$ is the same as the energy to close that crack of length Δa. The relationship for calculating the energy required to close the crack of length Δa for 2D modelling with linear quadrangle elements is:

$$\Delta E^e = \frac{1}{2}(X_n . \Delta u_m + Z_n . \Delta w_m) \tag{2.121}$$

where X_n (resp. Z_n) is the reaction force in mode I (resp. mode II) at point n and Δu_m (resp. Δw_m) is the displacement jump between nodes m and m* in mode I (resp. mode II) as shown in (Fig. 2.29).

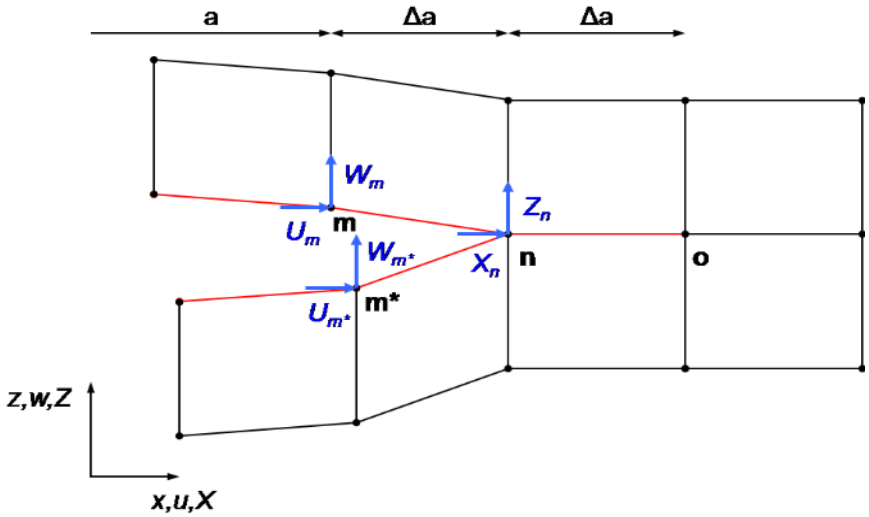


Figure 2.29: Principle of the VCCT method [86].

Another approach, called Modified Virtual Crack Closure Technique (MVCCT), exists in the literature. This method allows the calculation of the energy restitution rate and mode mixing, for a given crack length, in a single calculation. The loads and displacements required to calculate the energy restitution rate at the crack tip are recovered at point n for the loads and at points m and m* for the displacements (Fig. 2.29), contrary to the classical VCCT method which recovers these two data at point n by two successive calculations. Note that in order to use the MVCCT method, it is assumed that the crack propagation does not undergo a large perturbation between two propagated

states (i.e. the crack maintains an almost identical geometry when propagating from a length a to a length $a + \Delta a$).

The energy restitution rate G is then calculated by $G = \Delta E^e / \Delta A$ where ΔA is the area closed during the calculation. In addition, it is possible to decompose the total energy at the crack tip according to the failure modes in order to determine the mode mix Eq. (2.122):

$$G = G_I + G_{II} + G_{III}$$
$$\alpha_{II} = \frac{G_{II}}{G_I + G_{II} + G_{III}}, \qquad \alpha_{III} = \frac{G_{III}}{G_I + G_{II} + G_{III}} \tag{2.122}$$

Where G_I (resp. G_{II} et G_{III}) is the part of the energy G related to mode I (resp. mode II and mode III) and α_{II} (resp. α_{III}) is the mode mix defined by the energy in mode II (resp. mode III) on the total energy. When the energy restitution rate G reaches the critical threshold G_C, delamination propagation is then possible but usually requires a remeshing process at the crack tip. The last step consists in calculating the toughness value for the mixed mode as seen by the crack front. A propagation criterion, identified by the different tests from fracture mechanics, is then used. In order to best fit the experimental results obtained, several propagation criteria have been proposed. Among the criteria most commonly used in the literature for carbon/epoxy laminates, we find the Power Law criterion [87], whose general form is

$$\left(\frac{G_I}{G_{IC}}\right)^m + \left(\frac{G_{II}}{G_{IIC}}\right)^n + \left(\frac{G_{III}}{G_{IIIC}}\right)^p \geq 1 \tag{2.123}$$

where m, n and p are parameters for adjusting the experimental points. This criterion makes it possible to find the classic criteria: the linear criterion ($m = n = p = 1$) and the quadratic criterion ($m = n = p = 2$) :

$$\left(\frac{G_I}{G_{IC}}\right) + \left(\frac{G_{II}}{G_{IIC}}\right) + \left(\frac{G_{III}}{G_{IIIC}}\right) \geq 1 \tag{2.124}$$

$$\left(\frac{G_I}{G_{IC}}\right)^2 + \left(\frac{G_{II}}{G_{IIC}}\right)^2 + \left(\frac{G_{III}}{G_{IIIC}}\right)^2 \geq 1 \tag{2.125}$$

These criteria can be written in general terms as:

$$\left(\frac{G_I}{G_{IC}}\right)^\alpha + \left(\frac{G_{II}}{G_{IIC}}\right)^\alpha + \left(\frac{G_{III}}{G_{IIIC}}\right)^\alpha \geq 1 \tag{2.126}$$

with α a shape parameter.

More recently, Benzeggagh et al. [88] have also proposed a propagation law. This criterion is expressed in 2D by:

$$G_C = G_{IC} + (G_{IIC} - G_{IC}) \left(\frac{G_{II}}{G_I + G_{II}}\right)^\alpha \tag{2.127}$$

The writing of this criterion in 3D has been expressed in different ways allowing to differentiate or not the mode II and the mode III of rupture:

$$G_C = G_{IC} + (G_{IIC} - G_{IC}) \left(\frac{G_{II} + G_{III}}{G_I + G_{II} + G_{III}}\right)^\alpha \tag{2.128}$$

$$G_C = G_{IC} + (G_{IIC} - G_{IC})\left(\frac{G_{II}}{G_I + G_{II} + G_{III}}\right)^{\alpha}\left(\frac{G_{II} + G_{III}}{G_I + G_{II} + G_{III}}\right)^{\alpha-1} + (G_{IIIC} - G_{IC})\left(\frac{G_{III}}{G_I + G_{II} + G_{III}}\right)^{\alpha}\left(\frac{G_{II} + G_{III}}{G_I + G_{II} + G_{III}}\right)^{\alpha-1} \quad (2.129)$$

Fig. 2.30 illustrates all these criteria in the plane (G_{II}, G_I).

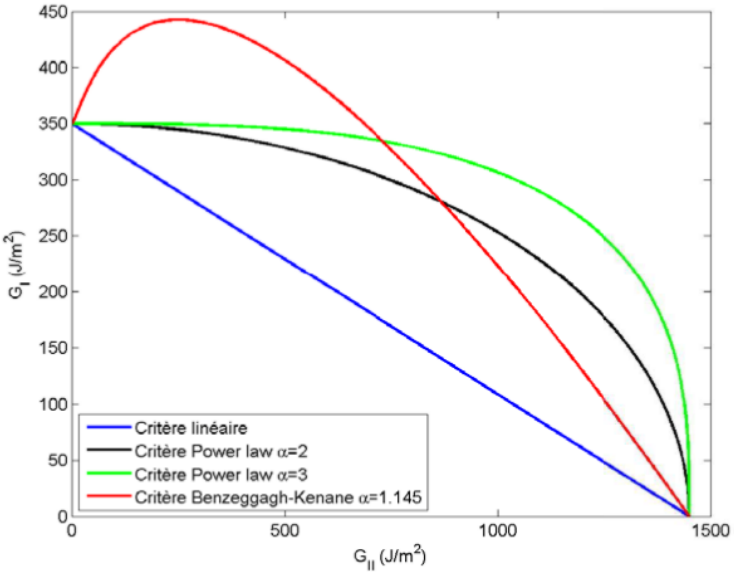


Figure 2.30: Presentation of different propagation criteria for G_{IC} = 350 J/m² and G_{IIC} = 1500 J/m² [78].

While this approach is simple to implement, quick to use and effective in determining delamination propagation, its use requires the presence of a crack in the structure. Thus, it has been used to study delamination failure in compression impact testing or stiffener debonding [89]. However, it does not allow the study of delamination initiation. Finally, the range of validity of this approach is limited to linear behaviour due to the assumptions of linear elastic fracture mechanics.

2.6.3. Cohesive zone elements

In order to study the initiation and propagation of delamination, an approach based on damage mechanics has been developed: cohesive zone models. These models were first proposed by Dugdale [90] to determine the plastic zone at the bottom of the notch. Subsequently, studies by Barenblatt et al. [91] refined the principle of cohesive zone models. This approach has been further developed, notably in works [92], [93] and used to study delamination in composite structures [94], [95].

Recently, H. Patrick et al. [96] have studied CFRP under bending load and investigated the effect of different parameters such as scaling techniques and failure models. Also, they incorporate the cohesive surface for simulate delamination where the non-linearity prediction of 45° and 90° lay-ups is improved. Cao et al. [97] examined intra-interlaminar failure in a curved composite laminated by incorporating cohesive elements into the intermediate finite elements within the 90 plies and along the ply interfaces, they have suggested an FE model for delamination and matrix failure. Y. Yang et al. [98] have investigated the behaviour of the composites laminated behaviour and compared the analysis results with the experiments tests which incorporated the cohesive zone method to simulate delamination.

The principle of cohesive zone models resides in the description of the relationship between the displacement jumps of two initially superimposed nodes and the associated cohesive loads via a softening law (Fig. 2.31).

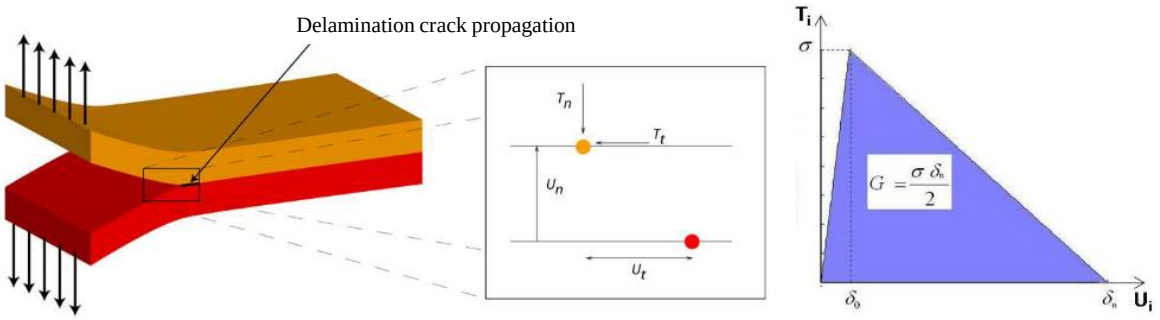


Figure 2.31: Principle of a cohesive zone model.

There are many forms of softening laws in the literature: bilinear [99], multi-linear, exponential [100], trapezoidal [90], polynomial [101], etc. Whatever the form of the law used, there are three parts (Fig. 2.32): (i) an increase in the interlaminar stress until a maximum is reached (PART I), (ii) a decrease corresponding to the loss of rigidity of the interface which becomes damaged (damage may appear from the first part of the curve) (PART II) and (iii) a cancellation of the interlaminar stress for a critical displacement jump, corresponding to the failure of the interface (PART III). For a stable and regular propagation, it has been shown that the description of the propagation is almost independent of the shape chosen for the cohesive zone. Note that these cohesive zone models therefore have a stress initiation threshold (usually linear or quadratic) which can be seen as a failure criterion and a propagation criterion from fracture mechanics. These models can therefore be related to bi-criteria approaches that are based on the same mechanisms. In this respect, the authors [102] have shown similarities between these two approaches.

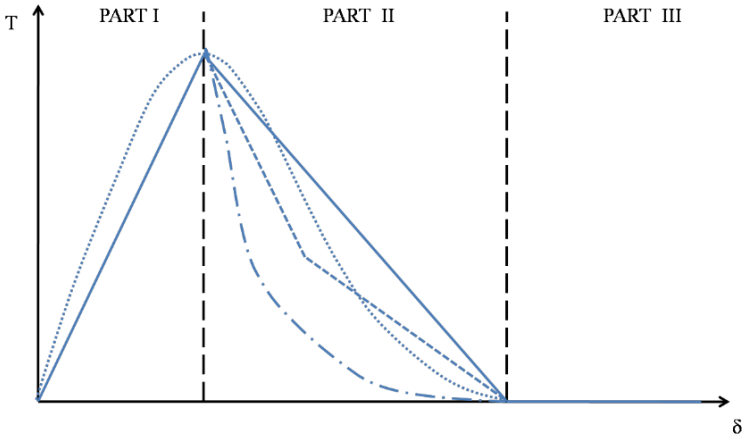


Figure 2.32: Description of the different parts, with several possible shapes, of a cohesive zone model.

Currently, the predominant computational approach for predicting delamination between plies in laminated composites relies on cohesive zone models. These models offer a comprehensive framework that combines strength-based and energy-based fracture models, providing a versatile solution for various applications where singular strength or energy criteria may not be adequate. By employing traction-separation laws, cohesive zone models effectively capture highly localized inelastic processes, connecting the cohesive traction transmitted along a discontinuity line or surface to the displacement jump characterized by the separation vector [103]–[105]. To address

different fracture modes, separate cohesive laws are utilized for opening mode I, and sliding and tearing modes II and III, respectively. This implies that the toughness and interfacial strength values differ for the three modes. Additionally, by following the approach proposed in [106], it is possible to assume the same cohesive law for shear modes II and III.

In order to model delamination by the cohesive zone models, the softening law equation is related to the two physical parameters of the interface, for each failure mode, which are: (i) the critical interlaminar stress σ_c and (ii) the toughness G_c. The toughness corresponds to the area under the traction/displacement jump curve. Thus, it is defined for the three failure modes by:

$$G_{IC} = \int_0^{\delta_{f,\ \text{mode I}}} \sigma_{33}(\delta) d\delta_3 \tag{2.130}$$

$$G_{IIC} = \int_0^{\delta_{f,\ \text{mode II}}} \tau_{13}(\delta) d\delta_1 \tag{2.131}$$

$$G_{IIIC} = \int_0^{\delta_{f,\ \text{mode III}}} \tau_{23}(\delta) d\delta_2 \tag{2.132}$$

To describe the propagation of mixed mode delamination, the propagation criteria, already presented in the section on linear elastic fracture mechanics, are used. However, the implementation of the propagation laws can be difficult depending on the model used. Also, in the literature, the Power Law criterion and the one proposed by Benzeggagh are generally associated with a bilinear form of the cohesive zone.

The simulation of interlaminar damage will be conducted using the cohesive zone approach, employing the Abaqus three-dimensional cohesive element COH3D8 at the interfaces between plies. The study focuses on the quasi-static regime. In the traction-separation law formulation, the cohesive zone is assigned a nonzero elastic stiffness. This choice is motivated by the reduced stiffness of the matrix-rich interface layer, which deviates from a perfect bond between the matrix and fibers. From a numerical perspective, this elastic stiffness can be viewed as a penalty-type enforcement of displacement continuity within the elastic range. Various guidelines have been proposed for determining the interface stiffness. Daudeville et al. [107] calculated the stiffness based on the interface thickness and elastic modulus. Camanho et al. [108] adopted a fixed value of $10^6\ N/mm^3$ for modelling graphite fiber/epoxy matrix laminates, which is a sufficiently large numerical parameter to ensure displacement continuity at the interface. Turon et al. [109] put forward the following relationship:

$$K = \alpha E_3 / t_{max} \tag{2.133}$$

The coefficient α, where α is significantly larger than 1, is incorporated into the relationship, along with t_{max} representing the greater thickness between the sub-laminates adjacent to the cohesive layer. The selection of α must consider the detrimental effects of relatively high stiffness values on both (i) the conditioning of the global stiffness matrix for implicit methods, and (ii) the critical time step for explicit methods. To meet these criteria, Turon et al. [109] proposed an α value of 50. For the damage initiation criterion in the cohesive zone model, a quadratic stress criterion is employed, as described in previous studies [80], [108], [110]. Mathematically, it can be expressed as follows:

$$\left(\frac{\langle\sigma_n\rangle}{f_I}\right)^2+\left(\frac{\sigma_s}{f_{II}}\right)^2+\left(\frac{\sigma_t}{f_{III}}\right)^2\geq 1 \tag{2.134}$$

Here, σ_n represents the stress in the pure normal mode, σ_s corresponds to the stress in the first shear direction, and σ_t denotes the stress in the second shear direction. The peak strength values in these respective directions are denoted as f_I, f_{II} and f_{III}. The relationship between these variables can be expressed as follows (based on Macaulay's symbol):

$$\langle\sigma_n\rangle=\sigma_n \quad \text{for } \sigma_n>0 \qquad and \qquad \langle\sigma_n\rangle=0 \quad \text{for } \sigma_n \leq 0 \tag{2.135}$$

As compressive normal stresses do not contribute to crack opening, they do not initiate crack propagation.

In the present work, the interlaminar damage model Benzeggah–Kenane criteria [88] have been adopted for damage evolution of the interface elements on the assumption of a critical energy release rate of mixed failure mechanisms. As shown below, the damage progression of the interface elements could be expressed.

$$G_{\mathrm{C}}=G_{\mathrm{IC}}+(G_{\mathrm{IIC}-}G_{\mathrm{IC}})\left(\frac{G_{\mathrm{II}}+G_{\mathrm{III}}}{G_{\mathrm{I}}+G_{\mathrm{II}}+G_{\mathrm{III}}}\right)^{\eta} \tag{2.136}$$

Parameters: $\{G_{\mathrm{II}}$, G_{II} and $G_{\mathrm{III}}\}$ related to the energy release rates of modes {I, II and III}, respectively. Also, $\{G_{\mathrm{IC}}$ and, $G_{\mathrm{IIC}}\}$ are related to the critical energy release rates of modes {I and II}, respectively, and η represent the Benzeggagh–Kenane criterion parameter.

2.7. Numerical modelling technique

Finite Element Method (FEM) simulations enable the modelling of complex structures, providing valuable information on displacements, strains, and stress components. These simulations, coupled with theoretical models and strength values, allow for progressive failure analysis. However, this task is not straightforward, as certain models require significant computational resources, leading to prolonged analysis times. Moreover, materials exhibiting softening behaviour often encounter convergence challenges, particularly in implicit finite element programs [76], where the Jacobian matrix loses positive definiteness. Despite these challenges, computational simulations offer cost-effective alternatives to characterize composite materials and facilitate material optimization processes.

The finite element model plays a crucial role in accurately representing composite materials. It should encompass the ply orientation, stacking sequence, thickness variation, and adequately capture the global stress field, through-thickness stress variations, local stress concentrations, and failure modes.

Abaqus/CAE, a comprehensive software package, offers built-in capabilities for composite modelling. Within Abaqus, users can define composite layups using three types of elements: continuum shell elements, conventional shell elements, and solid elements. The documentation for Abaqus [111] provides detailed information on the extensive list of solid 3D elements available.

When analysing composites using Abaqus, it is recommended to use solid elements when (i) transverse shear effects are significant, (ii) normal stress cannot be neglected, and (iii) accurate interlaminar stress analysis is desired. These considerations ensure a reliable representation of composite behaviour and enhance the accuracy of the simulation results.

Various approaches exist for modelling composite materials in finite element analysis, each offering different trade-offs between accuracy, versatility, applicability, and computational cost. Understanding the capabilities of these approaches can help users select the most suitable material representation and element type for their specific problem. The following overview provides insights into commonly available approaches, allowing users to make informed choices.

It is important to note that the presented approaches are applicable to both implicit and explicit finite element analysis. However, for distinguishing between these two analysis types and making an appropriate selection, Section 2.7.2 should be referred to.

By considering these factors and understanding the differences between implicit and explicit analysis, users can make informed decisions when choosing the modelling approach and analysis type that best align with their requirements and constraints.

2.7.1. Element type

In this thesis, three types of elements were utilized: conventional shell elements, continuum shell elements, and solid elements. Finite element analysis (FEA) offers a diverse range of elements not only for stress analysis in laminates and laminate structures (2D or 3D), but also for the analysis of residual stresses and delamination. The following summary outlines the capabilities and applicability of typical commercial element types for representing laminates.

The initial consideration when selecting an appropriate element type is determining how the local thicknesses of the laminate structure should be represented in the finite element (FE) model. For geometries with small thicknesses relative to their lateral extension, it may be advantageous to simplify the geometry to its mean surface, resulting in a locally 2D flat representation without a geometric extension in the through-thickness direction. In this case, the local thickness of the structure is treated as a material parameter. Alternatively, the local thickness of the structure can be retained in the discretized geometry, leading to a fully three-dimensional FE representation of the structure. This decision regarding the geometric representation of the structure has an impact on the choice of element types described below, as well as the suitable material definition method.

2.7.1.1. Shell vs. Continuum Elements

In the computation of FRPs (Fiber Reinforced Polymers), two types of elements are commonly used: 2D (shell) elements and 3D (continuum or solid) elements, as shown in Fig. 2.33. Selecting the appropriate element type for the analysis is not a straightforward decision. A crucial factor in the element selection process is the stress state within the component. When a two-dimensional stress state cannot be assumed, the use of continuum elements becomes necessary. Solid elements are particularly suited for accurately capturing stresses in the out-of-plane direction (σ_3, τ_{23} and τ_{13})[112].

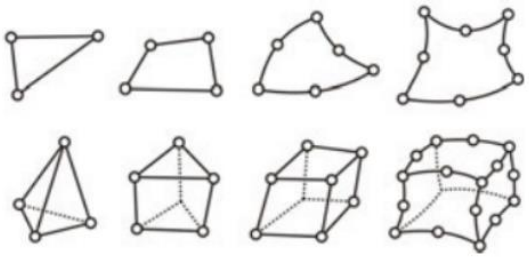


Figure 2.33: Upper row: 2D elements, lower row: 3D elements. Quadratic elements feature an extra node along each edge of the element.

Another general guideline is that if the slenderness ratio of a composite (ratio between length and thickness of the part) exceeds 5 to 7, there is no need for discretization using solid elements. In such cases, continuum elements can be used instead. While continuum elements offer greater accuracy compared to the 2D approach due to their increased number of nodes, they also result in higher computational costs. Therefore, the analysis engineer must strike a balance between computation time, number of nodes, accuracy, and costs to find the optimal solution.

In load application areas, three-dimensional stress states are commonly encountered. In cases where these areas are subjected to high loads, a three-dimensional approach becomes necessary. However, to manage costs without compromising accuracy, a cost-effective strategy is to perform a global analysis using the two-dimensional approach, and subsequently run smaller sub models using solid elements on specific regions of interest. This approach proves beneficial when the geometry is sufficiently large, allowing significant time savings with the 2D model.

2.7.1.2. Solid element

Solid continuum elements are typically not recommended for discretizing geometries with small thicknesses compared to their lateral extension due to the requirement of maintaining balanced spatial proportions for accurate results. This often necessitates a lateral discretization density equal to or greater than the lamina thickness, which can be computationally expensive. However, the use of solid continuum elements for representing laminate structures offers distinct advantages. Unlike other element types, solid continuum elements do not rely on axiomatic assumptions about displacement, stress, or strain fields. As a result, the results are expected to converge as the number of elements stacked in the z-direction increases. Furthermore, solid continuum elements provide valuable information such as through-thickness stress (σ_z) and strain components (ε_z), making them particularly suitable for conducting comprehensive 3D failure and post-failure analyses, especially in the context of generalized laminate behaviour (see Chapter 5).

Another unique feature of solid continuum elements is their ability to reproduce orthotropic material behaviour, similar to continuum shell elements. These elements have three translational degrees of freedom for each node, and they are available in linear and quadratic variants, with the number of nodes depending on the element shape (8 or 6 for linear elements, 20 or 9 for quadratic elements). In contrast to shell elements, solid elements are capable of accurately predicting transverse compression or tension. Therefore, when transverse loading is present in the model, such as in load application areas, the use of solid elements becomes indispensable.

2.7.1.3. Shell elements

Shell elements are the preferred choice for representing geometries with small thicknesses compared to their lateral extension. These elements are specifically designed to discretize locally two-dimensional structures without any significant expansion in the thickness direction. In the case of shell elements, the thickness information of the structure is incorporated into the material definition.

There are two types of shell elements available: one based on Kirchhoff kinematics, which is suitable for thin structures, and another based on Reissner kinematics, which is applicable to thick structures. The Reissner kinematics formulation takes into account through-thickness shear

contributions resulting from bending deformation, providing a more accurate representation of the behaviour of thick structures.

In a three-dimensional modelling space, thin shell elements possess three translatory degrees of freedom

$$\bar{u} = [u_x, u_y, u_z], \tag{2.137}$$

but only two rotatory degrees of freedom r_x and r_y. These elements are capable of evaluating the in-plane strain components $\varepsilon_x,\ \varepsilon_{y,}\ and\ \gamma_{xy}$.

On the other hand, thick shell elements offer a complete set of translatory degrees of freedom $\bar{u}$ and rotatory degrees of freedom $\bar{r}$, allowing for the inclusion of through-thickness shear strains γ_{xz} and γ_{yz}. In both cases, the governing differential equations only consider the in-plane stress components σ_x, σ_y and τ_{xy}. Consequently, these quantities are the results obtained through the solution derived from the Principle of Virtual Displacement (PVD). Additionally, Abaqus provides postprocessed results of through-thickness shear stress τ_{xz} and τ_{yz}, which are obtained by applying the equilibrium equations.

$$\frac{\partial \sigma_x}{\partial x} + \frac{\partial \tau_{yx}}{\partial y} + \frac{\partial \tau_{zx}}{\partial z} = 0 \tag{2.138}$$

$$\frac{\partial \tau_{xy}}{\partial x} + \frac{\partial \sigma_y}{\partial y} + \frac{\partial \tau_{zy}}{\partial z} = 0 \tag{2.139}$$

$$\frac{\partial \tau_{xz}}{\partial x} + \frac{\partial \tau_{yz}}{\partial y} + \frac{\partial \sigma_z}{\partial z} = 0 \tag{2.140}$$

Stress σ_z and strain components ε_z in the through-thickness direction are not directly output when using shell elements. Typically, boundary conditions are applied to the mean surface of the shell element. However, in some advanced FEA packages, it may be possible to apply boundary conditions to the outermost integration points in the z-direction, allowing for a continuous displacement field over bi-material interfaces in a stacked shell discretization.

If this capability is not available, it is not recommended to stack shell elements for representing laminates and laminate structures. Consequently, a layer-wise material representation is also not advisable in such cases.

In Abaqus, there are two main categories of shell elements available:

• Conventional Shell Elements

• Continuum Shell Elements

Conventional shell elements are suitable for representing two-dimensional geometries in a three-dimensional space. On the other hand, continuum shell elements encompass both thick and thin shell elements, such as S8R5 and S8R, respectively. These elements are equipped with 5 degrees of freedom (DOF) per node for thin shell elements and 6 DOF per node for thick shell elements.

Thin shell elements enforce the Kirchhoff constraints, resulting in the transverse shear deformations γ_{13} and γ_{23} being set to zero. In contrast, thick shell elements employ the First-order Shear Deformation Theory (FSDT) to provide more accurate predictions of transverse deformations. This requires specifying input values for the transverse shear stiffness.

Continuum Shell (CS) elements, such as SC6R and SC8R, are classified as solid elements and therefore require a three-dimensional (3D) geometry. These elements employ additional nodes to represent the thickness of the shell. Each node in these elements possesses only three degrees of freedom (DOF) for translation, enabling them to be stacked and connected to standard solid elements.

CS elements adhere to the First-order Shear Deformation Theory (FSDT), ensuring a constant thickness throughout the element. Unlike conventional shell elements, continuum shell elements lack rotational DOF and are only available with reduced integration. This characteristic makes them susceptible to a phenomenon known as "hourglassing." To address this issue, Abaqus implements hourglass control measures for these elements.

Each continuum shell element is defined by eight nodes, as opposed to conventional shells where only the mid-plane surface is defined. The integration point is situated in the middle of the element, as illustrated in Fig. 2.33. Additionally, continuum shell elements employ a finite strain formulation to accurately capture material behaviour.

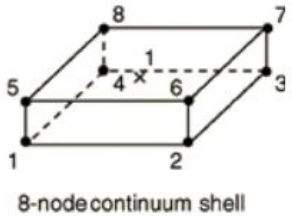


Figure 2.34: Continuum shell elements SC8R.

Continuum shell elements utilize the same section specification as conventional shell elements, employing integration schemes like Gauss quadrature or Simpson's rule. These integration points span the thickness of the element, allowing for the calculation of transverse shear stresses and the shear correction factor, which is analogous to the procedure followed for conventional shells. In the case of unidirectional bending along one axis, the strain energy is equated.

The primary advantage of continuum shell (CS) elements over solid elements lies in their ability to avoid aspect ratio problems. As previously mentioned, CS elements can be stacked, and as the number of stacked elements increases, the accuracy of transverse shear predictions approaches the exact analytical solution [112]. For composite materials with relatively low in-plane shear modulus, it is advisable to model them as thick shells. This can be accomplished using conventional shell elements like S3R, S3RS, S4R, S4RS, S4RSW, S8R, or continuum shell elements like SC6R and SC8R if a more accurate prediction of transverse shear deformation is required.

2.7.2. Numerical solution

The choice between implicit and explicit finite element analysis (FEA) does not have a significant impact on the representation of laminates and laminate structures. However, it becomes relevant when implementing user-defined materials. The progressive damage model employed in this thesis focuses on predicting material behaviour in the quasi-static domain, where factors such as time, velocity, and inertia are not considered in the material models and related analyses (unlike in the dynamic domain). In the context of nonlinear FEA, this scenario is typically associated with an implicit solution of the equation systems.

The distinction between implicit and explicit solution strategies for differential equations is fundamental, not just in terms of mathematical approaches [113]. The choice between them is left to the user and has a significant influence on the accuracy and computational costs of the FEA. In quasi-static analyses, the integration steps are commonly referred to as time increments, although their interpretation is implicitly reduced to load increments.

Both implicit and explicit processes employ a numerical time integration scheme to determine the unknown displacement solution at the end of each time step. This displacement solution serves as the foundation for calculating the resulting strains and stresses. Explicit integration schemes, such as the Central Difference method [114], assume a linear variation in displacement throughout each time step. They compute the displacements at the end of the time step using the state variables, which encompass the material description in the case of damage analysis, at the beginning of the time step. The updated state variables are then utilized to calculate the subsequent time step. This procedure involves a linear extrapolation based on the material's tangent moduli and, in dynamic scenarios, the velocity and acceleration at the start of the time step.

Implicit integration schemes, such as the Newmark Forward Differencing method [115], assume a constant average load increase and, in dynamic scenarios, a constant acceleration throughout each time step. At the end of each time step, the governing equation is evaluated using the actual state variables.

The main distinction between implicit and explicit algorithms lies in the treatment of the structural stiffness matrix. The implicit solution method requires a matrix inversion of the stiffness matrix, while the explicit solution method does not. However, it's important to note that the implicit scheme is unconditionally stable for large time steps, whereas the explicit scheme is only stable if the time step size is smaller than the critical time step size specific to the simulated structure. The undamped critical time step size is typically a very small value, around $2/w_{max}$, where w_{max} represents the largest natural circular frequency. This requirement for a small-time step size in the explicit scheme makes it suitable for short transient situations. Despite potentially having a significantly higher number of time steps compared to the implicit scheme, the explicit solution can still be more computationally efficient since it doesn't involve matrix inversion.

It should be emphasized that neither the implicit nor the explicit solution is universally superior in all cases. The choice between the two depends on factors such as the stability requirements, the nature of the problem being solved, and the desired computational efficiency.

When considering the implementation of degrading material behaviour, the explicit and implicit approaches differ in their requirements for the material user subroutine. In the explicit approach, the definition of the material's constitutive behaviour in terms of tangent moduli is essential. However, in the implicit approach, this requirement does not exist.

For implicit analysis in Abaqus, an acceptable solution is obtained by making an initial guess for the displacement field at the end of the time step, referred to as an "attempt" within Abaqus. Based on the actual constitutive behaviour associated with this guess, the solver evaluates whether the equilibrium equations are satisfied within specified tolerances. If the equilibrium is not met, the guess is adjusted accordingly.

Both the original guess and the subsequent corrections are based on the material's Jacobian matrix, which is calculated at the end of the previous time increment or attempt. This matrix defines the change in resulting stress component increments for each change in individual strain components. In both the explicit and implicit cases, the definition of these stiffnesses is crucial. For

increments $\partial\Delta\bar{\sigma}/\partial\Delta\bar{\varepsilon}$, it effectively contains information corresponding to the tangent explicit approach. The accuracy of the tangent stiffnesses directly affects the accuracy of the results in the explicit case. However, in the implicit case, the quality of the stiffness definition only influences the quality of the guesses and the convergence process, but not the solution itself.

2.8. Numerical implementation

In this section, we focus on the implementation of the research objectives within the commercial FE software Abaqus. However, one of the main goals of this study is to expand the capabilities of simulating failure scenarios for laminated composites beyond the failure models currently available in Abaqus. Abaqus/CAE provides interfaces that enable users to incorporate general constitutive equations.

To simulate progressive material damage in laminated composite structures using Abaqus, a user-defined material subroutine called Umat can be utilized. This Umat subroutine, written in FORTRAN, incorporates the Puck and Schürmann failure criteria along with a gradual degradation model for composite laminates. In order to numerically implement the PFA (Progressive Failure Analysis) model, Abaqus requires the user to provide the Umat subroutine along with a specific input file. It should be noted that the current version of Abaqus/CAE is limited to Hashin's failure criteria.

2.8.1. Umat subroutine

The user-defined material behaviour subroutine (Umat) presented here is specifically designed for explicit finite element analyses (FEAs) and encompasses all the components of Puck's Theory for fiber fracture, inter-fiber fracture prediction, determination of plane fracture angle, and gradual degradation rules in both 2D and 3D scenarios.

The primary objective of the Umat subroutine is to provide the following:

- ✓ The corresponding stress state for a given strain input.
- ✓ The relevant parameters and state variables associated with Puck's failure theory.
- ✓ The Jacobian matrix ($\partial\Delta\sigma/\partial\Delta\varepsilon$) for all stress and strain components, capturing their interdependencies.

2.8.2. implementation via Umat in Abaqus

Fig. 2.35 illustrates the flow chart of the integration between the Umat subroutine and Abaqus™ for progressive failure analysis. This process involves a series of iterations to calculate the stress state, update the material model variables, and assess the occurrence of failure modes. The integration starts by invoking the Umat subroutine for each finite element integration point and lamina at every analysis time step.

The primary purpose of the Umat subroutine is to determine the material model state variables and the strain tensor for the current step (step 1 in Fig. 2.35). These variables are essential for subsequent calculations. Once the material model variables and strain tensor are identified, the Jacobian matrix, which represents the sensitivity of stress with respect to strain, is computed. With this matrix, the stress state is predicted (step 1 in Fig. 2.35). Subsequently, the calculated stress state is evaluated using the damage model implemented through Umat (step 2 in Fig. 2.35).

The damage model assesses the extent of material degradation or failure. If any failure mode occurs, the damage variables are updated accordingly (step 3 in Fig. 2.35). These variables reflect

the level of damage or failure in the material. After the update, the state variables are modified based on the damage variables and passed to the next step to update the stress tensor. If failure does not occur, the predicted stress state is considered accurate. In this case, a Residual (R) is calculated as the difference between the internal and external force vectors. The magnitude of R is compared to a tolerance threshold set by the user. If R is lower than the tolerance value (e.g., 0.005 which is adequate for engineering applications [111]), indicating convergence, a new load step is applied, and the analysis continues. However, if R exceeds the tolerance threshold, Abaqus^{TM} stops the numerical analysis as the solution process has diverged.

Divergence typically occurs when the material properties exhibit significant degradation, and the structure lacks sufficient strength to withstand the applied loads. Localization problems can arise due to abrupt reductions in material properties. The density of the finite element mesh also plays a crucial role in handling such situations. Additionally, it is important for the material model assumptions to be physically consistent to avoid incoherent predictions.

In summary, the integration between Umat and Abaqus^{TM} for progressive failure analysis involves iterations to calculate the stress state, update the material model variables, and assess failure modes. This process allows for the simulation of material degradation and structural response under varying loads, providing valuable insights into the behaviour of complex systems.

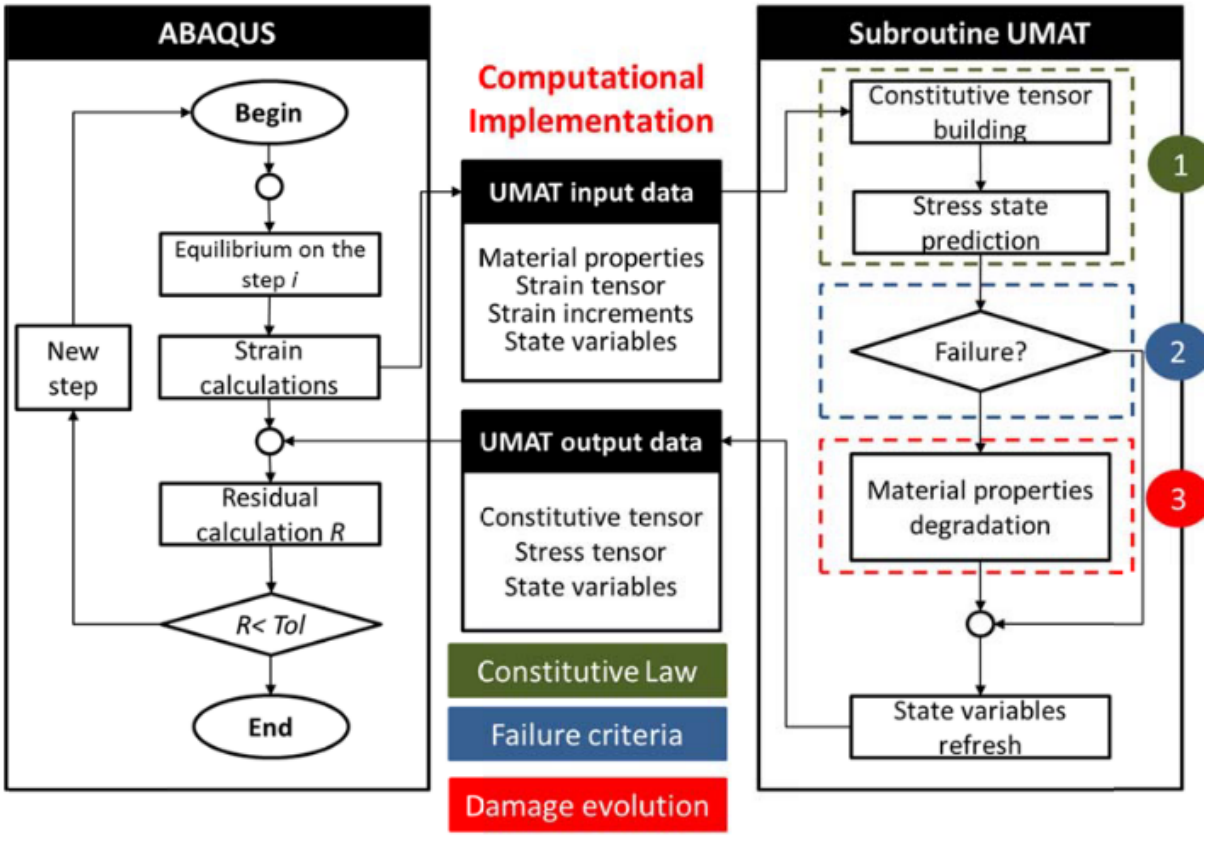


Figure 2.35: Flow chart for AbaqusTM and Umat integration.

2.9. Conclusion

This chapter has provided a comprehensive overview of composite materials and their behaviour. It covers the definition of composite materials, their areas of use, classification, and design rules for parts based on laminates. The chapter discusses the failure analysis of laminated composite

structures, which shows that the first damage mode generally observed in experimental tests is matrix failure in the layer misaligned with the loading axis. In contrast, fiber failure is considered a total failure of the layer as it results in a catastrophic drop in stiffness. Whereas, delamination can be coupled with the other two failure modes and is due to a three-dimensional stress state because of the low out-of-plane strength of the laminates.

Following the discussion on failure analysis, we delved into the various failure criteria associated with the intra/interlaminar damage process. We highlighted the applicability and limitations of each criterion and the importance of selecting the appropriate one based on the nature of the damage and the material under consideration. Additionally, we discussed numerical modelling techniques used to simulate and analyse the behaviour of composite laminates. This included a detailed explanation of the element types and numerical solution methods used to achieve accurate and reliable results.

The knowledge gained from this chapter can be used to improve the performance and reliability of composite laminates in various industries and unlock the full potential of composite materials for innovation and competitiveness.

Chapter 3: Progressive failure analysis of composite laminates under tensile loading

Overview

- *Introduction*
- *Computational analyse procedure*
- *Results and discussion*
- Conclusion

3.1. Introduction

In the first place, the study of problems of plane stress in thin composite laminates using progressive damage analysis under tensile loading is crucial for understanding the behaviour of composite materials and designing reliable and efficient structures. Composite materials are widely used in industries such as aerospace, automotive, and marine due to their high strength-to-weight ratios and durability. For example, in the aerospace industry, composite materials are used in aircraft structures such as wings, fuselage, and tail sections.

Progressive damage analysis is a powerful tool that can be used to predict the strength and stiffness of composite laminates under tensile loading and identify areas prone to damage and failure. This information can be used to optimize the design of composite structures to improve their durability and fatigue life, leading to cost savings and improved product quality. For example, if a composite structure is subjected to cyclic loading, such as during take-off and landing of an aircraft, progressive damage analysis can help identify areas of the structure that are prone to fatigue damage and failure. Furthermore, the impact of studying problems of plane stress in thin composite laminates using progressive damage analysis under tensile loading is significant in the industry sector, where it can help enhance overall competitiveness. By using progressive damage analysis, engineers can optimize the design of composite structures to improve their performance and efficiency. For instance, by identifying areas of high stress in a composite structure, engineers can add more material or increase its thickness in those areas to improve its strength and stiffness. This can lead to lighter and more efficient designs, reducing manufacturing costs and making the product more competitive in the market.

Besides, matrix cracking and fiber damage are two main damage modes within the thin composite laminates. The damage mechanism has been analysed for decades since transverse matrix cracking and fiber damage reduce the effective stiffness and strength of laminates. They also provide easy access for moisture or other leaking fluids. It has been suggested in the literature that the primary damage mode in the laminate is usually transverse matrix cracking when a laminate experiences mechanical loading. After sufficient number of matrix cracks have developed in the laminate, fiber damage starts to initiate from the tip of matrix cracks where local stress concentrations exist and propagate across the laminate. In other words, the density of matrix cracks increases until a certain value known as saturation crack density, and the secondary damage mechanism may change to fiber damage induced by transverse cracks.

Various failure criteria have been developed to predict damage initiation in composite laminates [35], [116]–[118], but traditional criteria like maximum stress/strain or Tsai-Hill fail to separate intralaminar failure modes. Hashin's failure criteria, proposed in 1980 [38] , address this issue by distinguishing between fiber and matrix failure based on the fracture plane's orientation. Puck's failure theory, an extension of Hashin's criteria, has been widely validated through experiments and numerical analysis [3], [5], [30], [31], [119], making it a preferred choice for accurately describing laminate degradation. Despite its complexity and limited commercial software support, Puck's criterion is crucial in industries like wind turbine blades, aeronautics, and construction sectors where precise estimation of fiber and matrix failure is necessary for design and fabrication.

In this chapter, various evaluation methods for the initial and progressive failure of different open-hole composite laminated have been proposed and assessed based on several failure criteria (Puck and Hashin) and coupled with damage mechanics (Discount methods and continuum damage mechanic), respectively (See chapter 2).

On one hand, the interest in studying progressive failure in open-hole composite laminates is primarily to improve the understanding of how these structures behave under load and to develop more reliable and safer composite structures. Open-hole composite laminates are commonly used in aerospace and other industries where high-performance and lightweight structures are required. However, these structures are also susceptible to failure, especially at the hole locations where stress concentrations can be high. Therefore, understanding the progressive failure mechanism in open-hole composite laminates is crucial for designing more robust and safe structures.

On the other hand, finite element analysis (FEA) is a powerful tool that can be used to simulate the progressive failure of open-hole composite laminates. However, there are several challenges associated with FEA modelling of composite structures, including:

- Accurately modelling the composite material behaviour, including its anisotropic properties, damage initiation, and propagation mechanisms.
- Accounting for the interaction between the composite material and the hole geometry, which can significantly affect the stress distribution and failure mechanism.
- Developing appropriate failure criteria to predict the onset of damage and the subsequent progression of damage in the composite structure.
- Considering the impact of manufacturing defects, such as voids or delamination, on the overall performance and reliability of the composite structure.

Overcoming these challenges requires a deep understanding of the underlying physics of composite materials and the ability to accurately model the complex interaction between the material and the hole geometry. It also requires access to advanced simulation tools and techniques, as well as extensive experimental validation to ensure the accuracy and reliability of the FEA models.

Accordingly, this study aimed to model the behaviour and the damage phenomenon in different composite laminates with several schemes under tensile loading while considering the effect of different stacking sequences, specimen sizes, stress concentration as well as the interactions between damage modes. Hence, a user-defined subroutine Material (Umat) has been successfully implemented, using finite element software Abaqus, through coupling all the presented parts of Puck's theory and gradual degradation methods (Constant stress exposure and Element weakening method) to enable accessible use of failure analysis. However, the analysis results comprise the prediction of the failure load, failure modes and load vs displacement curves which were compared to the experimental/numerical findings already provided in the literature as well as the study of the mesh dependency for a range of composite materials to assess the accuracy and applicability of the applied methods.

3.2. Computational analyse procedure

The following section provides a clear description of the computational analysis procedure using FEA, including the applied methods and the choice of materials utilized in the present work.

Hashin and Puck failure criteria (see section 2.3) have input stresses, strains and material properties for each element in order to predict the initial failure of composite laminates under tensile loading [9], [38]. Once the failure was detected, the material stiffness of the initially failed element was degraded following the aforementioned progressive failure methods. Those methods are the so-called element weakening method (EWM), the constant stress exposure method (CSE) and the method offered by Abaqus which is based on Matzenmiller's approach [55], [63], [64] (see section

2.4 and 2.5). It should be noted that, in the finite element software, problems may appear at the convergence level during the calculating of the failed elements. However, the elements should be degraded to a value close to zero and the damage variable values are updated depending on the failure mode. The application conditions for those methods are described in the previous section.

Table 3.1. Marking.

Symbol	Concept	Symbol	Concept
SDV1	Puck's fiber failure in tension	HSNFTCRT	Hashin's fiber in tension
SDV2	Puck's fiber failure in compression	HSNFCCRT	Hashin's fiber in compression
SDV3	Puck's matrix failure in tension	HSNMTCRT	Hashin's matrix in tension
SDV4	Puck's matrix failure in compression	HSNMCCRT	Hashin's matrix in compression
SDV6	Damage variable for fiber tensile	DAMAGEFT	Damage variable for fiber tensile
SDV7	Damage variable for fiber compressive	DAMAGEFC	Damage variable for fiber compressive
SDV8	Damage variable for matrix tensile	DAMAGEMT	Damage variable for matrix tensile
SDV9	Damage variable for matrix compressive	DAMAGEMC	Damage variable for matrix compressive

As a result, we have implemented the theory of the Puck failure criterion and the material stiffness degradation models, including both the EWM and the CSE, by using a user-defined subroutine Umat in the commercial FEA code (Abaqus). Besides, the solution dependence of state variables (STATEV) presents the failure index and damage variables for the failure modes in the mentioned UMAT. The concept of the symbols, within the UMAT subroutine as well as in the Abaqus model, has been displayed in Table 3.1. Also, the algorithm of computation for this case is presented in Fig. 3.1 below.

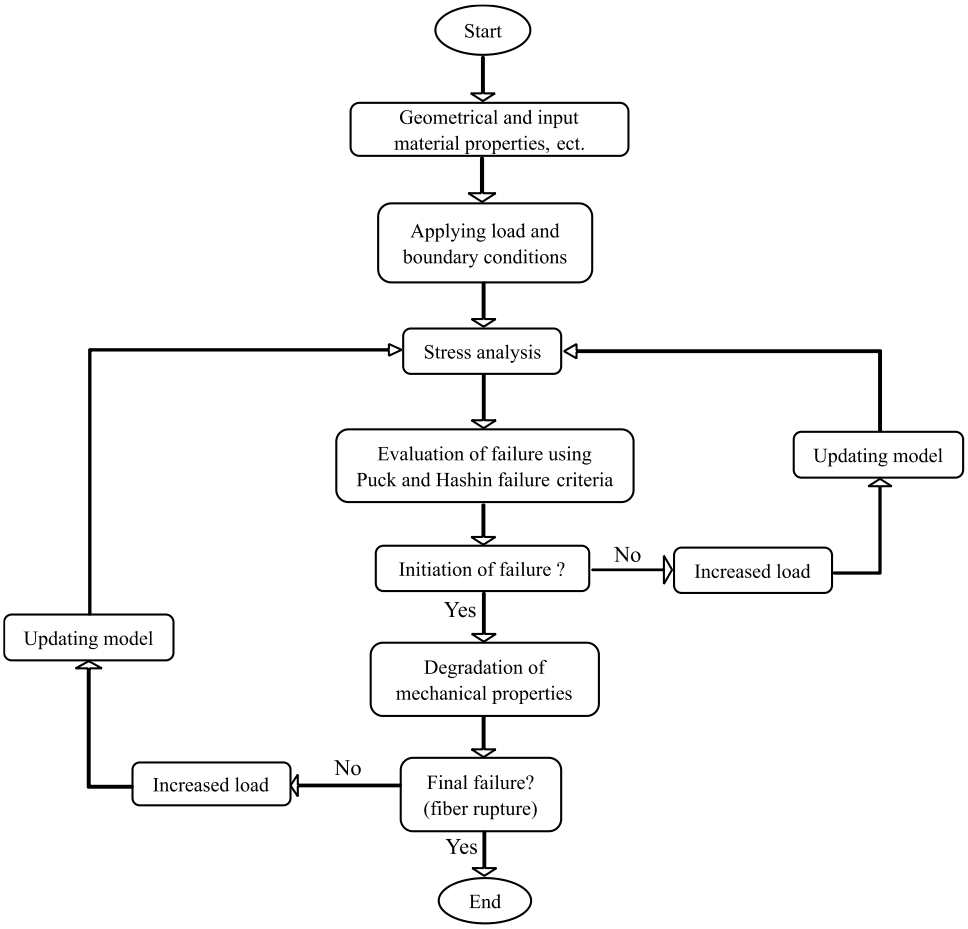


Figure 3.1: The computational algorithm used.

Both an initial failure analysis and a complete failure analysis were performed, as shown in this Fig. 3.1 above. Using the constitutive Eqs. ((2.63) – (2.71)), the stiffness matrix, strains and stresses are carried out for each element at every integration point in the material during the analysis. Once the onset of failure has been predicted, based on Hashin and Puck failure criteria in a single element using Eqs. ((2.11) – (2.14)) and Eqs. ((2.55) – (2.57), (2.61), (2.62)) respectively, the material stiffness was degraded in accordance with the following progressive failure models; EWM using Eqs. ((2.72) – (2.82)), CSE using Eqs. ((2.83) – (2.91)) and the model offered by Abaqus based on Matzenmiller's approach using Eqs. ((2.104) – (2.113)). Moreover, we repeatedly calculated the stresses and strains until the affected areas completely failed.

3.3. Results and discussion

3.3.1. T300/1034C Carbon/Epoxy composite laminates

To study the applicability and efficiency of the proposed methods, numerical simulations of the progressive failure of the composite laminates containing a central through-hole and is subjected to a uniform in-plane tensile load have been carried out. In addition, the analysis included the prediction of failure load, failure mode and the load-displacement curves in agreement with the aforementioned models. On the other hand, there are several experimental and numerical results available for an open-hole composite laminate under in-plane loading as Chang's research team, Tan et al., Chen et al. and Miami et al.[47], [53], [120], [121] were selected for validating the methods proposed.

3.3.1.1. Composite laminates with an open-hole

The laminate samples considered in this study are composed of T300/1034C carbon/epoxy composite plies. The dimensions and geometry are presented in Table 3.2 and Fig. 3.2, respectively. Using the function already available in Abaqus "composite layup", we modelled the laminated composite with three integration points through the thickness for each ply. Since the laminates and load are symmetrical, only one-quarter of the laminate is simulated.

In addition, the FE model boundary conditions of a quarter laminate considered along the x and y symmetry planes are shown in (Fig. 3.3). For this reason, all nodes on the vertical centreline cannot move in the horizontal direction (x). Similarly, as well as the nodes on the horizontal central line cannot move in the vertical direction (y). The laminate has been subjected to the controlled load by tensile displacement. To simulate it, a linear constraint equation was employed at the loading surface with displacement-controlled loading being applied at a reference point (RP) and is appointed to the left lower corner of the loaded surface.

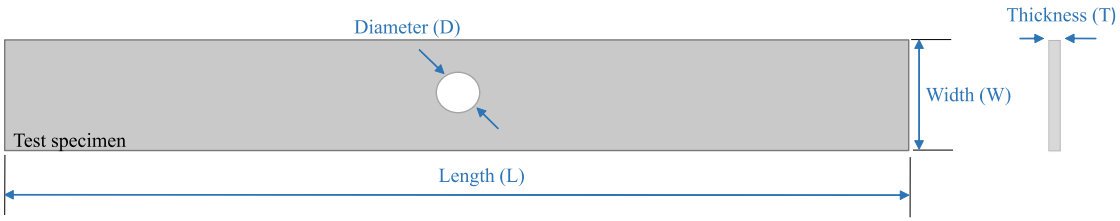


Figure 3.2: Geometrical of T300/1034C test specimen.

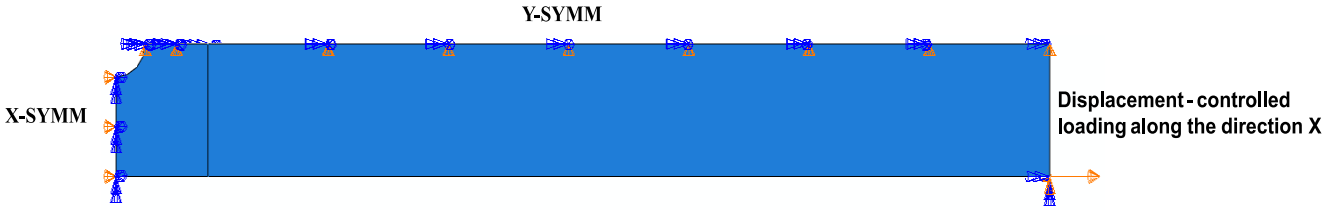


Figure 3.3: Loading and boundary conditions for T300/1034C composite laminates.

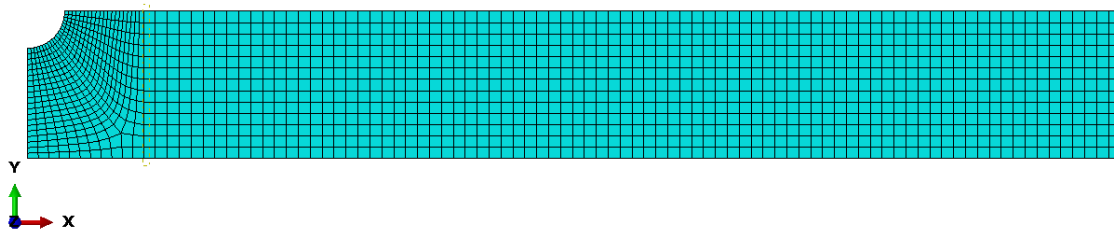


Figure 3.4: One-quarter of the finite element model of open-hole laminate.

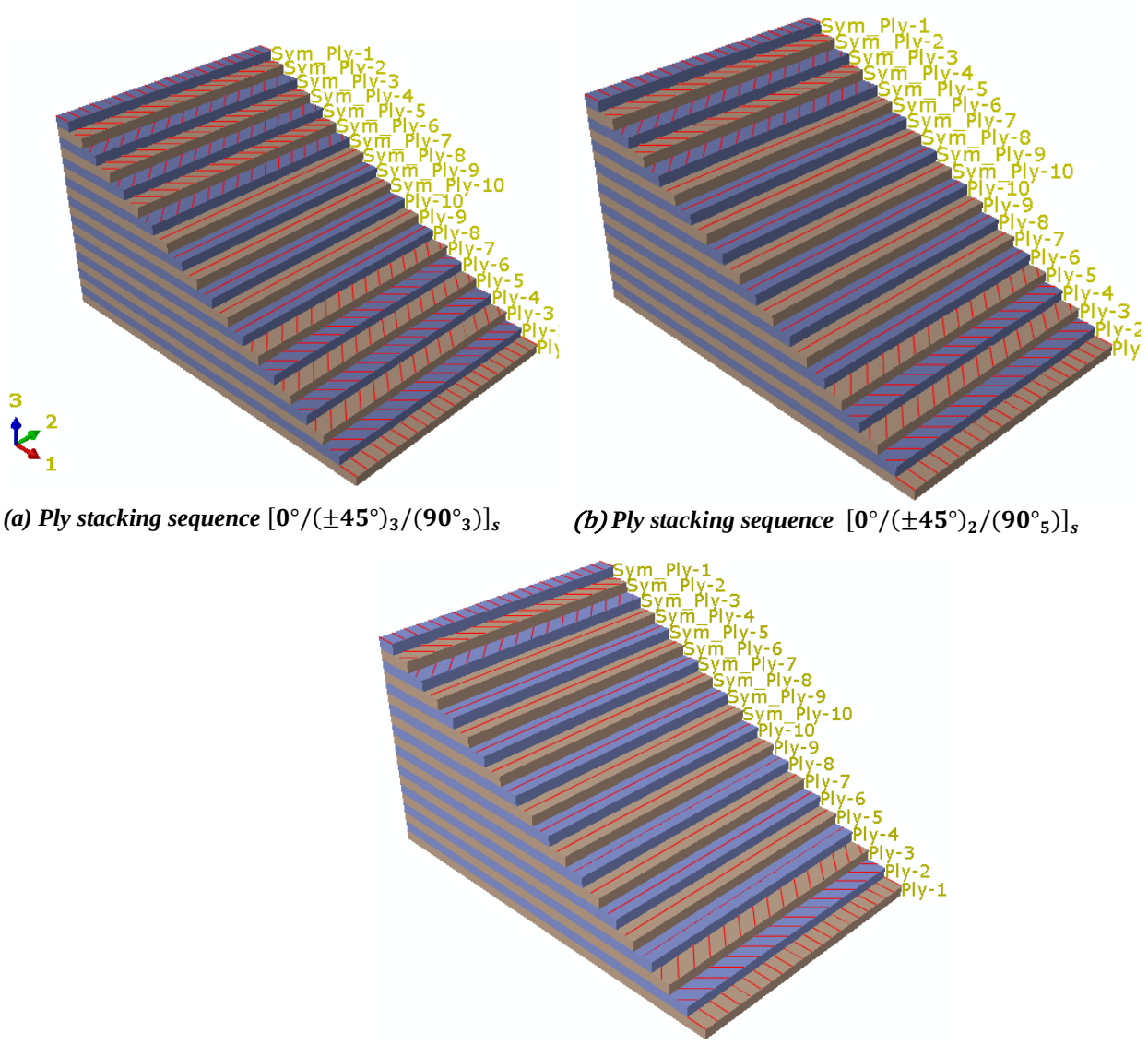
Table 3.2. Dimensions of the specimen used in this study.

Label	Length (mm)	Thickness (mm)	Width (mm)	Diameter (mm)
D	203.2	2.616	25.4	3.175

Table 3.3. Material properties of T300/1034C test specimens.

Properties	T300/1034C
$\mathbf{E_{11}}$ (GPa)	146.8
$\mathbf{E_{22}}$ (GPa)	11.4
$\mathbf{G_{12}}$ (GPa)	6.1
$\boldsymbol{\nu_{12}}$	0.3
$\boldsymbol{\nu_{23}}$	0.3
$\mathbf{E_f}$ (MPa)	230,000
$\boldsymbol{\nu_{f12}}$	0.2
$\mathbf{X_T}$ (MPa)	1730
$\mathbf{X_C}$ (MPa)	1379
$\mathbf{Y_T}$ (MPa)	66.5
$\mathbf{Y_C}$ (MPa)	268.2
$\mathbf{S_{12}}$ (MPa)	58.7
$\mathbf{G_{1t,c}}$ ($\mathbf{N/mm}$)	89.83
$\mathbf{G_{1c,c}}$ ($\mathbf{N/mm}$)	78.27
$\mathbf{G_{2t,c}}$ ($\mathbf{N/mm}$)	0.23
$\mathbf{G_{2c,c}}$ ($\mathbf{N/mm}$)	0.76

The purpose of that is to ensure that the displacements would be uniform across all nodes on that loaded surface and the reference point RP. As a result, the reaction force and displacement of the surface can be obtained at that reference node. As shown in (Fig. 3.4), the laminates have been modelled using continuum shell elements SC8R provided by Abaqus. Further details are provided in the following subsections.



(a) Ply stacking sequence $[\mathbf{0}°/(\pm\mathbf{45}°)_3/(\mathbf{90}°_3)]_s$ *(b) Ply stacking sequence* $[\mathbf{0}°/(\pm\mathbf{45}°)_2/(\mathbf{90}°_5)]_s$

(c) Ply stacking sequence $[\mathbf{0}°/(\pm\mathbf{45}°)_1/(\mathbf{90}°_7)]_s$

Figure 3.5: Plies stacking sequence with different cases and with identical thickness for T300/1034C composite laminate.

Besides, we used three different layers of materials that have been selected for the laminates $[0°/(\pm45°)_3/(90°_3)]_s$, $[0°/(\pm45°)_2/(90°_5)]_s$, $[0°/(\pm45°)_1/(90°_7)]_s$. Fig. 3.5(a, b, c) demonstrates the total stacking sequence in the Abaqus finite element model. Data on material properties, as well as the parameters of models used in finite element simulations, are listed in Table 3.3 and they have been extracted from the references [47], [122]. Likewise, the relevance of this selection was verified by comparing the load-displacement curve predicted, using these parameters with those suggested by the works of Maimi et al. [47] and Chen et al. [122].

3.3.1.2. Validation for failure load and the load-displacement curves

As mentioned in the previous section, two kinds of comparison approaches have been adopted for validating the proposed analysis methods that are the initial and the progressive failure of open-hole composite laminates under tensile loading. Furthermore, those approaches have been

predicted by comparing the failure load, failure mode and the load-displacement curves with the experimental and numerical tests that are indicated already in the literature.

Both failure criteria of Puck, Hashin and the degradations models of CSE, EWM and Matzenmiller's approach have been used for modelling the initial and the failure progression, respectively. As a result, we have predicted the failure load for an open-hole T300/1034C composite laminate and compared the results with those reported by the following references [47], [53], [120], [122] and the test data taken from Chang et al. [123].

The predicted results, using numerical modelling, are shown in Table 3.4. Moreover, to obtain the failure stresses σ_u we used the following formula $\sigma_u = P_u/WT$, where P_u is the failure load, T and W are the thickness and the width of the specimen, respectively.

Generally, geometric discontinuities such as holes have a weakness that quickly promotes their damage to structures. These structures are usually subjected to tension, which is among the most dangerous stresses, along with other loads that can undoubtedly accelerate their failure. During loading, the stacking sequence plays a determining role in the values of resistance and structural response that have been evaluated in this work.

Table 3.4. Comparison of the failure stresses of T300/1034C carbon/epoxy laminates (Label D).

Layup	**Failure stress (MPa)**							
	The applied models (Present Work)			**Data found in the literature**				
	PUCK + EWM	**PUCK +CSE**	**Built-in**	**Chen**	**Tan**	**Maimí**	**Chang**	**Test data**
$[\mathbf{0°}/(\pm\mathbf{45°})_3/(\mathbf{90°}_3)]_s$	214.9	243.37	187.26	238.30	248.21	263.1	179.26	235.80
$[\mathbf{0°}/(\pm\mathbf{45°})_2/(\mathbf{90°}_5)]_s$	171.01	196.42	173,034	205.83	158.58	200.1	151.68	185.47
$[\mathbf{0°}/(\pm\mathbf{45°})_1/(\mathbf{90°}_7)]_s$	133.94	149.45	103,87	135.67	199.95	148.2	103.42	159.96

Lay-up	**Error (%)**						
	The applied models			**Chen**	**Tan**	**Maimí**	**Chang**
	PUCK+EWM	**PUCK+CSE**	**Built-in**				
$[0°/(\pm45°)_3/(90°_3)]_s$	8.863	3.21	20.58	1.06	5.26	11.6	23.98
$[0°/(\pm45°)_2/(90°_5)]_s$	7.796	5.9	11,90	10.98	14.50	7.7	18.22
$[0°/(\pm45°)_1/(90°_7)]_s$	17.89	6.56	30,49	15.19	25.00	7.4	35.34

As shown in Table 3.4, the failure stresses predicted by different works are found to be different in many cases. This is because the prediction of the failing laminate and failure modes by different failure theories is usually not unique. Each time a failure is detected by a failure theory, the material

properties of the failing laminate degrade. Since the failure mode and the failing laminate may differ between failure theories, material degradation is applied to each failure theory separately.

The Built-in model in Abaqus, cannot perfectly predict the failure load of the three-layup used in this study and has a higher error compared to the test result. On the other hand, both PUCK+CSE and PUCK+EWM have a good results and are more accurate than the computational predictions made by Chang et al. [53]. However, PUCK+EWM has a precision less than PUCK+CSE. This is explained by the accurate prediction of Puck's theory for the fibers and matrix in Fiber Reinforced Polymer (FRP) compared to Hashin's theory.

Because the prediction of the final load is quite complex, a more accurate prediction of damage is difficult. This problem is attributed to many reasons, among which we find progressive failure models and failure criteria that, for the most part, do not take into account realistic phenomena that can appear during the damage process and that could have an effect on it, such as micro-defect pointed and material heterogeneity at the microstructure scale. In addition, the importance of the in-situ effect has been neglected; the adjacent lamina of a broken ply has a supporting effect, where the actual strength of an embedded ply is higher than that of an individual lamina. Neglecting the in-situ effect leads to a more conservative analysis of the laminate. Further investigations about the in-situ can be found in [124]. Moreover, the interlaminar damage between adjacent layers (i.e., delamination) has been ignored even if it has a small effect on the mechanical behaviour of composite laminates. The different results between the Built-in model, PUCK+CSE and Puck+EWM are due to the different criteria and damage degradation models to capture the occurrence and propagation of failure, respectively.

For Puck's criterion being one of the most accurate, Puck pointed out the importance of knowing the fracture angle of the fracture plane where it was incorporated into this analysis code unlike the Hashin criterion included in Abaqus. Furthermore, regarding the degradation properties of the lamina, the discount methods such as CSE and EWM have the ability to track stiffness degradation during laminate failure, where the lamina’s stiffness parameters are reduced according to their stress exertion. Therefore, according to the discount methods, the residual stiffness of ply is taken into account, unlike the continuum damage mechanics where Matzenmiller’s approaches based on it neglect this factor.

Moreover, the results presented by Chang et al. and Tan et al. differ significantly from the experimental result. However, Tan et al. have used an explicit formulation of damaged laminates where it is apparent that it has a strong dependence on the laminate that contains the damaged layer. As a result, this leads to significant limitations in the formulation of laminate stiffness relationships after the first layer failure and could influence the predicted failure load, this explains the errors in the outcomes obtained where the error rate ranges from 5.26–25% [120].

The predicted results found by Chang et al., who produced one of the first damage progression models and consider the in-plane damage modes, underestimated the ultimate load by approximately 18–35.34%. They have incorporated an empirical law, that is identical for all the damage mechanisms and is performed by adjusting the material properties of the damaged material to zero within a set number of time steps [53]. This approach is quite unreliable as the post-failure behaviour is entirely unaccounted for.

It can be seen that the estimated relative error in the prediction of Chen's model [122] increases with the increase in the number of plies with [90°] in the laminates. This could indicate the inexact prediction of matrix failure using the Hashin failure theory.

The failure load of the first degraded ply and ultimate failure load of the composite laminated depend upon the type of layup configuration, boundary conditions, material and the geometry of the composite laminate. Based on the above results, it was observed that the strength of the laminate is slightly reduced by placing the 90° plies adjacent to the laminate mid-plane. As a result, the ultimate load-carrying capacity of the laminated composite is influenced significantly by the ply orientation and stacking sequence.

3.3.1.3. Analysis results and discussions for progressive failure and load-displacement curves

Figs. (3.6 – 3.8), to evaluate load-displacement behaviour, illustrate the prediction of the tensile results of the open-hole composite laminates from label D. using the models proposed in this work and those reported by J. F. Chen et al. [122] and Maimí et al. [47].

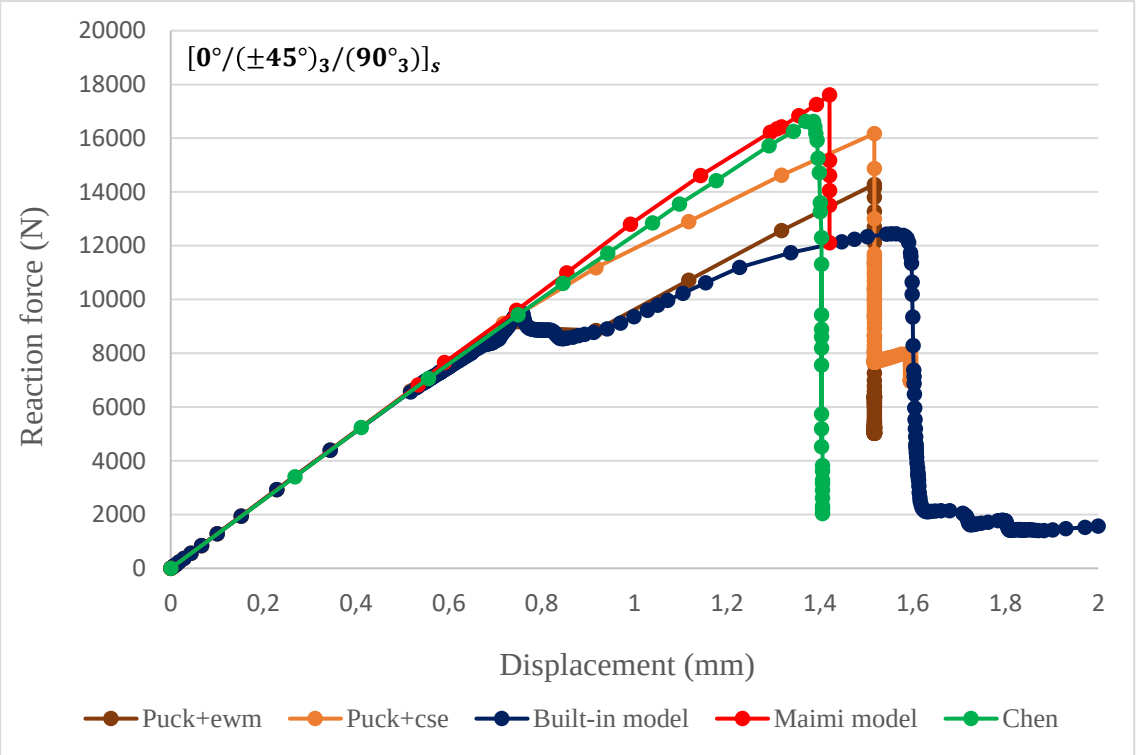


Figure 3.6: Predicted load vs. displacement curves of T300/1034C [0 / (±45)$_3$/ (90)$_3$)]$_s$ composite laminates.

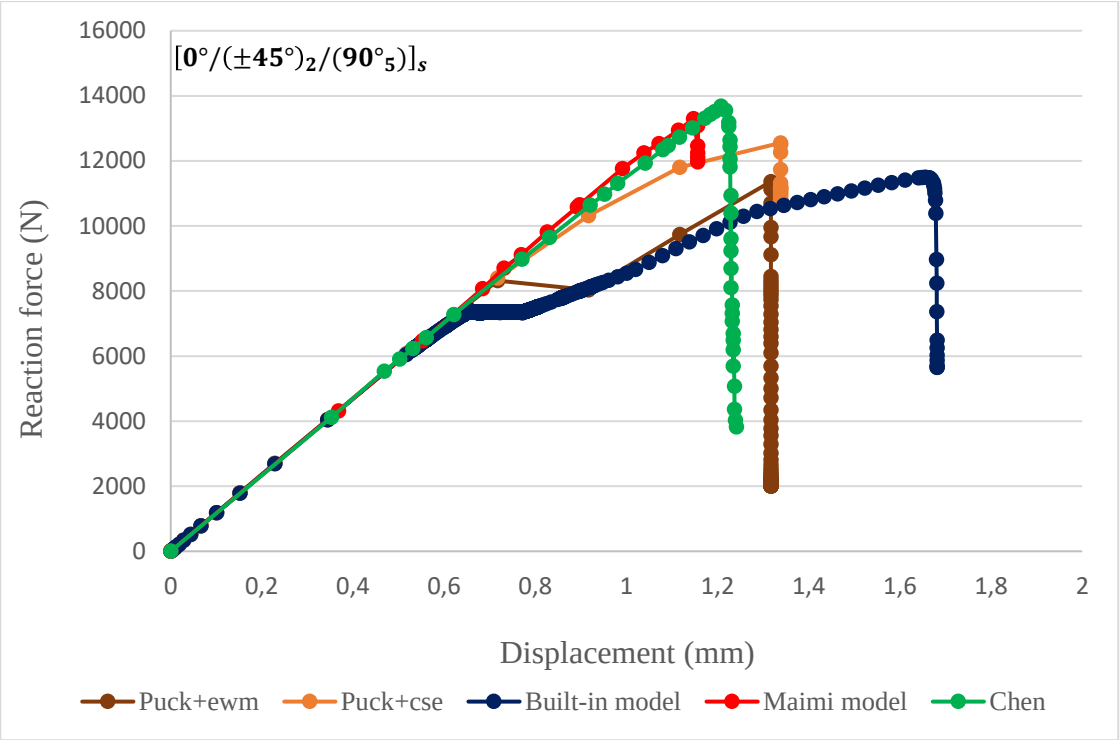


Figure 3.7: Predicted load vs. displacement curves of T300/1034C [0 / (±45)$_2$/ (90)$_5$)] $_s$ composite laminates.

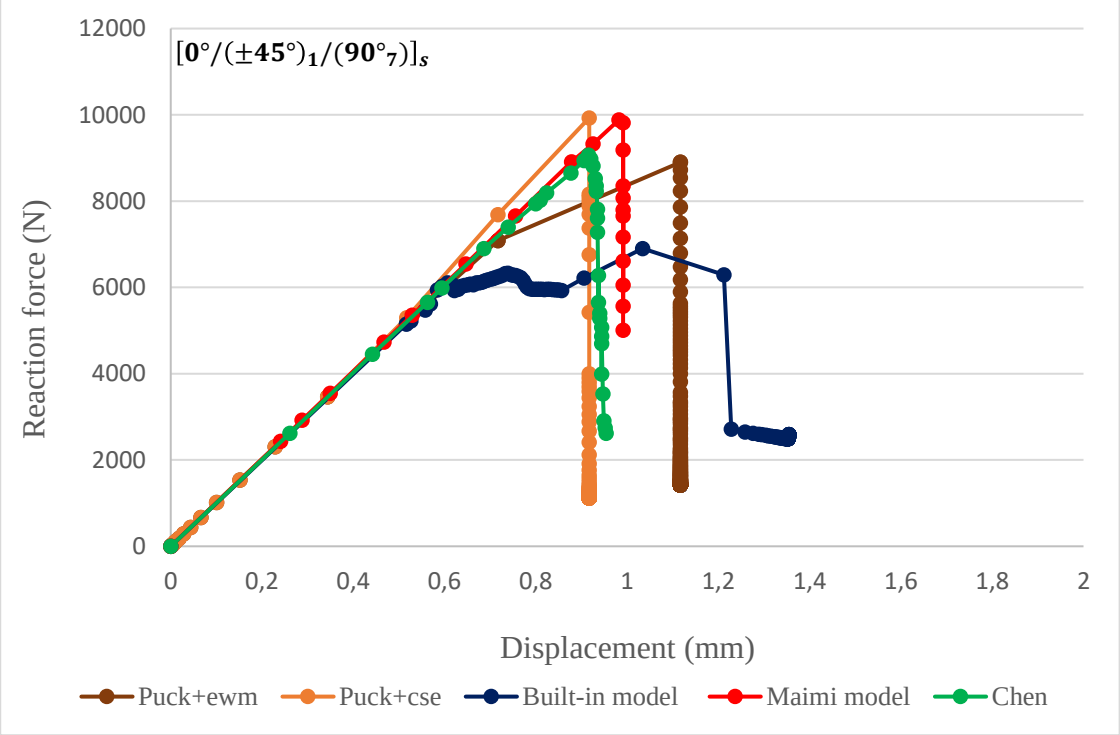


Figure 3.8: Predicted load vs. displacement curves of T300/1034C [0 / (±45) / (90)$_7$)] $_s$ composite laminates.

In the first step for a linear problem, there is no initial degradation of stiffness or material properties. However, once the failure criteria and degradation models are reached due to a certain amount of damage within a ply, the damage can lead to a subsequent stress redistribution in the laminate. Another ply will fail, even if the load could increase and thus the stiffness properties

decrease again. Also, it is ascertained that even after the first ply failure, the laminate still has much strength left in it [36].

The stiffness reduction can be observed in the above curves of the laminate under investigation, where the bends shown in the plot are an indicator of the appearance of damage and consequently the behaviour of the material becomes non-linear.

The tensile load on the damaged composite specimens showed a significant decrease near their failure point. Comparing the maximum load values between the different types (Fig. 3.6, Fig. 3.7 and Fig. 3.8), it was observed that the type shown in Fig. 3.6 had a higher maximum load. This difference can be attributed to the presence of a greater number of 90° folds in the middle of the type shown in Fig. 3.7 and Fig. 3.8 compared with that shown in Fig. 3.6.

The differences in the present results could be attributed to the fact that Chen et al. used an elastoplastic damage model that takes into account the irreversible deformation caused by plasticity effects [122], they have chosen a one-parameter plastic potential for the condition of plane stress with anisotropic hardening function that was already treated by Sun, C T et al. [125]. In comparison with the proposed models PUCK+EWM and PUCK+CSE that have adjustment factors for the non-linear behaviour of the shear moduli after the damage appears in the matrix which may not be able to give a perfect prediction, in contrast, the built-in model neglects this aspect.

As well, in the model proposed by Maimí et al. [47], a continuum damage model has been used considering the in-situ effect through the application of the LaRC04 criteria. Besides, only a nonlinear shear stress-strain relation has been used to model the nonlinear phenomenon found under shear loading and the non-linearity that occurs under transverse loading has been underestimated.

For the discount methods used in this work, it can be said that the difference in prediction ability with Matzenmiller's approach is due to an additional reduction in stiffness and strength of the elements adjacent near the hole that leads to the elimination of these elements. Therefore, faster divergence can be seen.

Generally, for each failure mechanism, all properties of an element will decrease equally. Moreover, if fiber failure occurs in an element, all properties will be failed in that element and it cannot carry on the transversal and shear loads, unlike the continuum damage mechanics models. Discount methods have an amount of stacking degradation more than Matzenmiller's approach in a shorter period of time, which causes a reduction in the loading capacity of the composite laminate as shown in Figs. ((3.6)−(3.8)) above. In numerical analysis, the divergence time of discount methods was less than Matzenmiller's approach.

In fact, constitutive strain-softening models have convergence problems when using global approaches, in particular for damage in the longitudinal (fiber) direction. For this purpose, Maimi et al. have proposed a viscous model and implemented a regularisation for the energy dissipated within the material to mitigate the convergence difficulties associated with this behaviour. Consequently, both the load-displacement curves and failure load anticipated by their model showed a good correlation with test results.

For further clarification of the damage process, (Fig. 3.9) shows the initiation and the progression of damage with the three different methods used. As illustrated, the matrix begins to fail in the 90° oriented layers at the same charge for the PUCK+CSE, PUCK+EWM and the Built-in model. For

the Built-in model, the initial fiber failure occurred in the first layer that oriented at 0° with a low load of 6.566 KN, less than PUCK+CSE and PUCK+EWM which have 9.122 KN and 8.997 KN, respectively. The failure of the tensile fibers is noticed to appear at the layer with an orientation of 0°, because of the longitudinal tension that has the maximum amount of damage. it could be explained that the existence of the 45° layers next to the 0° layer leads to the creation of a severe in-plane shear tension, which has a great influence on the equations of Hashin and Puck for tensile fiber failure. Thus, this issue must be taken into account in the designing process [122].

After the initial failure of both fiber and matrix, composite laminate can show some non-linearity but not up to the plastic behaviour as shown in the load vs. displacement curves where so-called the "knee" or the "bend". Besides, this can be explained by the apparition of more cracks in a matrix within layers that have an orientation of $\pm 45°$. In other words, this means a gradual degradation of the strength and stiffness of the material. The reduction process of layers can be observed as long as the failed layers are able to create more cracks. After reaching a certain number of cracks in the damaged layers, the load-displacement curve continues linearly until the next layer fails.

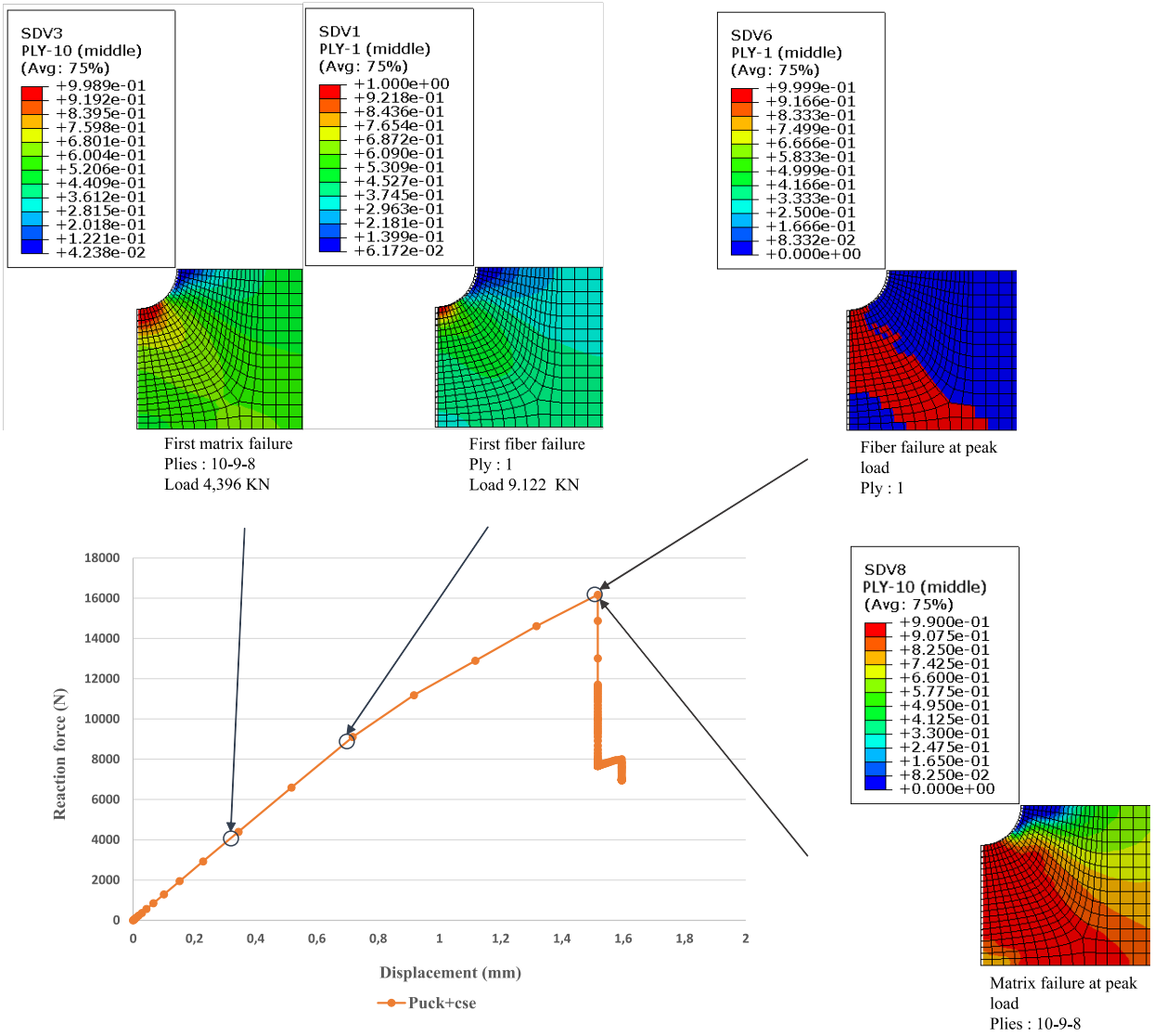


Figure 3.9a: Load vs. displacement curve for PUCK+CSE.

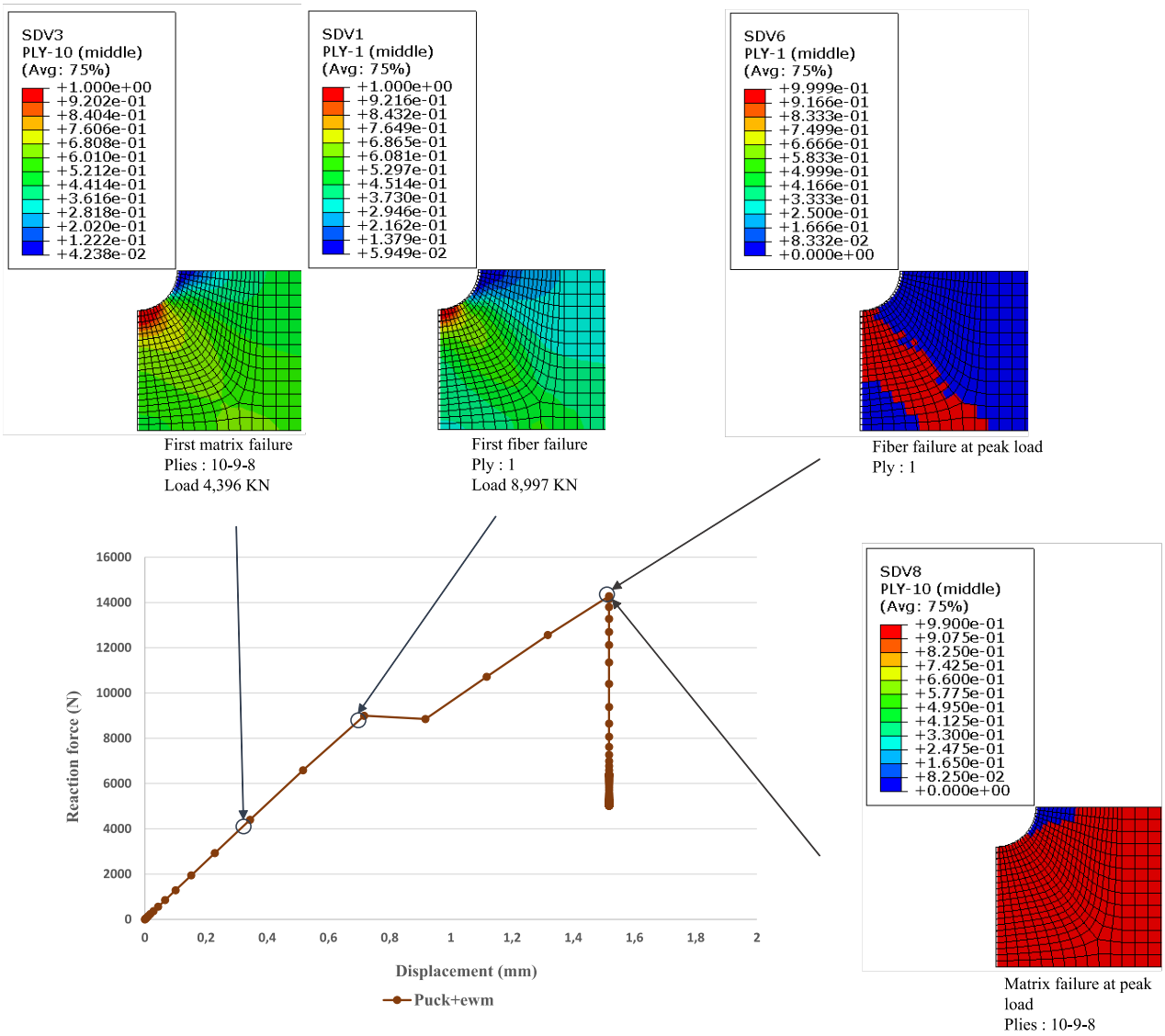


Figure 3.9b: Load vs. displacement curve for PUCK+EWM.

In the maximum tensile fiber failure load, which has 214.9 MPa (**-8.863% error)** and 243.37 MPa (**3.21 % error)** for PUCK+EWM and PUCK+CSE respectively, due to a loss in all material features, sudden failure collapse occurs through the layers. In addition to the matrix failure mode, there is a small amount of damage to the 0° orientation layers resulting in inconsiderable damage to the 0° layers.

In peak load, the Built-in model has 187.26 MPa (**-20.58 % error**) for the fiber tension failure mode, the damage variable exceeds one ($d_{ft} = 1$) after the full load resulting in the complete fracturing of the composite laminate. Due to the obvious stress concentration, the fracture started at the open-hole edge. Furthermore, catastrophic damage does not occur for failure fiber in layers with 90° orientation, wherein in this failure mode, the damage variable of Matzenmiller's approach only reduces the fiber stiffness. For tensile matrix failure, damage happened for all the orientations of the layers due to the large maximum load.

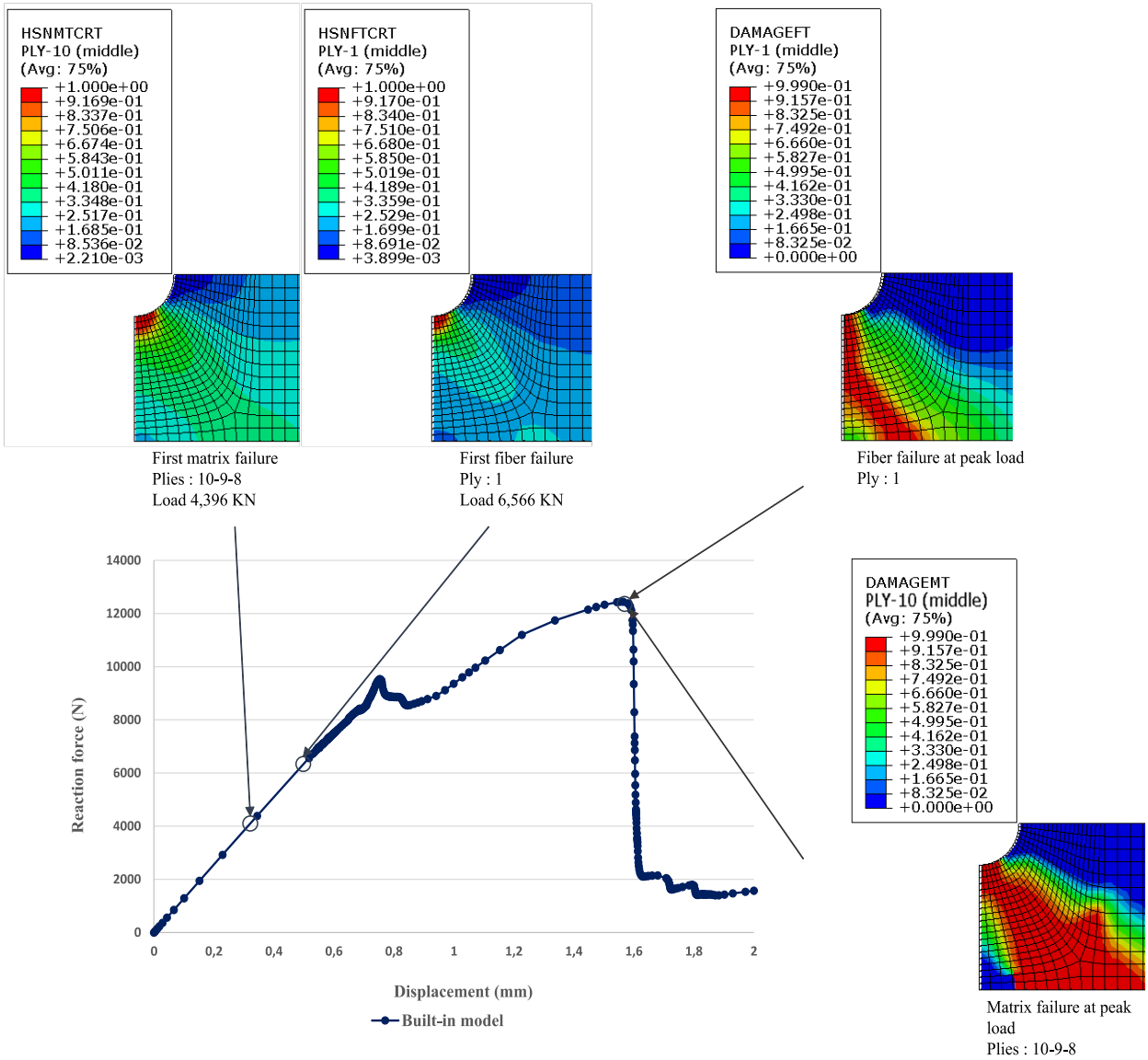


Figure 3.9c: Load vs. displacement curve for the Built-in model.

Figure 3.9: Load vs. displacement curves for the different methods used in this work.

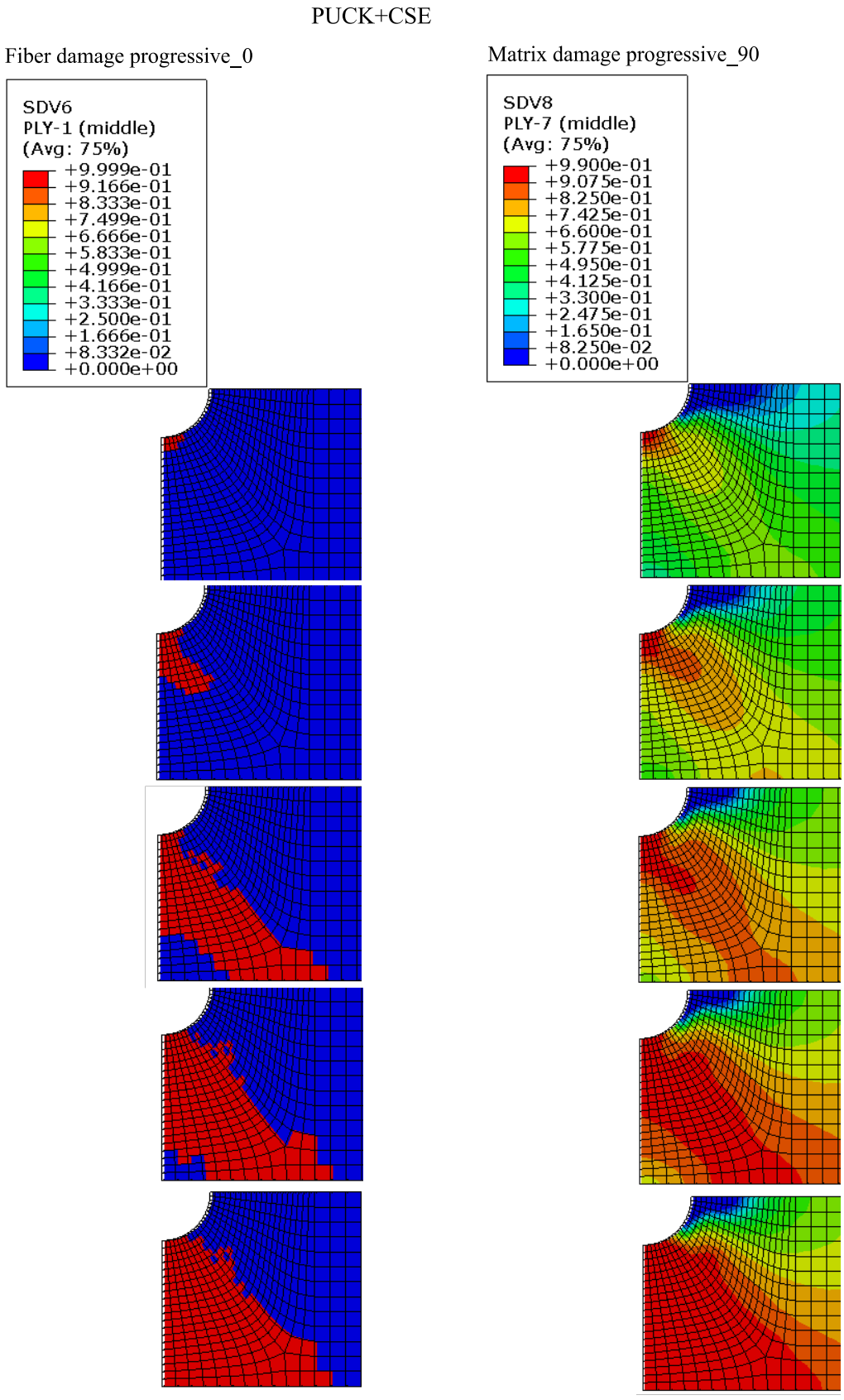


Figure 3.10a: The progress of failure for PUCK+CSE.

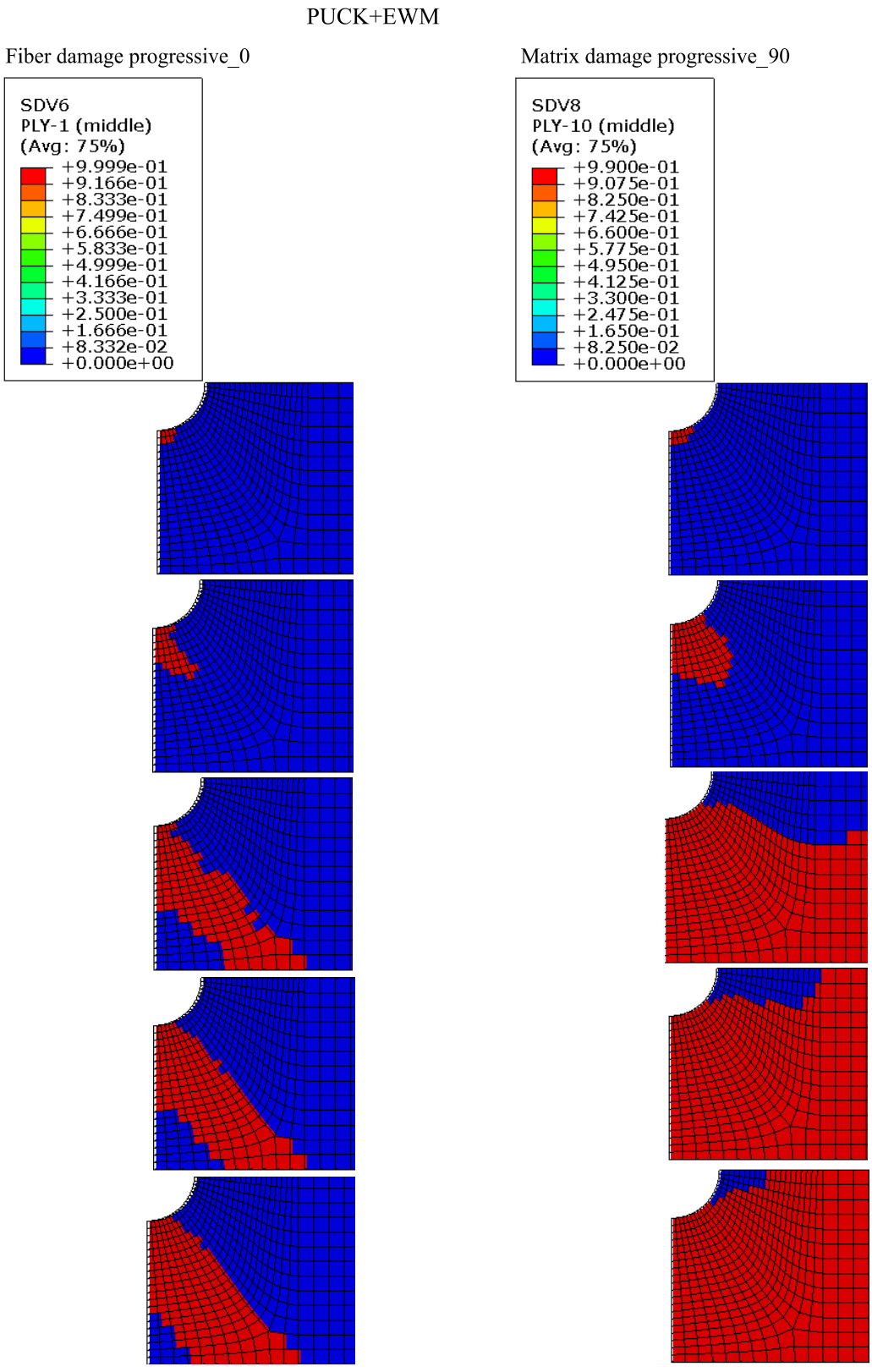


Figure 3.10b: The progress of failure for PUCK+EWM.

Built-in model

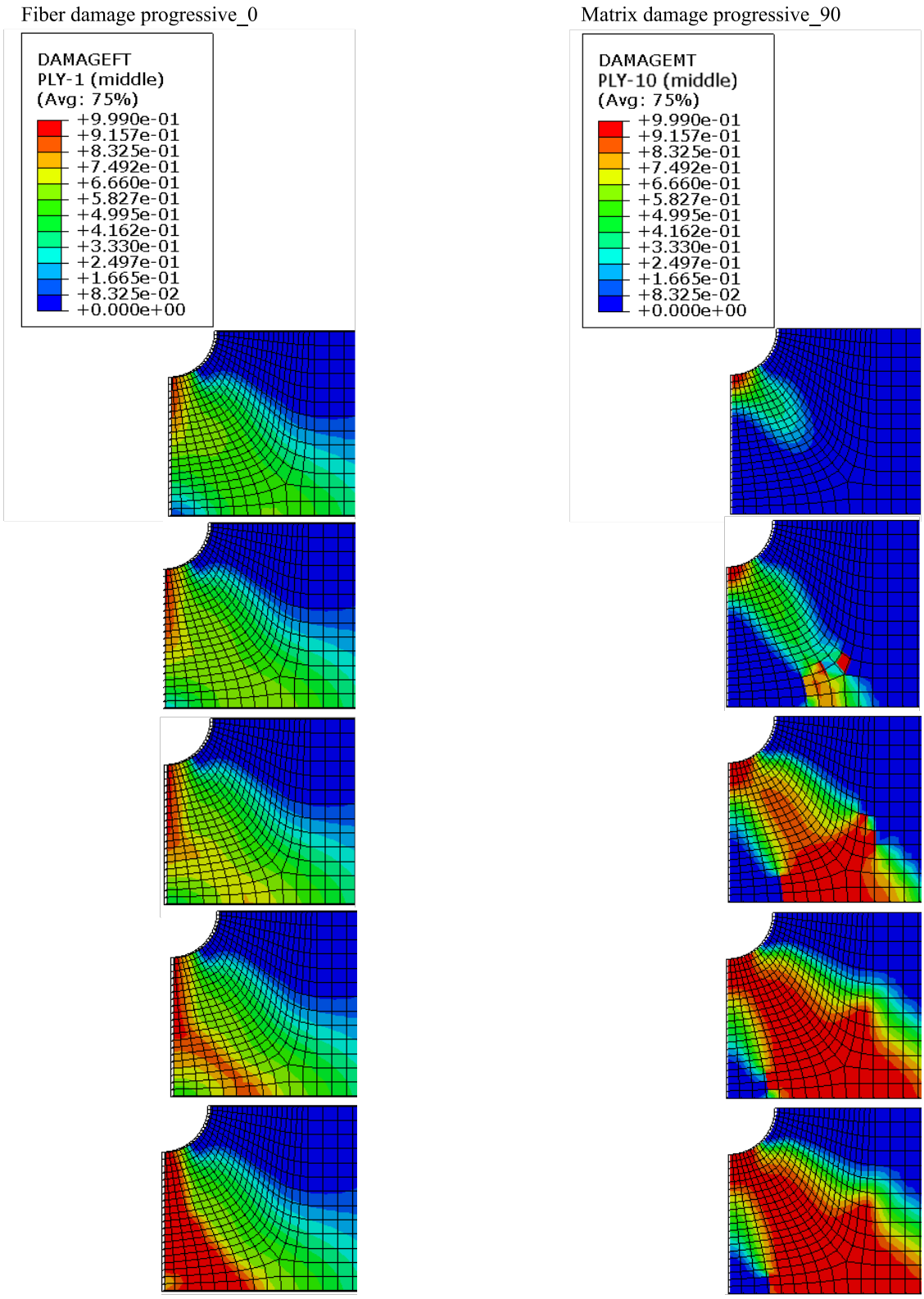


Figure 3.10c: The progress of failure for Built-in model.

Figure 3.10: The progress of failure for different progressive damage models.

Fig. 3.10 shows the progress of fiber and matrix failure modes for layers with an orientation of 0° and 90° using PUCK+CSE, PUCK+EWM and the Built-in model. The figures involve five different time steps, tensile fiber failure is indicated for 0° layers and tensile matrix failure is presented for 90° layers.

The progressive failure behaviour patterns for both PUCK+CSE and PUCK+EWM models are quite similar, especially in fiber damage. However, the matrix damage increases progressively tangentially to the hole in the fiber direction for both models and the contour damage of the PUCK+EWM diffuses more than the contour damage in the PUCK+CSE since the EWM leads to the failure of more elements at a faster rate than the CSE method. Therefore, the stiffness is instantly reduced in the EMW and leading to the development of larger deformations within the material.

The main difference between the Built-in model and the discounts methods is in the way of defect propagation, which can be noticed in the final failure of the matrix and fibers. Indeed, the fiber damage progresses along the net-tension failure plane until it reaches a certain point, after which it propagates to the edge. This procedure is not observed in PUCK+EWM and PUCK+CSE.

3.3.1.4. Mesh dependency study using T300/1034C

The different mesh densities can have a significant impact on the numerical modelling; as a result, it is necessary to choose the appropriate mesh density following the proper model that has less influence on the mesh dependency to ensure better accuracy of the results and minimise the time consumption. It should be noticed that the mesh density in the high-stress locations differs from the other places. Furthermore, the failure loads were used to compare the models because they constituted the desirable parameters of the analysis. In addition, the number of existing elements in the thickness is fixed and only the in-plane mesh density was examined. The presently Figs. (3.12 - 3.14) computed the load-displacement curves, for an open-hole T300/1034C composite laminates with the stacking sequences $[0°/(\pm 45°)_3\ (90°_3)]_s$, to evaluate the mesh dependency for the previously considered methods using different mesh cases around the hole as shown in (Fig. 3.11).

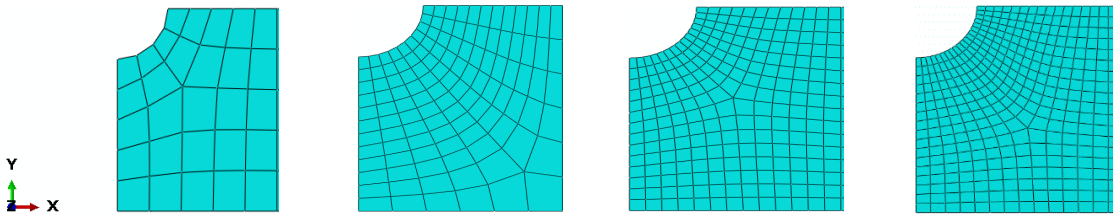


Figure 3.11: Different mesh numbers near the open-hole to verify the mesh dependency of PFA.

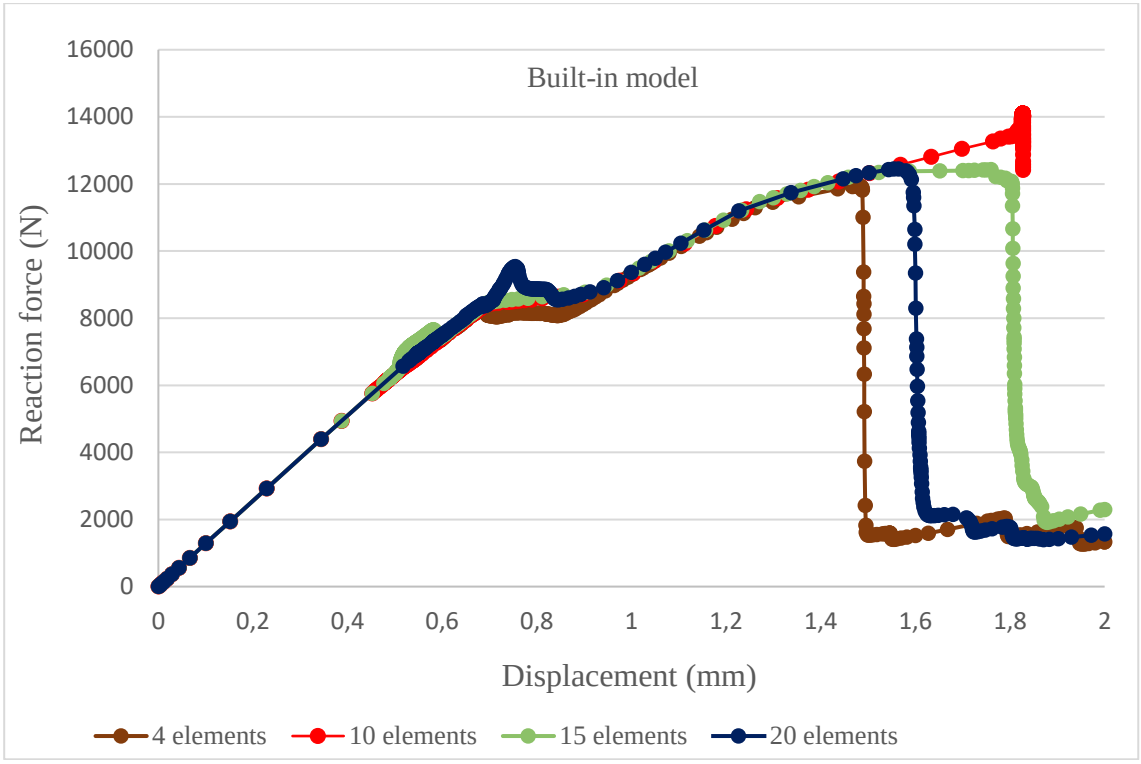


Figure 3.12: Load vs. displacement curves for different mesh cases using the Built-in model.

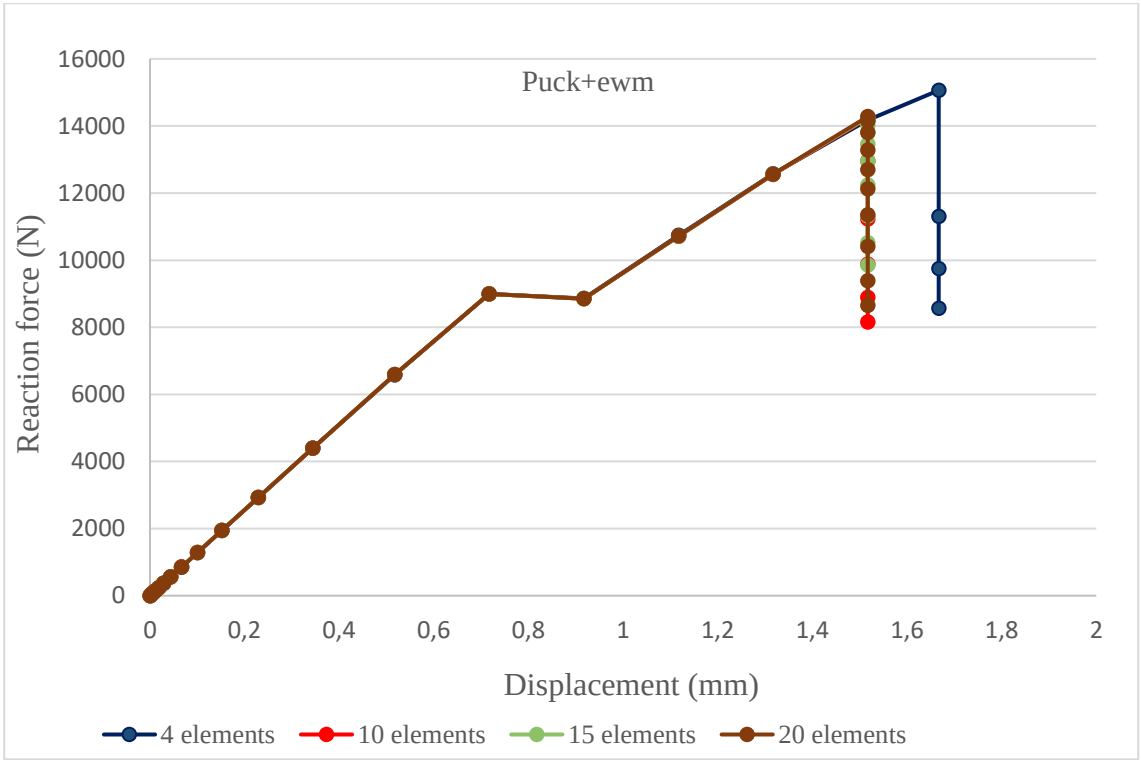


Figure 3.13: Load vs. displacement curves for different mesh cases using the PUCK+EWM model.

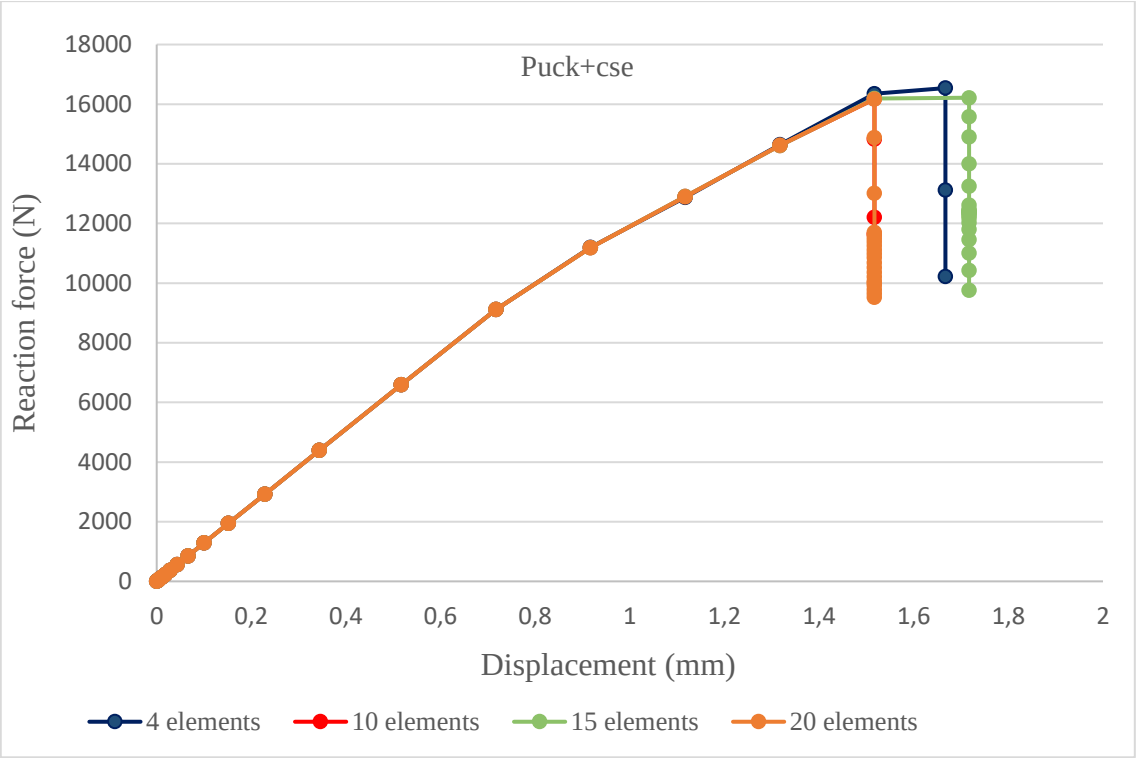


Figure 3.14: Load vs. displacement curves for different mesh cases using the PUCK+CSE model.

The Built-in model applied PFA provides various peak load values, where the response behaviour of the laminate is significantly different. Likewise, in the different meshes employed, the maximum displacement at which the laminate breaks varies. Fig. 3.15 shows the normalized failure load variation as a function of the overall number of elements near the open-hole for the PFA conducted with PUCK+CSE, PUCK+EWM and the Built-in model. The predicted load was divided by the experimental load to get the normalized failure load. **23.8 %** of the maximum load error was detected in the Built-in model with 4 elements and coinciding with the refinement of the mesh, the error starts to decrease until it converges towards the value of **-20.58%**. Besides, the numerical predictions using continuum damage mechanics, which is the case in the built-in model, have a higher mesh dependency. In addition, the amount of energy released by damage is strongly dependent on the meshes' size and element number, which tends to be zero near the limit of a highly refined mesh.

However, the strong mesh dependency in the continuum damage model arises from the fact that the failure energy, which is the amount of energy required to break an element, depends on the size and number of elements in the mesh. Specifically, as the size of the mesh decreases and the number of elements increases, the failure energy required to break each element also decreases. This is because smaller elements are inherently weaker than larger elements, and the more elements there are, the more opportunities there are for failure to occur. As a result, when using the damage variables in the continuum damage model, it is important to choose a mesh size and element density that is appropriate for the material being studied. If the mesh is too coarse or sparse, the model may underestimate the amount of damage and the material may appear stronger than it actually is. On the other hand, if the mesh is too fine or dense, the model may overestimate the amount of damage and the material may appear weaker than it actually is.

Many authors have analysed the problem of mesh sensitivity in which the material's constituent model must be supported with a mathematical condition that prevents fracture localization in an arbitrarily slighter area [105], [126].

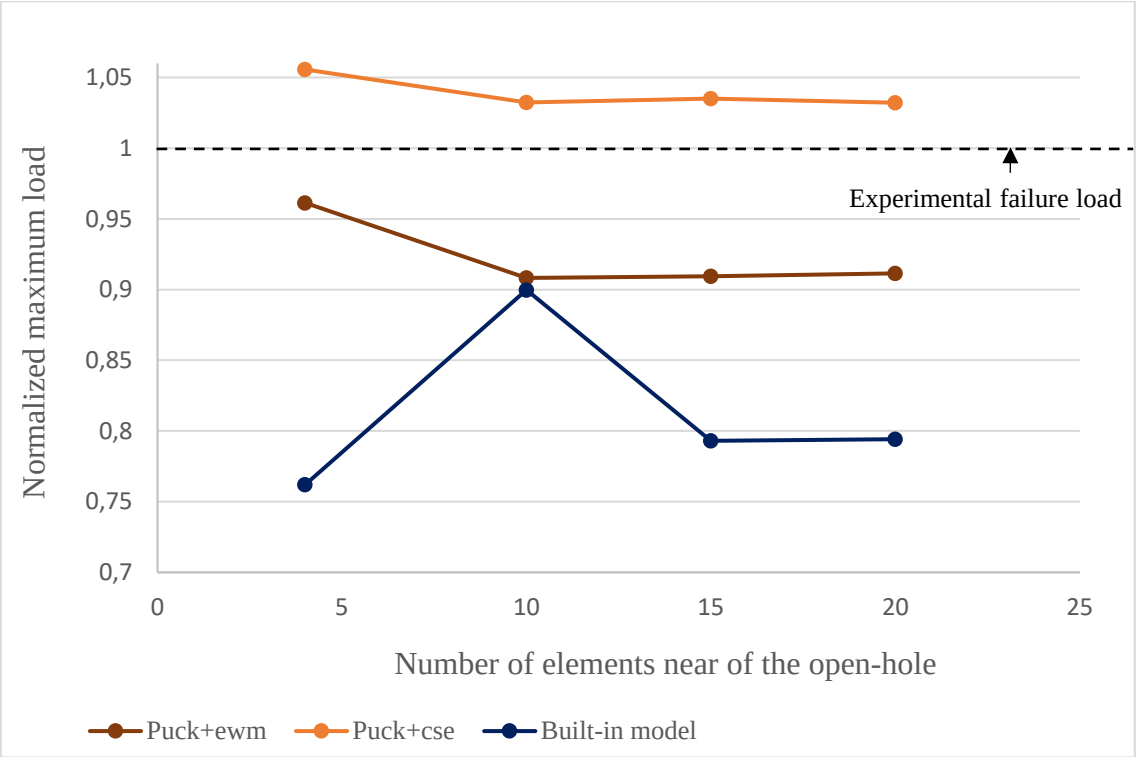


Figure 3.15: Failure load values according to the number of elements near the open-hole.

On the other hand, the applied PFA models of PUCK+CSE and PUCK+EWM display less influence on the mesh dependency, of which they give slightly different values for different meshes. The PUCK+EWM model shows accepted results, with an error of less than **8.86 %** compared to the Built-in model, which begins to stabilize after a fine mesh that has elements greater than 10 around the open-hole as plotted in (Fig. 3.13). Whereas (Fig. 3.14) exposes an error of **5.56 %** with 4 elements using the PUCK+CSE model, as the results converge to the experimental data, the PUCK+CSE model shows a very reliable result with an error of less than **3.2 %** when increasing the number of elements.

3.3.2. AS4/PEEK composite laminates

The second part of this chapter is aimed to investigate the progressive failure behaviour of AS4/PEEK composite laminates under in-plane tensile loading conditions, incorporating the effect of size as well as stress concentration. AS4/PEEK composites are known for their excellent mechanical properties, such as high strength, stiffness, and toughness, as well as their resistance to fatigue and corrosion. AS4/PEEK exhibits low thermal expansion properties, making it suitable for applications where dimensional stability is crucial under varying temperature conditions. To this end, numerical simulations were conducted using a linearly elastic, transversely orthotropic material model. In addition to examining the failure load and the corresponding load-displacement curves, various failure criteria were employed to identify the failure initiation and progression damage mechanisms of the composite laminate. The results obtained from this study can provide valuable insights into the design and optimization of composite structures, as well as contribute to

the development of advanced computational tools for predicting the failure behaviour of composite materials made with AS4/PEEK.

On the other hand, there are numerous numerical findings available in the literature as Chen et al., Mandal et al. [121] [127] and the experimental data reported by Maa and Cheng [128] were chosen to compare and validate the proposed approaches. The dimensions and the properties of the employed laminate are presented in Table 3.5, Table 3.6, respectively.

Table 3.5. Dimensions of the specimen used in this study.

	Length (mm)	Height (mm)	Thickness (mm)	Diameter (mm)
AS4/PEEK	100	20	2	2
				5
				10

Table 3.6. Material properties of AS4/PEEK test specimen [64].

Properties	***AS4/PEEK***
E_{11} (GPa)	127.6
E_{22} (GPa)	10.3
G_{12} (GPa)	6.0
ν_{12}	0.32
ν_{23}	0.45
X_T (MPa)	2023.0
X_C (MPa)	1234.0
Y_T (MPa)	92.7
Y_C (MPa)	176.0
S_{12} (MPa)	82.6
$G_{1t,c}$ (N/mm)	128.0
$G_{1c,c}$ (N/mm)	128.0
$G_{2t,c}$ (N/mm)	5.6
$G_{2c,c}$ (N/mm)	9.31

To create a numerical representation of the specimen, we utilized four-nodes linear reduced integration (SC8R) quadrilateral elements with a size of 1 mm x 1 mm. The resulting model consisted of 6424 elements and 8490 nodes, allowing for a highly detailed and accurate analysis of the specimen's behaviour. While other types of elements could have been used, the SC8R elements were selected due to their superior performance in accurately capturing the behaviour of thin-walled structures, like the laminate we were analyzing.

by implementing displacement-controlled loading at the reference point, strategically positioned at the corner side of the loading nose, we were able to achieve uniform displacements across all nodes on the loaded surface as well as the reference point. This approach ensured consistent and controlled deformation throughout the composite structure, allowing for accurate analysis of its mechanical response. To enforce this displacement control, a linear constraint equation was employed at the loading surface, effectively regulating the applied displacement and enabling us to precisely determine the reaction force and displacement at the specified reference node. This methodology provided a reliable means to study and understand the structural behaviour of the composite laminate under the applied loading conditions, facilitating comprehensive analysis and valuable insights into its performance.

Due to the obvious problem's symmetry, we were able to simulate one-quarter of the model similar to the previous case. The laminates are made up of eight layers of equal thickness with a lamination scheme $[0/45/\ 90/-45]_{2s}$.

3.3.2.1. Analysis Results and discussions for failure load and progressive damage

The predicted results of failure load for an open-hole AS4/PEEK composite material using numerical modelling are shown in Table 3.7. These results provide crucial information about the material's structural integrity and its ability to withstand certain loading conditions. It's important to note that these results are based on certain assumptions and limitations of the numerical modelling process, such as the accuracy of the material properties and the idealizations made in the model. However, by carefully considering these factors and interpreting the results in context, designers and engineers can use the failure load data to inform safety assessments and optimize the performance of the AS4/PEEK composite material. Additional details can be found in the accompanying text, and visual aids such as graphs may be used to help illustrate the model in this case incorporate puck's failure criteria and CSE to model the initiation and progressive failure.

Table 3.7. The failure loads (KN) of AS4/PEEK carbon/epoxy laminates.

Hole diameter	Chen	Mandal	Present model	Built-in model	Test
2	21.649	27.287	23.0033	15.0855	22.98
5	16.431	22.493	17.5565	12.2399	15.31
10	10.581	14.701	10.1929	7.68998	9.22

The discrepancies in these failure load values can indeed be attributed to differences in the failure theories employed to model the material, as well as several other influential factors.

One crucial factor contributing to the variations in failure load predictions is the inherent complexity of composite materials. AS4/PEEK composites consist of reinforcing fibers (such as carbon fibers) embedded in a polymer matrix (PEEK). The interactions between the fibers and the matrix, as well as the orientation and distribution of the fibers, significantly influence the material's strength and failure behaviour. Additionally, the presence of an open hole in the composite structure introduces stress concentrations, which further complicate the failure analysis. Stress concentrations occur around the hole due to the redistribution of stresses, leading to localized regions of higher stress.

The failure theories used to model the material must appropriately consider these stress concentrations to provide accurate predictions. Another factor influencing the discrepancies in failure load predictions is the specific experimental conditions and test setups employed in each study. Variations in specimen geometry, loading configurations, strain rates, temperature, and humidity can all impact the failure behaviour of composite materials. Even slight differences in these experimental parameters can yield different results and contribute to the observed variations in failure load predictions.

Moreover, the choice of failure criteria and the assumptions made within each theory can also affect the accuracy of failure load predictions. Failure theories, such as the Tsai-Wu criterion, Tsai-Hill criterion, Hashin criteria, and Puck criteria, make different assumptions about the material behaviour and the failure mechanisms at play. These assumptions may or may not capture the full range of failure modes and interactions occurring within the composite material, leading to variations in predicted failure loads. To address these challenges, researchers are continuously

working to refine and improve failure theories for composite materials. They strive to develop more sophisticated and accurate models that can account for the complex nature of AS4/PEEK composites, including stress concentrations around holes and the anisotropic behaviour of the material. Furthermore, efforts are being made to standardize testing procedures and establish guidelines for characterizing the failure behaviour of open-hole AS4/PEEK composites. This helps to minimize discrepancies arising from variations in experimental setups and enables better comparison and understanding of the material's performance across different studies.

The built-in model in Abaqus and the model presented by Mandal et al. [127] have been found to be insufficient in accurately estimating the failure load, with significant errors compared to test results. One reason for this is the failure criteria used to detect failure, which do not account for the determination of the fracture angle. In addition, the loss control variables for the shear stiffness induced by the matrix's tensile and compression failures were overlooked in the stiffness discount strategy used by Mandal et al. [127].

The present model demonstrates good agreement with the test results, indicating its effectiveness in predicting the failure behaviour of the composite material. One of the reasons for this accuracy is the utilization of Puck's criteria, which are known for their precision. Puck's criteria incorporate the fracture angle of the fracture plane, emphasizing its significance in failure analysis. By considering this aspect, the model can provide more accurate predictions of failure load and failure modes. Moreover, the present model employs a progressive process that allows for the monitoring of stiffness degradation. As the stress increases, the stiffness characteristics of the lamina are gradually reduced. This approach ensures that the model considers the residual stiffness of the lamina, which can have a notable impact on the overall failure behaviour. In contrast, the Matzenmiller method, which neglects this element, may lead to less accurate predictions. Furthermore, it's important to recognize that the ultimate failure load of the composite laminate is influenced by various factors.

The configuration of the laminate, including its load and boundary conditions, plays a significant role. Additionally, the material properties and size of the composite laminate contribute to the ultimate failure load. It's crucial to consider these factors in order to accurately predict and understand the failure behaviour of the composite material. However, it's essential to acknowledge the limitations of the present model. While it demonstrates good agreement with the test results, certain assumptions and simplifications are made. The model assumes specific material properties and failure criteria, which may not fully capture the behaviour of the composite material in all situations. Different loading conditions or material variations may require additional considerations or adjustments to the model.

Moreover, it's worth noting that the present model may not encompass all possible failure modes and processes that could occur under different loading conditions. The complexity of composite materials and the interaction of various factors make it challenging to develop a model that covers all scenarios. Ongoing research and further refinement of the model are necessary to improve its accuracy and comprehensiveness. Despite these limitations, the present model provides a valuable tool for predicting the failure load of open-hole AS4/PEEK composites and can be used to inform design decisions and safety assessments

In order to gain a more comprehensive understanding of the damage process within the composite material, a detailed analysis was conducted to examine the initiation and progression of damage using the applied models. The results of this analysis, depicted in Figs. (3.16, 3.17), provide valuable visions into the failure behaviour of the material. The analysis shows that the matrix

failure initiates in the layers with a 90° fiber orientation at the same load for both the Present model and the built-in model. This consistent behaviour indicates that the failure of the matrix is independent of the specific model used and can be attributed to the inherent characteristics of the material. Layers with a 90° fiber orientation are known to be more susceptible to shear stresses, which can lead to delamination (in some cases) and matrix cracking. The orientation of the fibers in these layers may also render them less effective in transferring loads, resulting in higher stress concentrations within the matrix material. These factors contribute to the observed matrix failure in the layers with a 90° orientation. Interestingly, the analysis suggests that the orientation of the layers does not significantly influence the occurrence of matrix failure. This finding implies that the failure behaviour of the matrix material is primarily determined by factors such as shear stresses and stress concentrations, rather than the specific fiber orientation of the layers.

Furthermore, the analysis reveals that the initial failure of the fibers occurs in the first layer with a 0° fiber orientation, and this failure occurs at a relatively low load of 6.96 KN. This observation indicates that the fibers in this layer experience significant stress concentrations, potentially due to the load transfer inefficiency caused by their orientation. The relatively low load required for initial fiber failure highlights the critical role of the fiber-matrix interface and the need for effective stress transfer mechanisms to prevent early fiber damage. The results of our analysis show that the failure of the tensile fibers tends to occur in the layer with an orientation of 0°, which experiences the highest quantity of damage. One possible explanation for this observation is the formation of severe in-plane shear stress caused by the presence of the adjacent 45° layers. This shear stress can significantly impact the Hashin and Puck equations for tensile fiber failure, which in turn affects the overall strength and performance of the material. Understanding the underlying mechanics of the failure process is crucial for predicting the behaviour of the material under different loading conditions and for developing effective strategies to improve its strength and durability. By shedding light on the role of in-plane shear stress in fiber failure, our analysis provides important insights into the behaviour of the material and can inform future design and manufacturing decision.

Our analysis also exposes that catastrophic failure occurs throughout the layers when the material is subjected to the maximum tensile fiber failure load, which for the Present model is 23.0033 KN. This failure is a consequence of a decrease in all material properties, including stiffness and strength, and it can have serious consequences for the overall performance of the material. Interestingly, in parallel to the matrix failure mode, we observed little damage to the layers with a 0° orientation, leading to an insignificant loss in these layers. This observation suggests that the 0° layers are more resilient to damage and may be better able to withstand high stress levels, compared to the layers with other orientations. These findings have important implications for designing and manufacturing materials that can resist catastrophic failure under different loading conditions. By identifying the layers that are most susceptible to failure and the ones that are more resilient, our analysis provides valuable insights into the behaviour of the material and can inform future research and development efforts.

The Built-in model reports that it has a peak load of 15.0855 KN for the fiber tension failure mode, which is lower than the corresponding value for the Present model. Moreover, we observed that the damage variable surpassed one after the maximum load, resulting in total fracture of the composite laminate. This fracture started at the open-hole edge due to the noticeable stress concentration, highlighting the importance of designing and manufacturing materials with appropriate stress distribution to prevent premature failure. Interestingly, we observed that severe

damage did not occur for the failure fiber in layers with a 90° orientation, indicating that these layers are more resilient to damage and may be better able to withstand high stress levels. In contrast, Matzenmiller's method simply lowers the fiber stiffness in this failure mode, suggesting that it may not accurately capture the full extent of damage in the material.

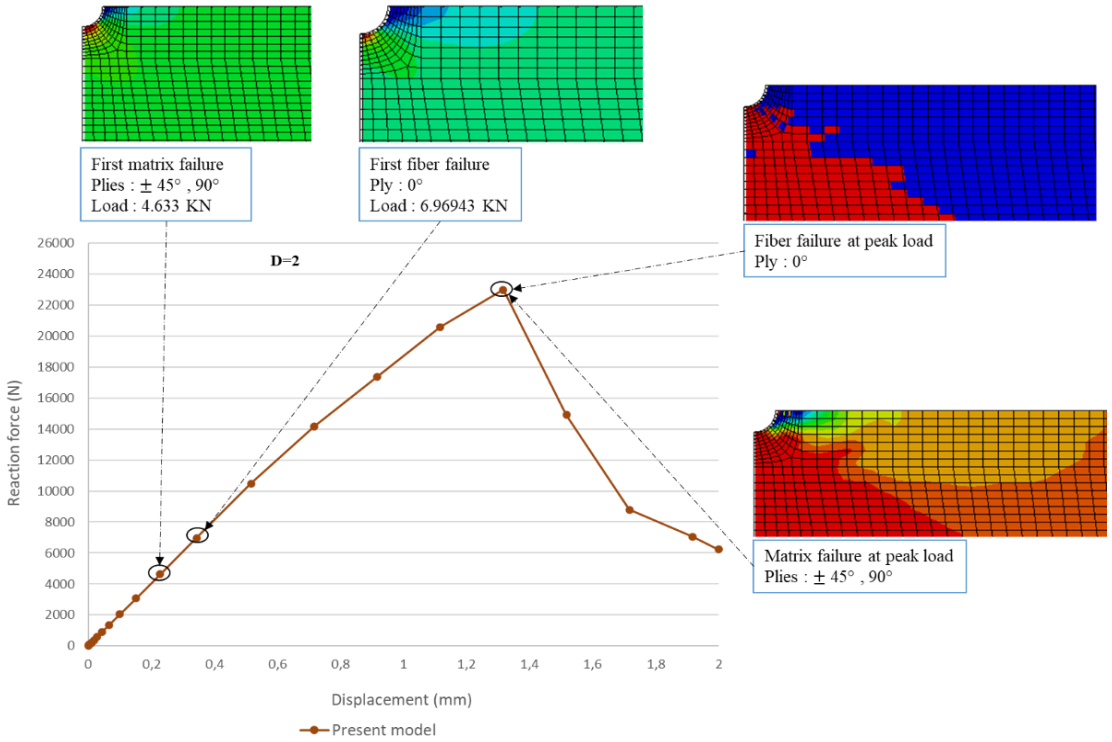


Figure 3.16: Load vs. displacement curve for the Present model.

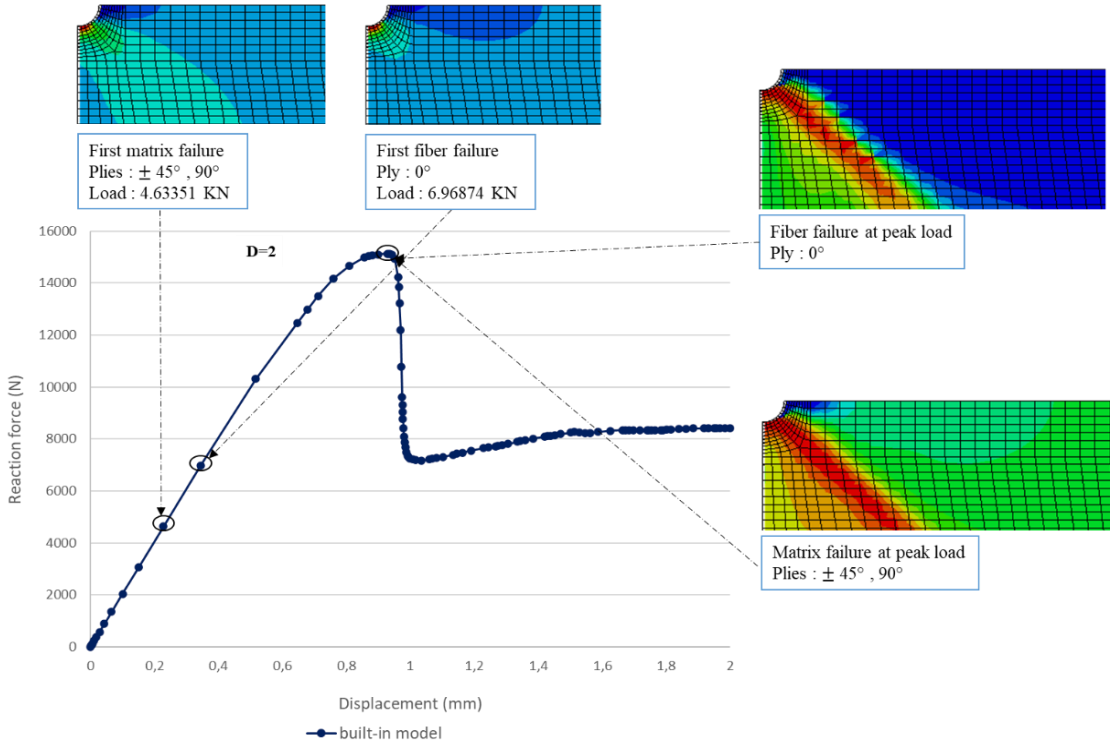


Figure 3.17: Load vs. displacement curve for the built-in model.

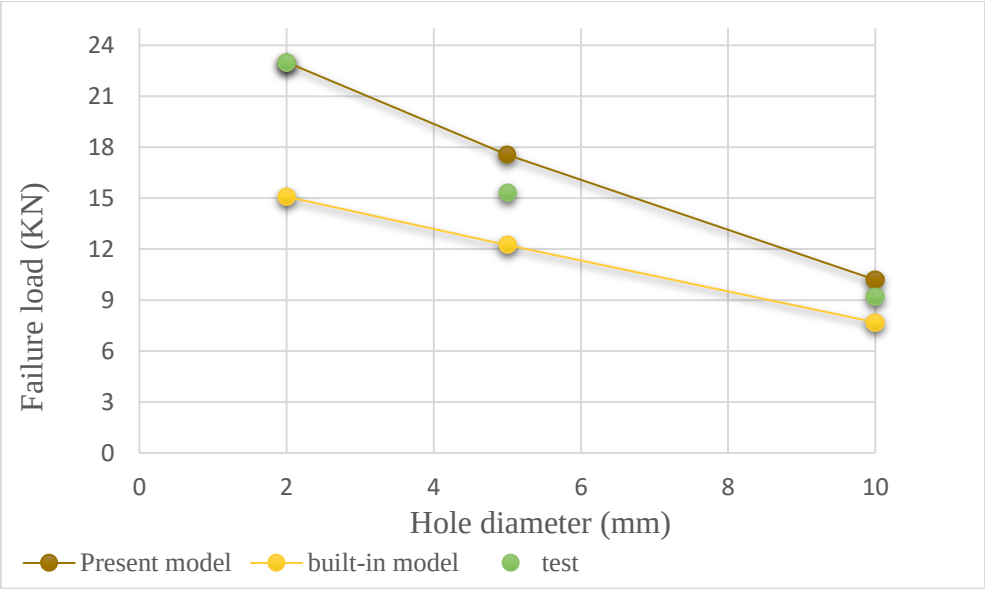


Figure 3.18: Relationships between failure load and different diameters.

In Fig. 3.18, we present the failure load predictions based on the Present model and the built-in model, compared to the experimental values obtained from the AS4/PEEK constituents fabricated from the same laminate and having identical stiffness. However, it is worth noting that the ultimate load of this laminate strongly depends on the specimen size. As seen in the figure, both the predicted ultimate load and the experimental values decrease as the hole diameter increases. This trend highlights the significant impact of the specimen size on the strength and load-bearing capacity. To analyse the effect of specimen size on the open-hole composite laminate, we used the Present model and found that most of our predictions were within the confidence interval. This indicates that our model is capable of accurately predicting the failure load of the composite material under tensile loading conditions and can provide valuable insights into the mechanics of failure in composite laminate. In contrast, the integrated model gave a higher error during the failure load analysis with different hole diameters, suggesting that it may not be as accurate in predicting the behaviour of the material.

These findings underscore the importance of considering specimen size using appropriate models and methods to accurately predict the behaviour of composite materials under different loading conditions. By identifying the strengths and limitations of different models and methods, our analysis provides important insights into the mechanics of failure in composite materials and can inform future research and development efforts aimed at improving their strength, durability, and performance.

3.3.2.2. Mesh dependency study using AS4/PEEK

The present study evaluated the progressive failure analysis of an open-hole AS4/PEEK composite laminate with D=2 using different finite element meshes around the hole, as shown in Fig. 3.19. The load-displacement curves computed in Fig. 3.20 indicate that the different mesh cases produced similar peak load values, but the post-peak response behaviour of the laminate varied slightly between the meshes. The finest mesh produced a slightly different maximum displacement at which the laminate completely failed. Interestingly, the results indicate that the degradation model and Puck's failure criteria had less influence on the mesh dependency, as shown in Fig. 3.21

where the normalized failure load was observed to vary according to the total number of elements near the open hole.

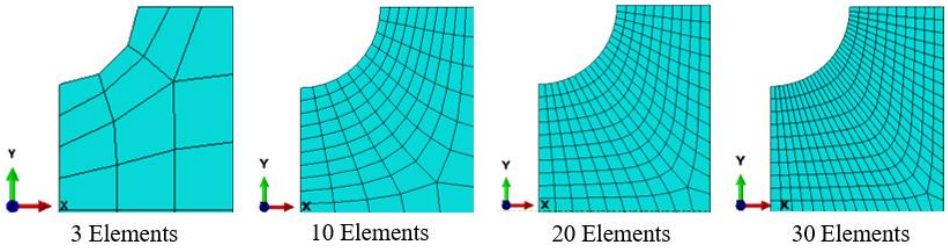


Figure 3.19: Various mesh densities around the hole.

However, the numerical predictions based on continuum damage mechanics are highly sensitive to the size of the finite element mesh as shown for in the case of T300/1034C. This is because the energy released by the damage depends on the size and number of elements in the mesh, which tends to decrease to zero around the limit of an extremely refined mesh which known as spurious mesh sensitivity, and it has been assessed by many researchers.

To overcome this issue, the constituent model of the material must be supplemented with a mathematical condition that avoids the localization of cracks occurring in a randomly smaller area. This is necessary because the model's ability to predict the failure of the material depends on the accuracy of the numerical simulations, which in turn depends on the mesh size and distribution. By addressing the issue of spurious mesh sensitivity, researchers can improve the accuracy of their numerical simulations and increase the reliability of their predictions [129], [130].

Furthermore, there is another problem of mesh dependency for the continuum damage model called mesh objectivity. Mesh objectivity refers to the property that the results of the finite element analysis should not depend on the element size or shape, provided that they are sufficiently small to resolve the relevant features of the problem. In other words, the material model should be insensitive to the mesh size and distribution, and the results obtained from different meshes should be the same or nearly the same.

However, in some cases, the continuum damage model may exhibit mesh objectivity problems, especially when the mesh is not properly designed or when the damage is localized in specific regions of the structure. This can lead to inaccurate predictions of the material behaviour and failure, which can have serious implications for the design and safety of engineering structures.

To address the issue of mesh objectivity, researchers use various techniques, such as adaptive meshing, mesh convergence analysis, and model validation against experimental data. These techniques aim to ensure that the numerical simulations are sufficiently accurate and reliable, and that the results are independent of the mesh size and distribution.

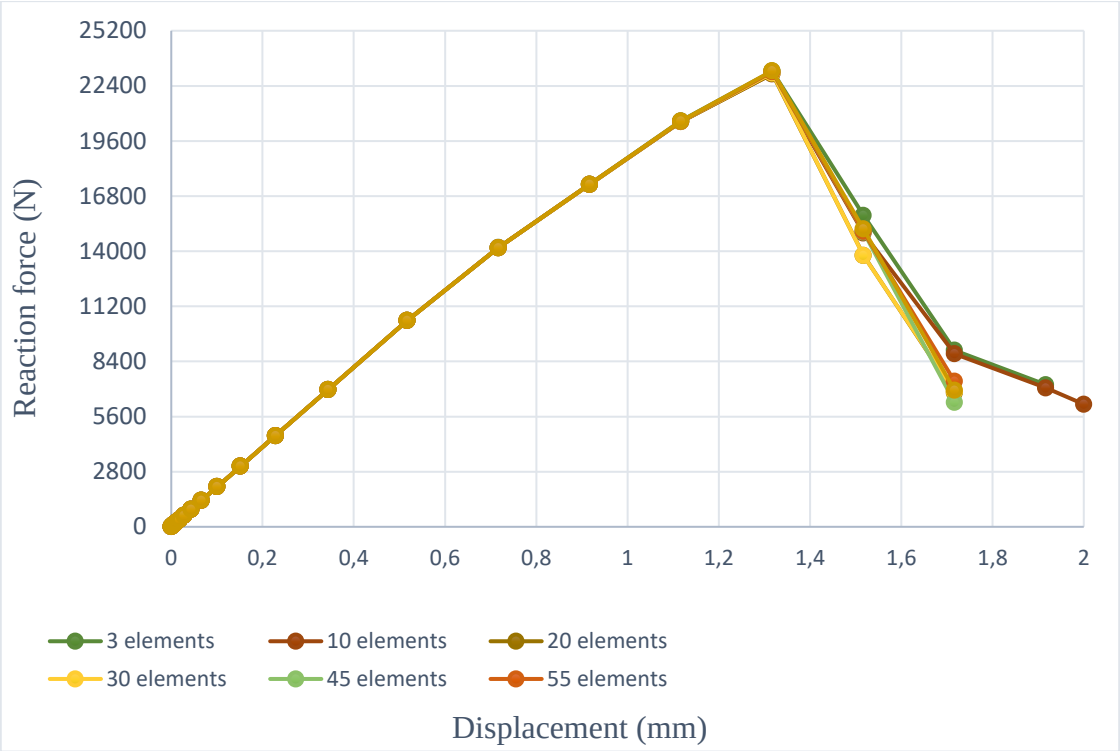


Figure 3.20: Load-displacement curves for different mesh cases with a diameter of $D = 2$.

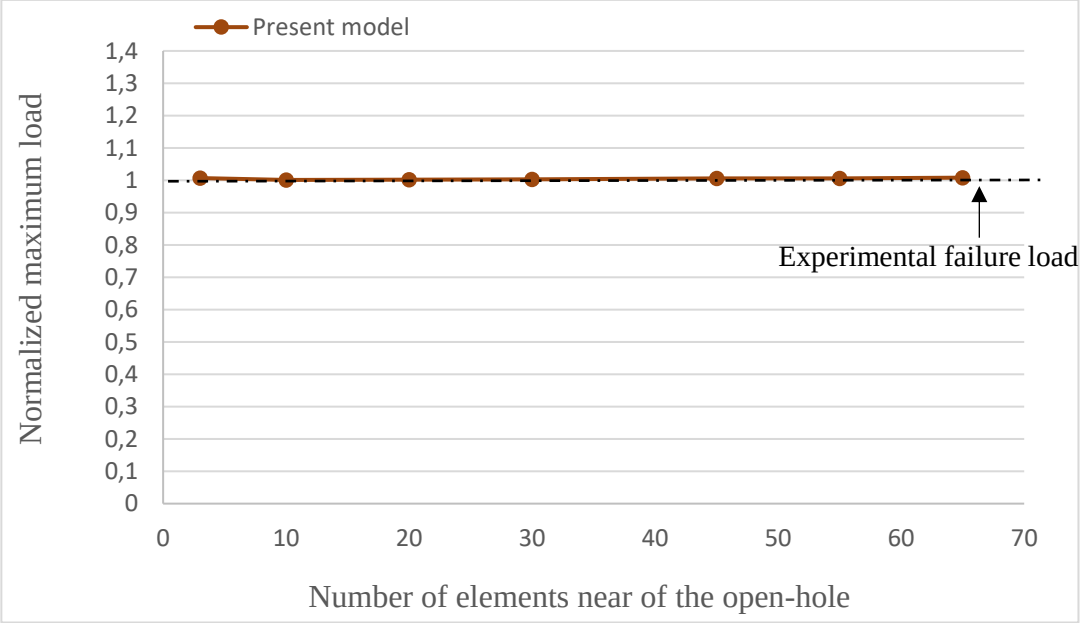


Figure 3.21: Failure load value according to the number of elements near the open-hole.

3.4. Conclusion

In conclusion, this chapter focused on analysing the behaviour of various open-hole composite laminates under pure tensile loading. The objective was to predict the damage progression, determine failure load and failure modes, and consider influential parameters such as specimen size, stress concentration, and layup.

To achieve these goals, a new computational analysis was developed using the UMAT subroutine integrated into the Abaqus finite element analysis package. Advanced assessment functions like

the Puck failure criteria and gradual degradation models, CSE and EWM, were successfully employed to estimate and predict the failure load, failure modes, and damage progression. A comparison was also made with the Built-in Abaqus model based on Hashin failure criteria and Matzenmiller's approach, as well as with existing literature.

The main research findings can be summarized as follows:

- ✓ The Puck failure criterion proved to be powerful and accurate in predicting initial and final failure loads of composite laminates when coupled with a degradation model. No parameter calibration was required.
- ✓ Simulation results correlated well with reported composite failure results when comparing initial/final failure loads and damage progression for various stacking sequences.
- ✓ Structural failure analyses of large complex composite structures are possible, although the analysis time increases due to the iterative process involved in obtaining the angle of the fracture plane for each increment.
- ✓ The constant stress exposure method used in the applied model was found to be accurate and faster than the element weakening method and Matzenmiller's approach, despite being more computationally expensive.
- ✓ Considering the size of holes in the design of structures is crucial and appropriate mitigating measures should be implemented to address the negative effects of larger hole diameters.
- ✓ Comparisons made in this study revealed that PUCK+CSE provided good agreement with experimental and computational results reported in the literature for failure load, size effect, and load vs. displacement curves. PUCK+CSE also exhibited better stiffness prediction than PUCK+EWM and the Built-in model, which had higher errors.
- ✓ Careful selection of material properties for the matrix and fibers is essential in the design of fiber-reinforced composites to optimize reinforcement and fiber breaking strength. Numerical predictions demonstrated the sensitivity of the overall material response to properties such as Young's modulus and stiffness for both fibers and matrix.
- ✓ The applied PFA models of PUCK+CSE and PUCK+EWM yielded less mesh-dependent results compared to the built-in model.

In summary, this study contributes to the understanding of open-hole composite laminate behaviour under tensile loading. The findings emphasize the effectiveness of the employed models and provide valuable insights for designing and analysing composite structures. Further research can expand on these findings and explore additional aspects of composite material behaviour.

Chapter 4: Flexural behaviour modelling of carbon/epoxy laminates using the Puck-EWM approach

Overview

- *Introduction*
- *Intralaminar damage initiation and evolution*
- *Experimental setup*
- *Numerical simulation*
- *Results and discussion*
- *Conclusion*

4.1. Introduction

Composite materials have achieved widespread adoption in numerous industries, thanks to their exceptional strength-to-weight ratio and desirable properties. However, their behaviour under different loading conditions remains poorly understood, and predicting their failure mechanisms proves complex. Among the various methods used to study the mechanical behaviour of composites, the three-point bending test has emerged as a common approach, particularly in aerospace and automotive applications.

A critical area of research revolves around understanding the progressive failure of composite laminates under three-point bending. This phenomenon involves the gradual formation and propagation of damage within the material, carrying the potential for catastrophic failures that significantly impact the performance and safety of composite structures. Hence, it is crucial to develop accurate models that can predict the initiation and propagation of damage under various loading conditions [131], [132].

In this chapter, we propose a progressive damage model to predict the flexural behaviour and progressive damage of different composite laminates subjected to three-point bending. This is accomplished by implementing a user-defined subroutine (UMAT) in Abaqus, providing an accessible and computationally efficient approach to perform failure analysis. The model utilizes Puck's failure criteria to predict initial failure and the element weakening method (EWM) to simulate the degradation of material properties.

To validate the progressive damage model, three-point bending tests were conducted on prepreg T700/Epoxy composite specimens. The experimental results were used to compare and assess the accuracy of the numerical simulations, including failure load, failure modes, and the influence of different specimen sizes. By evaluating the competence of the finite element model in predicting the mechanical response and progressive failure of the composite, we aim to enhance the understanding of composite behaviour under three-point bending.

The primary objective of this chapter is to provide a comprehensive overview of the progressive failure of composite laminates under three-point bending and the role of the proposed progressive damage model in predicting the behaviour of composite materials. By developing accurate models, we strive to improve the design and optimization of composite structures, ultimately enhancing their performance and safety in real-world applications. Through the integration of experimental and numerical analysis, this chapter aims to contribute to the broader field of composite materials by advancing our understanding of progressive failure mechanisms. By doing so, we aspire to enable more effective design strategies, leading to enhanced performance, reliability, and safety in composite structures across various industries.

4.2. Intralaminar damage initiation and evolution

Fiber fracture, matrix cracking, and delamination are common failure mechanisms in fiber reinforced composite laminates. In this context, fiber fracture/splitting and matrix cracking are classified as intralaminar damage, while delamination is considered interlaminar damage. A composite damage model was developed and implemented in Abaqus/standard, focusing on intralaminar damage. Hashin proposed unique failure functions for intralaminar damage, highlighting the limitations of conventional failure criteria. The Hashin failure function consists of a tensile part and a compression part, with additional terms for matrix failure under compressive

loads. Puck and Schürmann have gained credibility in the community by adopting the physically-based and mathematically-formulated Hashin criterion technique for brittle fracture [9][38].

The assessment of damage growth until final failure in composite materials requires an appropriate approach that aligns with the identified damage within the material. In this study, the elements weakening method (EWM) [63] is employed, which involves a gradual reduction in stiffness during the finite element (FE) procedure (see Chapter 2). The degradation process is assumed to represent the growth of crack density. It is important to note that delamination has a minimal impact on the mechanical response of composite laminates with embedded plies under in-plane loads; therefore, the approach used in this study does not consider delamination failure [133].

In terms of damage phenomenology, the initiation and spread of failures within a material depend largely on the degradation of the material's potential, which is most evident in the decrease in stiffness. The progressive failure, characterized by the accumulation of internal material damage and a corresponding loss of stiffness, can be quantitatively expressed[28]. When the stress exposure reaches a critical value, typically equal to one, the selected elastic properties of the elements are reduced to zero, as specified by the equations for inter-fiber failure. This reduction in properties affects the modulus perpendicular to fibers and the in-plane shear modulus. In the case of fiber failure, all elastic properties are reduced.

4.3. Experimental setup

4.3.1. Materials

The experimental study is performed using a three-point bending test to investigate the strength of composite structures, as shown in Fig. 4.1, which consists of a beam simply supported between two supports with the load applied at the midpoint. However, the evaluation process is easy to set up and the results are simple to understand. In addition, for the characterization of composite materials, the three-point bending test generally provides satisfactory results.

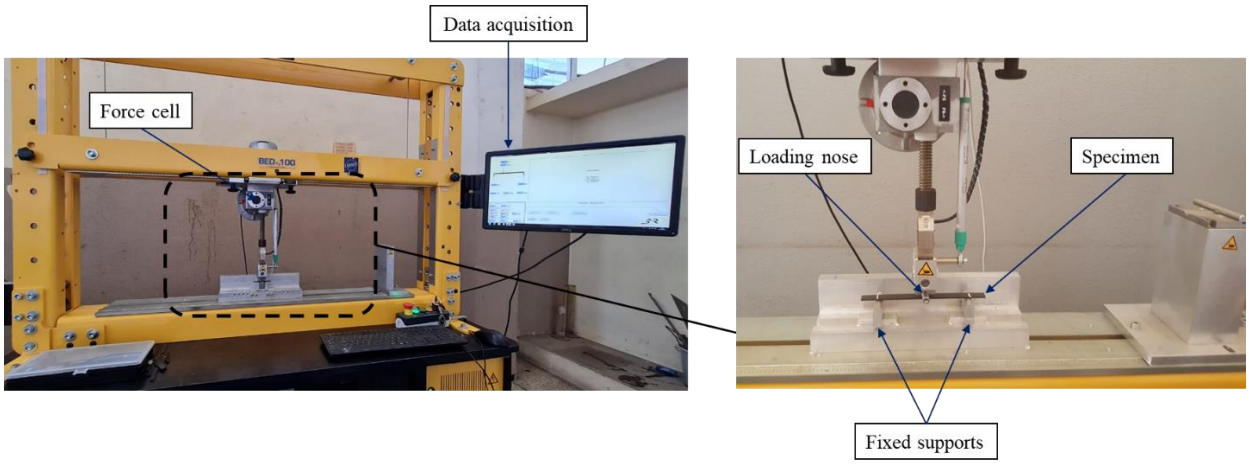


Figure 4.1: Three-point bending test.

However, its use is restricted since it necessitates the previous identification of failure mechanisms and their impact on the macroscopic load vs. deflection curves.

The procedure is followed according to ASTM D790 [134]. The specimen layup consisted of 6 plies with a stacking sequence given by an orthogonal laminate $[0/90]_6$. The dimensions of

specimens, geometrical and the material properties of prepreg T700/epoxy used, are presented in Fig. 4.2 and Table 4.1, respectively.

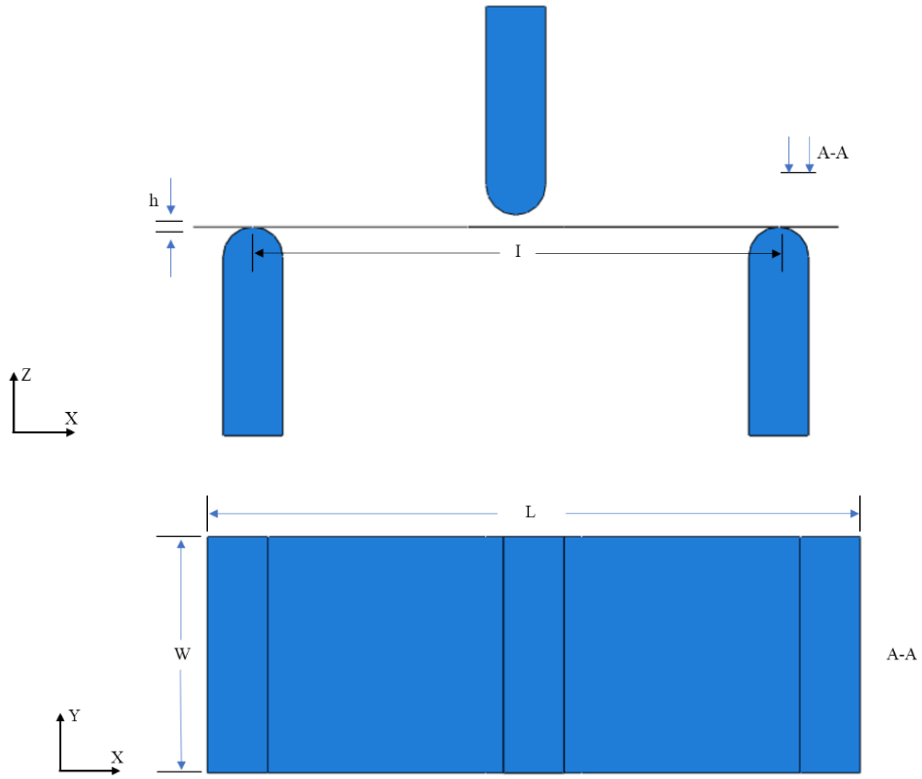


Figure 4.2: The geometry of the composite specimens for three-point bend experiments.

Table 4.1. Dimensions of the specimens used in this study in (mm).

Material	Label	Length (L)	Width(W)	Thickness(h)	Span (l)	Ratio l /h
Prepreg carbon T700/epoxy	K	54	20	2.2	44	20
Graphite/epoxy	A	75	25	3.6	57.5	16
	B	150	25	3.6	115.0	32
	C	150	25	3.6	136.5	38
	D	75	10	3.6	57.5	16

4.3.2. Preparation of the samples

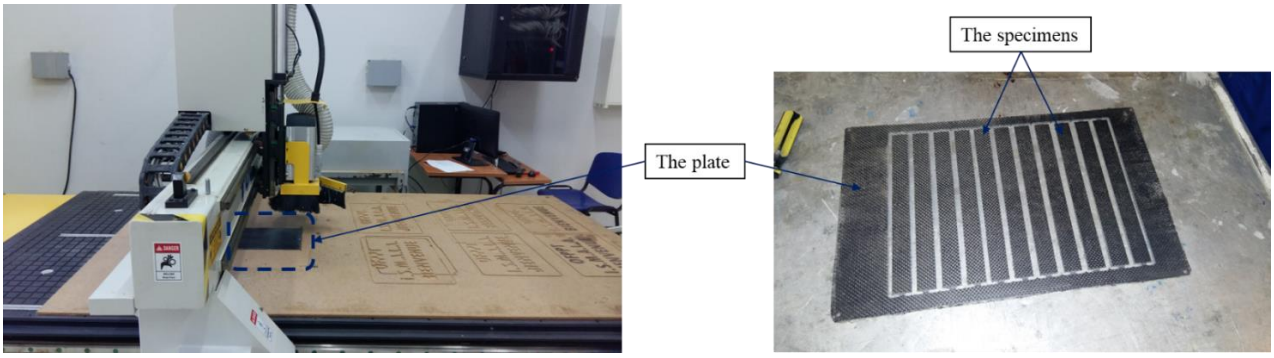
In the experimental setup, a prepreg material plate is cured in an oven at a temperature of 120°C for a duration of 60 minutes, with a controlled ramp-up rate of 2°C per minute. This curing process ensures the proper consolidation and bonding of the composite laminate structure. During the lamination process, meticulous attention is given to aligning the fiber orientations accurately, as this plays a crucial role in determining the mechanical properties of the composite.

To obtain specimens for testing, a computer numerical control (CNC) milling machine, depicted in Fig. 4.3, is utilized. The cured plate is cut into desired shapes using the CNC milling machine, ensuring precise dimensions and reproducibility of the specimens. To minimize any potential milling-induced damage, the edges of the samples are permanently machined with a diamond wheel, which helps in achieving clean and smooth surfaces.

The specimens obtained are subjected to testing as per the guidelines specified by the ASTM regulation [134]. This ensures standardized and consistent testing procedures across different laboratories. Fig. 4.1 illustrates the setup where deformation measurements during testing are collected using a computer connected to the equipment. The QuantX software is employed to store and analyse the gathered data, facilitating accurate evaluation of the mechanical response and behaviour of the composite specimens.

To track the progression of damage and observe the final failure of the specimens, a digital microscope is employed. This allows for detailed examination of the material's microstructural changes, crack initiation and propagation, and the overall failure mechanisms occurring during the testing process.

The combined use of controlled curing, precise specimen preparation, standardized testing procedures, deformation measurement software, and a digital microscope enables comprehensive characterization and analysis of the composite laminate's mechanical properties, damage progression, and ultimate failure modes. This experimental approach provides valuable insights into the material's performance and helps in advancing the understanding of composite laminate behaviour in various applications.



(a) (b)

Figure 4.3: The CNC milling machine: (a) Cutting the specimens by CNC milling machine; (b) The specimens obtained by cutting.

4.4. Numerical simulation

4.4.1. Finite element model

In this study, a finite element (FE) model, as depicted in Fig. 4.4, was created using Abaqus 2017 to simulate three-point bend events conducted on composite specimens with different lay-up configurations, namely $[0/90]_6$ and $[\,[+45°/-45°/90°/0°]_3\,]_s$. To reduce the need for extensive physical testing while ensuring accurate results, a virtual specimen was discretized using three-node triangular (S3) elements with a size of 1 mm × 1 mm. Although triangular finite elements exhibit more rigidity in bending problems due to their constant deformation characteristics, they are suitable for accurately capturing the behaviour of the laminate under investigation. The integration of a user-defined material subroutine (UMAT) in the FE model ensures the simulation accurately represents the mechanical response of the composite material during loading.

To validate the FE model and optimize computational efficiency, a mesh size convergence study was conducted and is presented in this chapter. The study involved analysing the effect of different

mesh sizes on the numerical results to identify the optimal mesh size that balances accuracy and computational cost effectively.

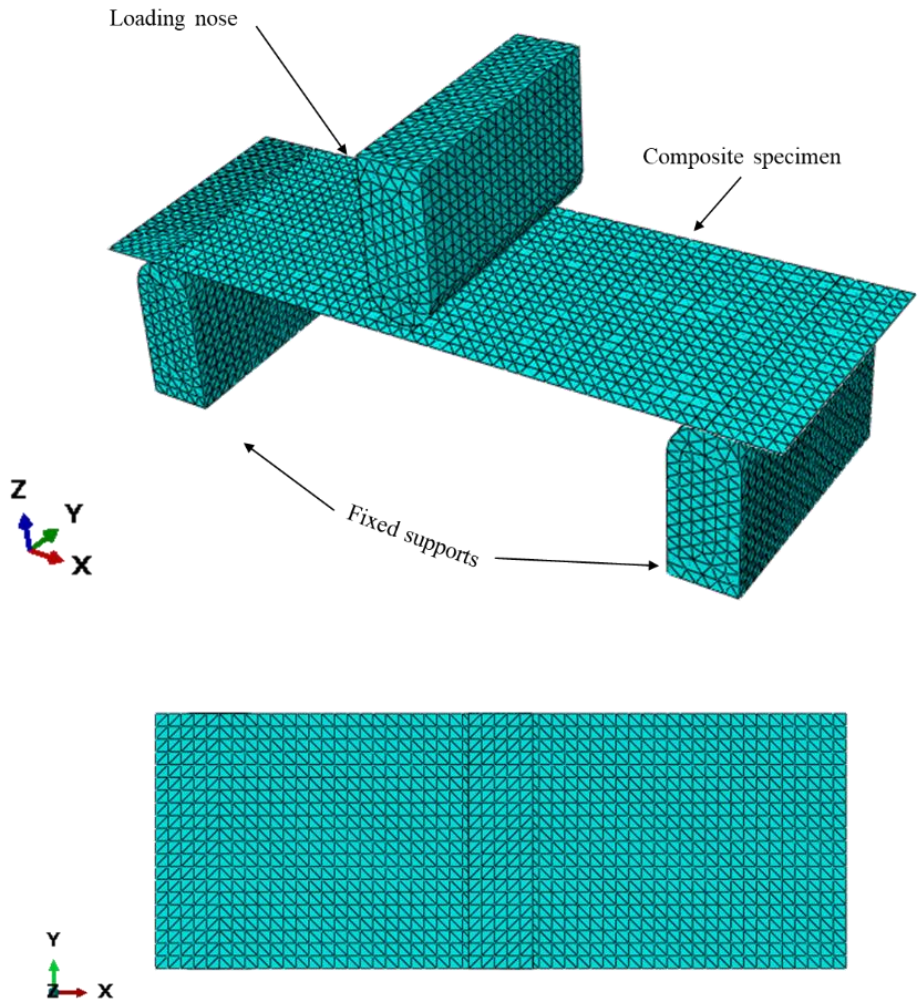


Figure 4.4: The FE models.

In the three-point bend simulations, the composite laminate was subjected to a displacement-controlled load. To accurately represent the loading conditions, a linear constraint equation was employed, where the displacement imposed on a reference point (RP) located on the underside of the loading nose controlled the loading on the surface. The primary objective was to ensure uniform displacements between all nodes of the loaded surface and the RP reference point. This approach facilitated the calculation of reaction forces and surface displacements at the reference node, providing valuable data for analysis.

To achieve computational accuracy, the simulations were performed in double precision. This choice helped minimize accumulation errors that can occur during the simulation, ensuring reliable and accurate results. Additionally, a stable time increment of less than 1e-02 s was employed to maintain numerical stability and capture the behaviour of the composite laminate during loading.

The computational efficiency of the simulations was optimized by utilizing the available computational resources effectively. The simulations were carried out on a workstation equipped with 12 CPUs and 32GB of RAM. With these specifications, the approximate run time for the simulations was less than 1 hour. This efficient runtime allowed for the completion of multiple

simulations, enabling a comprehensive analysis of the mechanical response of the composite laminate under three-point bend loading conditions.

4.4.2. Properties for model input

In this study, we used two different composite laminates to ensure the applicability and the efficacity of the applied methodology. The mechanical properties for both materials prepreg T700/epoxy and graphite/epoxy, such as strength and modulus, were obtained from the datasheet [135] provided by the ABC composite and the work presented by J. Echaabi et al. [136], respectively, which presented in Table 4.2.

Table 4.2. Material properties of the specimens used.

Properties	**Graphite/epoxy** [136]	**Prepreg T700/epoxy** [135]
$\mathbf{E_{11}}$ **(GPa)**	116	120
$\mathbf{E_{22}}$ **(GPa)**	6.9	120
$\mathbf{G_{12}}$ **(GPa)**	5.6	11.5
$\boldsymbol{\nu_{12}}$	0.3	0.28
$\boldsymbol{\nu_{23}}$	0.3	0.28
$\mathbf{E_f}$ **(MPa)**	230,000	224,000
$\boldsymbol{\nu_{f12}}$	0.2	0.6
$\mathbf{X_T}$ **(MPa)**	1860	2023.4
$\mathbf{X_C}$ **(MPa)**	1590	92.7
$\mathbf{Y_T}$ **(MPa)**	59	2023.4
$\mathbf{Y_C}$ **(MPa)**	207	92.7
$\mathbf{S_{12}}$ **(MPa)**	110	186

4.4.3. Model implementation

This section provides a comprehensive overview of the computational analysis process using the Finite Element Method (FEM), following the methodology outlined in the flow chart presented in Fig 4.5. It is important to note that this process involves iterations to ensure accuracy and convergence of the results.

The analysis begins by utilizing the UMAT subroutine, which plays a crucial role in computing the stress state and the compatible Jacobian matrix. Eqs. ((2.63) – (2.71)) are employed to determine the stress state for each step, considering all integration points within each lamina and for each analysis time step. The UMAT subroutine also handles the calculation of material properties, state variables, and deformation tensor as the initial step in the analysis.

Once the material properties and deformation tensor are determined, the Jacobian matrix is computed, and the stress field is predicted using appropriate equations. Additionally, a damage model, implemented via the UMAT subroutine, is employed to evaluate the stress state based on Puck's single element failure criteria, as described by Eqs. ((2.55) – (2.57), (2.61), (2.62)). If a failure mode is detected, the material stiffness is degraded using the Element Weakening Method (EWM) outlined in Eqs. ((2.72) – (2.82)). In our study, the assumption of an elastic brittle material implies that the damage variables are not explicitly derived or formulated through mathematical expressions. Instead, they serve as indicators of the failure state within the material. We assign a value of "1" to these damage variables to represent complete damage or failure when the failure has been detected by the Puck failure criteria. This representation is in line with the brittle behavior

assumed for the material, where failure occurs abruptly without significant plastic deformation. Given the assumption of an elastic brittle material, the formulation of the damage variables is not explicitly required or considered in our study. Consequently, the damage variables are updated to reflect the occurrence of damage. It is noteworthy that the computationally expensive search for the fracture plane angle, using Puck's failure criteria, persists as a restricting factor. Researchers have addressed this challenge, such as J. Wiegand et al. [137] who developed an algorithm incorporating a numerical search of the extremes of the function making it possible to reduce the amount of computation time needed to accurately locate the precise orientation of a potential fracture plane.

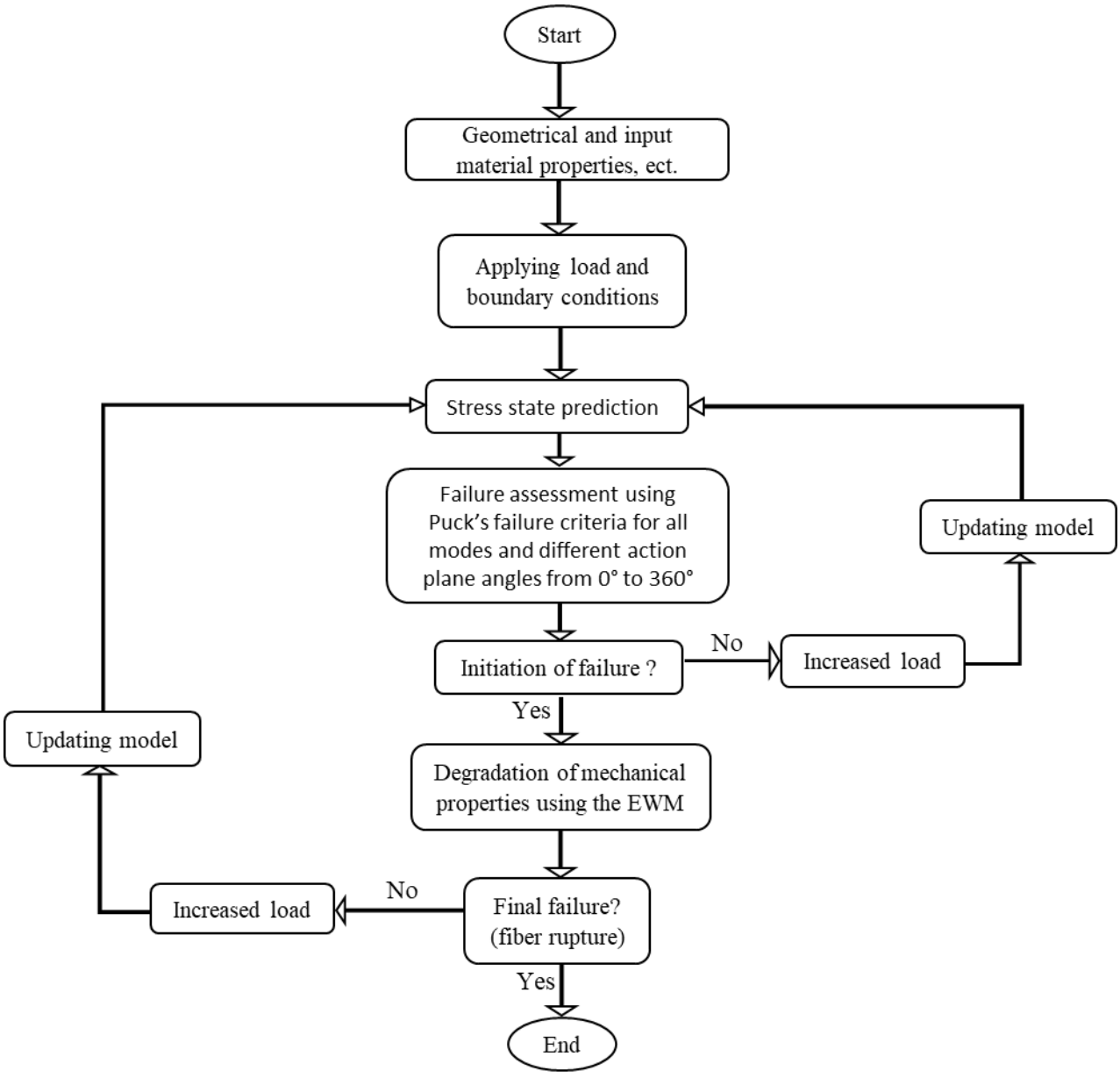


Figure 4.5: The computational algorithm.

Furthermore, the failure index and damage variables for the failure modes in the UMAT are shown by the solution dependence of state variables (STATEV). Table 4.3 depicts the symbol notion within the UMAT subroutine. Subsequently, the state variables are updated with the damage variables, and these variables are taken to the next step to update the stress field.

Table 4.3. Marking.

Concept	Symbol
Puck's fiber failure in tension	SDV1
Puck's fiber failure in compression	SDV2
Puck's matrix failure in tension	SDV3
Puck's matrix failure in compression	SDV4
Damage variable for fiber tensile	SDV6
Damage variable for fiber compressive	SDV7
Damage variable for matrix tensile	SDV8
Damage variable for matrix compressive	SDV9

Additionally, we repeatedly computed stresses and strains until the affected areas were completely ruptured (fibers failure), as the laminate was no longer able to support further loading due to many reasons such as fracture crack propagation in the 0° oriented plies in the Y-direction, fiber matrix debonding, and delamination between the plies. If the damage does not occur, then the stress state prediction is assumed to be correct. Next, a residual (R) is computed as the difference between the internal and external force vectors, and the residual is compared to the tolerance threshold defined by the user. A new load step is applied if there is convergence, i.e. if R is less than the tolerance (value adapted to engineering requirements), Abaqus stops the numerical analysis. It is necessary to point out that during the calculation of the failed elements, difficulties in the finite element software may occur at the convergence level.

Nonetheless, depending on the failure scenario, the elements must be degraded to a value close to zero, and the values of the damage variables must be updated. The previous section describes the application conditions of the different approaches.

On the other hand, R is estimated to have declined during the iterations for each load stage. When R rises, the response process diverges, and the numerical analysis comes to a halt. Divergence occurs when the material characteristics have degraded to a high degree and the strength of the structure is no longer sufficient to carry on the applied loads.

It should be mentioned that, when a user-defined material (UMAT) subroutine is used, the stiffness matrix is not directly computed by the program as it is in the standard element formulations. Instead, the UMAT subroutine returns the incremental constitutive matrix, which describes the material behaviour for the current integration point. The incremental constitutive matrix is then used to assemble the element stiffness matrix, which is a linearized form of the nonlinear equation system. The linearization is performed by assuming that the current stress state is close to the previous stress state and approximating the constitutive matrix as a linear function of the strain increments. This approximation is known as the tangent stiffness matrix and is used to update the stiffness matrix at each iteration of the solution process.

During the solution process, the tangent stiffness matrix is updated based on the current state of the model and used to solve the linearized equation system. This iterative process continues until the solution converges to a stable solution or until a maximum number of iterations is reached. Overall, the use of UMAT subroutine in Abaqus allows for the inclusion of complex material behaviours, but requires the user to provide an accurate and efficient description of the material behaviour through the UMAT subroutine, and may increase the computational cost due to the nonlinear iterative solution process.

4.5. Result and discussion

In this section, we will present the experimental results finding in this investigation for the prepreg T700/epoxy and the simulation results using the developed model. The macroscopic curves obtained from the specimens examined are shown in Fig 4.6 combined with the results produced by damage morphology. As can be seen, three macroscopic failures are observed for the orthogonal laminated K with a sequence layer $[0/90]_6$. However, a smaller ratio of span distance and thickness (l/h) induces stress normal to the median plane of the specimen, which leads to the creation and propagation of the intralaminar damage as illustrated when the loaded up from 309 N to 353 N. In conjunction with the rise of the load up to 360 N, we observed a total collapse appears in all layers as seen in the Figure.

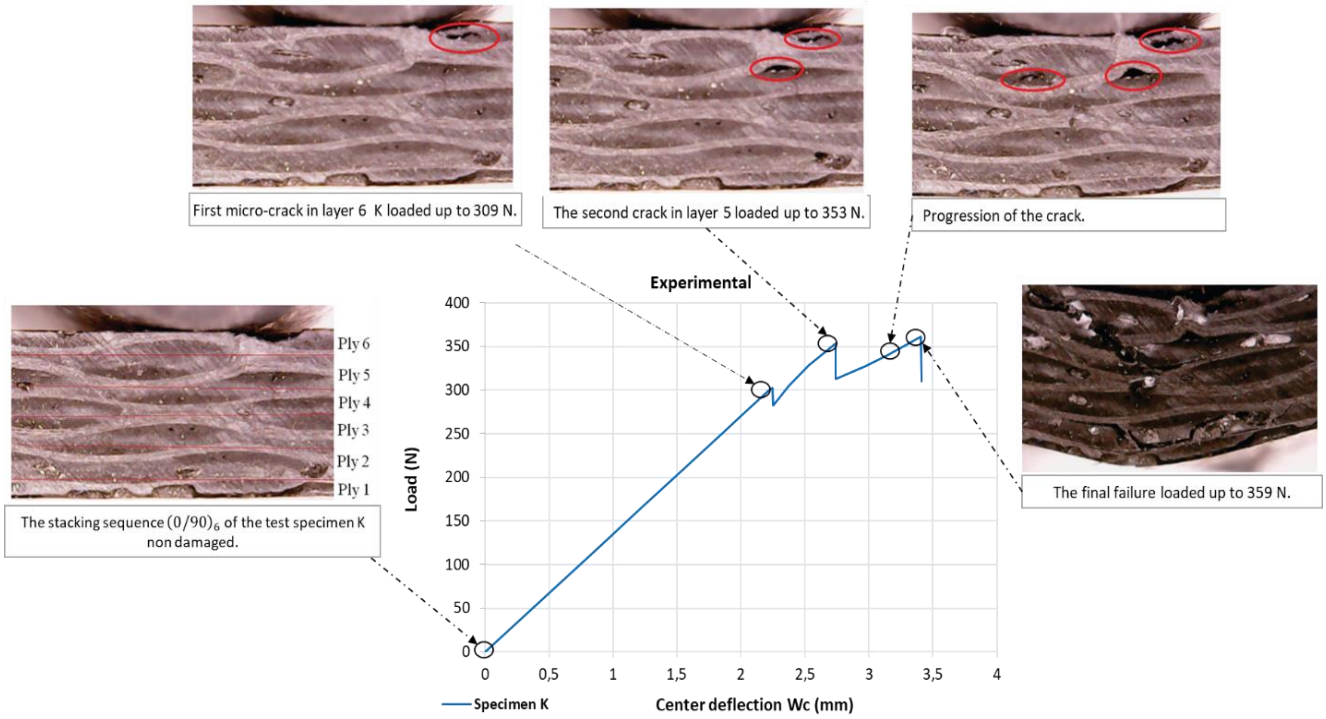


Figure 4.6: Experimental macroscopic curves with damage progressive of specimen K.

4.5.1. Analysis results and discussions for failure load

From the simulation side, the results deduced from this modelling are the successive failure, the modes of failure, deflection at failure load, the initiation and evolution of the damage and the macroscopic curves.

In the first step, we model our fabric prepreg "carbon/epoxy" by analogy with a [0°/90°] laminate [138]. The predicted results, using numerical modelling are shown in Tables (4.4 – 4.5) and have been compared with the experimental tests. Moreover, we will exploit the results found by J. Echaabi et al [136] for the graphite/epoxy to evaluate the applicability of our proposed model.

Table 4.4. Comparison of the failure load and the displacement at failure load with the test results.

Material	Layup	Label	Failure Load (N)		
			The Present model	**Experiment**	**Error (%)**
Prepreg carbon T700/epoxy	$[0°/90°]_6$	K	392,311	361,661	8.47
Graphite/epoxy	$[\,[+45°/-45°/90°/0°]_3\,]_s$	A	2991,36	2883,27	3.75
		B	1349,52	1210,03	11.52
		C	1079,74	969,194	11.37
		D	1182,64	1082,44	9.25

Deflection at Failure Load (mm)			
Label	**The Present model**	**Experiment**	**Error (%)**
K	3,4	3,40491	0.144
A	3,70891	3,8961	4.88
B	13,5267	13,6364	0.81
C	18,4638	18,3847	0.43
D	3,95891	3,92253	0.93

During loading, the ratio (l/h) and the width of the test specimen play a determining role in the values of resistance, the number of successive failures and the structural response that have been evaluated in this work. As shown in Table 4.4, the failure loads are predicted by a different ratio (l/h) for both prepreg T700/epoxy and graphite/epoxy are in good agreement with a slight difference between the experimental results where the error does not exceed more than 11.52%. However, the displacement anticipated at the failure load exhibits a meaningful correlation with the test results.

The accurate prediction of ultimate load and damage in composite laminates is a complex task due to various factors that are often overlooked in existing models and criteria. One of the main challenges is the consideration of realistic features that can occur during the damage process and significantly influence it. Micro-defects and material heterogeneity at the microstructure scale are important aspects that can affect the overall behaviour of the laminate, but they are often not adequately accounted for in current predictive models.

Progressive failure models and failure criteria, which are commonly used to predict damage in composite laminates, may not fully capture the influence of micro-defects and material heterogeneity. These models typically assume uniform properties throughout the material, ignoring the inherent variations and irregularities that can exist at the microscale. As a result, the predicted damage may not accurately reflect the actual behaviour of the laminate under loading.

Another aspect that is often neglected in predicting ultimate load and damage is the in-situ impact. When a fracture occurs in a laminate, the adjacent lamina provides support, resulting in a higher strength for the fractured layer compared to an individual lamina. Neglecting this in-situ effect can lead to overly conservative predictions, where the analysis of the laminate underestimates its actual strength.

In-depth studies on the in-situ impact and its influence on composite laminates can be found in reference [124]. These studies aim to better understand and quantify the effect of adjacent layers on the strength and damage behaviour of fractured laminates. By incorporating the in-situ impact in predictive models, more accurate predictions of ultimate load and damage can be achieved.

Interlaminar damage between adjacent layers is another factor that is often ignored in the analysis of composite laminates. While it may have a minimal effect on the overall mechanical behaviour of the laminate, it can still contribute to the overall damage process. Neglecting interlaminar damage can result in incomplete predictions of the damage progression and its impact on the ultimate load capacity.

The progressive damage model employed in our study based on the puck failure criteria has a restricted ability to predict delamination, which focuses solely on intralaminar damage, specifically fiber/matrix failure within the laminate. While these failure criteria adequately capture the observed failure modes of the prepreg T700/epoxy material, including the phenomenon of false delamination represented by longitudinal cracks within the laminate, as demonstrated in Fig 4.6, it does not encompass the prediction of delamination itself. However, delamination in bending occurs, in case of a very low (l/h) ratio, under the effect of higher interlaminar stresses σ_{33}, σ_{13} and σ_{23} [139]. Accordingly, we have observed experimentally that the primary failure mechanism is false delamination rather than conventional interlaminar delamination. In view of this experimental evidence and in order to simplify the computation and reduce the processing time, we have opted for a plane stress problem, neglecting interlaminar stresses in our numerical model. This approach enables us to focus on the intralaminar damage, which is the dominant failure mechanism observed in our experiments. Furthermore, the stress plane assumption reduces the number of elements and nodes required in the finite element model. Consequently, it lowers computational costs and improves efficiency, making it feasible to analyse larger and more complex composite structures within practical time frames. However, composite laminates are often designed with thin layers of fiber-reinforced materials. In these cases, the stress plane assumption is applicable because the out-of-plane stresses are typically negligible compared to the in-plane stresses. By focusing on the dominant in-plane stresses, we can accurately capture the laminate's behaviour under bending loads.

The failure load of the first damaged layer and the final failure load of the composite laminate are governed by the type of layup configuration, material, boundary circumstances and geometry of the composite laminate. Based on the above results, it was observed that the strength of the laminate is reduced by increasing the ratio (l/h) for specimens A, B and C. In addition, for specimen D only the width has been changed and therefore the failure load has been increased, which means that the width also has an effect on the failure of the composite under three-point bending.

4.5.2. Discussion and analysis results for progressive damage and load-deflection curves

The Figs. (4.7 – 4.11), to evaluate load-deflection behaviour, illustrate the prediction of the three-point bending results of all the labels (K, A, B, C, D) and correlated with failure modes using the applied method and the experimental test. In the initial stage of a linear problem, where there is no initial deterioration in stiffness or material properties, the composite laminate behaves according to linear elastic principles. The stiffness properties of the plies are considered intact, and the load distribution is based on these properties.

However, when damage occurs within a ply, it can have significant implications for the overall behaviour of the laminate. As the damage progresses and reaches the failure criteria and degradation patterns, the stiffness properties of the damaged ply may decrease. This reduction in stiffness leads to a redistribution of stresses within the laminate, as the intact plies take on a larger share of the load.

The stress redistribution effect occurs due to the load-sharing mechanism among the plies. When one ply is damaged and experiences a decrease in stiffness, the adjacent intact plies absorb a portion of the load previously carried by the damaged ply. This redistribution helps to mitigate stress concentrations and prevents localized failure, thereby enhancing the overall structural integrity of the laminate.

If the load continues to increase, and the stiffness properties of the remaining intact plies decrease as well, another layer may eventually reach its failure criteria and degrade. This process can lead to a cascade of layer failures, where each failure triggers the next one. The laminate experiences a progressive failure mechanism, with each damaged ply influencing the load distribution and failure progression.

Despite the occurrence of ply failures, it is often observed that the composite laminate retains a considerable amount of strength even after the first layer fails. This residual strength is due to the load-sharing effect among the intact plies. The intact plies continue to contribute to the load-bearing capacity of the structure, effectively compensating for the loss of strength in the failed layers.

The ability of the laminate to maintain its overall strength even after the failure of individual plies is a desirable characteristic of composite materials. It provides a measure of robustness and damage tolerance, allowing the structure to sustain loads beyond the initial failure point. This behaviour is advantageous in engineering applications where safety and structural integrity are critical. Furthermore, we can observe the reduction in stiffness for both composite materials, where the sharp curves shown in the plot are an indicator of the occurrence of damage and consequently the behaviour of the material is getting non-linear. In addition, the ratio (l/h) is a primary factor in geometric nonlinearity. Indeed, laminated beams with a low ratio exhibit linear behaviour as shown in Fig. 4.6 and non-linear responses correspond to beams with relatively large l/h ratio (Figs ((4.9) – (4.10))).

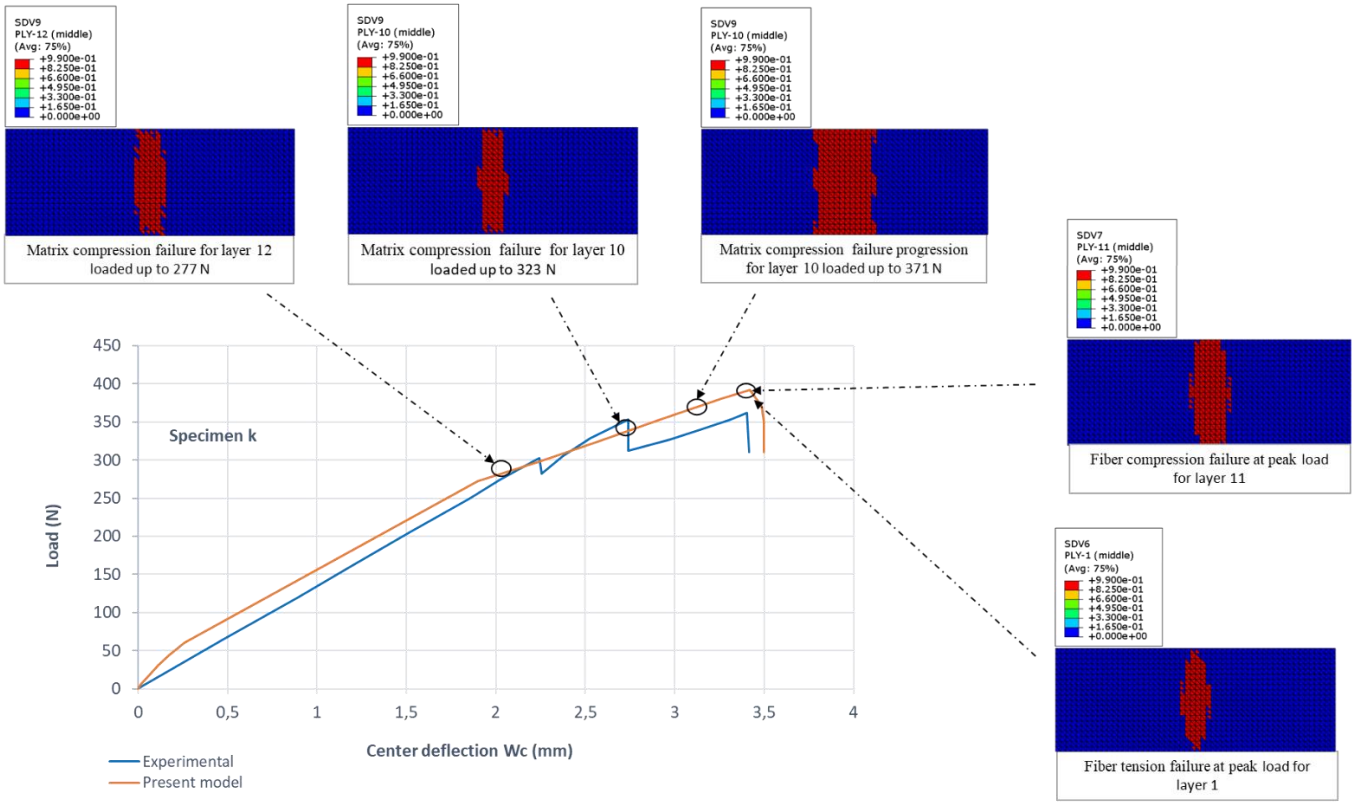


Figure 4.7: Load-deflection curves of specimen K.

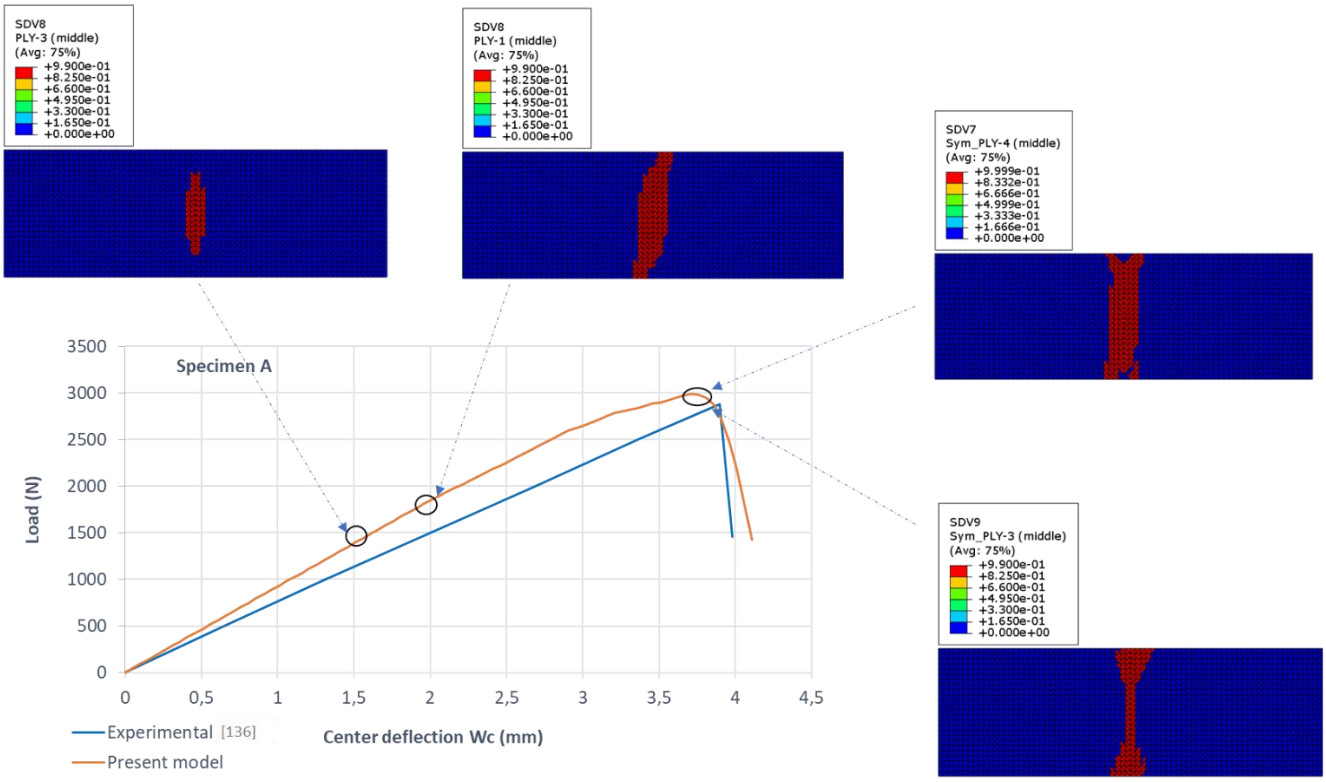


Figure 4.8: Load-deflection curves of specimen A.

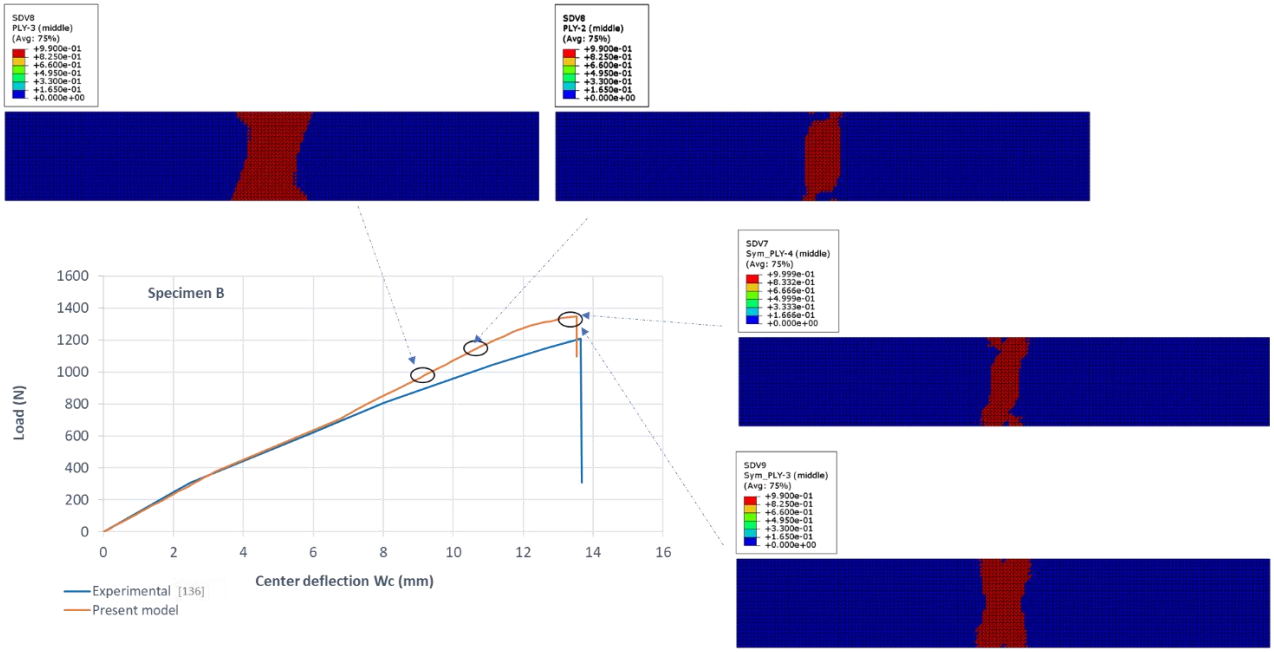


Figure 4.9: Load-deflection curves of specimen B.

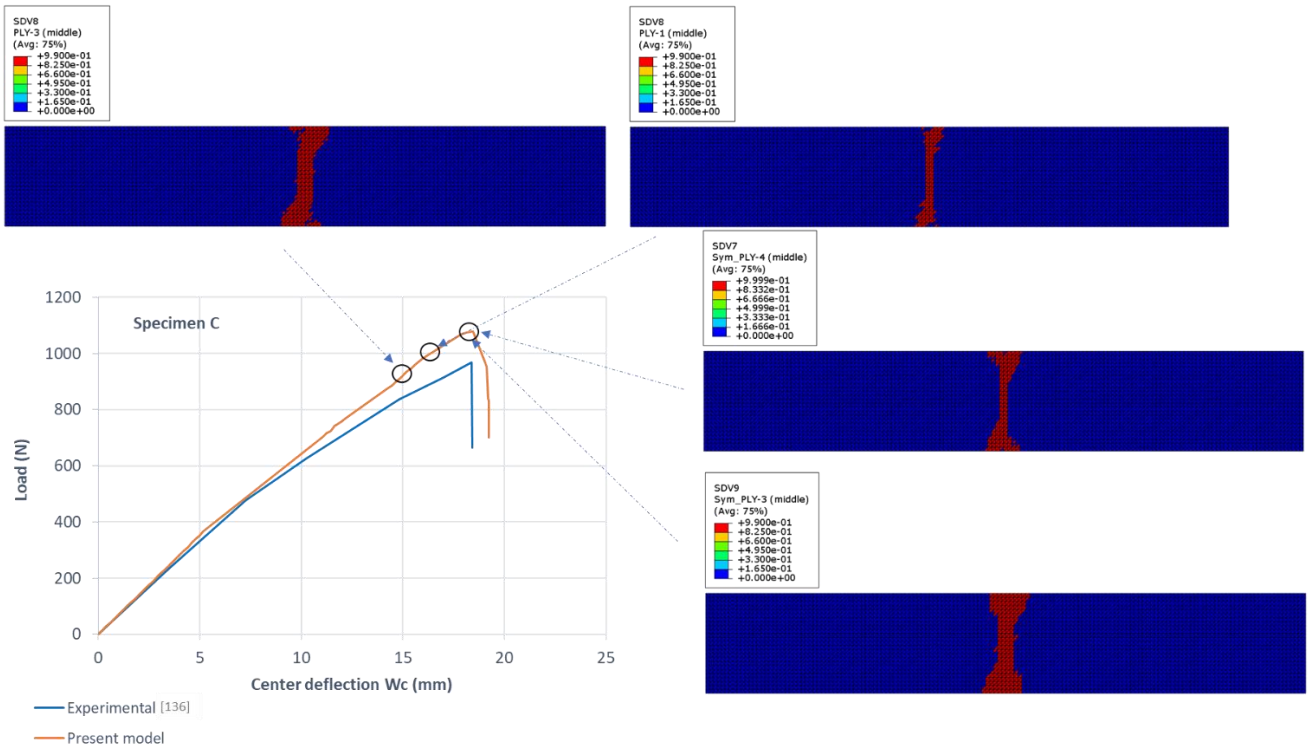


Figure 4.10: Load-deflection curves of specimen C.

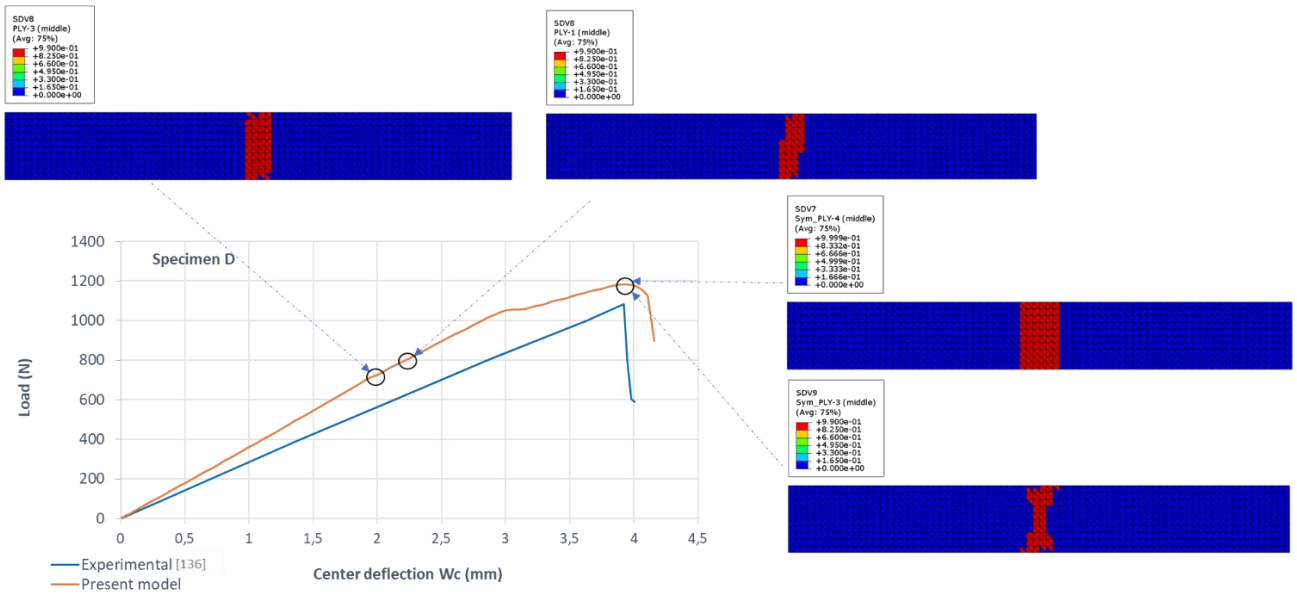
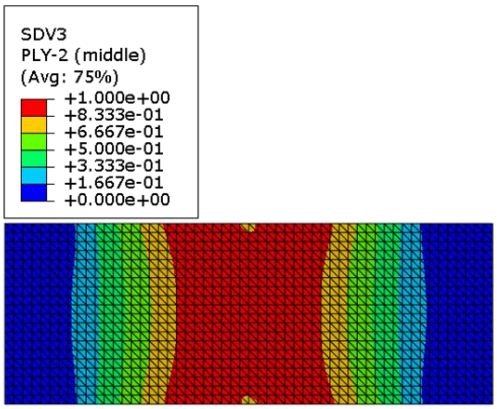
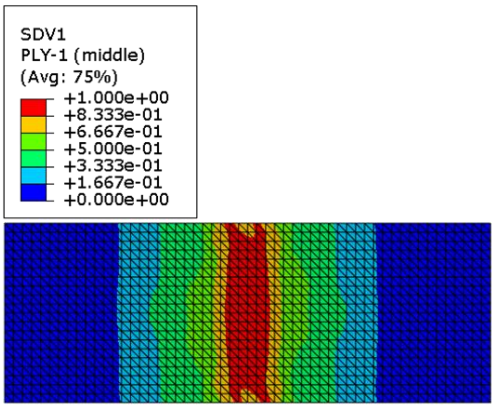


Figure 4.11: Load-deflection curves of specimen D.

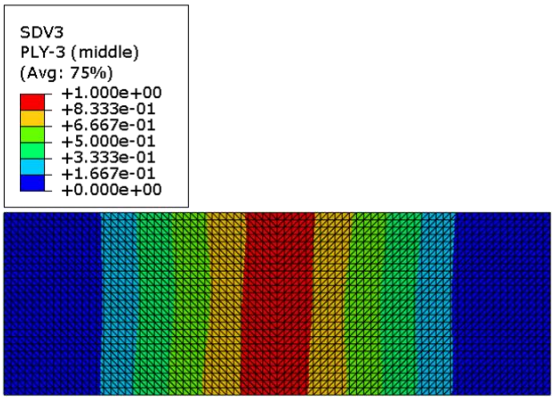
The difference in prediction ability of load vs deflection curves (all the labels) using the Puck-EWM with the test result, which is noticed in the final failure deflection, is due to a further reduction in the rigidity and strength of the elements, resulting in the removal of these elements, hence, faster divergence can be seen. Typically, with each failure mechanism, all properties of an element will reduce equally. Furthermore, in case fiber failure occurs in an element, then all properties of that element will fail and it will not be able to withstand the transverse and shear loads when a larger amount of laminate degradation takes place in a shorter period, leading to a decreased loading capacity of the composite laminate.



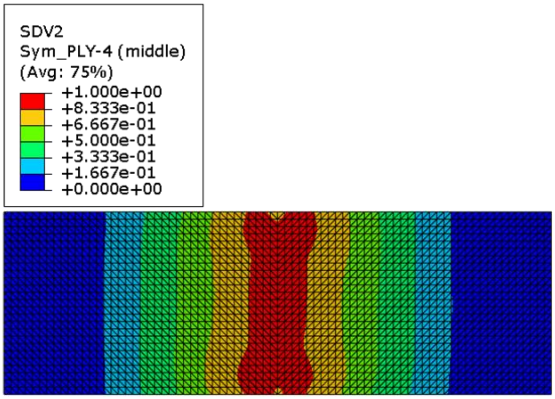
(a) Matrix failure contour (specimen K)



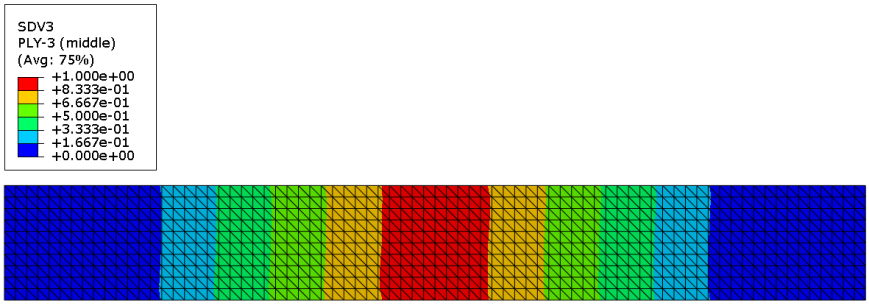
(b) Fiber failure contour (specimen K)



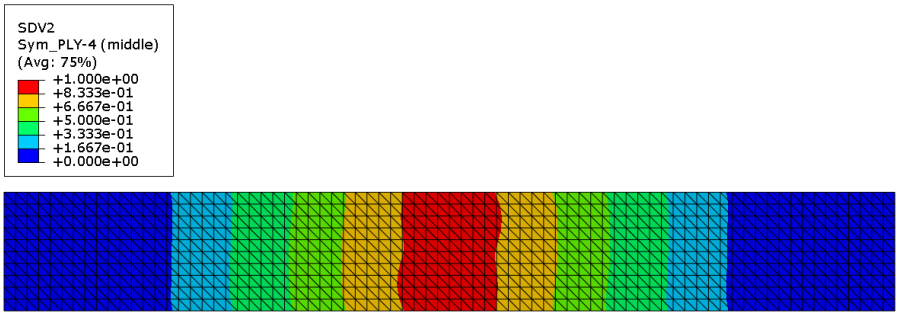
(c) Matrix failure contour (specimen A)



(d) Fiber failure contour (specimen A)



(e) Matrix failure contour (specimen D)



(f) Fiber failure contour (specimen D)

Figure 4.12: Progressive failure contours using the applied method for specimen K, A and D.

Table 4.5. Results obtained by finite element method for test specimen A, D and K.

Specimen	Failure sequence	F (N)	Layer number	Angle (°)	Type of failure
K	1	56.0043	2	90	SDV3
	2	84.5651	4	90	SDV3
	3	117.773	6,1	90,0	SDV3
	4	147.395	12	90	SDV4
	5	147.395	3	0	SDV3
	6	195.845	10	90	SDV4
	7	195.845	5	0	SDV3
	8	259.617	8	90	SDV4
	9	259.617	14	90	SDV4
	10	298.139	11	0	SDV4
	11	324.579	7	0	SDV3
	12	392,311	9	0	SDV2
A	1	1583.63	3	90	SDV3
	2	1630.08	1	45	SDV3
	3	1766.41	2	-45	SDV3
	4	2264.25	5	45	SDV3
	5	2473.57	7	90	SDV3
	6	2556.94	21	0	SDV2
	7	2596.71	24	45	SDV4
	8	2596.71	6	-45	SDV3
	9	2630.04	23	-45	SDV4
	10	2886.22	20	45	SDV4
	11	2974.87	17	0	SDV2
	12	2991,36	All remaining layers	-	SDV2, SDV4
D	1	655.432	3	90	SDV3
	2	655.432	1	45	SDV3
	3	706.3	2	-45	SDV3
	4	934.573	5	45	SDV3
	5	981.677	24	45	SDV4
	6	1027.84	7	90	SDV3
	7	1027.84	21	0	SDV2
	8	1042.16	6	-45	SDV3
	10	1042.16	23	-45	SDV4
	11	1147.56	17	0	SDV2
	12	1182,64	All remaining layers	-	SDV2, SDV4

For further clarification of the damage process, Table 4.5 shows the successive failure that occur in the specimens (K, A, D) and failure contour of fiber and matrix have been presented in Fig. 4.12. The result was obtained by coupling the Puck's failure criteria and EWM.

For the label K, the crack initiates from the lower plies with 90°. Besides, the density of the cracks increases with the load and turns into the upper layers. As the damage spreads in the matrix, macroscopic failure is occurring which may lead to a separation between plies as a result of the growth of longitudinal cracks.

Fig. 4.7 shows the numerical results of the damage evolution for the Prepreg T700. As can be seen, the matrix compression starts failing in the middle of the specimen through the layer oriented with 90° ply 12 and move to layer with the same orientation ply 10. Then, the failure propagates within layer with 371 N. However, in the peak load layer with orientation 0° (plies 11 and 1) failed where the plies have lost, they strength. Besides, the failure of the fibers is noticed to appear at the layer with an orientation of 0°, because of the longitudinal tension that has the maximum amount of damage.

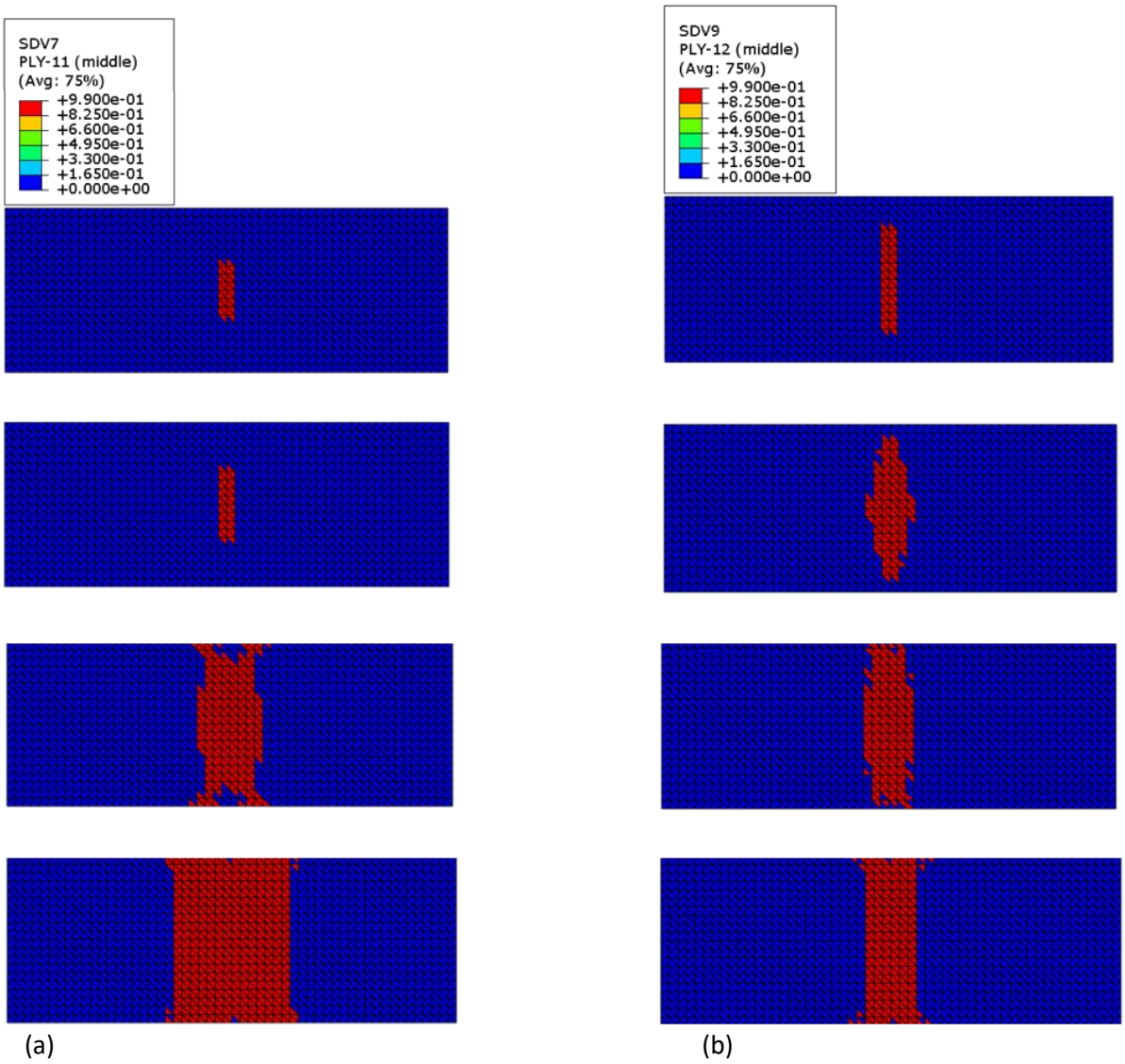


Figure 4.13: Failure patterns of Prepreg T700: (a) Fiber damage progressive in the 0° ply; (b) Matrix damage progressive in the 90° ply.

Besides, Fig 4.13 shows the patterns of fiber and matrix failure modes for layers with an orientation of 0° and 90° using Puck-EWM. The figures involve four different time steps, compression fiber failure is indicated for 0° layers and compression matrix failure is presented for 90° layers.

However, the matrix damage increases progressively tangentially in the fiber direction and the contour damage of the Puck-EWM diffuses a little more than the experiment found. The stiffness is instantly reduced in the EMW and leading to the development of larger deformations within the material which the EWM leads to the failure of more elements. The fiber damage progresses perpendicular to fiber direction until it reaches a certain point, after which it propagates to the edge.

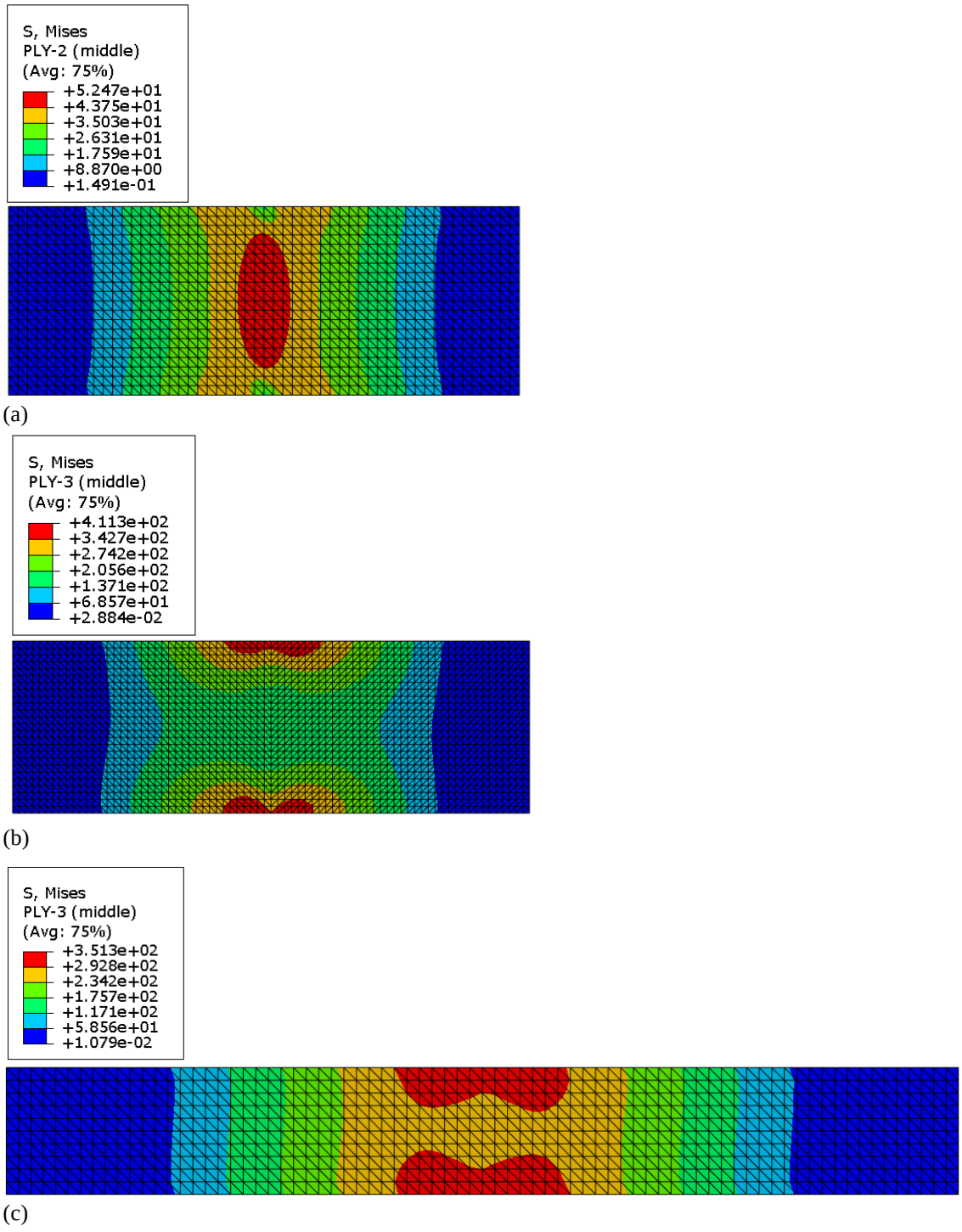


Figure 4.14: Contours of stress's Mises (MPa) in the 90° ply: (a) stress contour of specimen k at first ply failure; (b) stress contour of specimen A at first ply failure; (c) stress contour of specimen D at first ply failure.

However, the failure initiates at the bottom and grows to the top for both specimens (A, D) where the matrix cracking appears first in the 90° plies and grows to the 45° plies. Fig. 4.14 shows the stress contour at first-ply failure for the labels K, A and D, which indicates the appearance of stress concentration from the middle and bord of materials.

It should be underlined that the shear stresses support the inter-fiber failure if σ_n relates to tensile stress. Nevertheless, it would restrain inter-fiber failure if σ_n represents compressive stress by increasing the resistance to failure through shear stress. For this reason, separate equations are used to predict inter-fiber failure in tension and compression as shown above [140].

Furthermore, the fiber failure is noticed in the 0° plies which the first failure appears in the two upper 0° plies and is preceded by matrix cracking. The main difference in the result between the specimen (A, D) is the succession of damage after the occurring of macroscopic failure and is due to the different widths of the specimens. In peak load, the curves of load vs. deflection exhibit vertical jump that corresponds to macroscopic failures in plies orientated at 0 degrees and this value vary with the width and the ratio (l/h). Hence, catastrophic failure occurs across the layers due to the decrease in all material properties resulting in the complete fracturing of the composite laminate. Those predictions are in good correlation with the experimental result reported by J. Echaabi et al. [136] where errors of the simulated failure load and deflection at failure load do not exceed 11.52% and 4.88%, respectively. In some cases, the error of failure load does not surpass 3.75% such as label A. Additionally, for the deflection at failure load, most of the cases the error does not surpass 0.9% such as labels (B, C and D). Noted that the source of the errors using the numerical approach can be attributed to many reasons. The majority of the theories neglect such realistic phenomena, which can appear especially in the heterogonous material at the microstructural scale, such as the micro defect during the forming of materials or matrix-inclusion interaction which leads to high flow stress and then conservative analysis can be shown.

From these results, we found a strong correlation between the thickness ratio (l/h) and the macroscopic behaviours of the specimens, with a low ratio (l/h) resulting in a linear response and a high ratio (l/h) resulting in a nonlinear response. In addition, this parameter, thickness ratio (l/h), does not influence the microscopic behaviours observed, because, for different values of (l/h), the progressive damage and the failure mode remain the same.

4.5.3. Mesh dependency

The choice of mesh density plays a crucial role in numerical modelling, as it can significantly impact the accuracy of the results and the computational efficiency of the simulation especially under different load scenario. Different mesh densities can lead to variations in the predicted behaviour of the structure, making it important to select an appropriate mesh density that balances accuracy and processing time.

In numerical modelling, the mesh represents the discretization of the geometry into smaller elements or cells. The accuracy of the simulation is generally expected to improve with finer meshes, as they can capture more detailed features and variations in the structure. However, using excessively fine meshes can also result in increased computational costs, including longer processing times and higher memory requirements.

To strike a balance, it is essential to choose an appropriate mesh density that minimizes the influence of mesh dependency while ensuring the highest possible accuracy of the results. Mesh dependency refers to the sensitivity of the simulation results to changes in the mesh density.

Ideally, the chosen mesh density should provide stable and consistent results that are not excessively influenced by further mesh refinement.

Determining the appropriate mesh density often involves performing mesh convergence studies. In these studies, the simulation is repeated with varying mesh densities, and the results are compared to assess the convergence of the solution. The convergence is typically evaluated by examining the changes in key output quantities, such as displacements, stresses, or strains, as the mesh is refined. The goal is to identify a mesh density beyond which further refinement has a minimal impact on the results.

When investigating large or complex structures, choosing the appropriate mesh density becomes even more critical. The computational resources required to analyse such structures can be substantial, and processing time can become a limiting factor. Therefore, it is necessary to strike a balance between accuracy and computational efficiency.

In practice, there are several approaches to manage mesh density for large structures. One common strategy is to use a combination of coarse and fine meshes, focusing the finer mesh on areas of interest or regions where higher accuracy is required. This technique, known as adaptive meshing, allows for a more efficient allocation of computational resources while maintaining accuracy in critical regions.

Additionally, advanced meshing techniques, such as mesh morphing or adaptive mesh refinement, can be employed to dynamically adjust the mesh density during the simulation based on specific criteria or solution behaviour. These techniques aim to optimize the mesh density in real-time, focusing computational efforts where they are most needed.

Furthermore, the failure loads have been chosen to evaluate the applied model as suitable parameters for the analysis. The number of existing elements in the in-plane mesh density has been addressed. Fig. 4.15 shows the load-deflection curves for composite laminate Graphite/epoxy with the following stacking sequences $[\,[+45°/-45°/90°/0°]_3\,]_s$, to assess the mesh dependency using the previously considered method with different mesh cases as shown in Fig. 4.16.

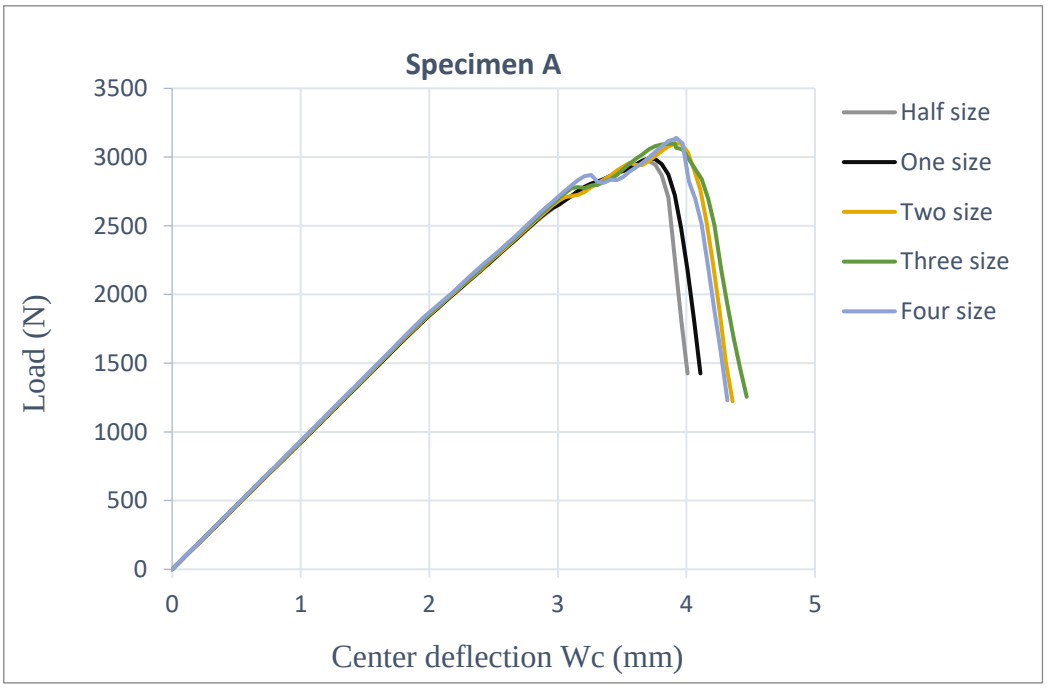


Figure 4.15: Load vs. deflection curves for the different mesh sizes.

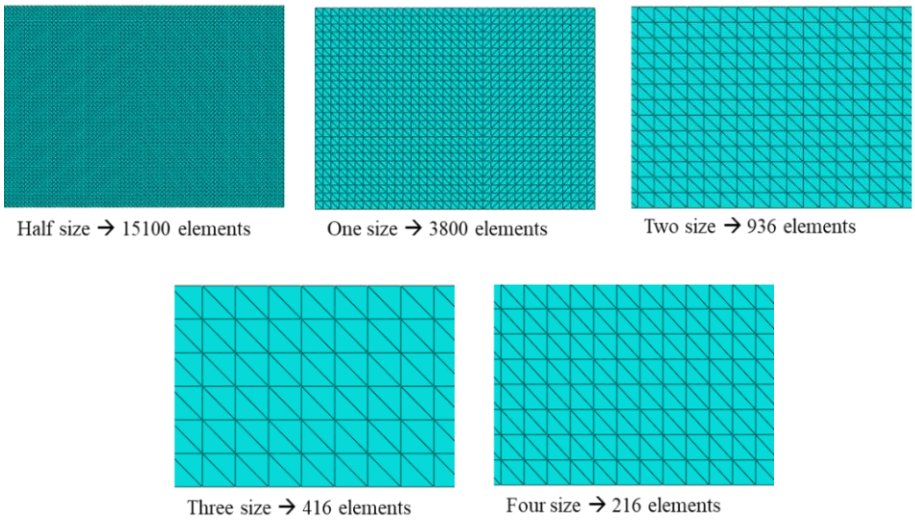


Figure 4.16: Different mesh numbers to verify the mesh dependency of the applied model.

The implemented PFA model exhibits less influence on the mesh dependence, resulting in slightly different values for the different meshes. The deflections at the ultimate load vary slightly in the different meshes used. Further, Fig. 4.17 depicts the variation of the normalized failure load plotted vs. the total number of elements for FPA carried out with the Puck-EWM. The applied model exposes an error of less than 8,8 % (with 216 elements = size of 4 mm*4mm), as the results converge to the experimental data, it shows a very reliable result with an error of less than 3.7 % when increasing the number of elements (by starting with 3800 elements = size of 2 mm* 2mm).

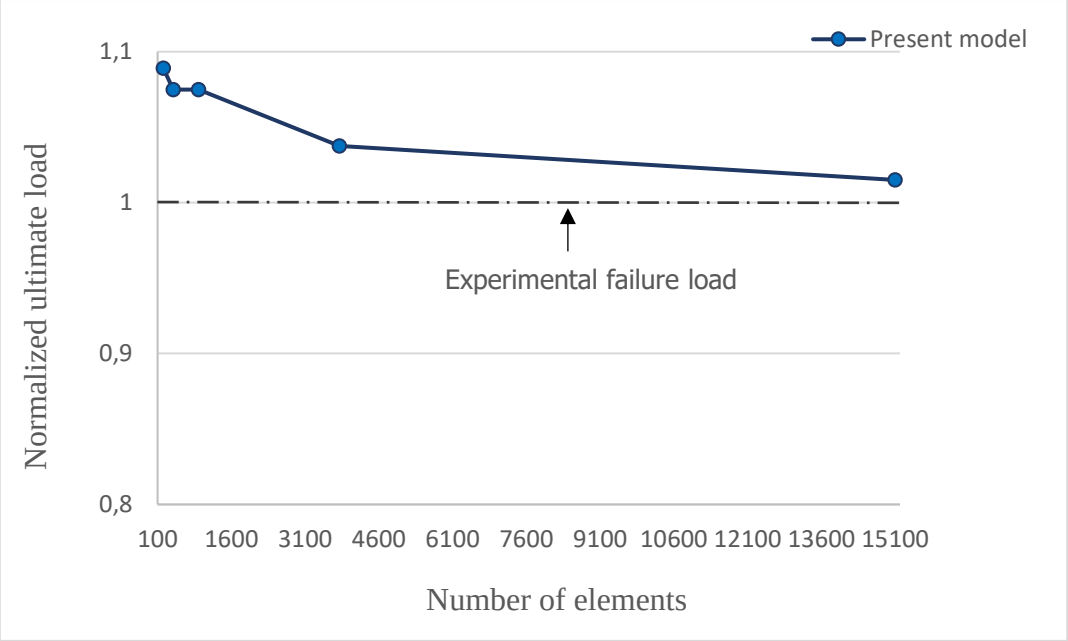


Figure 4.17: Failure load values according to the number of elements.

4.6. Conclusion

In this chapter, we conducted a comprehensive study on two different composite laminates subjected to three-point bending. Our objective was to analyse the damage progression from the initial onset of damage to the final failure. To achieve this, we developed a finite element model

incorporating Puck's failure criteria and an element weakening method, which accurately captured the behaviour of the specimens.

Additionally, we conducted an experimental investigation of the Prepreg T700/epoxy woven laminates under three-point bending tests. By comparing the experimental results with our finite element model predictions, we were able to draw several important research findings.

Firstly, we found that Halpin's analogy, which considers the woven laminate as a two-layer laminate [0/90], demonstrated a strong correlation with the experimental findings. This observation was evident in the accurate prediction of deflection and failure load.

Moreover, we identified that the ratio (l/h) and the width of the specimens played a crucial role in the successive failure and overall resistance of the composite laminate. Specifically, we observed that increasing the ratio (l/h) negatively impacted the strength of the laminate. These findings highlight the significance of these geometric parameters in determining the structural integrity and failure behaviour of the composite laminate.

Furthermore, our research demonstrated the feasibility of conducting structural failure assessments for highly complex composite structures. However, it is important to note that the implementation of Puck's criteria in our analysis required an iterative process to determine the fracture plane angle at each integration point for each increment. As a result, the analysis time was significantly longer.

Chapter 5: Intra/interlaminar damage modelling of composite laminates using a 3D progressive failure model

Overview

- *Introduction*
- *Failure theory*
- *Modelling*
- *Results and discussion*
- *Conclusion*

5.1. Introduction

Modern aerospace structures make extensive use of composite structures. Developments in this field of expertise should improve the performance of these materials in the future. In recent years, there has been also a substantial increase in the use of composite materials in the transportation industry such as automotive and marine. The efficiency of these structures is in fact determined to a certain extent based on the characteristics and understanding of the materials. However, out-of-plane failure modes that occur in composite laminates are frequently driven by interlaminar and transverse stresses. A safe design of lightweight FRC structures requires an efficient and reliable failure prediction model for a general three-dimensional (3D) state of stress. Laminated structures commonly have geometries with thicknesses small relative to their lateral dimensions. The deformations of such structures are usually analyzed by using a 2D structural model that is based on the plane stress state assumption. The governing equations and the associated boundary conditions of the reduced-order model are derived by making suitable kinematic assumptions on the displacement field in the thickness direction, and integrating through the thickness various moments with respect to the thickness coordinate of the partial differential equations governing 3D deformations of a continuous body.

However, the complexity of the failure mechanisms of laminated composites is related to many factors, such as interfacial fiber/matrix decohesion, matrix cracking, delamination between plies and fiber failure (buckling or kinking) in independent or mixed modes. Due to the high anisotropy of these structures and the dependence on temperature, time, ambient light and humidity, many measurements are required to fully qualify a material. Certain of these features are difficult to quantify and may not be possible to identify them at all [141]. The collapse of composite structures is part of a progressive degradation process. Furthermore, it is important to note that local failure causes load redistribution, allowing multiple failure mechanisms to emerge, which diminishes the strength of the composite structure, decreases the capacity of carrying the stress, and ultimately leads to global rupture of the composite. Moreover, it is difficult to accurately represent the stiffness behaviour of a fiber carbon-reinforced polymer coupon due to numerous interacting aspects, such as treatment techniques, distribution and arrangement of the fibers and matrix.

On the other hand, flexural testing leads to beneficial mechanical parameters for composite laminates, such as flexural modulus and shear stress, as well as a better ability to comprehend and describe the cohesive inter-layer interactions. The advantage of three-point bending tests is that they have advantages in terms of specimen generation, they allow progressive tracking of specimen degradation to final failure, the location of the failure is foreseeable, and they also allow validation of the strength of composite structures. Once a specimen is subjected to a bending load, the three basic stress states of the material are induced, namely tension, compression and shear. The failure of composite material is controlled mainly by one of the three basic stresses that will be the first to attain its ultimate value. Parallel to this, previous studies of damage composites under bending load have assumed equal compressive and tensile responses, resulting in over- or underestimation of composite resistance. In order to improve the accuracy of the post-processing analysis and reduce effectively time and costs and exploit fully the profits of composite structures under different loads, more credible failure theories and damage propagation approaches are urgently required.

Nevertheless, progressive damage modelling of composite laminates has gained significant attention in over the last years due to its ability to accurately predict the mechanical behaviour and failure mechanisms of these materials under bending load [96], [97], [142], [143]. A model of

progressive damage based on the Hashin failure criteria and cohesive zone method was developed by Y. Yang et al. [98] to investigate the behaviour of the composites laminated under three-point bending and compared the analysis results with the experiments tests. The implementation of their energy-based model requires a large number of input parameters, which makes it computationally intensive. The inter-laminar damage response of glass/epoxy composite laminates of different L/h ratios under 3-point bending loading has been investigated by Liu et al. [144]. The failure mechanism was highly sensitive to the stacking sequence of the glass fiber reinforced epoxy layers. M. Demiral et al. [145] have studied the size effect in unidirectional (GFRP) subjected to quasi-static bending loading, and it was observed that the flexural failure triggered the multiple delaminations. L. B. Andraju et al. [146] used a finite element model that included the 3D Hashin failure criteria and a cohesive zone model to forecast failures, including the effect of matrix tensile strength, plies orientation, and damage interlaminar resistance on the failure of curved laminates. Their research shows that it is possible to increase the out-of-plane strength of curved laminates through a suitable sequence of layup selection as well as matrix strength properties. P. Hu et al. [147] have investigated the influence of intralaminar damage on interlaminar delamination properties of laminated composites through a novel two-step mechanical test. They found that intralaminar damage promotes fiber bridging in the transverse direction, which ultimately influences the out-of-plane properties significantly.

Over the years, there has been growing interest in understanding the interaction between intra/interlaminar damage in composite materials, as evidenced by several recent studies [148]–[150]. Ferreira, Gregório F.O. et al. [151] have presented a novel approach to modelling composite laminates and analysing the progressive damage under bending load. The approach is based on Carrera's unified formulation and continuum damage mechanics (CDM) principles. However, the study only considers progressive damage in-plane and does not address out-of-plane damage mechanisms which can be an important factor in many practical applications where composite laminates are subjected to complex loading conditions and occur due to transverse cracking, delamination, or fiber breakage perpendicular to the plane of the laminate. M. A. Caminero et al. [152] have carried out a three-point bending test of symmetric cross-ply CFRP in order to identify the initial failure mechanism and where it occurs for engineering reasons, as well as to define the mechanical response in terms of strength using sub-laminate level technique and ply level. The thicker laminates were observed to have lower strength and strain at finale failure but exhibited higher flexural stiffness and a meaningful switch in flexural behaviour as a function of stacking sequence and spalling type.

Most of the above literatures require more computational effort and time, and only concentrate by the forecast of the onset of damage, while disregarding the development of the defect, as equally relevant to damage assessment of the composite. Also, often they do not take into consideration of the Interaction of multiple damage mechanisms: In composite laminates, multiple damage mechanisms can occur simultaneously, which makes it challenging to predict the evolution of damage.

In addition, in the meantime, the composites begin to lose their load carrying capacity once the ultimate stress point in the load versus deflection graph has been crossed, however, some of the load can be retained, thus there is a window of opportunity for remedial action. For this reason, it is very necessary to have a more accurate estimation of the damage evolution in order to be able to follow the damage process and to better predict the strength remaining [98]. The continuum damage mechanics approach (CMD), whereby the stiffness tensor factors of the laminate are

reduced, is an equivalent replacement for these methods. To predict damage initiation and damage evolution in composite structures, progressive damage analysis (PDA) is widely employed. Moreover, the three main aspects of the (PDA) model are the behaviour's laws of the material used, damage criteria for predicting the occurrence of failure and the material degradation model.

In this chapter, we propose a new progressive damage model that takes into account both inter and intralaminar failure modes to accurately predict the flexural behaviour and damage evolution of composite laminates under three-point bending. The proposed model incorporates a progressive failure algorithm and gradual stiffness degradation rules through a user defined subroutine UMAT to predict further damage evolution following damage initiation, estimated by the combination of the three-dimensional Puck failure criteria and the cohesive zone model.

One of the objectives of this research is to develop a finite element model (FEM) capable of simulating the behaviour of different composite laminates under three-point bending, to reduce effectively processing time and testing costs. As part of the investigations carried out in this study on the damage mechanics of two types of composite laminates IMS194/CYCOM977-2 and AS4/PEEK, we considered the prediction of ultimate load and stiffness. The results showed significant agreement with the experiments [98], [153], as well as degradation trends in the load vs. deflection curves. In addition, the interaction of matrix cracking and delamination as well as the impact of cohesive zones elements on material strength. Corrodingly, we found that the interface strength should be considered, to fully exploit the laminate features, and to reduce the effect of delamination which causes intra-laminar longitudinal cracks to appear under the effect of higher inter-laminar stresses. Furthermore, a mesh dependency of the model used has been conducted, to determine the optimal mesh size and shape required to accurately capture the behaviour of the composite laminates.

The significance of our study lies in the development of a more accurate and reliable progressive damage model that can improve the design and engineering of composite laminate. By taking into account interaction between inter and intralaminar failure modes, the proposed model can provide a better understanding of the damage mechanism of composite laminates, which is crucial for designing more reliable and durable composite structures. The illustrative synopsis below summarises the work carried out in this chapter.

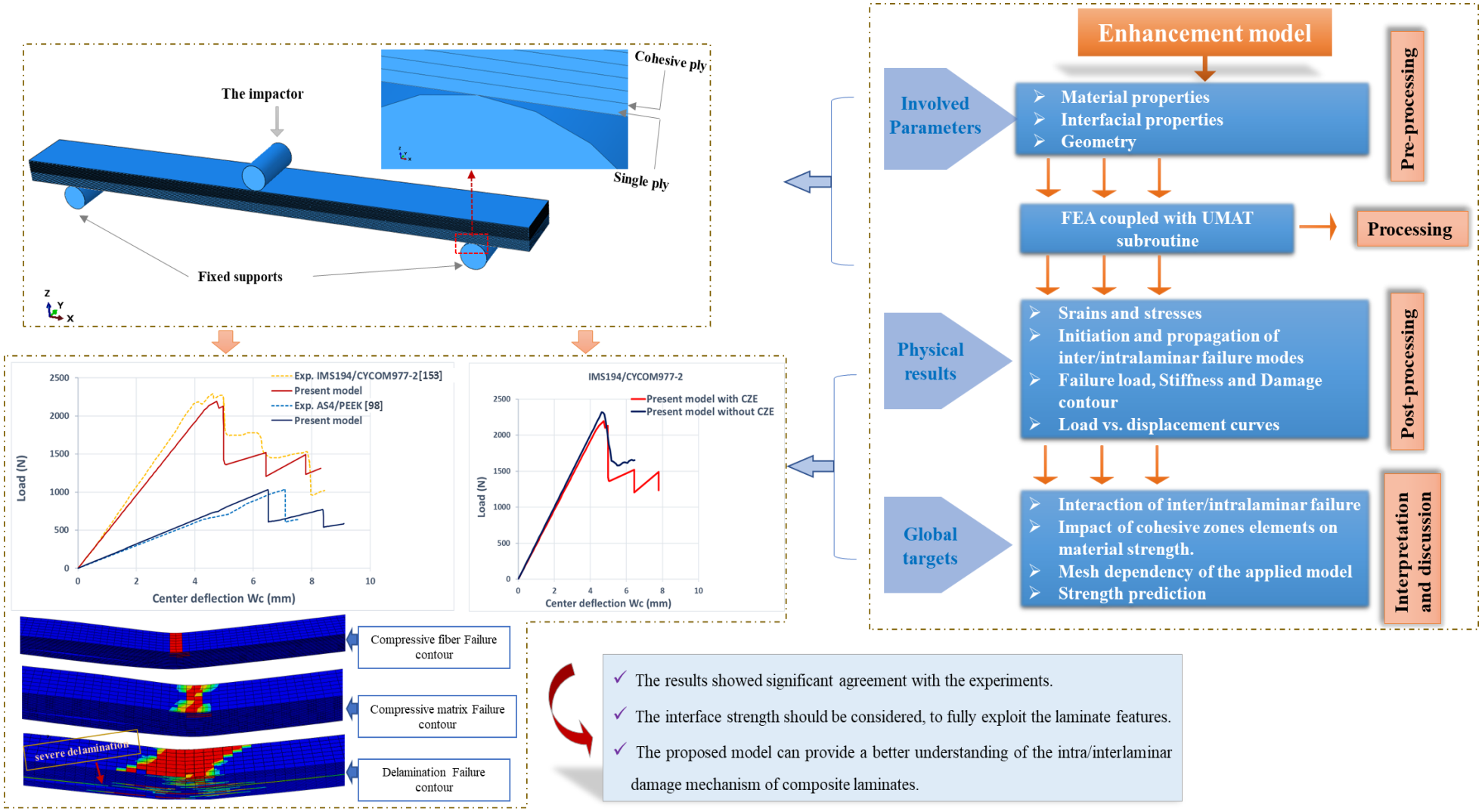


Figure 5.1: The illustrative synopsis.

5.2. Failure theory

5.2.1. Intralaminar damage initiation

To predict damage initiation and failure modes for the laminated composites, the combined failure criteria including the Puck criteria and the cohesive zone method have been established. As a result of the highly anisotropic and inhomogeneous nature of composites, it is possible to observe multiple failure mechanisms at different loads (bending, tension, compression...). Phenomenological models based on the hypothesis of Coulomb and Mohr have been suggested to assess the failure of unidirectional fiber-reinforced composites by Puck and Schürmann [9], [154].

Puck and Schürmann proposed distinct stress-based criteria for the initiation of failure in both the fiber and matrix components of unidirectional (UD) composite laminates. In their models, both the matrix and fiber materials are considered to undergo linear elastic deformation and experience brittle failure. This assumption disregards any inelastic effects and assumes infinitesimal deformations. Additionally, the failure plane for the matrix is assumed to be parallel to the fibers, and the initiation criterion depends on whether the normal stress on the plane is tensile or compressive. When the normal stress on the matrix failure plane is compressive, it is believed to impede the sliding of one surface over the other. As for matrix failure, the elastic properties of the material degrade once failure initiation occurs. On the other hand, fiber failure is assumed to be catastrophic, meaning that the fiber fails instantaneously when the failure criterion is satisfied.

For 3D deformations, the influence of transverse normal stresses, σ_{22} and σ_{33}, on the fiber failure is considered because fibers are confined in the matrix. Puck and Schürmann hypothesized that (i) the effect of transverse normal stresses σ_{22} and σ_{33} on the axial strain induced in the fiber is enhanced due to the presence of the matrix, (ii) at failure the axial strain in the fiber embedded in a ply deformed in uniaxial tension equals that in an isolated fiber deformed in uniaxial tension (See section 2.3.4).

The Puck failure criteria include five failure modes, namely, fiber failure under tension/compression as well as inter-fiber failure (IFF) with modes (A, B, C) under transverse tension, in-plane shearing and high transverse compression (See Section 2.3.4).

5.2.2. Intralaminar damage evolution

Progressive damage models (PDM) based on finite element (FE) analysis are now well recognised to be extremely capable methods for both damage assessment and ultimate strength prediction.

In the analysis of failure, the appropriate approach must be applied to assess the growth of damage to final failure, in the same manner as the damage identified in the composite material.

There are several explanations behind this. Firstly, isotropic ductile materials have been the target of most damage models. Therefore, it is challenging to adapt a general damage model to brittle anisotropic materials. Secondly, it takes a lot of effort to set the material characteristics of such a damage model. This means that an immense series of measurements has to be taken in order to get the accurate material data. Consequently, in the present Chapter, the damage occurrence and evolution have been identified based on the Puck criteria coupled with the material stiffness degradation method so-called (constant stress exposure (See section 2.4.2.3)), respectively. This concept is quite straight forward and has been frequently employed by researchers in the field of composites engineering for both strength prediction and gradual failure analysis. In the case of

quasi-static analysis, constitutive models relate the state of stress to the state of strain. It assumes that the material is linearly elastic with transversely orthotropic material behaviour.

5.2.3. Interlaminar damage initiation and evolution

Another important way in which composites fail is by delaminating between layers. To simulate interlaminar delamination in this chapter, a cohesive zone model (CZM) [75] has been applied in the interlayer sections. In order to simulate the interlaminar delamination in the samples using Abaqus, cohesive layers are introduced between each ply. Besides, the (CZM) represent the delamination process as a gradual failure of the interface between composite plies, rather than a sudden fracture. This gradual failure allows for a more realistic representation of the delamination behaviour and provides valuable information about the onset and progression of delamination.

A bi-linear formulation was used for this study according to the traction-separation law (TSL), which is characterized by critical energy release rates, a penalty stiffness, and maximum interlaminar tractions as a function of the failure mechanism. However, the largest permissible reduction of the penalty stiffness has been constrained to 0.95, as well as the viscous regularisation that incorporated using a viscous coefficient to enhance the convergence and robustness of the FEA. For damage initiation of interface elements, a quadratic stress criterion has been applied. On the other hand, in the interlaminar damage model, Benzeggah–Kenane criteria [88] have been adopted for damage evolution of the interface elements on the assumption of a critical energy release rate of mixed failure mechanisms (See section 2.5.3).

5.3. Modelling

5.3.1. Initial/progressive failure analysis procedure using Abaqus Umat subroutine

The workflow of the developed finite-element model, including both the interlaminar and intralaminar damage progressive model, is schematically shown in Fig. 5.2. A clear description of the process of computational analysis is provided using FEM, as well as the applied methodology utilized in the present work. It should be noted that the process consists of iterations.

On the intralaminar side, the UMAT subroutine is used to compute the stress state and the Jacobian matrix compatible using Eqs. ((2.63) – (2.71)) with the given strain state for each i-th step, including all finite element integration points (at each lamina) and for each analysis time step. However, the determination of the material properties, state variables and deformation tensor are the initial step carried out by the UMAT. Then, the Jacobian matrix is calculated and the stress field is predicted. Besides, the damage model implemented via UMAT, based on Puck's single element failure criteria, verifies the stress state calculated using Eqs. ((2.55) – (2.57), (2.61), (2.62)). In addition, the fracture plane oriented at the angle of θ_{fp} is determined by calculating FI_M for all plane ranging from $\theta = -90$ to $\theta = 90$ with one step. In case of a failure mode occurrence, the material stiffness will be degraded by the following CSE using Eqs. ((2.83) – (2.91)), and as a consequence, the damage variables are updated. Furthermore, the failure index and damage variables for the failure modes in the UMAT are shown by the solution dependence of state variables (STATEV). Table 5.1 depicts the symbol notion within the UMAT subroutine. Subsequently, the state variables are updated with the damage variables, and these variables are taken to the next step to update the stress field.

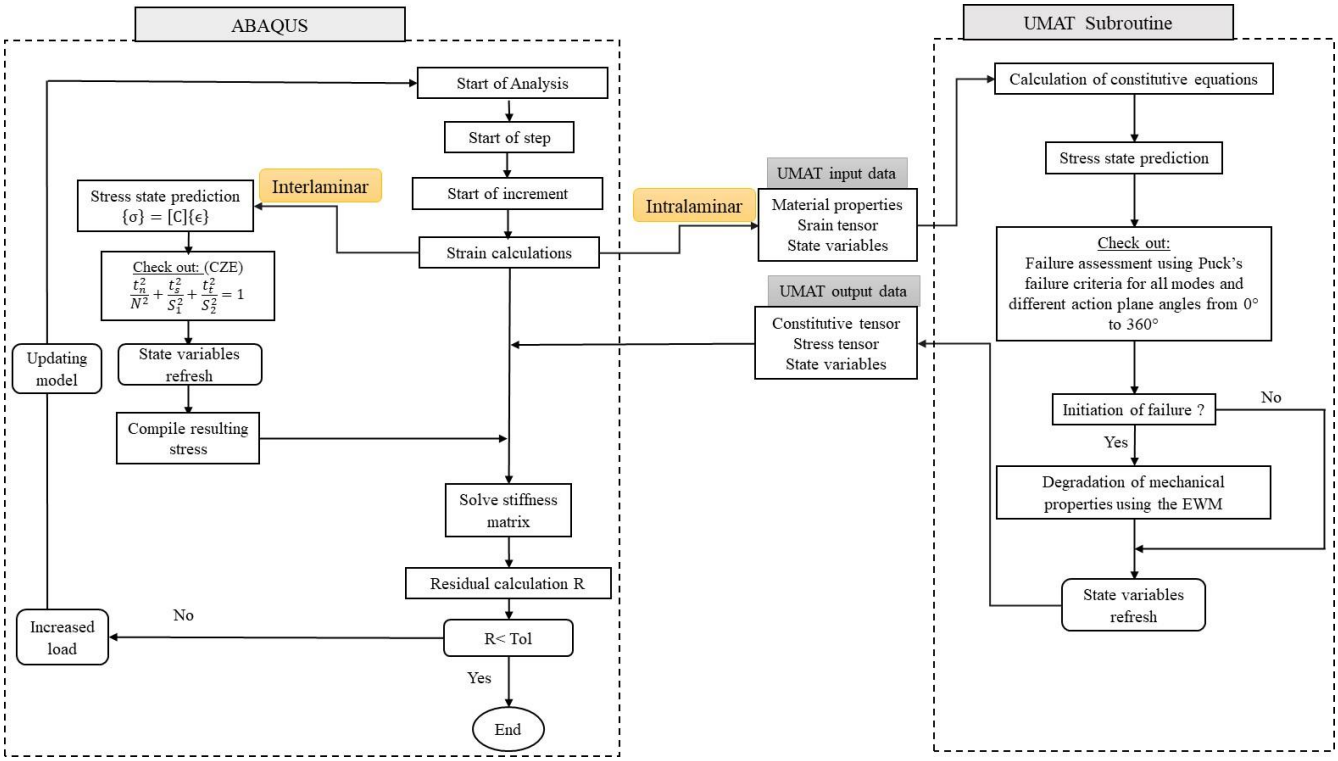


Figure 5.2: The computational algorithm of the progressive damage simulation using UMAT subroutine.

Table 5.1. Labelling.

Concept	Symbol
Puck's fiber failure in tension	SDV1
Puck's fiber failure in compression	SDV2
Puck's matrix failure in tension	SDV3
Puck's matrix failure in compression	SDV4
Damage variable for fiber tensile	SDV6
Damage variable for fiber compressive	SDV7
Damage variable for matrix tensile	SDV8
Damage variable for matrix compressive	SDV9
Status of all damage modes	SDV10
Stiffness degradation Scalar	SDEG

On the interlaminar side, cohesive layers are modelled using the traction-bilinear-separation responses. Usually, adjoining layers are assumed to be perfectly bonded to each other. The interlaminar boundaries that are surfaces of abrupt discontinuities in material properties are usually sites of failure initiation in the form of interlaminar cracks and/or delamination.

Likewise, mixed mode delamination is simulated by applying the quadratic nominal stress criterion and having off-plane stresses as input. As soon as the delamination initiation criterion is fulfilled, it starts to spread following the above delamination propagation criterion using Eqs. ((2.134) – (2.136)). The state of delamination can be visualised by the scalar stiffness degradation variable option (SDEG) available in Abaqus, which ranges between 0 (no delamination) to 1 (delamination).

The computation of stresses and strains until complete rupture of the affected areas in the composite laminate provides valuable insights into the failure behaviour of the material. The

occurrence of factors such as fracture crack propagation, fiber matrix debonding, and delamination can significantly impact the structural integrity and load-carrying capacity of the laminate. Understanding these failure mechanisms is crucial for predicting the structural response and ensuring the safety and performance of composite components in real-world applications.

Convergence is an important aspect of the numerical analysis process. The residual (R) is calculated by comparing the internal and external force vectors, and its evaluation against a tolerance threshold determines the convergence of the simulation. If the residual falls below the specified tolerance, indicating that the computed solution is sufficiently close to the true solution, the analysis is considered converged. This convergence criterion ensures accurate and reliable results. However, it is essential to select an appropriate tolerance value that balances accuracy and computational efficiency, considering the specific engineering requirements and the complexity of the problem at hand.

In situations where the residual does not meet the convergence criterion, several challenges may arise. Calculation of failed elements can pose difficulties in FEA software, particularly when the failure scenario involves the reduction of element stiffness properties close to zero. Achieving convergence in such cases may require careful consideration of numerical techniques and adjustments to the analysis settings. Additionally, refreshing the values of damage variables is necessary to accurately represent the progressive damage and failure of the material.

The behaviour of the residual (R) during iterations provides insights into the convergence or divergence of the analysis. A declining residual indicates progress towards convergence, suggesting that the material and structural response are within acceptable limits. On the other hand, an increasing residual signifies divergence, implying that the applied loads exceed the remaining strength of the structure, resulting in an unrealistic response. It is crucial to monitor the behaviour of the residual throughout the analysis to ensure the reliability and validity of the simulation results.

To enhance the convergence of the simulation, the viscous regularization method is employed. This method addresses the discrete form of the damage variables and aims to improve the stability and accuracy of the analysis. By introducing viscosity-like terms into the governing equations, the viscous regularization method helps control the numerical instabilities associated with damage evolution. It provides smoother and more robust convergence behaviour, ensuring reliable simulations of the progressive failure of composite laminates.

5.3.2. Materials for computational analysis

In order to evaluate the usability and performance of the suggested model, the progressive damage of various composite laminates subjected to three-point bending has been numerically simulated. The analysis also involved the identification of the ultimate load, the failure modes including delamination and the load-deflection curves. Moreover, the predicted results have been compared with experimental outcomes in the works conducted by L. Haibao [153] and Y. Yuxing [98].

5.3.3. Samples of composite laminates

In this study, we used two different stacking sequences $[45°/\,0°_2/-45°/0°/90°/0°_2/90°/0°/-45°/0°_2/45°)]_s$ and $[0°_3/90°_3]_{2s}$ that have been selected for the IMS194/CYCOM977-2 and AS4/PEEK composite laminates, respectively. Figs (5.3 - 5.4) demonstrate the plies sequences of composites laminates with the cohesive plies. Material properties and model parameters associated with finite element simulations are given in Tables (5.2 , 5.3) and they have been extracted from

the references [155], [156] and [122], [157], [158]. The importance of the selectivity was further checked by matching the intralaminar and interlaminar damage progressive, using these parameters with those suggested by the L. Haibao [153] and Y. Yuxing [98]. Also, the parameters of three-point bending experiments are shown in Table 5.4

Table 5.2. The mechanical properties of the materials used in this study.

Properties	IMS194/CYCOM977-2	AS4/PEEK [157]
$\mathbf{E_{11}}$ (GPa)	165	127.6
$\mathbf{E_{22}}$ (GPa)	8.17	10.3
$\mathbf{G_{12}}$ (GPa)	4.27	6.0
$\mathbf{G_{23}}$ (GPa)	3.0946	5.7
$\boldsymbol{\nu_{12}}$	0.33	0.32
$\mathbf{E_f}$ (MPa)	230,000	141,000
$\boldsymbol{\nu_{f12}}$	0.2	0.6
$\mathbf{X_T}$ (MPa)	3150	2023.4
$\mathbf{X_C}$ (MPa)	1450	1234.1
$\mathbf{Y_T}$ (MPa)	81.4	92.7
$\mathbf{Y_C}$ (MPa)	270	176.0
$\mathbf{S_{12}}$ (MPa)	108	186.0

Table 5.3. The materials properties of the cohesive plies.

Properties	IMS194/CYCOM977-2 [156]	AS4/PEEK [122], [158]
$\boldsymbol{K_n}$ (MPa/mm)	34500	$6.4*10^5$
$\boldsymbol{K_s = K_t}$ (MPa/mm)	3450	$6.4*10^5$
$\boldsymbol{\tau_n^0}$ (MPa)	12.8	43
$\boldsymbol{\tau_s^0 = \tau_t^0}$ (MPa)	24.2	55
$\boldsymbol{G_{IC}}$ (N/mm)	0.478	0.478
$\boldsymbol{G_{IC} = G_{IIIC}}$ (N/mm)	0.58	0.58

Table 5.4. The parameters of three-point bending experiments.

Materials	Length (mm)	Width (mm)	Thickness (mm)	Support span (mm)	Impactor nose radius (mm)	Support radius (mm)	(l/h)
IMS194/CYCOM977-2	130	13	5.264	105	3	3	20
AS4/PEEK	120	13	3	96	5	5	32

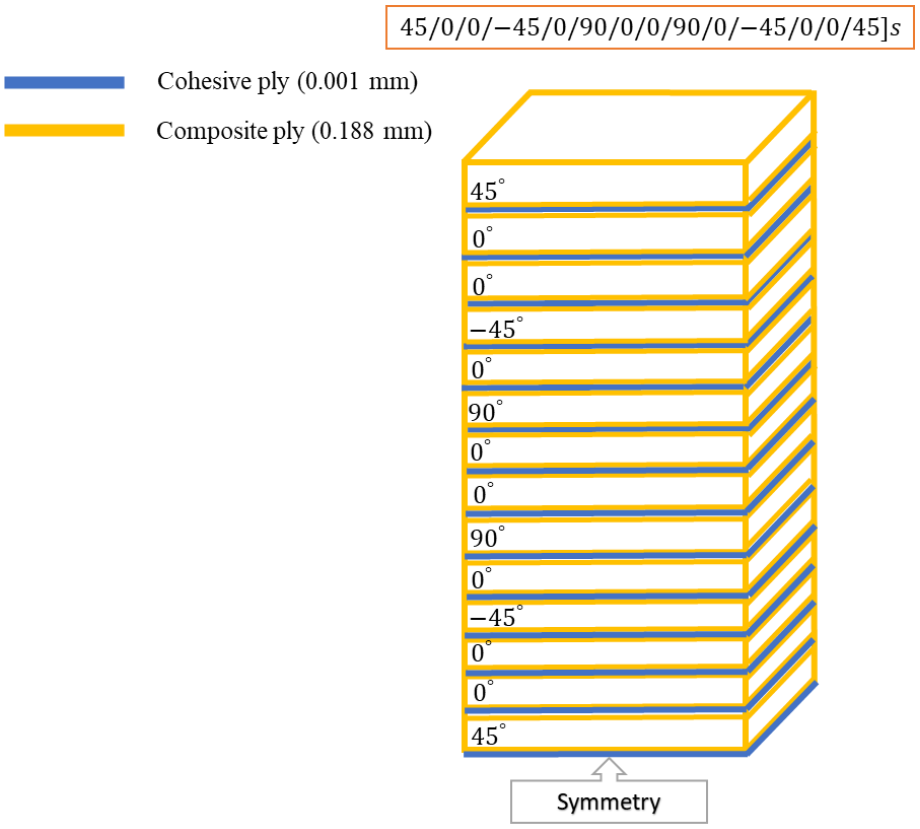


Figure 5.3: Plies stacking sequence with cohesive plies for IMS194/CYCOM977-2 composite laminates.

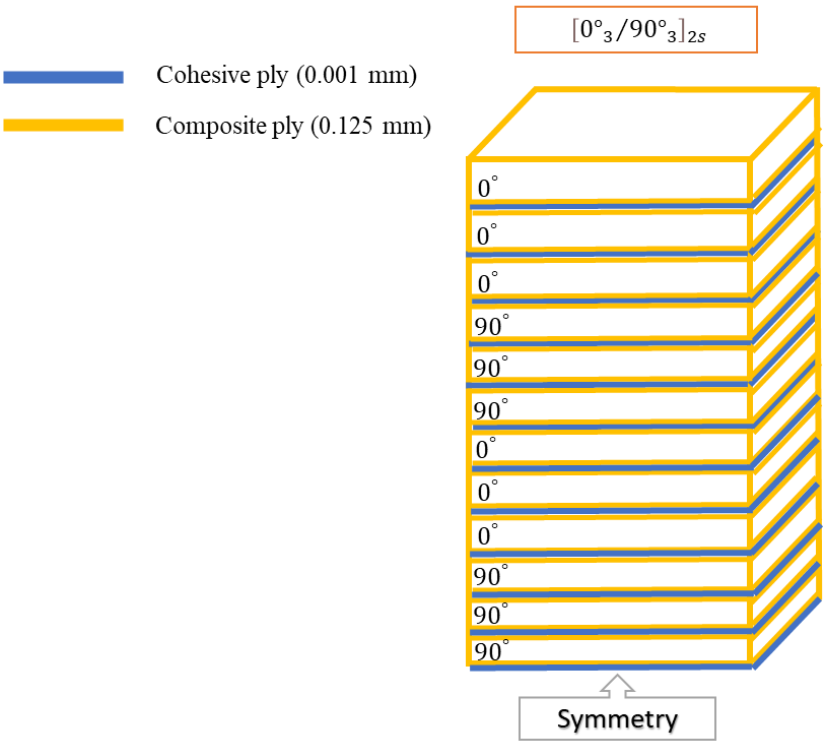


Figure 5.4: Plies stacking sequence with cohesive plies for AS4/PEEK composite laminate.

5.3.4. Finite element model

A three-dimensional FEM has been established within Abaqus/Standard which allows the progressive damage of composite laminates to be modelled and analysed under flexural loading. Fig. 5.5 illustrates the computer-assisted design (CAD) model generated using Abaqus 2017, followed by its subsequent conversion into a Finite-Element model as depicted in Fig. 5.6. Besides, the proposed user defined material (UMAT) subroutine has been incorporated with the cohesive element model so as to perform three-point bending simulations on the composite samples. A layer-by-layer analysis technique was used to model all the layers. Each layer was required to be modelled individually based upon its fiber orientation angle.

The interfaces between the composite layers were the main areas of delamination which has been created by offset method. Therefore, the embedded zero-thickness cohesive plies method, based on the traction-separation-method, is very suitable for guiding the delamination prediction. Eight-node linear reduced integration (C3D8R) solid elements, 2 mm × 2 mm in size, with enhanced hourglass control and second order accuracy have been applied to model each layer of the composite laminated through its thickness.

In addition, Cohesive layers are placed between every composite layer with a thickness of 0.001 mm and 0.188 mm per layer for both of IMS194/CYCOM977-2 and AS4/PEEK composite materials, respectively, using an 8-node cohesive element (COH3D8). The total number of elements in the FE model for the three-point bend simulation was 26403 and 19740 for the IMS194/CYCOM977-2 and AS4/PEEK composite laminates, respectively. Note the analytical rigid surfaces were employed for both the impactors and the fixed supports, and the surface interaction type has been specified between the cylinders and the composite element. The interaction properties are defined in terms of tangential behaviour with (frictionless) contact as well as normal behaviour with (hard) contact. The fixed supports are restricted to 6 DOF. Whereas, the impactor nose can only advance across the thickness of the sample. Moreover, the laminate has been exposed to a displacement-controlled load.

A linear constraint equation was used to simulate the loaded surface, where loading was controlled by the displacement imposed on a reference point RP on the underside of the loading nose. The main goal is to make sure that the displacements are both uniform between all nodes of the loaded surface and the RP reference point locate in the centre of the cylinder impactor. Consequently, the reaction force and surface displacement are obtained correspondingly at this reference node. It should be noted that all the coefficients of friction between parts in contact with each other are fixed at 0.2.

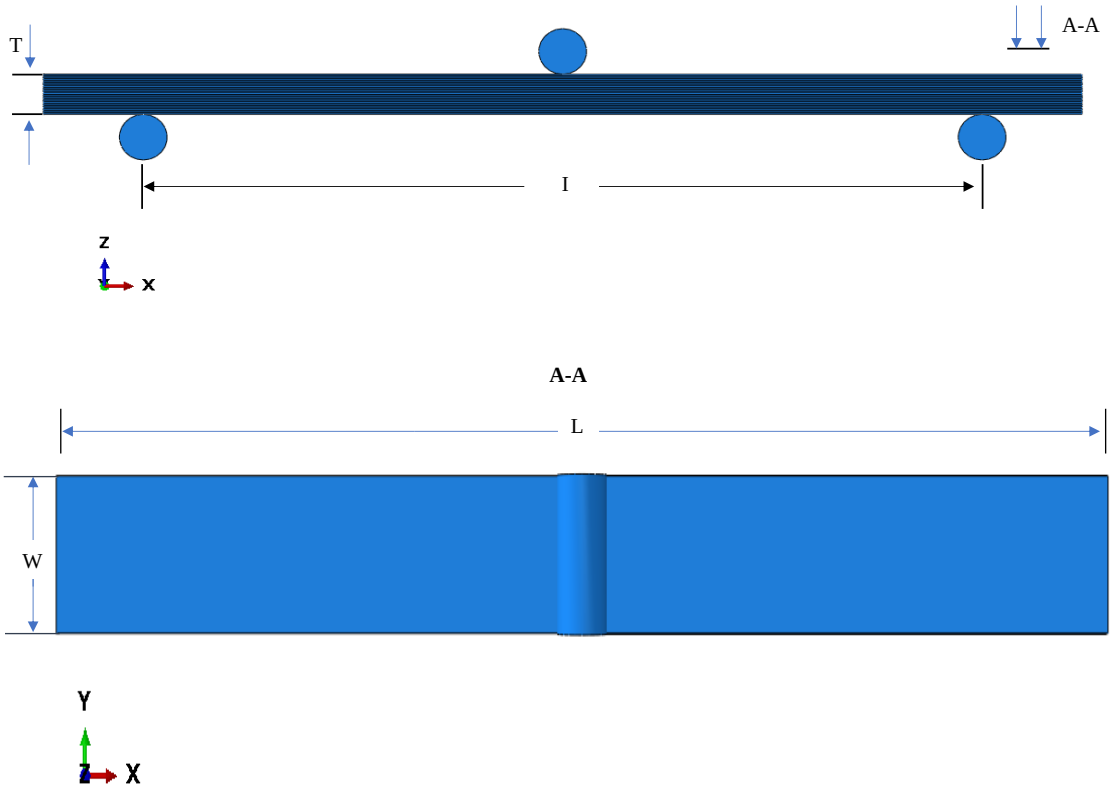


Figure 5.5: Computer-Aided Design (CAD) model using Abaqus software.

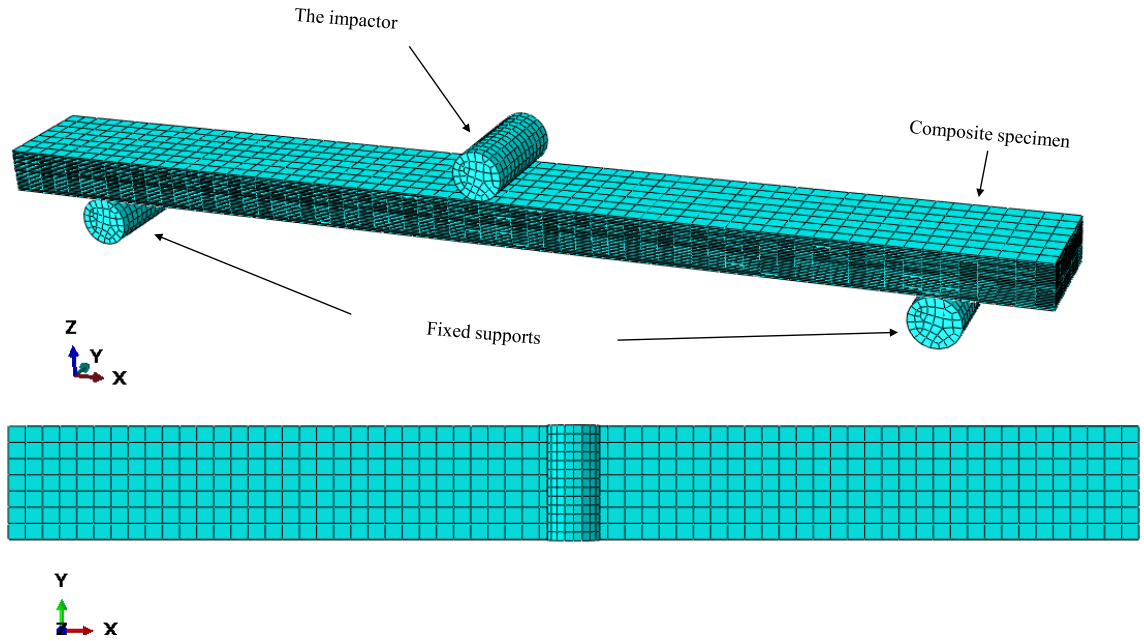


Figure 5.6: 3-Dimensional FEM for bending loading of the specimens.

In order to reduce the accumulation error during the simulation, the computational fidelity has been specified as double precision. Also, to achieve a reasonable trade-off between running time and accuracy, selective mass scaling was utilised. The run time is estimated to be 1 hour, with a time increment of less than 1e-04s on a 64-bit Intel core i7- 2.10 GHz processor with 32 GB RAM and 12 CPUs.

Mesh dependency study was carried out with the in-plane element size varying from 2.0 mm to 6.0 mm for IMS194/CYCOM977-2 composite laminates under 3-point bending. After matching the ultimate load with the mean value (relative error was found to be 4.23%, where the mean ultimate load was found to be 2289.74 N), Thus, the in-plane element size was chosen to be 2.0 mm.

On the other hand, it should be mention that advancing the computational efficiency and accuracy of modelling damage in composite laminates has been a driving force in research, prompting the exploration of innovative approaches. Among these, adaptive mesh refinement (AMR) has emerged as an interesting technique, offering exciting prospects for improving simulations while optimising computing resources. Adaptive mesh refinement (AMR) presents a promising approach to enhance the computational efficiency of modelling damage in composite laminates. By selectively refining the mesh based on local criteria, AMR optimizes resource allocation and captures detailed damage mechanisms while maintaining reasonable computational costs. This dynamic refinement strategy improves stress and strain predictions, enables tracking of evolving damage patterns, and facilitates the analysis of larger and more complex structures [159], [160].

However, AMR, as an alternative approach for enhancing computational efficiency in modelling damage problems in composite laminates, has a few drawbacks. First, its implementation complexity requires the development of algorithms and techniques, which can be time-consuming. Second, the use of AMR may increase memory requirements due to the storage of mesh hierarchy and connectivity information. Third, the effectiveness of AMR is sensitive to the chosen refinement criteria, requiring careful calibration. Finally, adaptive refinement can result in non-uniform mesh elements, potentially leading to poor mesh quality and numerical artifacts.

Accordingly, incorporating AMR into the modelling workflow may offers researchers valuable insights and opens new possibilities for simulating and understanding damage in composite laminates.

5.4. Results and discussion

5.4.1. IMS194/CYCOM977-2

5.4.1.1. Load-deflection behaviour

Firstly, the present model has been compared against the damage model provided by Linde [74] and confirmed by the test carried out by Y Yang et al [98]. Fig. 5.7 displays the load vs deflection curves obtained using the numerical models and the experiments. The stiffness can be derived directly from the linear region of the curve, which gives a stiffness of 480.68 N/mm compared to a standard deviation of -70.32 N/mm given by the experiments. Therefore, there is a reasonable relative error between the present model and the experiments in the amount of -12.8% regarding the stiffness. Besides, the ultimate strength has been found to be 2192.84 N compared to the experimental standard deviation of -96.9 N and 2.95% error of the deflection at failure load. 2304.86 N has been the expected value by Linde's model, it can then be seen after the ultimate load that the degradation pattern illustrated in the figure of the present model is significantly more in agreement with the experimental results compared to that of Linde's model. In fact, Linde's model is similar to a single sudden degradation model with no degradation stage. In other words, this model of Linde can be used for the purpose of estimating the stiffness and the strength of the composite material, rather than for predicting the remaining damage behaviour.

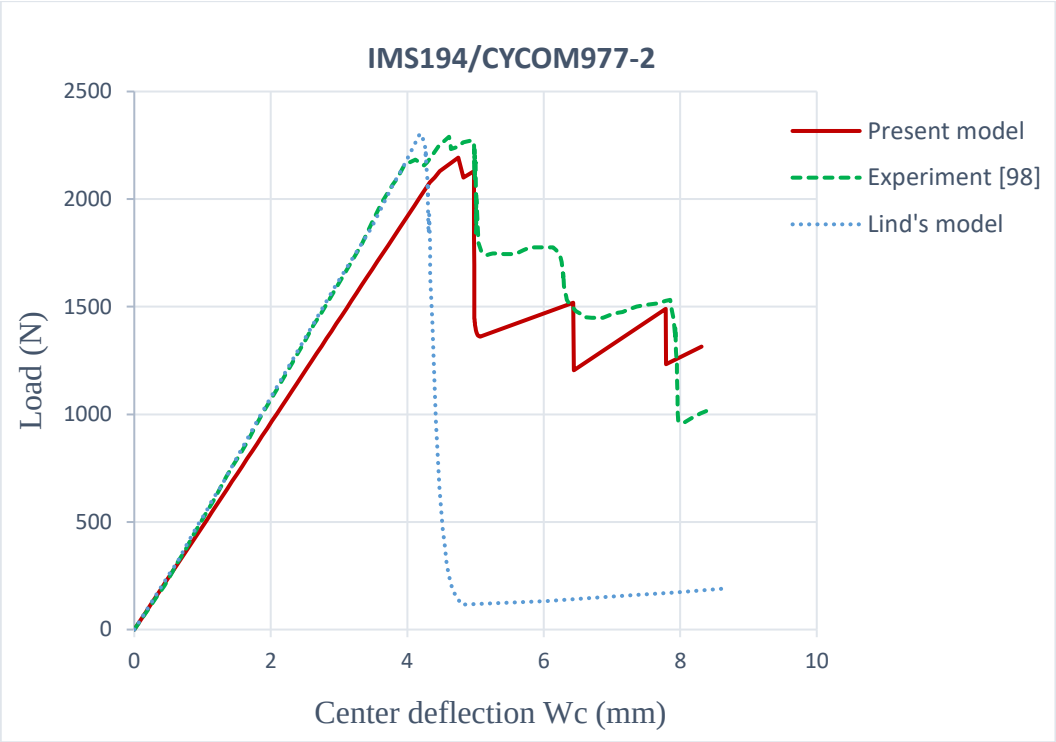


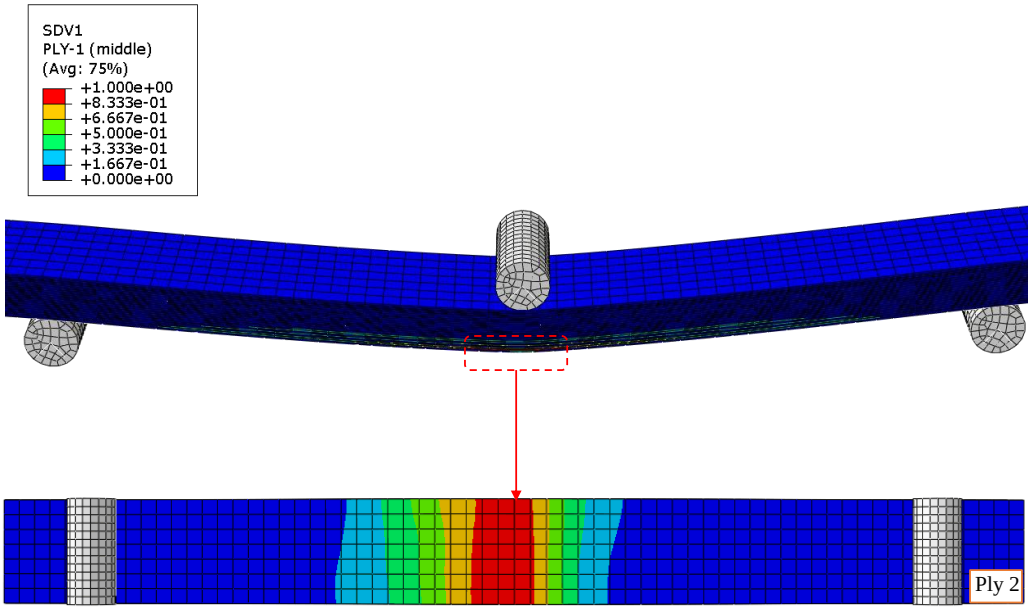
Figure 5.7: Predicted load vs. deflection curves of IMS194/CYCOM977-2 composite laminates.

Therefore, since there are no additional reduction steps by using Linde's model, it will not be a rival model for the simulation of damage evolution. In this Chapter, a progressive deterioration with more stages of degradation has been considered, which is very important and suitable for predicting the damage behaviour of laminated composites. Upon making a comparison with the test results, it has been discovered that the model prediction is in agreement with the experimental results in terms of the degradation trend, although it's slightly differentiated in terms of the values. However, the displacement anticipated at the ultimate load exhibits a meaningful correlation with the test results, with an error less than 3%. Consequently, not only the present model is good at predicting the load versus deflection curve of 3-point bending for composites, but also still has satisfactory numerical stability when the laminate fails completely. In case of practical application, the numerical simulation stops just after the final load, thus allowing adequate numerical accuracy to be achieved.

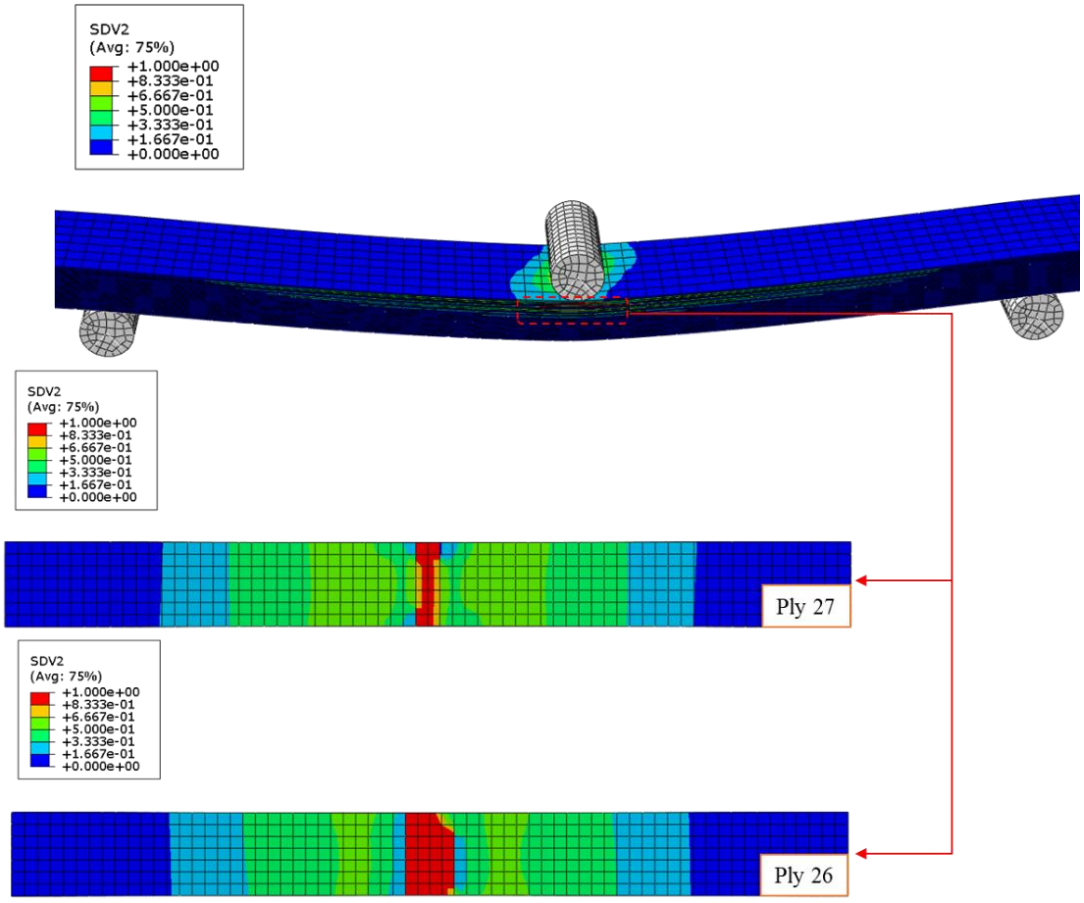
5.4.1.2. Damage prediction

Figs. (5.8 – 5.10) display the several modes of damage ***predicted*** by the present model at failure load. Whereas fiber tensile failure (Fig. 5.8 (a)) is spread along the base of the sample, as well as severe fiber compression failure (Fig. 5.8 (b)) is spread across the thickness towards the upper surface by high compression under the impactor nose. As can be seen from Fig. 5.9, There is damage to the elements in proximity to the apparent delamination area and precured by the cracking of the matrix in the plane which accelerated the emergence of delamination. As exposed in Fig. 5.10, the matrix tensile failure appears in the ply oriented with 45° close to bottom of specimen. However, in-plane matrix under compression occurs close to the top surface under the loading nose with several elements failed at the plies with $\pm 45°$. After the ultimate load, inter/intralaminar failure still propagate through the specimen as shown in Fig. 5.11. In the cohesive ply between ply 7 and ply 8, the largest amount of delamination is concentrated leading

to a complete collapse of the elements, due to severe out-of-plane shear stress close to the lower surface of the specimen under tensile loading, which induces ultimate failure of the lower plies.



(a) Fiber tension damage on the Bottom surface at Failure load.



(b) Fiber compression damage on the Top surface at Failure load.

Figure 5.8: Damage contour of fiber tension/compression of IMS194/CYCOM977-2 composite laminates.

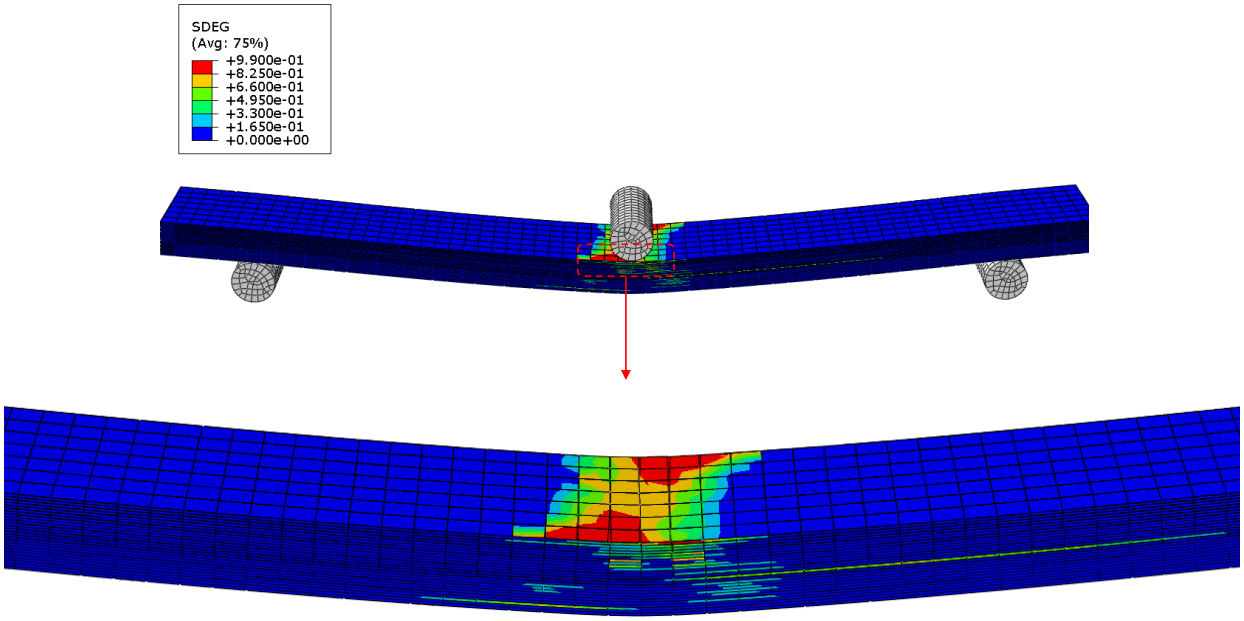
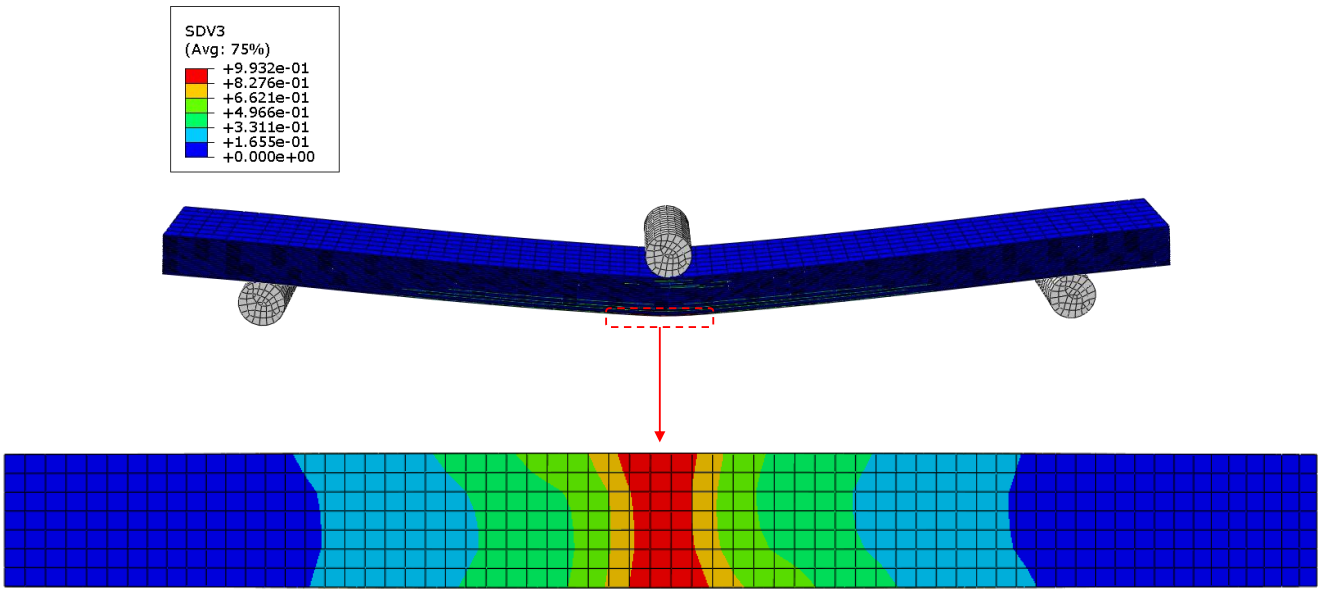
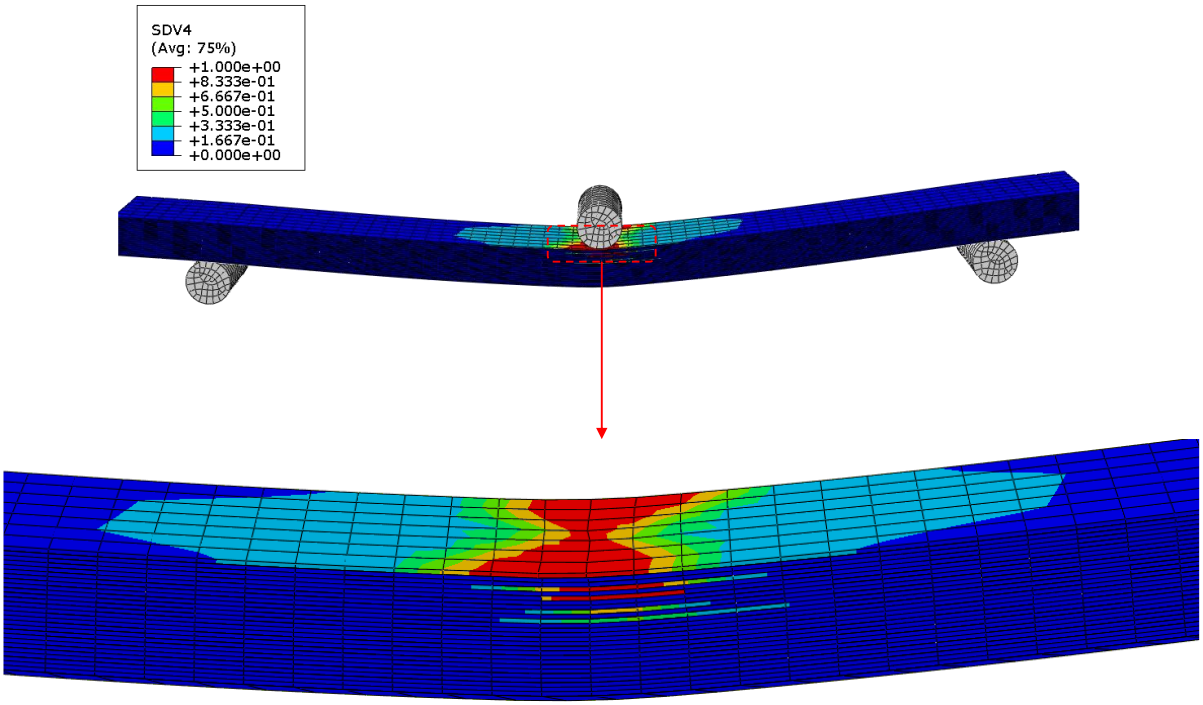


Figure 5.9: Delamination initiation at Failure load.

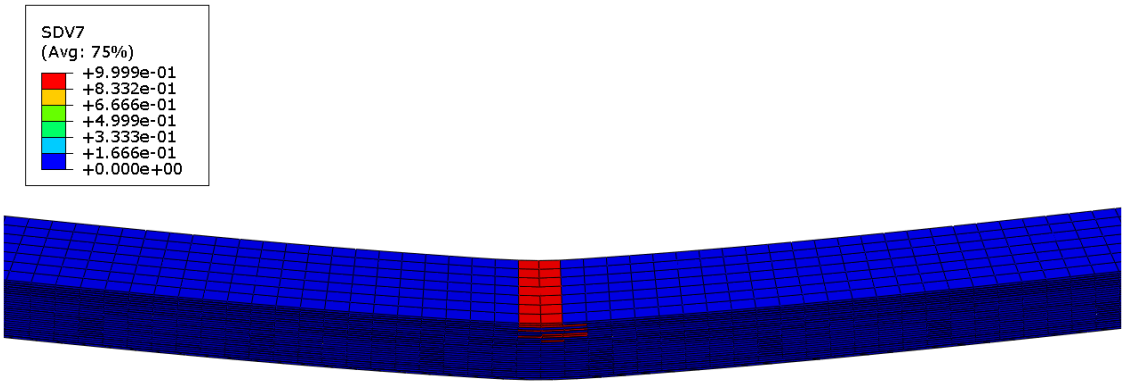


(a) Matrix tension damage on the Bottom surface at Failure load.

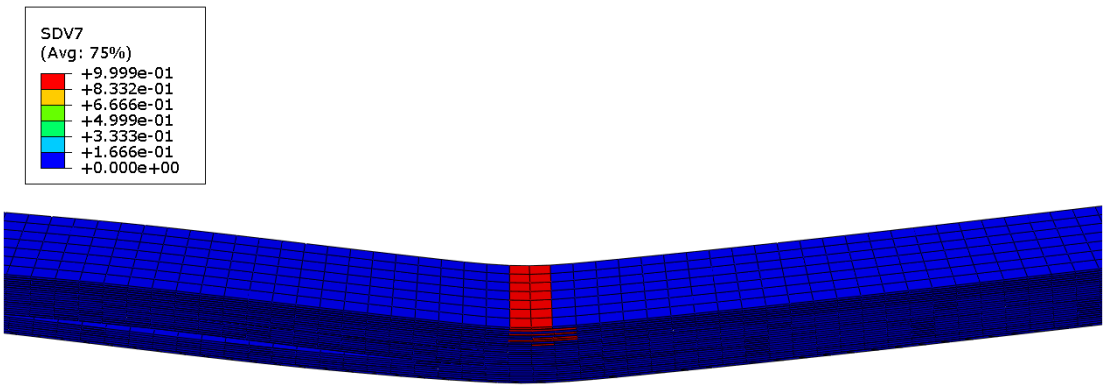


(b) Matrix compression damage on the Top surface at Failure load.

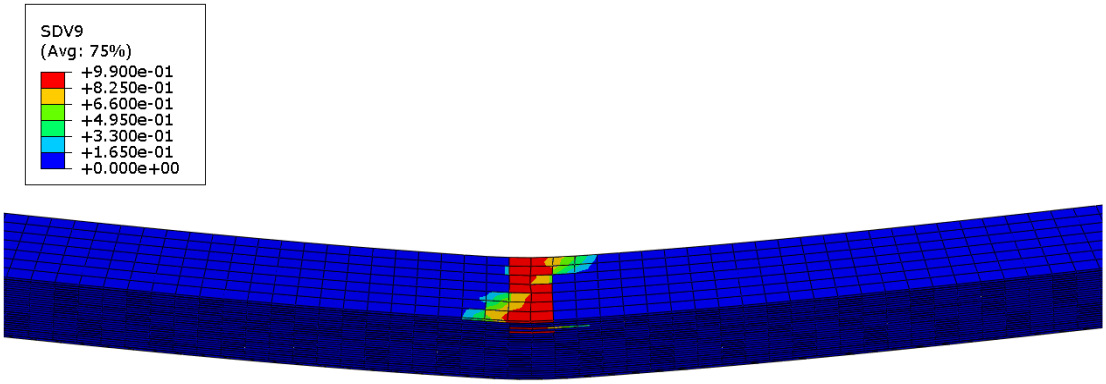
Figure 5.10: Damage contour of Matrix tension/compression of IMS194/CYCOM977-2 composite laminates.



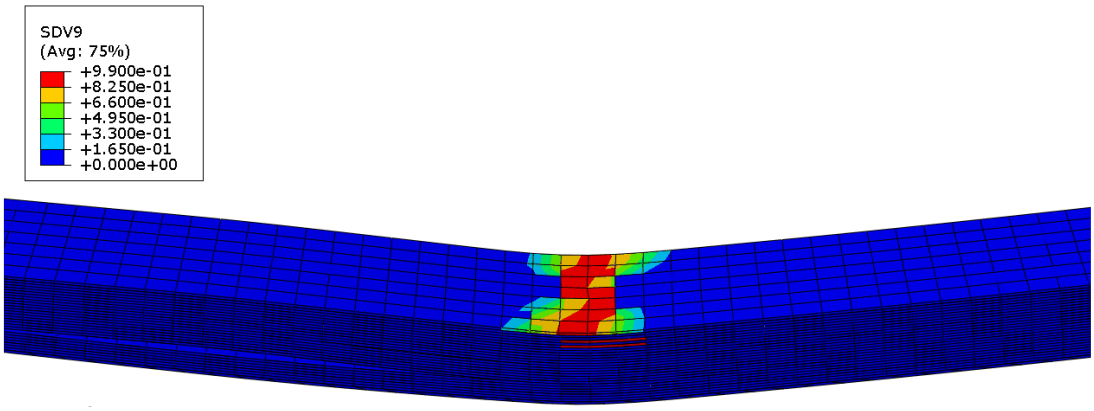
(a) Compressive fiber Failure at second fracture.



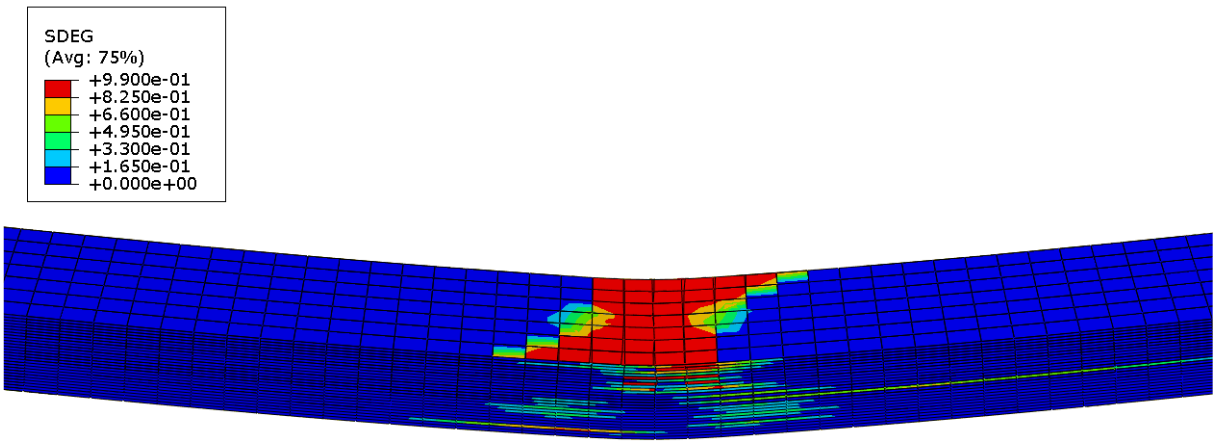
(b) Compressive fiber Failure at third fracture.



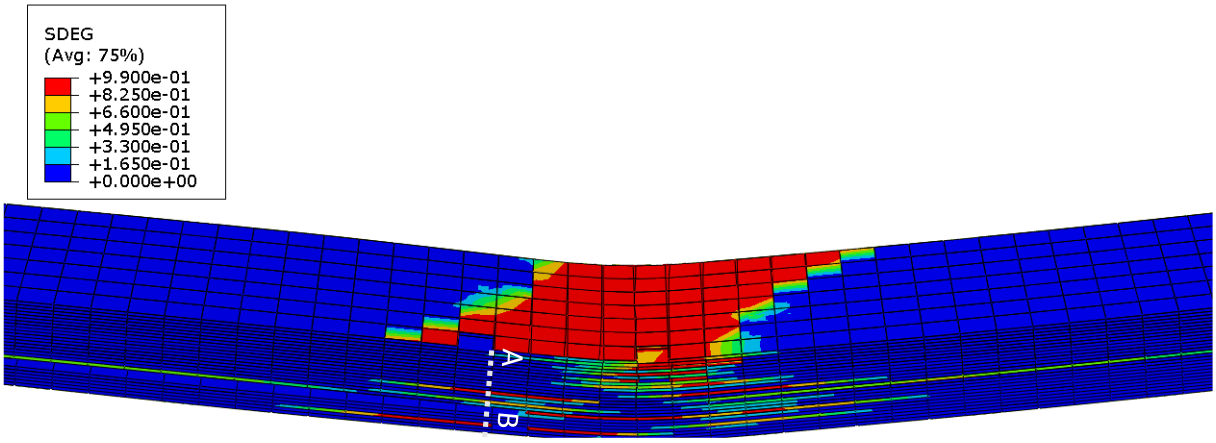
***(c) Compressive matrix Failure at second fracture*.**



(d) Compressive matrix Failure at third fracture.



(e) Delamination at second fracture.



(f) Delamination at third fracture.

Figure 5.11: Intra/interlaminar damage contour at second/third fracture of IMS194/CYCOM977-2 composite laminates.

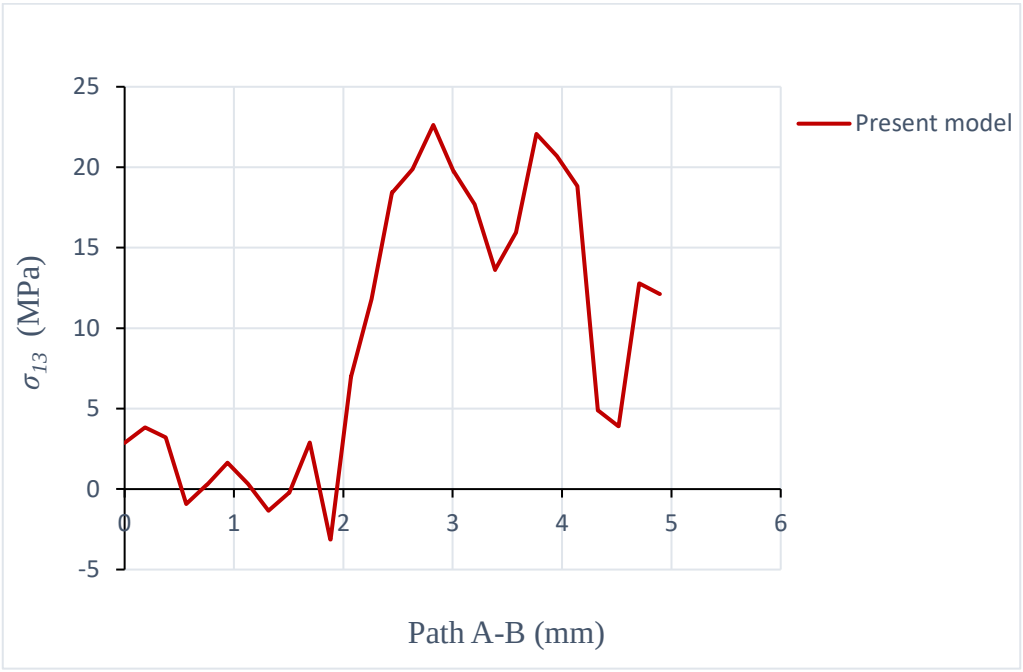


Figure 5.12: Distributions of σ_{13} along path A-B of IMS194/CYCOM977-2 composite laminates.

The contributions of first shear (mode 2) to the deformation of areas, the σ_{13} values along path A-B (Fig. 5.11 (f)), and the cohesive interface layer, were plotted in Fig. 5.12. It has been observed that the values of the normal mode and mode 3 were ignored, therefore they are not reported in this section. However, only mode 2 was significantly active in the middle range, since σ_{33} and σ_{23} have low and stable values. On the other hand, in the central region, while the values of σ_{33} and σ_{23} remain steady, σ_{13} increases in areas with severe delamination. First shear mode contribution becomes dominant which may be explained by the predominance of shear effects in a shorter specimen. Similarly, there appears to be small delamination between ply 14 and ply 15 due to out-of-plane shear stress under compression next to the middle within plies with 90° and the top surface of the sample.

The slight difference that can be found compared to the experimental may be attributed to composite materials that exhibit complex and heterogeneous behaviour, material variability which the properties of composite materials can vary significantly depending on the manufacturing process. Composite laminated exhibit behaviour at multiple scales, from the macro-scale behaviour of the entire laminate to the micro-scale behaviour of the fibers and matrix. Also exclude the effect of interface properties. It should be noted that the bonding quality between the composite plies, as well as the properties of the interlayer material used, can greatly affect delamination. A poorly bonded interface can result in a lack of energy dissipation and increased stress concentrations, promoting delamination. On the other hand, a high-quality bond can help distribute stress and absorb energy, reducing delamination.

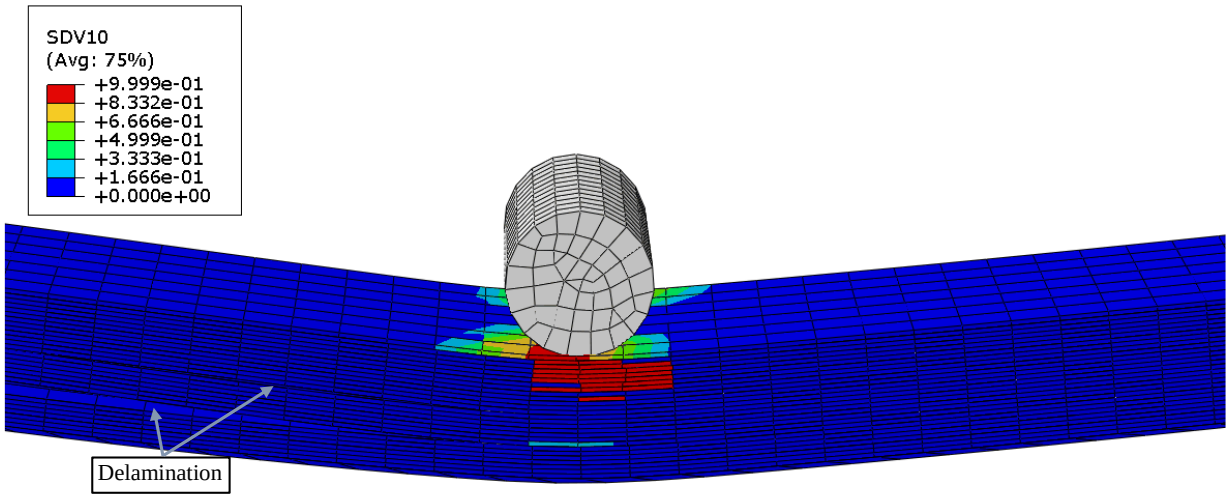


Figure 5.13: Status of all damage modes of IMS194/CYCOM977-2 composite laminates.

Moreover, next to the top surface, the breakage of fibers under compression (so-called fiber buckling) spreads more to adjacent plies with 0° orientation as well as the compression failure matrix that continues to appear across the thickness in the plies with ±45. The status of all damage modes has been shown in Fig. 5.13, as can be seen, the failures of plies on the top specimen have been completely extending through the nearby layers resulting in the sample being completely unable to support the load. The above results of damage distribution from the numerical results obtained from the applied model are quite similar to the test results found by [98].

5.4.1.3. Cohesive zone effect

Although the failure modes of the IMS194/CYCOM977-2 model are fiber/matrix failure. In fact, the cohesive elements (CE) have an extremely significant impact.
The IMS194/CYCOM977-2 model with (CE) and the IMS194/CYCOM977-2 model without (CE) is compared, as shown in Figs. (5.14, 5.15). At the peak load, the failure pattern of the matrix under compression in the model without (CE) is much lower than in the model with (CE). There is a migration of cracks to adjacent elements in the (Fig. 5.14 (b)) which adopts cohesive elements, as shown in the top of the specimen (plies with $\pm 45°$ and 90°). However, delamination promotes intra-laminar longitudinal cracking under higher interlaminar stresses σ_{33}, σ_{13} and σ_{23}. The model using (CE) is able to predict well the migration of cracks (inter-fiber failure), whereas the model with no cohesion elements cannot account for the migration of cracks. Furthermore, the failure inter/intralaminar is strongly related to the degradation of composite material resistance.

Altogether, the ultimate load of the model using (CE) was less compared to the model without (CE) which means that the strength increases while ignoring the delamination failure.

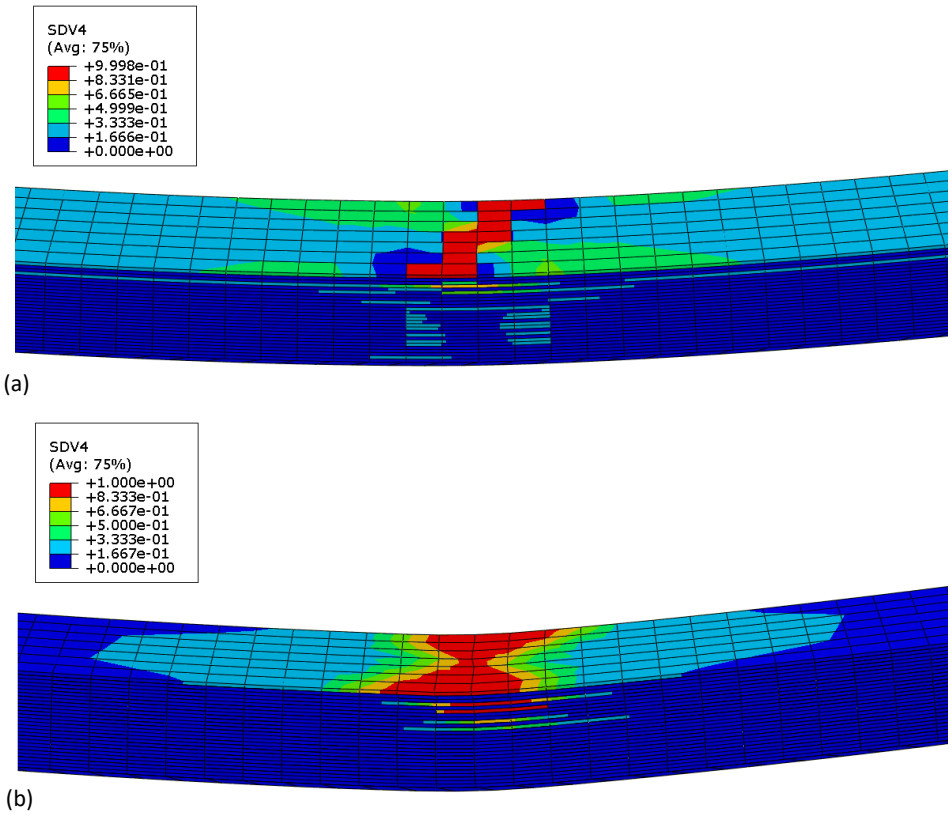


Figure 5.14 : Compression matrix damage contour. (a) model without CZE, (b) model with CZE.

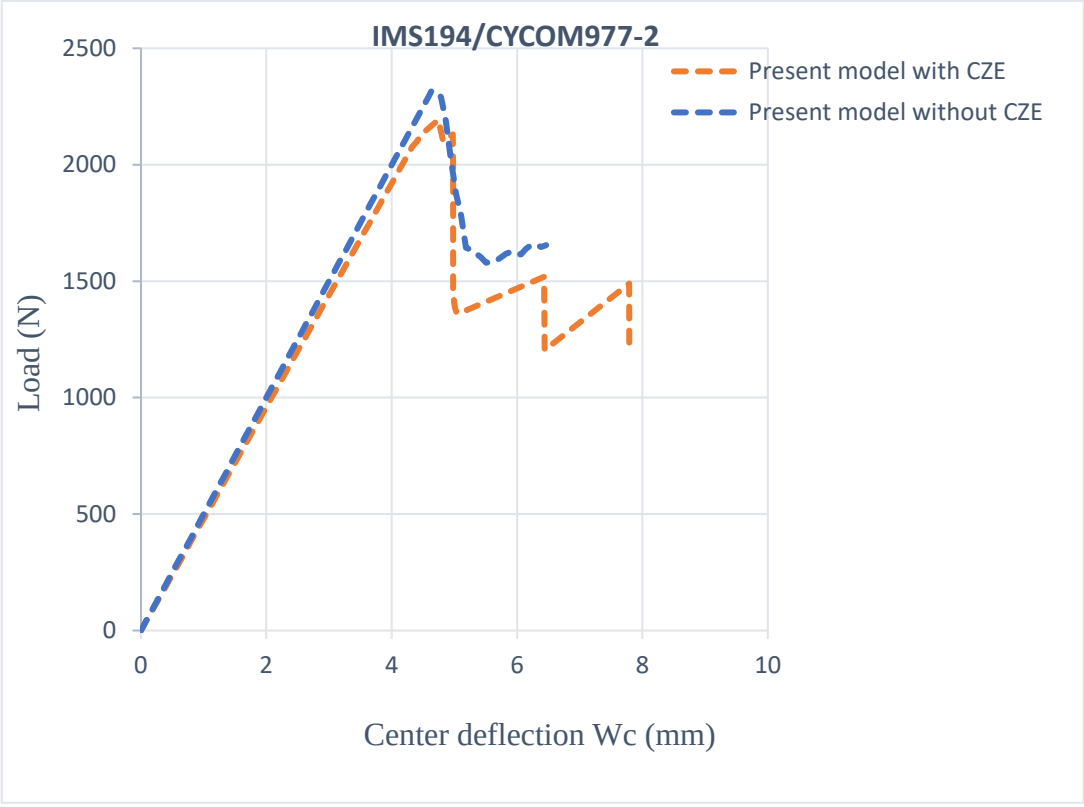


Figure 5.15: The comparison of load vs deflections of two model.

In general, the failure of a CFRP specimen under three-point bending loading is still dominated by failure in the plane of the plies (fiber fracture under tension or compression) and exhibits little sensitivity to the number of elements across the thickness of the geometry.

Additionally, delamination becomes more critical issue and different parameters can affect it such as the arrangement of the composite plies, the magnitude and distribution of the applied load as well as the shape of the specimen and interface properties. Also, mechanical properties of the matrix and fiber play a significant role in delamination. A matrix with low toughness, for example, may not absorb enough energy to prevent delamination initiation and propagation. Similarly, fiber reinforcements with low strength can be more susceptible to fracture, leading to delamination. The modulus of elasticity of the matrix and fiber can also affect the stress distribution within the composite and thus its delamination behaviour.

However, the adoption of cohesive element modelling can be useful for predicting delamination in composite laminates and has further enhanced the ability to understand and assess flexural strength especially in thick composite laminates.

5.4.1.4. Mesh dependency

Since different mesh densities could affect the numerical modelling significantly, the appropriate mesh density should be chosen according to the appropriate model having a lower effect on mesh sensitivity providing the highest quality of output and minimum computing time. This becomes critical in cases where we need to investigate rather huge structures for which the calculation process is often a constraint. Furthermore, the failure loads have been chosen to evaluate the applied model as suitable parameters for the analysis. The number of existing elements in the in-plane mesh density has been addressed. Fig. 5.16 shows the load-deflection curves for composite laminate Graphite/epoxy with the following stacking sequences $[45°/\,0°_2/-45°/0°/90°/0°_2/\,90°/0°/-45°/0°_2/45°)]_s$, to evaluate the dependency of the mesh according to the methodology already described, by using various mesh types, as seen in Fig. 5.17.

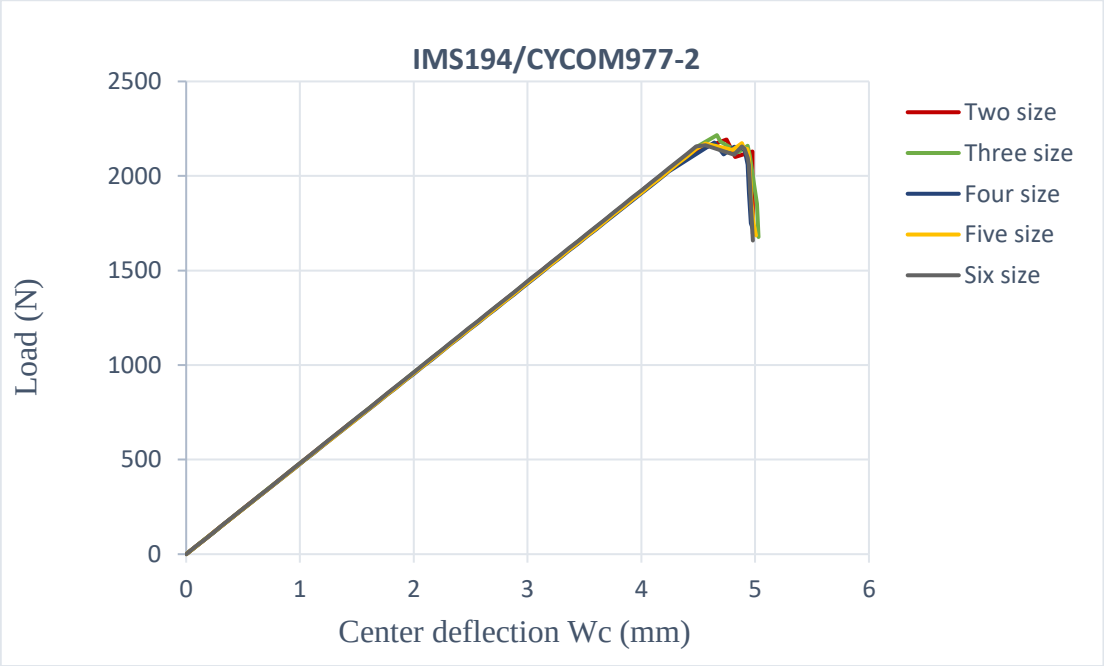


Figure 5.16: load-deflection curves for different sizes.

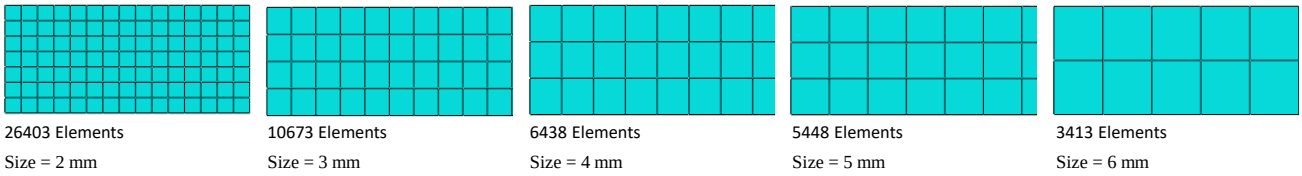


Figure 5.17: Different mesh numbers to verify the mesh dependency of the applied model.

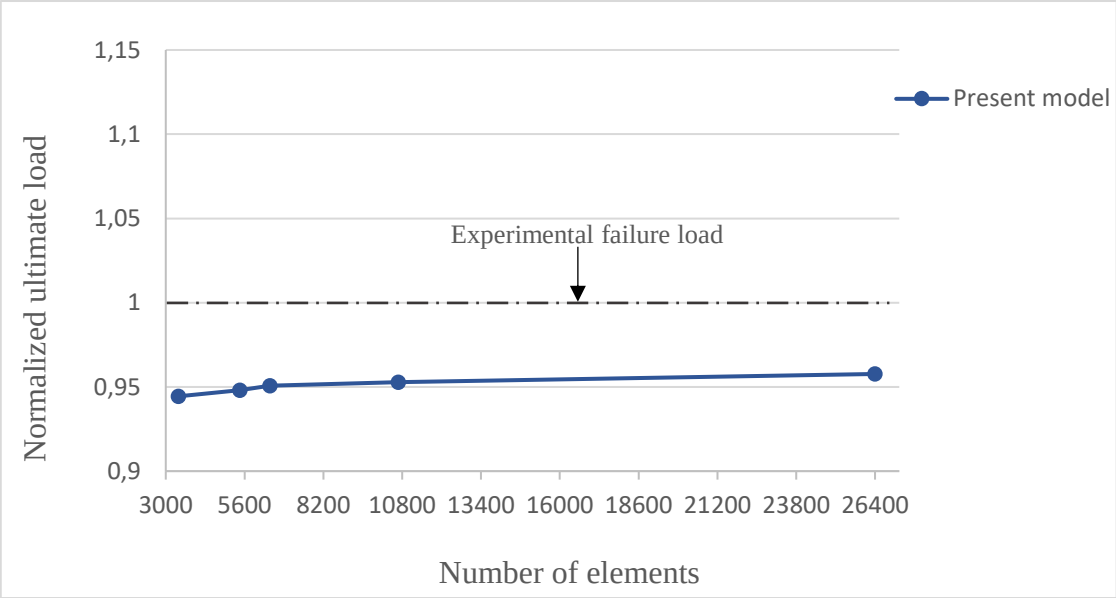


Figure 5.18: Failure load values according to the number of elements.

The implemented PFA model exhibits less influence on the mesh dependence, resulting in slightly different values for the different meshes. The deflections at the ultimate load vary slightly in the different meshes used. Further, Fig. 5.18 depicts the variation of the normalised ultimate loads plotted against the number of total elements for (PFA) carried out with the Puck-CSE. The applied model exposes an error of less than 5,5 % (with 3413 elements = size of 6 mm*6 mm), as the results converge to the experimental data, it gives a highly stable response, showing an error smaller than 4,5% as the number of elements increases (by starting with 6438 elements = size of 4 mm* 4mm).

5.4.2. AS4/PEEK

5.4.2.1. Load-deflection response

The load-deflection was obtained from both the simulation and the test achieved by [153]. The comparative load-deflection behaviour between the experimental and numerical results has been plotted in Fig. 5.19. Both the experimental and the computation results exhibit a linear elastic response during the initial phase, immediately preceded by a non-linear stage leading up to the failure limit. As shown in Table 5.5, the average ultimate load obtained experimentally have been correlated with the corresponding numerical findings. Furthermore, the mean ultimate load provided using the test results on average was 1041.34N whereas the predicted based on the applied (PFA) ultimate load was 1033.15N, representing just an error of 0.8% less than the mean value measured experimentally and error of 7.07% less than the deflection at ultimate load.

Table 5.5. Comparison of the failure load and the deflection at failure load with the test results.

Material	Layup	Failure Load (N)		
		The Present model	Experiment	Error (%)
IMS194/CYCOM977-2	$[45°/\,0°_2/-45°/0°/90°/\,0°_2/90°/0°/-45°/0°_2/45°)]_s$	2192,84	2289,74	4,23
AS4/PEEK	$[0°_3/90°_3]_{2s}$	1033,15	1041,34	0,8

Deflection at Failure Load (mm)		
The Present model	Experiment	Error (%)
4,75	4,61	2,95
6,49	6,99	7,07

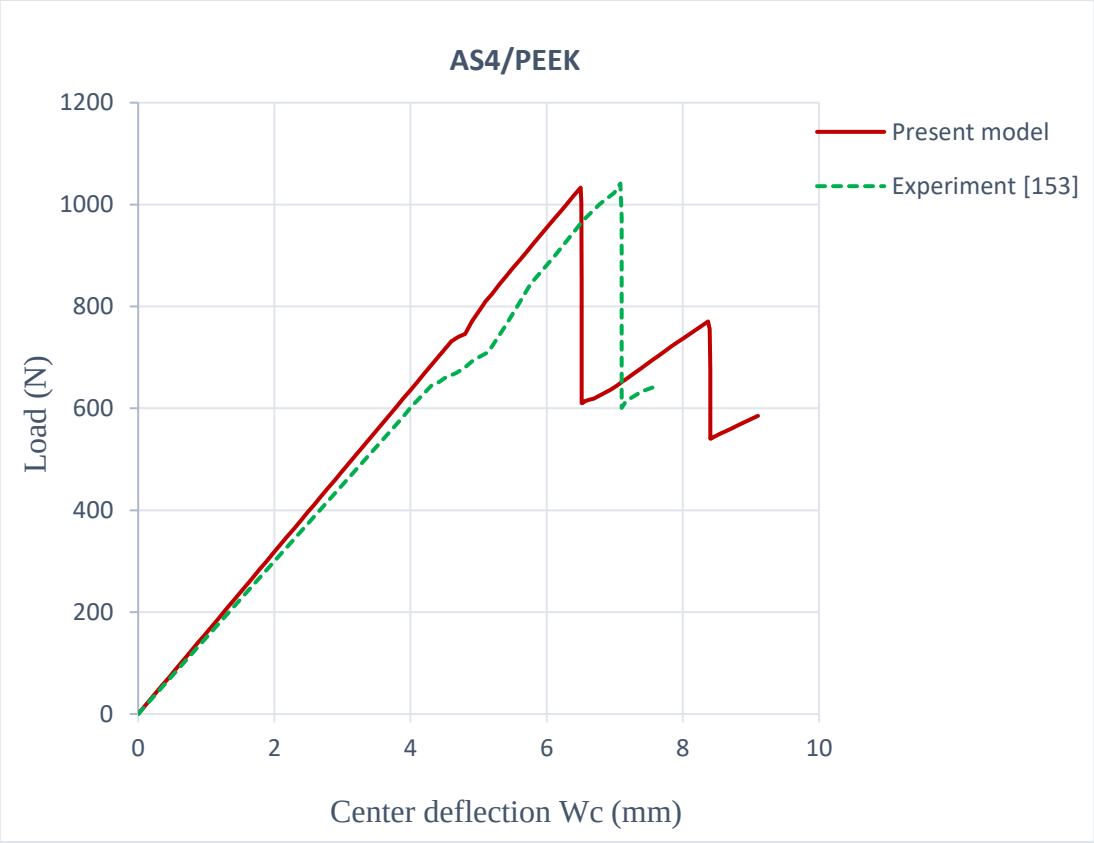
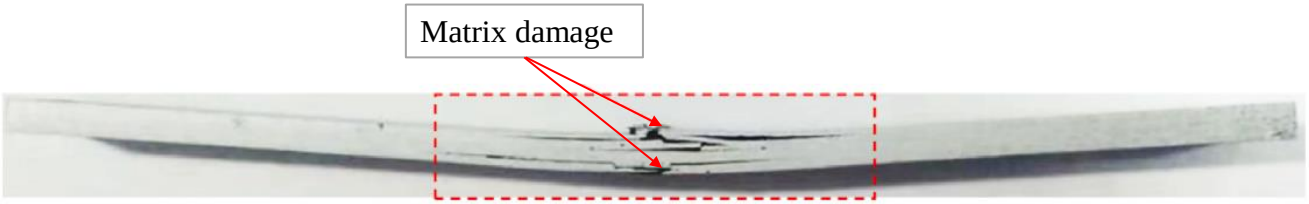


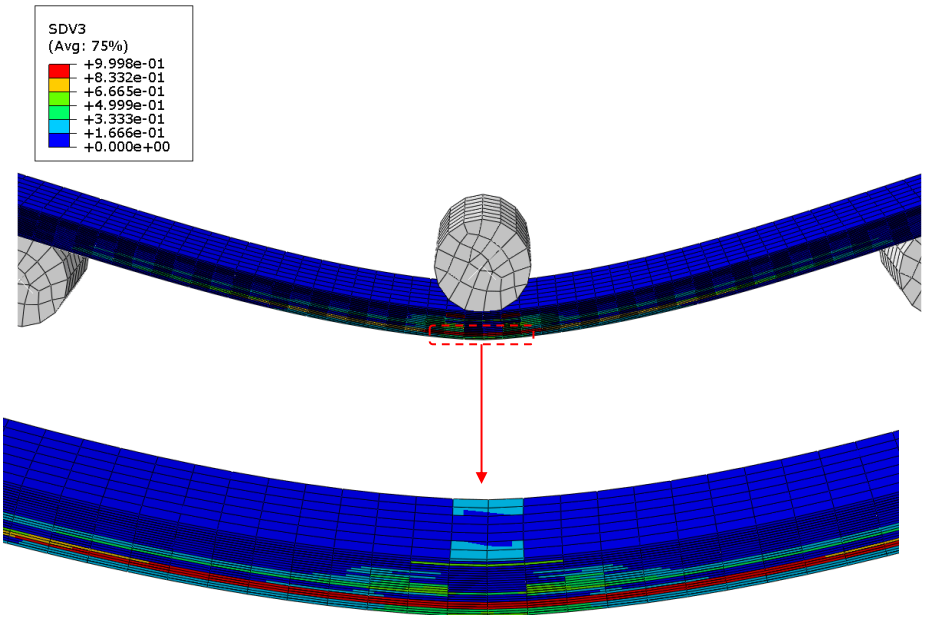
Figure 5.19: Predicted load vs. deflection curves of AS4/PEEK composite laminates.

5.4.2.2. Damage prediction

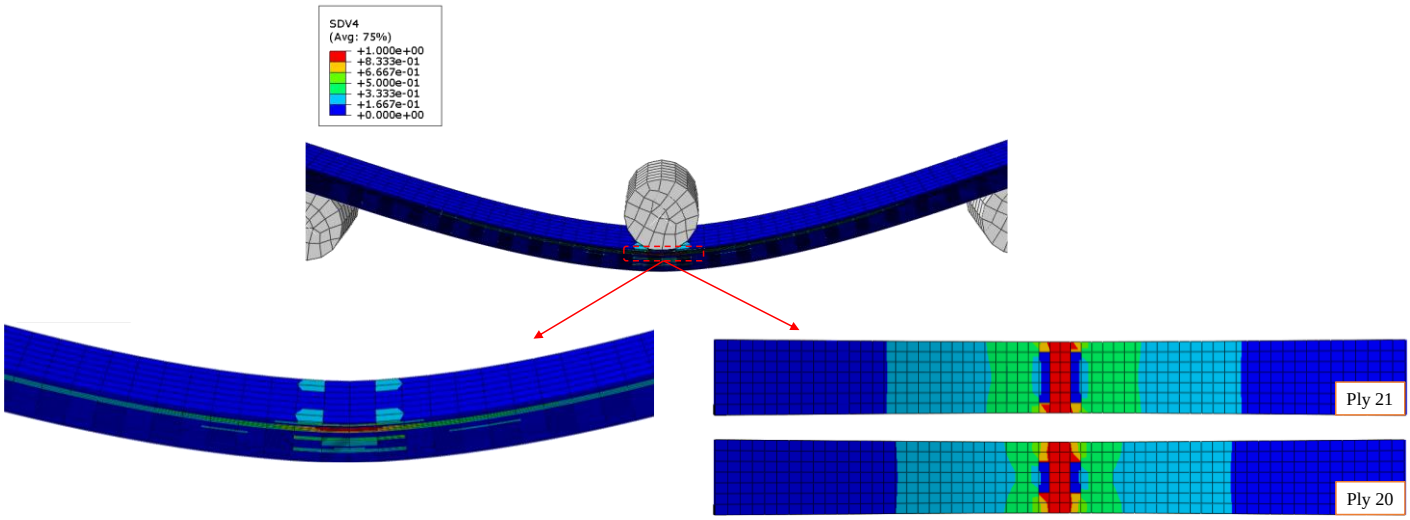
The developed damage model can predict the initiation and progression of in-plane damage within the laminated composites. The experimental matrix damage and the modelled damage contour at failure load are shown in Fig. 5.20. It can be seen from the picture of the test specimen that the matrix damage has occurred in the middle region of the sample which was further supported with numerical computation as shown in (Figs. 5.20 (a, b)). The compressive and tensile matrix damage occurred in the top and bottom laminate in the layers with 90° orientation, respectively. Further diffuses to the adjacent layers after the maximum load so that the elements are completely destroyed as shown in (Figs. 5.21 (a, b)). In terms of upper and lower fiber damage, Fig. 5.22 illustrates upper fiber damage under compression and lower fiber damage under tension, as extracted using the 3-point bending for experiment and simulation. It is evident that in both the upper and lower sections of the simulated samples, fiber breaks have been detected in the mid region of the layers with 0° orientation (tensile fiber damage at the bottom and compressive fiber damage at the top), matching closely with the reported experimental specimen. After the failure load, the specimen loses much of its strength, and the elements undergo tensile and compressive fiber failure very quickly and infect adjacent elements as illustrated in (Fig. 5.21 (c, d)).



(a) Matrix damage obtained from virtual post-tested composite specimen [153]**.**

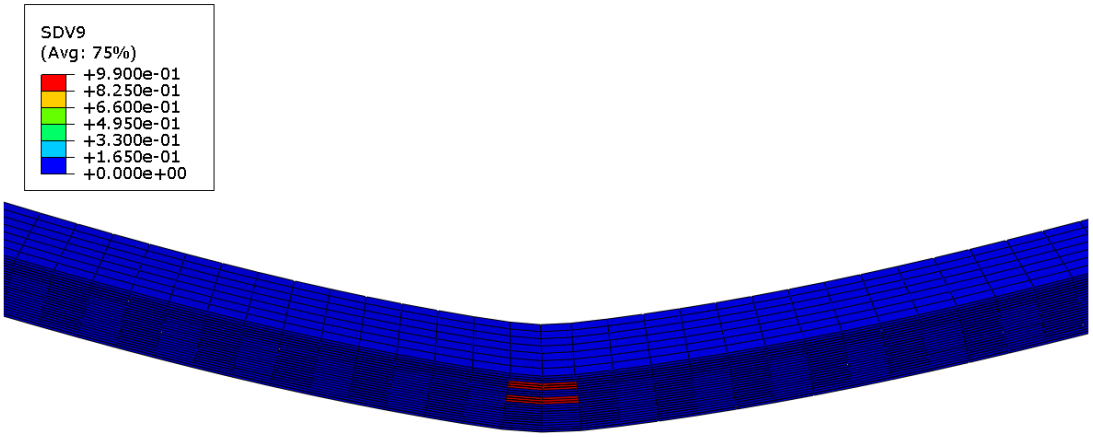


(b) Matrix tension damage on the Bottom surface at Failure load.

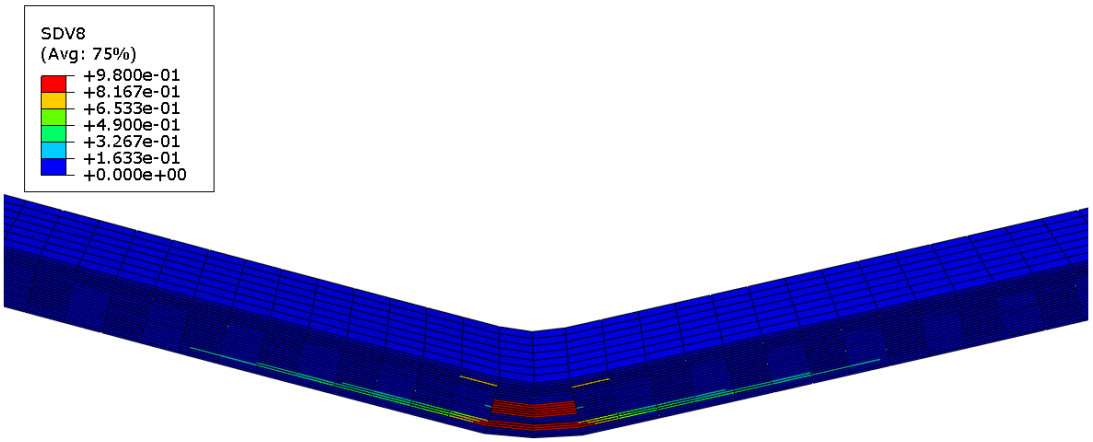


(c) Matrix compression damage on the Top surface at Failure load.

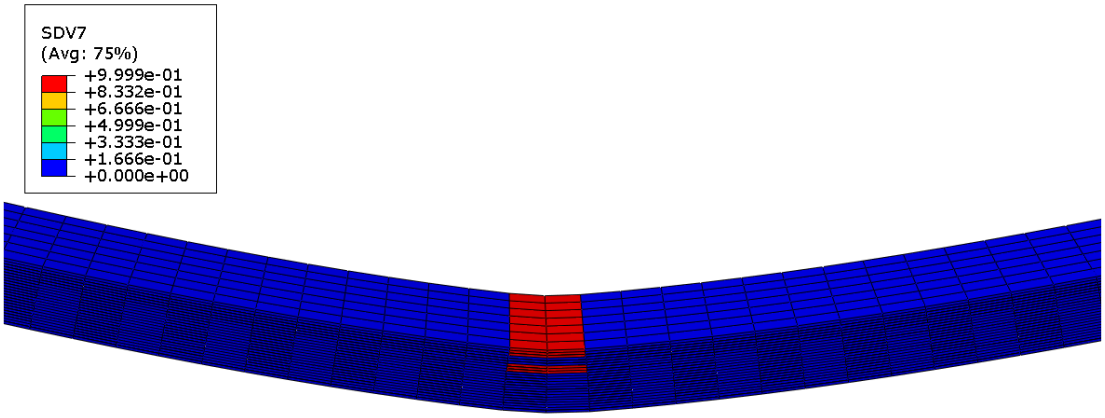
Figure 5.20: Matrix damage obtained from the experiments [153] and the damage contour from the simulation at failure load.



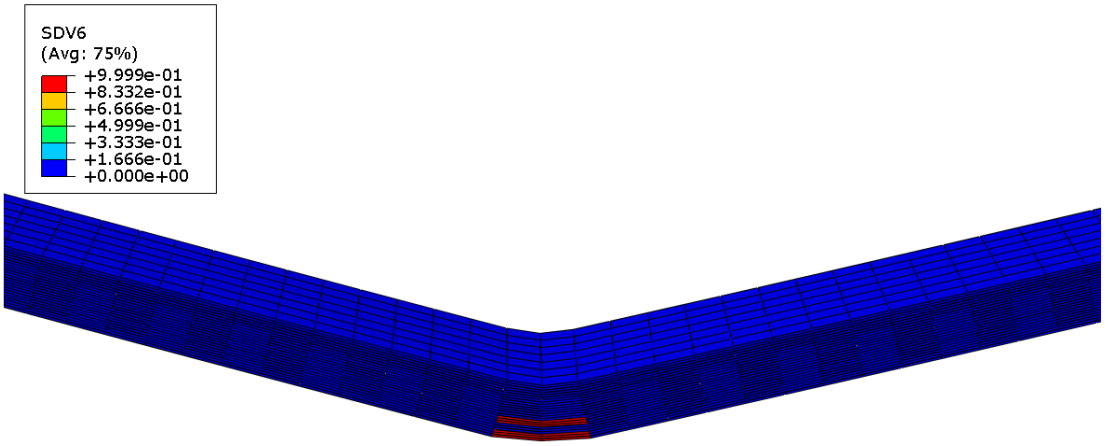
(a) compressive matrix Failure at second fracture.



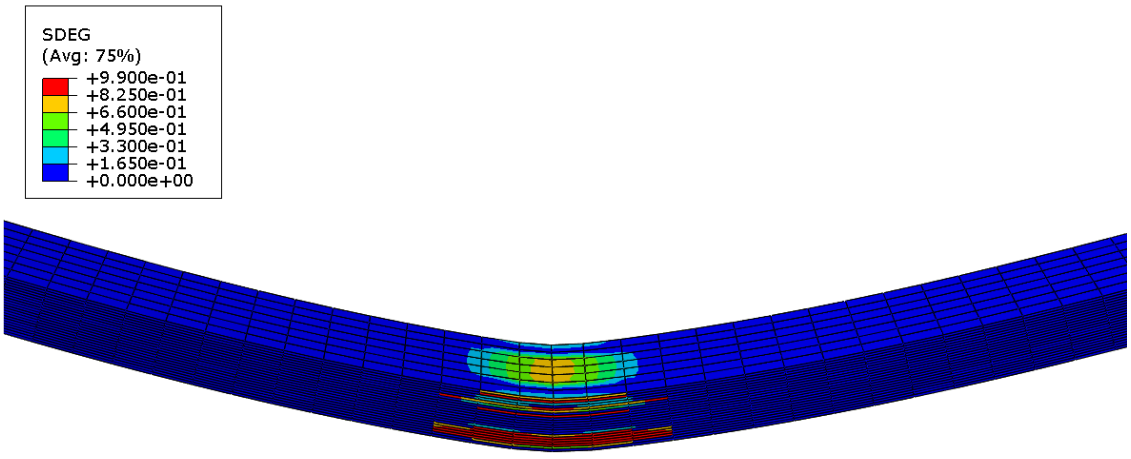
(b) tension matrix Failure at second fracture.



(c) Compressive fiber Failure at second fracture.

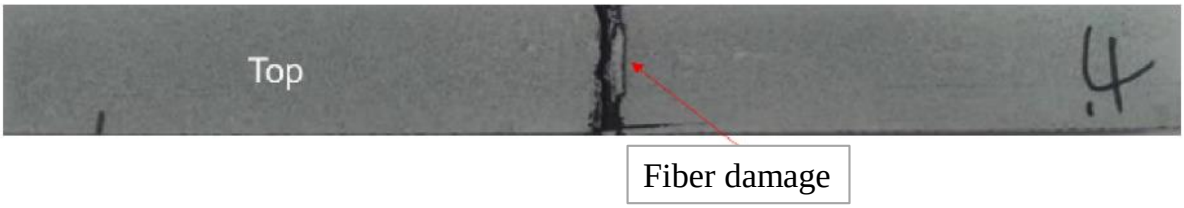


(d) tensile fiber Failure at second fracture.

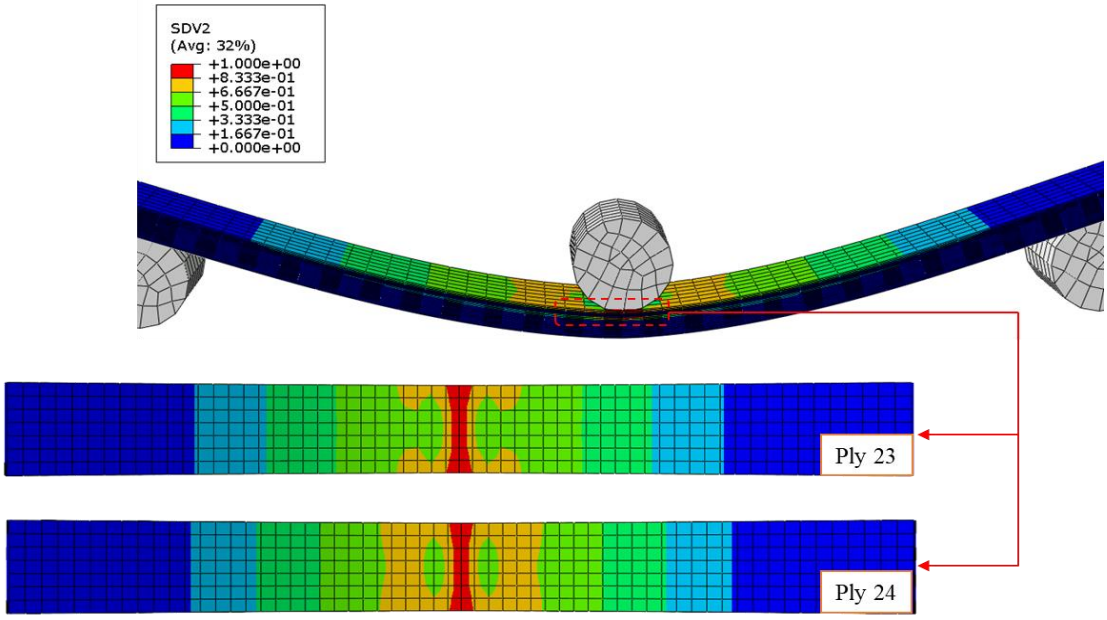


(e) Delamination at second fracture

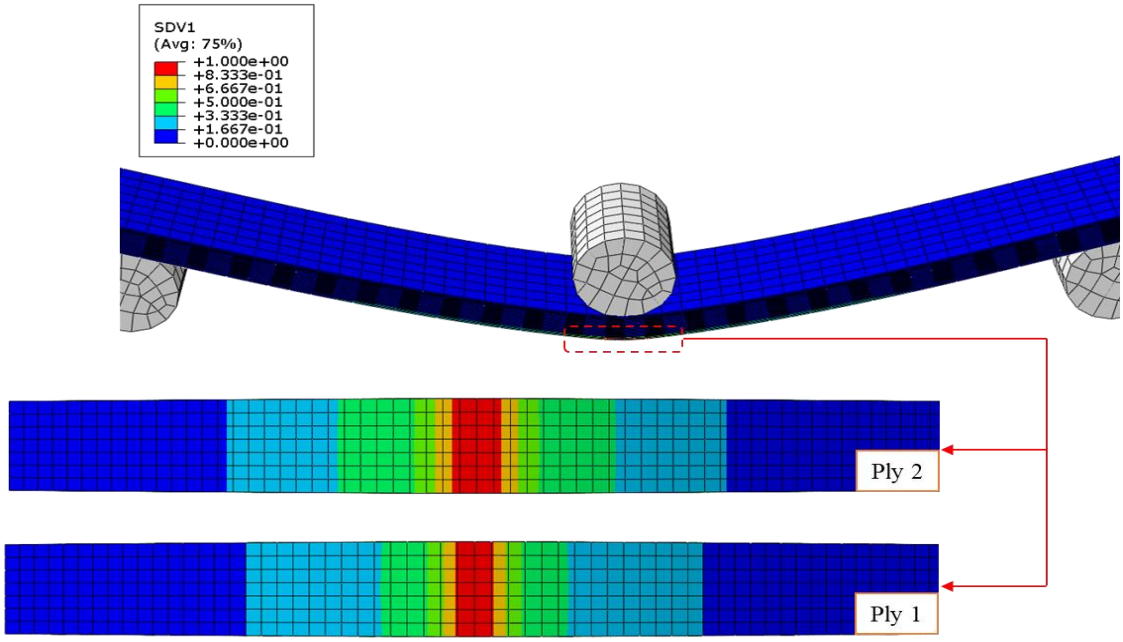
Figure 5.21: Intra/interlaminar damage contour at second fracture of AS4/PEEK composite laminates.



(a) fiber damage obtained from the virtual post-tested composite specimen [153] **.**

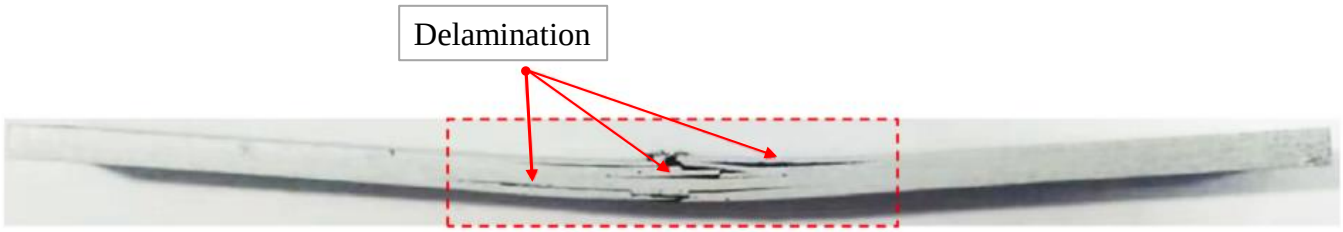


(b) Fiber compression damage on the Top surface at Failure load.

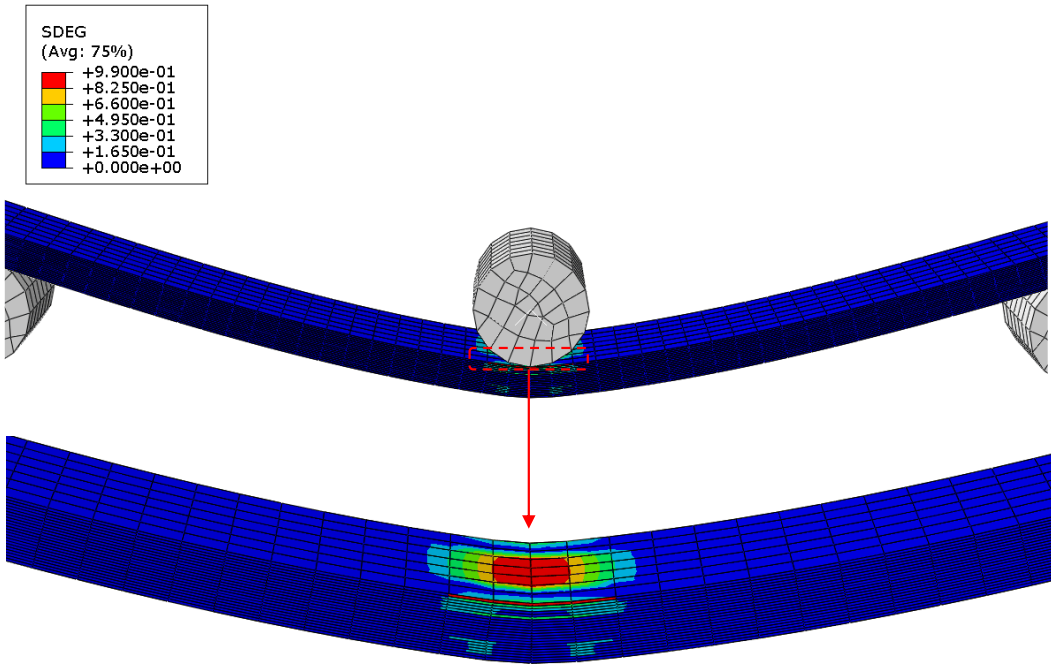


(c) Fiber tension damage on the Bottom surface at Failure load.

Figure 22. Damage contour of fiber tension/compression of AS4/PEEK composite laminates.



(a) Delamination damage obtained from virtual post-tested composite specimen [153]**.**



(b) Delamination initiation at Failure load.

Figure 5.23: Delamination obtained from post-tested with delamination damage contour obtained from simulation at failure load.

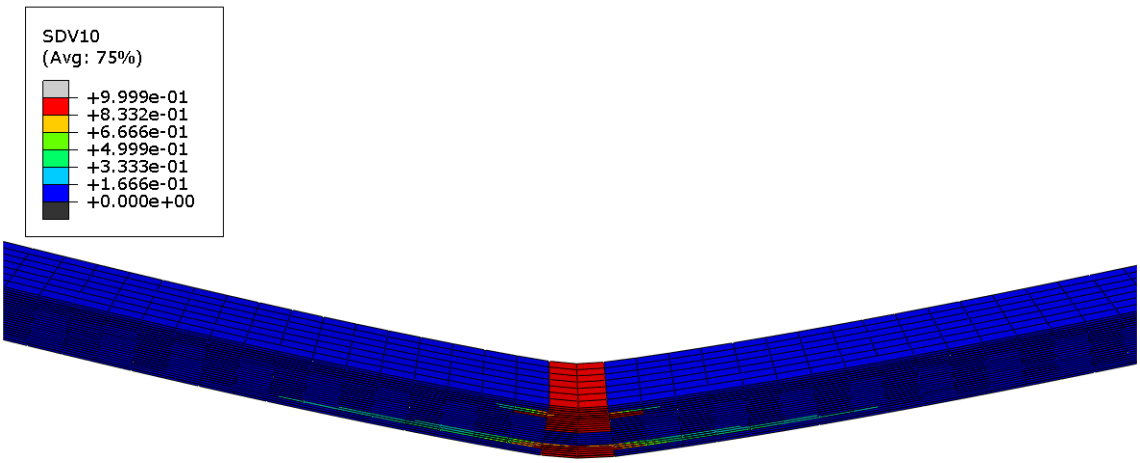


Figure 5.24: Status of all damage modes.

On the other hand, Fig 5.23 compares experimental and simulated inter-laminar damage. It is clear from the side aspect of the sample under test that substantial delamination damage has taken place through the composite laminated due to the three-point bending loading. The simulation using the applied method can display that the interlaminar damage where the delamination initiates in top of specimen at the failure load and propagate through the thickness which yielded close agreement with the reported experimentally data as demonstrated in the Fig. 5.23 (a). The status of different intralaminar damage modes have been presented in Fig. 5.24 which show that the majority of elements located in the middle have been completely destroyed. Besides, the results of the comparison between the test and simulation indicate that the proposed numerical model using progressive failure approach can successfully reproduce the failure mechanisms including fiber breakage under tension/compression, matrix failure and delamination as well as the whole damage pattern of the examined composite samples.

5.5. Conclusion

The aim of this chapter is to improve the finite element modelling of a three-point bending load, by incorporating multi-layered laminates and cohesive zone elements, utilizing the Umat subroutine. This approach enables accurate representation of intra/interlaminar damage progressive through composite laminates, while simultaneously reducing processing time and testing costs. To track the progressive damage within each ply, Puck's failure criteria and constant stress exposure are employed. Additionally, interlaminar damage between plies is predicted using a quadratic stress criterion coupled with Benzeggah-Kenane criteria.

The key research findings are outlined as follows:

- ✓ The computational results were observed to be in good agreement with the experimental data. The computed ultimate load and failure displacement exhibited errors of 4.23% and 2.95% for IMS194/CYCOM977-2, and 0.8% and 7.07% for AS4/PEEK, respectively, when compared to the mean values reported in the existing literature. This suggests that the computational model effectively captures the mechanical behaviour of the investigated composites, validating its reliability, flexibility and accuracy. In addition, it has been observed that the degradation trends in the load vs deflection curves following the peak load could be satisfactorily estimated using the proposed model.
- ✓ The incorporation of a cohesive zone model into finite element simulations has proven to be a valuable tool for investigating the delamination behaviour of composite laminates, offering insights that can enhance their design and performance. Additionally, delamination plays a significant role in promoting intralaminar longitudinal cracking under higher interlaminar stresses, thereby contributing to the degradation of the composite material's strength. The research demonstrated that neglecting delamination failure leads to an underestimation of the failure load, highlighting the importance of considering delamination effects for accurate failure predictions.
- ✓ The applied model demonstrates reduced mesh dependency, which can be attributed to its distinctive approach in simulating the progressive damage behaviour of composite materials. Unlike traditional methods relying on energy release rate approaches that exhibit higher mesh dependency, our model utilizes a novel damage propagation scheme based on element deletion techniques. This advancement contributes to improved accuracy and reliability in capturing the damage evolution regardless of mesh refinement.

- ✓ The design of high-performance composite structures in the aerospace or automotive industry could benefit greatly from this new high integrity damage modelling approach. It is believed that this damage modelling approach has potential for wider application to various loading configurations, such as impact, fatigue loading and this will be explored in future work.

Chapter 6: Conclusions and recommendations for future research studies

Overview

- *Introduction*
- *Conclusions*
- *Recommendation for future research works*

6.1. Introduction

This chapter summarises the main findings of the study in each of these researches including:

- ☞ The applicability and effectiveness of different progressive damage model.
- ☞ Implementation and development of progressive damage model.
- ☞ Numerical simulation of different composite laminated behviour under tension and three-point bending loading.
- ☞ The interaction between inter/intralaminar damage using three-dimensional finite element model as well as the interest of using cohesive zone elements.

In addition, recommendations for future research studies to improve or extend current works are also provided.

6.2. Conclusions

To accurately predict the mechanical response and progressive damage of composite materials under tensile loading, and also to reduce the computational time and cost and fully exploit the advantages of composite structures, it is necessary to apply a suitable approach to assess the growth of damage to final failure.

For this purpose and following the discussion on failure analysis, we delved into the various failure criteria associated with the intra/interlaminar damage process. We highlighted the applicability and limitations of each criterion and the importance of selecting the appropriate one based on the nature of the damage and the material under consideration. Additionally, we discussed numerical modelling techniques used to simulate and analyse the behaviour of composite laminates.

However, it is hard to come up with a universal definition for what constitutes "failure" of a composite structure since many failure theories and analytical models are available in the literature. The World-Wide Failure exercise (WWFE) summarized twenty-three different failure criteria. All test cases presented in the WWFE are laminates assembled from continuous fiber reinforced unidirectional laminae subjected to 2D in-plane loading. Among the twenty-three failure criteria studied in the WWFE, predictions from Puck and Schürmann's failure criteria showed good agreement with most of the experimental data. The current state of some failure criteria was described in Chapter 2. The revolutionary Hashin's failure criteria for FRP composites based on the concept of failure plane were discussed in some detail, and correlations between Puck and Schürmann's and Hashin's failure criteria are reviewed.

Accordingly, a new computational analysis was developed using the UMAT subroutine integrated into the Abaqus finite element analysis package which can be adapted for both 3D problem or plane stress state (2D) (Chapter 3). Advanced assessment functions like the Puck failure criteria and gradual degradation models, CSE and EWM, were successfully employed to simulate the behaviour of an open-hole composite laminate under pure tensile loading. Separate failure modes are considered for the matrix and the fiber of the laminates. The development of the subroutine widens the capability of the software for PFA using the finite element method.

The analysis has been included the prediction of the damage progression, failure load and failure modes. In addition, while taking into account the effect of parameters such as sample size, stress

concentration and stacking sequences, a comparison was also made with the Built-in Abaqus model which based on Hashin failure criteria and Matzenmiller's approach, as well as with others existing literature.

The main results of the research are described below:

- The accurate assessment of progressive failure in laminated composite structures relies heavily on the choice and application of appropriate failure criteria.
- The simulation results obtained using the applied models (PUCK+CSE and PUCK+EWM) demonstrated strong correlation with the reported composite failure results. This was evident in the comparison of initial and final failure loads, as well as the progression of damage across various stacking sequences.
- Despite the increased analysis time due to the iterative process involved in determining the angle of the fracture plane for each increment, it was found that structural failure analyses of large complex composite structures are feasible. The constant stress exposure method utilized in the applied model proved to be accurate and more time-efficient than the element weakening method and Matzenmiller's approach.
- The importance of considering the size of holes in structural design cannot be overstated. Mitigating measures should be implemented to address the adverse effects associated with larger hole diameters.
- The comparative analysis conducted in this study revealed that the PUCK+CSE model exhibited good agreement with experimental and computational results reported in the literature. It demonstrated accurate predictions of failure load, size effect, and load-displacement curves. Additionally, the PUCK+CSE model outperformed the PUCK+EWM model and the Built-in model in terms of stiffness prediction, displaying lower errors.
- The careful selection of material properties for both the matrix and fibers is crucial in the design of fiber-reinforced composites. Optimizing the reinforcement and fiber breaking strength relies on accurately determining properties such as Young's modulus and stiffness for both the fibers and matrix.
- In terms of mesh dependence, the applied PFA models of PUCK+CSE and PUCK+EWM yielded more consistent results compared to the Built-in model, demonstrating their reliability and suitability for accurate simulations.

On the one hand, the simulation of the three-point bending test holds significant interest in engineering and materials science. This simulation provides a platform for characterizing material properties, optimizing designs, predicting failure modes, and validating computational models. By replicating this test virtually, researchers and engineers can gain valuable insights into the mechanical behaviour of materials subjected to bending loads which is the case of Chapter 4. Our objective was to analyse the damage progression from the initial onset of damage to the final failure. To achieve this, we developed a finite element model incorporating Puck's failure criteria and the element weakening method, which accurately captured the behaviour of two different type specimens.

Additionally, we conducted an experimental investigation of the Prepreg T700/epoxy woven laminates under three-point bending tests. By comparing the experimental results with our finite element model predictions, we were able to draw several important research findings:

- Our study revealed that Halpin's analogy, which treats the woven laminate as a two-layer laminate [0/90], displayed a strong correlation with the experimental results. This was particularly evident in its ability to accurately predict deflection and failure load, providing confidence in its applicability to woven laminates.
- Additionally, our investigation highlighted the influential role of the ratio (l/h) and the width of the specimens in the successive failure and overall resistance of the composite laminate. Specifically, we observed a detrimental effect on the strength of the laminate as the ratio (l/h) increased. These findings underscore the critical importance of considering these geometric parameters when evaluating the structural integrity and failure behaviour of the composite laminate.

On the other hand, with advancements in simulation techniques, there has been a transition from simulating materials using stress plane state to more complex 3D problems. This transition has opened up new possibilities for a comprehensive understanding of material behaviour, particularly in the presence of delamination. The simulation of materials using stress plane state provided valuable insights into the stress distribution and failure mechanisms in two-dimensional models. However, as engineering applications became more complex, it became essential to consider the full three-dimensional nature of structures and materials. Simulating 3D problems allows for a more accurate representation of real-world scenarios, enabling engineers to capture the intricacies of material behaviour under various loading conditions. Integrating delamination effect into these 3D simulations has further enhanced the interest in this area which the aim of chapter 5. Hence,

The objective was improving the finite element modelling of a three-point bending load, by incorporating multi-layered laminates and cohesive zone elements, utilizing the Umat subroutine. Each layer was required to be modelled individually based upon its fiber orientation. This approach enables accurate representation of intra/interlaminar damage progressive through composite laminates, while simultaneously reducing processing time and testing costs. To track the progressive damage within each ply, Puck's failure criteria and constant stress exposure are employed. Additionally, interlaminar damage between plies is predicted using a quadratic stress criterion coupled with Benzeggah-Kenane criteria. This method can be applied in particularly to structures where 3D effects become significant. A numerical search method, was adapted to determine the failure plane angle in the matrix. The damage variable known as material degradation factors and the angle α of the failure plane are found by solving a system of non-linear equations which satisfy the matrix failure criteria.

The key research findings are outlined as follows:

- The Puck failure criterion was found to be effective in handling 3D stress states without the need for parameter calibration. When coupled with a degradation model, it accurately predicted the intralaminar progressive damage in composite laminates. This demonstrates the power and reliability of the Puck failure criterion in capturing the failure behaviour of composite materials.
- The computational results showed excellent agreement with experimental data, with small errors in ultimate load and failure displacement compared to existing literature. This indicates that the computational model successfully captures the mechanical behaviour of the investigated composites, validating its reliability, flexibility, and accuracy. The proposed model also accurately estimated the degradation trends in the load vs deflection curves after the peak load.

- The incorporation of a cohesive zone model into finite element simulations proved valuable in studying the delamination behaviour of composite laminates and enhancing their design and performance. Neglecting delamination failure leads to an underestimation of the failure load, emphasizing the significance of considering delamination effects for accurate failure predictions.
- The applied model demonstrated reduced mesh dependency due to its unique approach in simulating progressive damage behaviour. By utilizing an element deletion technique for damage propagation instead of traditional energy release rate approaches, the model achieved improved accuracy and reliability regardless of mesh refinement.
- The developed high integrity damage modelling approach holds great potential for the design of high-performance composite structures in aerospace and automotive industries. It can be further explored and applied to various loading configurations such as impact and fatigue loading in future research.
- By incorporating the UMAT subroutine into Abaqus, we have gained the capability to effectively examine the progressive failure under various loadings. These insightful examples serve as valuable tools for investigating more complex problem geometries and diverse loading conditions.

6.3. Recommendation for future research works

Since the research work in this thesis aimed to model the damage in composite structures, it was not possible to cover all aspects of the problem. A number of further research studies can be pursued to improve the understanding in this area:

- Development of advanced damage models: Future research can focus on the development and refinement of advanced damage models for composite laminates under different complex loading. These models should accurately capture the progressive damage and failure mechanisms, including multi-cracks propagation, kink-band and buckling of fiber, and interface debonding. Incorporating multiscale and Multiphysics approaches can help improve the accuracy of damage predictions.
- Impact and fatigue analysis: Progressive damage analysis under impact, thermo-mechanical and fatigue loading conditions is of great practical importance. Further research can investigate the behaviour of composite laminates under dynamic loading, including the development of accurate and efficient models to predict damage initiation, propagation, and residual strength.
- Manufacturing effects: The manufacturing process can have a significant impact on the damage behaviour of composite laminates. Future research should investigate the influence of manufacturing defects, such as voids, fiber misalignment, and resin-rich areas, on the progressive damage and failure of laminated structures. Developing models that incorporate manufacturing-induced defects will aid in optimizing the manufacturing process and improving the reliability of composite laminates.

These recommendations aim to address current challenges and push the boundaries of progressive damage analysis in composite laminates. By focusing on these areas, researchers can contribute to the development of more accurate, reliable, and efficient analysis methods, leading to improved design and performance of composite structures in various applications.

REFERENCES

[1] G. Marsh, “Composites lift off in primary aerostructures The take-off run for aerospace composites has been prolonged , but now that,” no. April, pp. 22–27, 2004.

[2] P. D. Soden, A. S. Kaddour, and M. J. Hinton, “Recommendations for designers and researchers resulting from the world-wide failure exercise,” *Fail. Criteria Fiber-Reinforced-Polymer Compos.*, pp. 1223–1251, 2004.

[3] P. D. Soden, M. J. Hinton, and A. S. Kaddour, “Lamina properties lay-up configurations and loading conditions for a range of fiber-reinforced composite laminates,” *Fail. criteria fiber Reinf. Compos. Elsevier*, pp. 30–51, 2004.

[4] P. D. Soden, M. J. Hinton, and A. S. Kaddour, “A comparison of the predictive capabilities of current failure theories for composite laminates,” *Compos. Sci. Technol.*, vol. 58, no. 7, pp. 1225–1254, 1998, doi: 10.1016/S0266-3538(98)00077-3.

[5] M. J. Hinton, A. S. Kaddour, and P. D. Soden, *A comparison of the predictive capabilities of current failure theories for composite laminates, judged against experimental evidence*, vol. 62, no. 12-13 SPECIAL ISSUE. 2002. doi: 10.1016/S0266-3538(02)00125-2.

[6] M. J. Hinton, A. S. Kaddour, and P. D. Soden, “Evaluation of failure prediction in composite laminates : background to ‘ part C ’ of the exercise,” vol. 64, pp. 321–327, 2004, doi: 10.1016/S0266-3538(03)00216-1.

[7] P. D. Soden, A. S. Kaddour, and M. J. Hinton, “Recommendations for designers and researchers resulting from the world-wide failure exercise,” *Compos. Sci. Technol.*, vol. 64, pp. 589–604, 2004, doi: 10.1016/S0266-3538(03)00228-8.

[8] R. G. Cuntze and A. Freund, “The predictive capability of failure mode concept-based strength criteria for multidirectional laminates,” vol. 64, pp. 343–377, 2004, doi: 10.1016/S0266-3538(03)00218-5.

[9] A. Puck and H. Schürmann, “Failure analysis of FRP laminates by means of physically based phenomenological models,” *Compos. Sci. Technol.*, vol. 62, no. 12-13 SPECIAL ISSUE, pp. 1633–1662, 2002, doi: 10.1016/S0266-3538(01)00208-1.

[10] N. V Nayak, “Composite Materials in Aerospace Applications,” 2014.

[11] H. Bisheh and Y. Abdin, “Carbon Fibers: From PAN to Asphaltene Precursors; A State-of-Art Review,” *J. Carbon Res.*, vol. 9, no. 1, p. 19, 2023, doi: 10.3390/c9010019.

[12] S. Drapier, “Mécanique des Composites Hautes Performances,” École Nationale Supérieure des Mines de Saint-Étienne, 2021.

[13] M. BELLAHKIM, “Modélisation du comportement mécanique non linéaire et de la rupture par délaminage d’un composite stratifié en carbone/époxyde en flexion trois points,” Université Hassan II, 2022.

[14] J. M. Berthelot, *Mécanique des Matériaux et Structures Composites ISMANS Institut Supérieur des Matériaux Le Mans, France et Mécaniques Avancés*. 2012.

[15] M. NOUARI, “Modélisation numérique de l’usinage des matériaux composites à matrice polymère et fibers longues de carbone,” Université de Lorraine, 2011.

[16] E. Lund, “NOTES ON STRUCTURAL ANALYSIS OF COMPOSITE SHELL STRUCTURES,” Aalborg University, 2001.

[17] L. Gornet, *Généralités sur les Matériaux Composites*. 2011.

[18] Z. Sekkate, A. Aboutajeddine, and A. Seddouki, “Elastoplastic mean-field homogenization: recent advances review,” *Mech. Adv. Mater. Struct.*, vol. 29, no. 3, pp. 449–474, 2022, doi: 10.1080/15376494.2020.1776431.

[19] M. Paley and J. Aboudi, “Micromechanical analysis of composites by the generalized cells model,” vol. 14, pp. 127–139, 1992.

[20] H. Moussaddy, “A New Definition of the Representative Volument Element in Numerical Homogenization Problems and its Application to the Performance Evaluation of Analytical Homogenization Models.,” 2013. [Online]. Available: http://publications.polymtl.ca/1091/1/2013_HadiMoussaddy.pdf

[21] A. Puck, “SHOULD FIBER-PLASTICS COMPOSITES BE DESIGNED WITH STRAIN OR STRESS CRITERIA.,” *KUNSTSTOFFE-GERMAN Plast.*, vol. 82, no. 5, pp. 431–434, 1992.

[22] J. Kopp, “Contribution to the stress and strength analysis of unidirectionally fiber reinforced plastics,” Technical University of Aachen, 2000.

[23] L. J. Hart-Smith, “PREDICTIONS OF A GENERALIZED MAXIMUM-SHEAR-STRESS FAILURE CRITERION FOR CERTAIN FIBROUS COMPOSITE LAMINATES,” *Compos. Sci. Technol.*, vol. 58, pp. 1179–1208, 1998.

[24] W. Michaeli, M. Mannigel, and F. Preller, “On the effect of shear stresses on the fiber failure behaviour in CFRP,” *Compos. Sci. Technol.*, vol. 69, no. 9, pp. 1354–1357, 2009, doi: 10.1016/j.compscitech.2008.09.024.

[25] S. LÜTZE, “Confocal Laser Scanning Photoelasticity : Improvement of Precision for Quantitative Photoelastic Studies on Model Composite Materials,” vol. 23, pp. 273–278, 2001.

[26] I. V Sela and O. Ishai, “Interlaminar fracture toughness and toughening of laminated composite materials : a review,” vol. 20, no. 5, 1989.

[27] F. Gu, X. Yuan, X. Zhu, X. Lu, D. Fang, and L. Li, “Numerical study of composite laminates subjected to low-velocity impact using a localized damage algorithm of Puck ’ s 3D IFF criterion,” vol. 228, no. September 2019, 2020, doi: 10.1016/j.engfracmech.2020.106901.

[28] C. S. Lee, J. H. Kim, S. K. Kim, D. M. Ryu, and J. M. Lee, “Initial and progressive failure analyses for composite laminates using Puck failure criterion and damage-coupled finite element method,” *Compos. Struct.*, vol. 121, pp. 406–419, 2015, doi: 10.1016/j.compstruct.2014.11.011.

[29] J. Gu, K. Li, and L. Su, “A Continuum Damage Model for Intralaminar Progressive Failure Analysis of CFRP Laminates Based on the Modified Puck ’ s Theory,” no. Cdm, 2019.

[30] G. Kress, “Examination of Hashin’s failure criteria for Part B of the second world-wide failure exercise: Comparison with test data,” *J. Compos. Mater.*, vol. 47, no. 6–7, pp. 867–891, 2013, doi: 10.1177/0021998312460260.

[31] Z. Zhao *et al.*, “Progressive failure simulation of notched tensile specimen for triaxially-braided composites,” *Materials (Basel).*, vol. 12, no. 5, pp. 1–19, 2019, doi: 10.3390/MA12050833.

[32] A. M. Gadade, A. Lal, and B. N. Singh, “Finite element implementation of Puck’s failure criterion for failure analysis of laminated plate subjected to biaxial loadings,” *Aerosp. Sci. Technol.*, vol. 55, pp. 227–241, 2016, doi: 10.1016/j.ast.2016.05.001.

[33] S. W. Tsai and V. D. Azzi, “Anisotropic Strength of Composites derived from unidirectional specimens alone,” pp. 283–288, 1965.

[34] P. Nali and E. Carrera, “A numerical assessment on two-dimensional failure criteria for composite layered structures,” *Compos. Part B Eng.*, vol. 43, no. 2, pp. 280–289, 2012, doi: 10.1016/j.compositesb.2011.06.018.

[35] S. W. Tsai and E. M. Wu, “A General Theory of Strength for Anisotropic Materials,” *J. Compos. Mater.*, 1971, doi: 10.1177/002199837100500106.

[36] R. Joshi, P. Pal, and S. K. Duggal, “Ply-by-ply failure analysis of laminates using finite element method,” *Eur. J. Mech. A/Solids*, vol. 81, no. January, p. 103964, 2020, doi: 10.1016/j.euromechsol.2020.103964.

[37] A. Puck, J. Kopp, and M. Knops, “Guidelines for the determination of the parameters in Puck’s action plane strength criterion,” *Compos. Sci. Technol.*, vol. 62, no. 3, pp. 371–378, 2002, doi: 10.1016/S0266-3538(01)00202-0.

[38] Z. Hashin, “Failure Criteria for Unidirectional Mr !,” *J. Appl. Mech.*, vol. 47, no. June, pp. 329–334, 1980.

[39] E. H. Irhirane, J. Echaabi, M. Aboussaleh, M. Hattabi, and F. Trochu, “Matrix and fiber stiffness degradation of a Quasi-isotrope graphite epoxy laminate under flexural bending test,” *J. Reinf. Plast. Compos.*, vol. 28, no. 2, pp. 201–223, 2009, doi: 10.1177/0731684407084213.

[40] Z. Hashin and A. Rotem, “A Fatigue Failure Criterion for Fiber Reinforced Materials,” *J. Compos. Mater.*, vol. 7, no. 4, pp. 448–464, 1973, doi: 10.1177/002199837300700404.

[41] C. G. Davila, P. P. Camanho, and C. A. Rose, “Journal of Composite Materials,” 2005, doi: 10.1177/0021998305046452.

[42] S. T. Pinho, C. G. Dávila, P. P. Camanho, L. Iannucci, and P. Robinson, “Failure Models and Criteria for FRP Under In-Plane or Three-Dimensional Stress States Including Shear Non-Linearity,” no. February, 2005.

[43] F. Paris and K. E. Jackson, “A Study of Failure Criteria Composite Materials of Fibrous,” no. March, 2001.

[44] A. Filippatos, A. Langkamp, and M. Gude, “Influence of gradual damage on the structural dynamic behaviour of composite rotors: Simulation assessment,” *Materials (Basel).*, vol. 11, no. 12, pp. 1–16, 2018, doi: 10.3390/ma11122453.

[45] B. G. Falzon and P. Apruzzese, “Numerical analysis of intralaminar failure mechanisms in composite structures. Part II: Applications,” *Compos. Struct.*, vol. 93, no. 2, pp. 1047–1053, 2011, doi: 10.1016/j.compstruct.2010.06.022.

[46] B. G. Falzon and P. Apruzzese, “Numerical analysis of intralaminar failure mechanisms in composite structures. Part I: FE implementation,” *Compos. Struct.*, vol. 93, no. 2, pp.

1039–1046, 2011, doi: 10.1016/j.compstruct.2010.06.028.

[47] P. Maimí, P. P. Camanho, J. A. Mayugo, and C. G. Dávila, “A continuum damage model for composite laminates: Part II - Computational implementation and validation,” *Mech. Mater.*, vol. 39, no. 10, pp. 909–919, 2007, doi: 10.1016/j.mechmat.2007.03.006.

[48] P. Maimí, P. P. Camanho, J. A. Mayugo, and C. G. Dávila, “A continuum damage model for composite laminates: Part I - Constitutive model,” *Mech. Mater.*, vol. 39, no. 10, pp. 897–908, 2007, doi: 10.1016/j.mechmat.2007.03.005.

[49] L. M. Kachnov, “Time of the rupture process under creep conditions,” *Izy Akad. Nank SSR Otd Tech Nauk*, vol. 8, no. 26–31, 1958.

[50] H. El Idrissi and A. Seddouki, “Analysis of The Progressive Damage of A Notched AS4 / PEEK Composite Laminate Subjected To Tensile Loading,” *Stat. Optim. Inf. Comput.*, vol. 11, pp. 125–135, 2023, doi: 10.19139/soic-2310-5070-1555.

[51] H. El Idrissi and A. Seddouki, “Modelling of Progressive Damage in a Notched Carbon/Epoxy Composite Laminate Subjected to Tensile Loading Using Different Assessment Methods Coupled with FEM,” *Fibers Polym.*, vol. 23, no. 11, pp. 3146–3162, 2022, doi: 10.1007/s12221-022-0019-4.

[52] H. El Idrissi and A. Seddouki, “Damage Modeling of Composites Laminate Containing Stress Concentrations,” in *2022 2nd International Conference on Innovative Research in Applied Science, Engineering and Technology (IRASET)*, 2022, pp. 1–5. doi: 10.1109/IRASET52964.2022.9737799.

[53] F. K. Chang and K. Y. Chang, “A Progressive Damage Model for Laminated Composites Containing Stress Concentrations,” *J. Compos. Mater.*, vol. 21, no. 9, pp. 834–855, 1987, doi: 10.1177/002199838702100904.

[54] D. Yoon, S. Kim, J. Kim, and Y. Doh, “Development and evaluation of crack band model implemented progressive failure analysis method for notched composite laminate,” *Appl. Sci.*, vol. 9, no. 24, 2019, doi: 10.3390/app9245572.

[55] A. Matzenmiller, J. Lubliner, and R. L. Taylor, “A constitutive model for anisotropic damage in fiber-composites,” *Mech. Mater.*, vol. 20, no. 2, pp. 125–152, 1995, doi: 10.1016/0167-6636(94)00053-0.

[56] J. N. REDDY and A. K. PANDEY, “A first-ply failure analysis composite laminates of,” *Comput. Methods Appl. Mech. Eng.*, vol. 25, no. 3, pp. 371–393, 1986.

[57] T. Y. Kam and T. B. Jan, “First-ply failure analysis of laminated composite plates based on the layerwise linear displacement theory,” vol. 32, pp. 583–591, 1995.

[58] I. I. T. Kharagpur and K. W. Bengal, “Progressive Failure Analysis of Cross-ply,” vol. 26, no. 5, 2007, doi: 10.1177/0731684406072533.

[59] B. G. Prusty, S. K. Satsangi, and C. Ray, “Journal of Reinforced Plastics and,” 2001, doi: 10.1177/073168401772679020.

[60] M. Knops and C. Bögle, “Gradual failure in fiber/polymer laminates,” *Compos. Sci. Technol.*, vol. 66, no. 5, pp. 616–625, 2006, doi: 10.1016/j.compscitech.2005.07.044.

[61] L. B. Lessard and F. K. Chang, “Damage Tolerance of Laminated Composites Containing an Open Hole and Subjected to Compressive Loadings: Part I-Analysis,” *J. Compos. Mater.*, vol. 25, no. 1, pp. 44–64, 1989, doi: 10.1177/002199839102500102.

[62] V. K. Goyal, N. R. Jaunky, E. R. Johnson, and D. R. Ambur, “Intralaminar and interlaminar progressive failure analyses of composite panels with circular cutouts,” *Compos. Struct.*, vol. 64, no. 1, pp. 91–105, 2004, doi: 10.1016/S0263-8223(03)00217-4.

[63] C. S. Lee, B. M. Yoo, M. H. Kim, and J. M. Lee, “Viscoplastic damage model for austenitic stainless steel and its application to the crack propagation problem at cryogenic temperatures,” *Int. J. Damage Mech.*, vol. 22, no. 1, pp. 95–115, 2013, doi: 10.1177/1056789511434816.

[64] H. M. Deuschle and B. Kroplin, “3D Failure Analysis of UD Fiber Reinforced Composites: Puck’s theory within FEA,” University of Stuttgart, 2010.

[65] P. Ladeveze and E. LeDantec, “Damage modelling of the elementary ply for laminated composites,” *Compos. Sci. Technol.*, vol. 43, no. 3, pp. 257–267, 1992, doi: 10.1016/0266-3538(92)90097-M.

[66] N. M. Hassan and R. C. Batra, “Modeling damage in polymeric composites,” *Compos. Part B Eng.*, vol. 39, no. 1, pp. 66–82, 2008, doi: 10.1016/j.compositesb.2007.02.001.

[67] J. Lemaitre and R. Desmorat, *Engineering Damage Mechanics - Ductile, Creep, Fatigue and Brittle Failures*. Springer, 2005.

[68] J. Lemaitre, *A Course on Damage Mechanics*. 1996. doi: 10.1007/978-3-642-18255-6.

[69] L. Kachanov, *New approach for fatigue life prediction of composite plates using micromechanical bridging model*, vol. 10. 1986. doi: 10.1177/0021998313518570.

[70] M. V. Donadon, S. F. M. de Almeida, M. A. Arbelo, and A. R. de Faria, “A Three-Dimensional Ply Failure Model for Composite Structures,” *Int. J. Aerosp. Eng.*, vol. 2009, pp. 1–22, 2009, doi: 10.1155/2009/486063.

[71] R. C. Pavan, B. F. Oliveira, S. Maghous, and G. J. Creus, “A model for anisotropic viscoelastic damage in composites,” *Compos. Struct.*, vol. 92, no. 5, pp. 1223–1228, 2010, doi: 10.1016/j.compstruct.2009.10.020.

[72] T. Flatscher and H. E. Pettermann, “A constitutive model for fiber-reinforced polymer plies accounting for plasticity and brittle damage including softening - Implementation for implicit FEM,” *Compos. Struct.*, vol. 93, no. 9, pp. 2241–2249, 2011, doi: 10.1016/j.compstruct.2011.03.012.

[73] S. Zhou, Y. Sun, B. Chen, and T. E. Tay, “Progressive damage simulation of open-hole composite laminates under compression based on different failure criteria,” *J. Compos. Mater.*, vol. 51, no. 9, pp. 1239–1251, 2017, doi: 10.1177/0021998316659776.

[74] P. Linde and H. de Boer, “Modelling of inter-rivet buckling of hybrid composites,” *Compos. Struct.*, vol. 73, no. 2, pp. 221–228, 2006, doi: 10.1016/j.compstruct.2005.11.062.

[75] P. P. Camanho and C. G. Dávila, “Mixed-Mode Decohesion Finite Elements for the Simulation of Delamination in Composite Materials,” *J. Appl. Mech*, vol. 28, no. 2, pp. 259–268, 2002.

[76] I. Lapczyk and J. A. Hurtado, “Progressive damage modeling in fiber-reinforced materials,” *Compos. Part A Appl. Sci. Manuf.*, vol. 38, no. 11, pp. 2333–2341, 2007, doi: 10.1016/j.compositesa.2007.01.017.

[77] P. Ba, “Crack band theory for fracture of concrete,” 1983.

[78] T. VANDELLOS, “DÉVELOPPEMENT D’UNE STRATÉGIE DE MODÉLISATION DU DÉLAMINAGE DANS LES STRUCTURES COMPOSITES STRATIFIÉES,” BORDEAUX, 2011.

[79] A. C. Orifici, I. Herszberg, and R. S. Thomson, “Review of methodologies for composite material modelling incorporating failure,” *Compos. Struct.*, vol. 86, no. 1–3, pp. 194–210, 2008, doi: 10.1016/j.compstruct.2008.03.007.

[80] J. C. Brewer and P. A. Lagace, “Quadratic Stress Criterion for Initiation of Delamination,” *J. Compos. Mater.*, 1988, doi: 10.1177/002199838802201205.

[81] N. Carrere, “Proposition of 3D progressive failure approach and validation on tests,” 2010, no. June.

[82] J. M. Whitney and R. J. Nuismer, “Journal of Composite Materials,” 2014, doi: 10.1177/002199837400800303.

[83] G. A. A, “The Phenomena o f Rupture and Flow in Solid,” *Philos. Trans. R. Soc.*, vol. 221, pp. 163–198, 1920.

[84] E. F. RYBICIU and M. F. RANNINEN, “A FINITE ELEMENT CALCULATION OF STRESS INTENSITY FACTORS BY A MODIFIED CRACK CLOSURE INTEGRAL,” *Eng. Fract. Mech.*, vol. 9, pp. 931–938, 1977.

[85] R. Krueger, “Virtual crack closure technique : History , approach , and applications,” vol. 57, no. 2, pp. 109–143, 2013, doi: 10.1115/1.1595677.

[86] I. G. R., *Fracture I*. Handbuch der Physik, 1958.

[87] W. J. D. Rankumar R. L., “Characterization of Mode I and Mixed-Mode Delamination Growth in T300/5208 Graphite/Epoxy,” *Delamination Debonding Mater. ASTM STP 876*, pp. 315–335, 1985.

[88] M. L. Benzeggagh and M. Kenane, “Measurement of mixed-mode delamination fracture toughness of unidirectional glass/epoxy composites with mixed-mode bending apparatus,” *J. Compos. Sci. Technol.*, vol. 56, pp. 439–449, 1996.

[89] R. Krueger, J. G. Ratcliffe, and P. J. Minguet, “Panel stiffener debonding analysis using a shell / 3D modeling technique q,” *Compos. Sci. Technol.*, vol. 69, no. 14, pp. 2352–2362, 2009, doi: 10.1016/j.compscitech.2008.12.015.

[90] D. D. S., “Yielding of steel CONTAINING SLITS,” vol. 8, pp. 100–104, 1959.

[91] B. G. I., “The Mathematical Thsory of Equilibrium Cracks in Brittle Fracture,” *Adv. Appl. Mech.*, vol. 7, pp. 55-129, 1962.

[92] P. L. Allix O., Lévêque D., “Identification and forecast of delamination in composite laminates by an interlaminar interface model,” *Compos. Sci. Technol.*, vol. 58, pp. 671–678, 1998.

[93] "Damage Allix O., Ladevèze P., Corigliano A., “Damage analysis of interlaminar fracture specimens,” *Compos. Struct.*, vol. 31, pp. 61–74, 1995.

[94] C. G. Dávila and N. Langley, “Effective Simulation of Delamination in Aeronautical Structures Using Shells and Cohesive Elements,” vol. 45, no. 2, 2008, doi: 10.2514/1.32832.

[95] A. Turon, P. P. Camanho, J. Costa, and J. Renart, “Accurate simulation of delamination growth under mixed-mode loading using cohesive elements : Definition of interlaminar strengths and elastic stiffness,” *Compos. Struct.*, vol. 92, no. 8, pp. 1857–1864, 2010, doi: 10.1016/j.compstruct.2010.01.012.

[96] P. Hale and E. G. Ng, “Three-point bending analysis with cohesive surface interaction for improved delamination prediction and application of carbon fiber reinforced plastics composites,” *Model. Simul. Mater. Sci. Eng.*, vol. 28, no. 3, 2020, doi: 10.1088/1361-651X/ab7054.

[97] D. Cao, H. Hu, Q. Duan, P. Song, and S. Li, “Experimental and three-dimensional numerical investigation of matrix cracking and delamination interaction with edge effect of curved composite laminates,” *Compos. Struct.*, vol. 225, no. June, p. 111154, 2019, doi: 10.1016/j.compstruct.2019.111154.

[98] Y. Yang, X. Liu, Y. Q. Wang, H. Gao, R. Li, and Y. Bao, “A progressive damage model for predicting damage evolution of laminated composites subjected to three-point bending,” *Compos. Sci. Technol.*, vol. 151, pp. 85–93, 2017, doi: 10.1016/j.compscitech.2017.08.009.

[99] G. Alfano and M. A. Crisÿeld, “Finite element interface models for the delamination analysis of laminated composites : mechanical and computational issues,” no. March 2000, pp. 1701–1736, 2001.

[100] X.-P. Xu and A. Needleman, “Void nucleation by inclusion debonding in a crystal matrix,” *Model. Simul. Mater. Sci. Eng.*, vol. 111, 1993.

[101] A. Needleman, “A Continuum Model for Void Nucleation by Inclusion Debonding,” vol. 54, pp. 525–531, 1987.

[102] C. Henninger, D. Leguillon, and E. Martin, “Crack initiation at a V-notch — comparison between a brittle fracture criterion and the Dugdale cohesive model,” *C. R. Mec.*, vol. 335, pp. 388–393, 2007, doi: 10.1016/j.crme.2007.05.018.

[103] O. Allix and P. Ladev, “Interlaminar interface modelling for the prediction of delamination,” vol. 22, pp. 235–242, 1992.

[104] M. L. Falk, A. Needleman, J. R. Rice, and A. Arbor, “A critical evaluation of cohesive zone models of dynamic fracture,” vol. 11, 2001.

[105] Z. P. Bažant and M. Jirásek, “Nonlocal Integral Formulations of Plasticity and Damage: Survey of Progress,” *Perspect. Civ. Eng. Commem. 150th Anniv. Am. Soc. Civ. Eng.*, no. November, pp. 21–51, 2003, doi: 10.1061/(asce)0733-9399(2002)128:11(1119).

[106] Q. Yang and B. Cox, “Cohesive models for damage evolution in laminated composites,” pp. 107–137, 2005, doi: 10.1007/s10704-005-4729-6.

[107] L. P. Daudeville L, Allix O, “Delamination analysis by damage mechanics. Some applications.,” *Compos Engng*, vol. 5, no. 1, pp. 17–24, 1995.

[108] P. P. Camanho, C. G. Davila, and M. F. De Moura, “Numerical Simulation of Mixed-Mode Progressive Delamination in Composite Materials,” *J. Compos. Mater.*, 2003, doi: 10.1177/002199803034505.

[109] P. P. Camanho and J. Costa, “An engineering solution for mesh size effects in the simulation of delamination using cohesive zone models,” vol. 74, pp. 1665–1682, 2007,

doi: 10.1016/j.engfracmech.2006.08.025.

[110] P. D. Mohammadi S, Owen DRJ, “A combined finite/discrete element algorithm for delamination analysis of composites,” *Finite Elem. Anal. Des.*, vol. 28, pp. 321–336, 1998.

[111] “Abaqus/Standard, V6.13-3, is a trademark of ABAQUS, Inc.,” *Simulia, Dassault Systèmes*. http://130.149.89.49:2080/v6.13/pdf_books/ANALYSIS_3.pdf

[112] E. J. Barbero, *Finite element analysis of composite materials using Abaqus (2013)*. 2013. [Online]. Available: https://books.google.com/books?hl=en&lr=&id=sKHT0WwTm2UC&pgis=1

[113] E. Hinton and D. R. J. Owen, “An introduction to finite element computations,” *Pineridge Press*, 1981.

[114] G. D. Smith, “Numerical solution of partial differential equations: finite difference methods,” *Oxford Univ. Press*, 1985.

[115] K. H. Huebner, D. L. Dewhirst, D. E. Smith, and T. G. Byrom, “The Finite Element Method for Engineers,” *John Wiley Sons*, 2001.

[116] Hill R, “Theory of mechanical properties of fiber-strengthened materials_III,” *J Mech Phys Solids*, vol. 13, pp. 189–98, 1965.

[117] S. W. Tsai, “Strength Theories of Filamentary Structures Fundamental Aspects of Fiber Reinforced Plastic Composites,” *New York WileyInterscience*, 1968.

[118] O. Hoffman, “The Brittle Strength of Orthotropic Materials,” *J. Compos. Mater.*, vol. 1, no. 2, pp. 200–206, 1967, doi: 10.1177/002199836700100210.

[119] H. El idrissi and A. Seddouki, “Damage Modeling of Composites Laminate Containing Stress Concentrations,” in *2022 2nd International Conference on Innovative Research in Applied Science, Engineering and Technology (IRASET)*, 2022, pp. 1–5. doi: doi: 10.1109/IRASET52964.2022.9737799.

[120] S. C. Tan, “A Progressive Failure Model for Composite Laminates Containing Openings,” *J. Compos. Mater.*, vol. 25, no. 5, pp. 556–577, 1991, doi: 10.1177/002199839102500505.

[121] B. Y. Chen, T. E. Tay, P. M. Baiz, and S. T. Pinho, “Numerical analysis of size effects on open-hole tensile composite laminates,” *Compos. Part A Appl. Sci. Manuf.*, vol. 47, no. 1, pp. 52–62, 2013, doi: 10.1016/j.compositesa.2012.12.001.

[122] J. F. Chen, E. V. Morozov, and K. Shankar, “A combined elastoplastic damage model for progressive failure analysis of composite materials and structures,” *Compos. Struct.*, vol. 94, no. 12, pp. 3478–3489, 2012, doi: 10.1016/j.compstruct.2012.04.021.

[123] F. K. Chang, R. A. Scott, and G. S. Springer, “Strength of bolted joints in laminated composites,” *MICHIGAN UNIV ANN ARBOR DEPT Mech. Eng. Appl. Mech.*, vol. 28, no. 1, pp. 9–10, 1984, doi: 10.3917/tf.071.0009.

[124] H. Bakhshan, A. Afrouzian, H. Ahmadi, and M. Taghavimehr, “Progressive failure analysis of fiber-reinforced laminated composites containing a hole,” *Int. J. Damage Mech.*, vol. 27, no. 7, pp. 963–978, 2018, doi: 10.1177/1056789517715088.

[125] C. T. Sun and J. L. Chen, “A simple flow rule for characterizing non-linear Behavior of Fiber composites,” *J. Compos. Mater.*, vol. 23, no. 1009–20, 1988, doi:

10.1177/002199838902301004.

[126] T. Belytschko, Z. P. Bažant, H. Yul-Woong, and C. Ta-Peng, “Strain-softening materials and finite-element solutions,” *Comput. Struct.*, vol. 23, no. 2, pp. 163–180, 1986, doi: 10.1016/0045-7949(86)90210-5.

[127] B. Mandal and A. Chakrabarti, “SIMULATING PROGRESSIVE DAMAGE OF NOTCHED COMPOSITE LAMINATES WITH VARIOUS LAMINATION SCHEMES,” vol. 22, no. 2, pp. 333–347, 2017, doi: 10.1515/ijame-2017-0020.

[128] R. H. Maa and J. H. Cheng, “A CDM-based failure model for predicting strength of notched composite laminates,” *Compos. Part B Eng.*, vol. 33, no. 6, pp. 479–489, 2002, doi: 10.1016/S1359-8368(02)00030-6.

[129] G. Am, “Girão-Coelho AM . Finite element guidelines for simulation of delamination dominated failures in composite materials validated by case studies . Archives of Computational Methods in Engineering 2016 , 1-26 . Finite Element Guidelines for Simulation of Del,” no. February, pp. 1–26, 2016.

[130] M. Ridha, C. H. Wang, B. Y. Chen, and T. E. Tay, “Modelling complex progressive failure in notched composite laminates with varying sizes and stacking sequences,” *Compos. Part A Appl. Sci. Manuf.*, vol. 58, pp. 16–23, 2014, doi: 10.1016/j.compositesa.2013.11.012.

[131] A. Mokhtari, M. Ould Ouali, and N. Tala-Ighil, “Damage modelling in thermoplastic composites reinforced with natural fibers under compressive loading,” *Int. J. Damage Mech.*, vol. 24, no. 8, pp. 1239–1260, 2015, doi: 10.1177/1056789515573900.

[132] E. H. Irhirane, M. Abousaleh, J. Echaabi, M. Hattabi, A. Saouab, and M. O. Bensalah, “Modeling and simulation of the failure and stiffness degradation of a graphite epoxy in a three point bending test,” *J. Eng. Mater. Technol. Trans. ASME*, vol. 132, no. 3, pp. 0310131–0310138, 2010, doi: 10.1115/1.3078392.

[133] J. F. Chen, E. V. Morozov, and K. Shankar, “Simulating progressive failure of composite laminates including in-ply and delamination damage effects,” *Compos. Part A Appl. Sci. Manuf.*, vol. 61, pp. 185–200, 2014, doi: 10.1016/j.compositesa.2014.02.013.

[134] ASTM Standard D790, “Standard test methods for flexural properties of unreinforced and reinforced plastics and electrical insulating materials.,” in *Annual book of ASTM Standards*, 1997, pp. 1–11.

[135] “ABC composites Standard Prepreg Range & Technical data sheets NT-FTP-022 (T700). index 3,” 2016.

[136] J. Echaabi, F. Trochu, X. T. Pham, and M. Ouellet., “Theoretical and Experimental Investigation of Failure and Damage Progression of Graphite-Epoxy Composites in Flexural Bending Test,” *J. Reinf. Plast. Compos.*, vol. 15, no. 7, pp. 740–55., 1996, doi: 10.1177/073168449601500707.

[137] J. Wiegand, N. Petrinic, and B. Elliott, “An algorithm for determination of the fracture angle for the three-dimensional Puck matrix failure criterion for UD composites,” *Compos. Sci. Technol.*, vol. 68, no. 12, pp. 2511–2517, 2008, doi: 10.1016/j.compscitech.2008.05.004.

[138] F. Dal Maso and J. Meziere, “Calcul des propriétés élastiques des tissus utilisés dans les matériaux composites,” *Rev. l’Institut Français du Pétrole*, vol. 53, no. 6, pp. 857–870,

1998, doi: 10.2516/ogst:1998073.

[139] M. A. Caminero, G. P. Rodríguez, and V. Muñoz, “Effect of stacking sequence on Charpy impact and flexural damage behavior of composite laminates,” *Compos. Struct.*, vol. 136, pp. 345–357, 2016, doi: 10.1016/j.compstruct.2015.10.019.

[140] R. J. Nuismer and S. C. Tan, *Constitutive Relations of a Cracked Composite Lamina*, vol. 22, no. 4. p. 306−321. doi: 10.1177/002199838802200401.

[141] D. C. Pham, X. Cui, X. Ren, and J. Lua, “A discrete crack informed 3D continuum damage model and its application for delamination migration in composite laminates,” *Compos. Part B Eng.*, vol. 165, no. October 2018, pp. 554–562, 2019, doi: 10.1016/j.compositesb.2019.02.045.

[142] Y. Lin, Y. Huang, T. Huang, B. Liao, D. Zhang, and C. Li, “Characterization of progressive damage behaviour and failure mechanisms of carbon fiber reinforced aluminium laminates under three-point bending,” *Thin-Walled Struct.*, vol. 135, pp. 494–506, 2019, doi: 10.1016/j.tws.2018.12.002.

[143] Y. Benbouras, M. Bellahkim, A. Maziri, E. Mallil, and J. Echaabi, “An analytical and experimental study of the nonlinear behaviour of a carbon/epoxy under a three-point bending test,” *Plast. Rubber Compos.*, pp. 145–153, 2021, doi: 10.1080/14658011.2021.1950457.

[144] C. Liu *et al.*, “Interlaminar failure behavior of GLARE laminates under short-beam three-point-bending load,” *Compos. Part B Eng.*, vol. 97, pp. 361–367, 2016, doi: 10.1016/j.compositesb.2016.05.003.

[145] M. Demiral, F. Kadioglu, and V. V. Silberschmidt, “Size effect in flexural behaviour of unidirectional GFRP composites,” *J. Mech. Sci. Technol.*, vol. 34, no. 12, pp. 5053–5061, 2020, doi: 10.1007/s12206-020-1109-0.

[146] L. Bahadur and G. Raju, “Continuum and cohesive zone damage models to study intra / inter-laminar failure of curved composite laminates under four-point bending,” *Compos. Struct.*, vol. 253, no. March, p. 112768, 2020, doi: 10.1016/j.compstruct.2020.112768.

[147] P. Hu, D. Pulungan, R. Tao, and G. Lubineau, “An experimental study on the influence of intralaminar damage on interlaminar delamination properties of laminated composites,” *Compos. Part A Appl. Sci. Manuf.*, vol. 131, p. 105783, 2020, doi: 10.1016/j.compositesa.2020.105783.

[148] B. Shen, H. Liu, S. Lv, Z. Li, and W. Cheng, “Progressive Failure Analysis of Laminated CFRP Composites under Three-Point Bending Load,” *Adv. Mater. Sci. Eng.*, 2022, doi: 10.1155/2022/3047319.

[149] K. Falkowicz, M. Ferdynus, and P. Rozylo, “Experimental and numerical analysis of stability and failure of compressed composite plates,” *Compos. Struct.*, vol. 263, p. 113657, 2021, doi: 10.1016/j.compstruct.2021.113657.

[150] P. Hu, X. Li, and G. Lubineau, “Prediction of a complex delamination front using a general cohesive model,” *Compos. Sci. Technol.*, vol. 233, 2023, doi: 10.1016/j.compscitech.2023.109911.

[151] G. F. O. Ferreira, J. H. S. Almeida, M. L. Ribeiro, A. J. M. Ferreira, and V. Tita, “A finite element unified formulation for composite laminates in bending considering progressive damage,” *Thin-Walled Struct.*, vol. 172, 2022, doi: 10.1016/j.tws.2021.108864.

[152] M. A. Caminero, G. P. Rodríguez, J. M. Chacón, J. M. Reverte, and I. García-Moreno, "Flexural damage response of symmetric cross-ply carbon fiber reinforced laminates: Effects of thickness and ply-scaling technique," *Mech. Adv. Mater. Struct.*, vol. 28, no. 2, pp. 212–219, 2021, doi: 10.1080/15376494.2018.1553260.

[153] H. Liu *et al.*, "Modelling damage in fiber-reinforced thermoplastic composite laminates subjected to three-point bend loading," *Compos. Struct.*, vol. 236, p. 111889, 2020, doi: 10.1016/j.compstruct.2020.111889.

[154] B. Paul, "A Modification of the Coulomb- Mohr Theory of Fracture 1," *J. Appl. Mech*, no. 2, pp. 259–268, 2016.

[155] *Cytec Inc, CYCOM 977-2 Epoxy Resin System Data Sheet*,. 2012. [Online]. Available: http://www.cytec.com/sites/default/files/datasheets/CYCOM_977-2_ 031912.pdf

[156] X. Li, W. Gao, and W. Liu, "Post-buckling progressive damage of CFRP laminates with a large-sized elliptical cutout subjected to shear loading," *Compos. Struct.*, vol. 128, pp. 313–321, 2015, doi: 10.1016/j.compstruct.2015.03.038.

[157] *CYTEC. APC-2-PEEK Thermoplastic Polymer 2012.*

[158] L. Wang, C. Zheng, H. Luo, S. Wei, and Z. Wei, "Continuum damage modeling and progressive failure analysis of carbon fiber/epoxy composite pressure vessel," *Compos. Struct.*, vol. 134, pp. 475–482, 2015, doi: 10.1016/j.compstruct.2015.08.107.

[159] H. Nguyen-Xuan, G. R. Liu, S. Bordas, S. Natarajan, and T. Rabczuk, "An adaptive singular ES-FEM for mechanics problems with singular field of arbitrary order," *Comput. Methods Appl. Mech. Eng.*, vol. 253, pp. 252–273, 2013, doi: 10.1016/j.cma.2012.07.017.

[160] W. Xu *et al.*, "An adaptive mesh refinement strategy for 3D phase modeling of brittle fracture," *Eng. Fract. Mech.*, vol. 284, no. December 2022, 2023, doi: 10.1016/j.engfracmech.2023.109241.